NASA

MEMORANDUM

A TRANSONIC WIND-TUNNEL INVESTIGATION OF

THE PERFORMANCE AND OF THE STATIC STABILITY AND CONTROL

CHARACTERISTICS OF A MODEL OF A FIGHTER-TYPE AIRPLANE

WHICH EMBODIES PARTIAL BODY INDENTATION

By Ralph P. Bielat

Langley Research Center
Langley Field, Va.

Declassified April 14, 1960

NATIONAL AERONAUTICS AND SPACE ADMINISTRATION
WASHINGTON

March 1959

L-476

NATIONAL AERONAUTICS AND SPACE ADMINISTRATION

MEMORANDUM 12-13-58L

A TRANSONIC WIND-TUNNEL INVESTIGATION OF

THE PERFORMANCE AND OF THE STATIC STABILITY AND CONTROL

CHARACTERISTICS OF A MODEL OF A FIGHTER-TYPE AIRPLANE

WHICH EMBODIES PARTIAL BODY INDENTATION

By Ralph P. Bielat

SUMMARY

An investigation was conducted to obtain the aerodynamic characteristics of a model of a fighter-type airplane embodying partial body indentation. The wing had an aspect ratio of 4, taper ratio of 0.5, $35°$ sweepback of the 0.25-chord line, and a modified NACA 65A006 airfoil section at the root and a modified NACA 65A004 airfoil section at the tip. The fuselage has been indented in the region of the wing in order to obtain a favorable area distribution. The results reported herein consist of the performance and of the static longitudinal and lateral stability and control characteristics of the complete model. The Mach number range extended from 0.60 to 1.13, and the corresponding Reynolds number based on the wing mean aerodynamic chord varied from 1.77×10^6 to 2.15×10^6.

The drag rise for both the cambered leading edge and symmetrical wing sections occurred at a Mach number of 0.95. Certain local modifications to the body which further improved the distribution of cross-sectional area gave additional reductions in drag at a Mach number of 1.00. The basic configuration indicated a mild pitch-up tendency at lift coefficients near 0.70 for the Mach number range from 0.80 to 0.90; however, the pitch-up instability may not be too objectionable on the basis of dynamic-stability considerations. The basic configuration indicated positive directional stability and positive effective dihedral through the angle-of-attack range and Mach number range with the exception of a region of negative effective dihedral at low lifts at Mach numbers of 1.00 and slightly above.

*The information presented herein was previously given limited distribution in NACA Research Memorandum SL54J15.

INTRODUCTION

The work of reference 1 has indicated that substantial reductions in the zero-lift transonic drag rise of wing-body combinations could be realized if the bodies were properly contoured for the wings in order to achieve favorable area distributions. As a result, it was considered desirable to investigate the aerodynamic properties at transonic speeds of a model of a fighter-type airplane which embodied partial body indentation. The model selected had a wing which was swept back 35° at the quarter-chord line with an aspect ratio of 4, a taper ratio of 0.5, and a thickness of 6 percent chord at the root and 4 percent chord at the tip. The wing was mounted in a "semihigh" position on the fuselage, and an all-movable horizontal tail was located slightly below the extended chord line of the wing. The fuselage was indented in the region of the wing in an effort to obtain a favorable area distribution for the purpose of reducing the transonic drag rise.

The purpose of the present investigation was to obtain the performance and static longitudinal and lateral stability and control characteristics of the model at transonic speeds. The effects of wing-profile, leading-edge chord-extensions, body modifications, wing-mounted air-to-air missiles, and speed brakes are also included. The Mach number range extended from 0.60 to 1.13 and the corresponding Reynolds number range extended from 1.77×10^6 to 2.15×10^6 based on the wing mean aerodynamic chord.

During the course of the investigation, the static longitudinal stability characteristics obtained on the model indicated a forward movement of the aerodynamic-center location in the Mach number range from 0.60 to 0.90, which resulted in a low static margin of stability. In order to determine whether the forward movement of the aerodynamic-center location could be due to Reynolds number effects, the model was tested also at low speeds and varying Reynolds numbers in the Langley low-turbulence pressure tunnel. The present paper, therefore, contains the results obtained at transonic speeds in the Langley 8-foot transonic tunnel and at low speeds in the Langley low-turbulence pressure tunnel.

COEFFICIENTS AND SYMBOLS

The stability system of axes used for the presentation of the data, together with an indication of the positive direction of forces, moments, and angles, is presented in figure 1. All moments are referred to the 25-percent-chord point of the mean aerodynamic chord. The coefficients have been based on the geometry of the symmetrical wing section.

C_L lift coefficient, $\dfrac{\text{Lift}}{qS}$, where Lift $= -Z$

C_D drag coefficient, $\dfrac{\text{Drag}}{qS}$, where Drag $= -X$ when $\beta = 0°$

ΔC_D incremental drag coefficient

ΔC_{D_F} incremental drag coefficient based on frontal area

C_X longitudinal-force coefficient, $\dfrac{\text{Longitudinal force}}{qS}$

C_{D_I} internal-drag coefficient of duct, $\dfrac{\text{Internal drag}}{qS}$

C_m pitching-moment coefficient, $M'/qS\bar{c}$

C_l rolling-moment coefficient, L'/qSb

C_n yawing-moment coefficient, N'/qSb

C_Y lateral-force coefficient, Y/qS

X force along X-axis

Y force along Y-axis

Z force along Z-axis

M' moment about Y-axis

N' moment about Z-axis

L' moment about X-axis

q free-stream dynamic pressure

S wing plan-form area based on symmetrical wing

A duct area

b wing span

c local wing chord, parallel to plane of symmetry

$\bar{c}$ mean aerodynamic chord of wing

M   Mach number

m   mass-flow rate, ρAV

R   Reynolds number based on $\bar{c}$

V   free-stream velocity

α angle of attack referred to fuselage reference line

β angle of sideslip

ϵ effective downwash angle

i_t stabilizer incidence referred to fuselage reference line

δ control surface deflection measured in plane perpendicular to hinge line

ρ free-stream air density

L/D   lift-drag ratio

W/S   wing loading

$\dfrac{\partial C_D}{\partial C_L^2}$ drag-due-to-lift parameter

$C_{L_\alpha} = \dfrac{\partial C_L}{\partial \alpha}$ per degree

$C_{m_{i_t}} = \dfrac{\partial C_m}{\partial i_t}$ per degree

$C_{m_{C_L}} = \dfrac{\partial C_m}{\partial C_L}$

$C_{l_\beta} = \dfrac{\partial C_l}{\partial \beta}$ per degree

$C_{n_\beta} = \dfrac{\partial C_n}{\partial \beta}$ per degree

$$C_{Y_\beta} = \frac{\partial C_Y}{\partial \beta} \quad \text{per degree}$$

$$C_{l_{\delta_f}} = \frac{\partial C_l}{\partial \delta_f} \quad \text{per degree}$$

$$C_{l_{\delta_r}} = \frac{\partial C_l}{\partial \delta_r} \quad \text{per degree}$$

$$C_{n_{\delta_r}} = \frac{\partial C_n}{\partial \delta_r} \quad \text{per degree}$$

$$C_{Y_{\delta_r}} = \frac{\partial C_Y}{\partial \delta_r} \quad \text{per degree}$$

$$\beta_{\delta_r} = \frac{C_{n_{\delta_r}}}{C_{n_\beta}} \quad \text{per degree}$$

Subscripts:

f	flap-type spoiler
i	inlet
o	free stream
r	rudder
max	maximum
min	minimum

APPARATUS AND MODELS

Tunnels

The investigation was conducted in both the Langley 8-foot transonic tunnel and Langley low-turbulence pressure tunnel. The 8-foot transonic tunnel is a dodecagonal, slotted-throat, single-return wind tunnel. This

tunnel is designed to obtain aerodynamic data through the speed of sound without the usual effects of choking and blockage. The tunnel operates at atmospheric stagnation pressures. A more complete description of the tunnel can be found in reference 2.

The Langley low-turbulence pressure tunnel is a rectangular, closed-throat, single-return wind tunnel. This tunnel operates with air to obtain low-speed data or with Freon-12 to obtain high subsonic data. The stagnation pressure can be varied to control the Reynolds number. A complete description of this tunnel can be found in references 3 and 4.

Models

A three-view drawing and physical characteristics of the model used in this investigation are presented in figure 2, and a photograph of the model on the sting support is shown in figure 3. The construction of the model was such that the effects of various components could be investigated. The term "basic configuration" as employed herein describes the model with original fuselage, wing with cambered leading edge, chordwise wing fences, and the horizontal- and vertical-tail surfaces. The basic configuration for this investigation had a 35° sweptback wing with a modified NACA 65A006 airfoil section at the root and a modified NACA 65A004 airfoil section at the tip. The wing had an aspect ratio of 4 and a taper ratio of 0.5 and was mounted in a semihigh position on the fuselage. The camber line of the basic wing was tangent to the mean line of the unmodified symmetrical wing section at the 0.40-chord station. The camber line of the basic wing gave approximately 8° of nose droop at the extreme leading edge. The leading edge of the basic wing could be removed in order to allow for the installation of an alternate symmetrical leading edge. A comparison of the wings with cambered leading edges and symmetrical leading edges is made in figure 4 and ordinates for the two wing sections are presented in table I.

Chordwise wing fences, located at the 0.52b/2 wing station (fig. 2), were tested in combination with the cambered-leading-edge wing. The fences had a maximum height of 0.065c and were faired to zero height at the 0.70c station.

Leading-edge chord-extensions were also tested in combination with the cambered-leading-edge wing. The leading-edge chord-extensions covered the outboard span of the wing from the 0.52 to the 1.00b/2 stations, and the chords were 10 percent of the local wing chord (fig. 2). The leading-edge chord-extensions were obtained by moving the front 10 percent of the basic airfoil forward along the camber line of the leading-edge camber and fairing in the gap produced.

Lateral control was obtained with a flap-type spoiler located on the upper surface of the wing as shown in figure 2. The spoiler extended from the 0.21 to the 0.84b/2 wing stations and was hinged at the 0.70c station. The spoiler chord was 14 percent of the local wing chord. Spoiler deflections were obtained by installing spoiler sections which had been machined to the desired deflections.

The original fuselage, which had an equivalent fineness ratio of 7.43 (equivalent fineness ratio is the ratio of the length of the configuration to the equivalent diameter corresponding to the maximum cross-sectional area of the configuration), had substantial indentation of the sides in order to obtain a favorable area distribution in the region of the wing. The area removed to obtain the basic fuselage was determined according to the concepts of reference 1. Three modifications on the original fuselage were investigated as shown in figures 2 and 5. The maximum indentation for modification 1 (fig. 2) was farther forward than that for the original fuselage and the maximum area was increased so that the equivalent fineness ratio was 7.28. Modification 2 (fig. 5) was used to give a smoother area distribution in the region of the leading edge of the wing and modification 3 (fig. 5) increased the base area and reduced the boattail at the rear of the fuselage. The axial distributions of cross-sectional area for these configurations are given in figure 6(a).

The model was also tested with air-to-air missiles, which were strut-mounted below the wing at the 0.58b/2 wing station. Details of the air-to-air missiles are presented in figure 7, and the axial distribution of the cross-sectional area of the missiles in combination with the basic configuration is given in figure 6(b).

An all-movable horizontal tail was mounted at the 0.069b/2 wing station below the extended chord plane of the wing. Stabilizer incidences were accomplished by pivoting the horizontal tail about a line through the 57.6-percent mean aerodynamic chord of the horizontal tail. Rudder deflections were obtained by providing several rudder surfaces with fixed angles of deflection.

The speed brakes which were investigated are shown in figure 2.

The jet-engine ducting was simulated on the model by the use of conventional subsonic twin side-scoop inlets. Faired plugs were used to close the inlets in order that some results could be obtained without flow through the ducts.

Some tests were conducted with fixed transition on the model by applying 1/8-inch-wide strips of No. 60 carborundum grains around the nose of the fuselage approximately 1 inch back from the nose and to the side inlets at the leading edge of the inlets and a strip on the wing

leading edge which extended from the 5-percent-chord station on the upper
surface to the 5-percent-chord station on the lower surface.

TESTS

Tests in Langley 8-Foot Transcnic Tunnel

Reynolds number.- For the tests in the Langley 8-foot transonic
tunnel, the Reynolds number based on the mean aerodynamic chord of the
wing and averaged for several runs is shown in figure 8 as a function of
test Mach number. The Reynolds number varied from 1.77×10^6 to
2.15×10^6 for the present investigation.

Measurements.- Six-component data were obtained by means of an
electrical strain-gage balance located inside the fuselage. Total-
pressure and static-pressure measurements were taken at the exit of the
jet-engine duct to determine the mass flow and internal-drag coefficient.
In addition, static pressures were measured within the balance chamber.
In general, dependent on model configuratior, measurements were taken
for two angle-of-attack ranges: -2^0 to 15^0 and -2^0 to 9^0 at Mach numbers
varying from 0.60 to 1.13. The angle of sideslip ranged from -8^0 to 4^0
for angles of attack of 0^0 and 6^0. Additioral tests were made through
an angle-of-attack range for fixed angles of sideslip approximately equal
to 0^0, -2.5^0, and -5^0. Load limits on the balance, however, prevented
the attainment of measurements over the entire angle ranges at all test
Mach numbers.

Corrections and accuracy.- No corrections to the free-stream Mach
number and dynamic pressure for the effects of model and wake blockage
are necessary for tests in the slotted test section of the Langley 8-foot
transonic tunnel (ref. 5). There is a range of Mach numbers above a
Mach number of 1.00 where the data are affected by reflected compressions
and expansions from the test-section boundary. From consideration of
the results of reference 2, it is believed that for Mach numbers up to
approximately 1.03 the effects of these disturbances on the measurements
made in the present investigation would be negligible. No test data,
however, were taken in the range where the reflected boundary disturbances
impinged upon the model. Visual schlieren observations were made during
the investigation to determine the Mach number at which the reflected
boundary disturbances cleared the base of the model.

The drag data have been corrected for base pressure such that the
drag corresponds to conditions where the base pressure is equal to the
free-stream static pressure. The drag data have also been corrected for
a buoyant force on the balance, which was obtained from measurements of
the static pressure in the balance chamber, and for the viscous force

on the unshielded portion of the sting inside the model. The internal drag has been subtracted for the open-duct configurations so that a net external drag was obtained. The variation with angle of attack of the internal-drag coefficient for the basic configuration is shown in figure 9.

No corrections for the forces and moments produced by the sting interference have been applied to the data. As indicated in reference 6 the significant corrections would be limited to small increments in pitching moment and drag and to the effective downwash angle.

The angles of attack and sideslip have been corrected for deflection of the sting support system under load. The angles of attack, sideslip, and control deflection are estimated to be accurate to within $\pm 0.1^\circ$.

The estimated consistency of the data at a Mach number of 0.60, based on the static calibrations and the repeatability of the data, is as follows:

C_L . . . . ± 0.01
C_D . . . . ± 0.0015
C_m . . . . ± 0.008
C_l . . . . ± 0.0007
C_n . . . . ± 0.0007
C_Y . . . . ± 0.005

These errors would be inversely proportional to the dynamic pressure and therefore would be lower at the higher Mach numbers.

Tests in Langley Low-Turbulence Pressure Tunnel

Reynolds number.- The investigation in the Langley low-turbulence pressure tunnel was made for Reynolds numbers, based on the wing mean aerodynamic chord, varying from 1.60×10^6 to 7.70×10^6.

Measurements.- The forces, moments, and pressures in the Langley low-turbulence tunnel were determined in a similar manner to those obtained in the Langley 8-foot transonic tunnel. Generally, the measurements were taken for an angle-of-attack range from -4° to 12°; however, in some cases, the range was increased to approximately 18°. The Mach number range varied from 0.148 to 0.489 for the tests conducted in air and from 0.390 to 0.842 for the tests conducted in Freon-12. The model caused the tunnel to choke at a Mach number of about 0.91; however, no data are presented in the Mach number range where it was believed that the data would be affected by partial choking.

Corrections.- Blockage corrections were determined by the methods described in references 7 and 8 and were applied to the Mach numbers and dynamic pressures. Jet-boundary corrections, applied to the angle of attack, drag, and pitching moments for the configurations with the horizontal tail, were calculated by using the methods of reference 9. The methods described in reference 4 have been used to correct the data obtained in Freon-12 to equivalent air conditions. The angle of attack has been corrected for deflection of the sting-support system under load. No tare corrections were applied.

<div align="center">RESULTS</div>

Throughout the present paper, the model having the original fuselage (fig. 2), the wing with cambered leading edge, the chordwise wing fences, and the horizontal- and vertical-tail surfaces is identified as the basic configuration. An index of the figures presenting the results is given in table II.

The first preliminary tests on the model indicated a high transonic drag-rise increment. The mass-flow ratio at the inlets at a Mach number of 1.00 was found to be approximately 0.35; whereas the design inlet mass-flow ratio on the airplane is 0.80. It was believed, therefore, that a combination of the low inlet-velocity ratio resulting from the low mass-flow ratio and the external spillage of the air around the inlets was responsible for the high drag. Examination of the model ducting indicated that extensive modifications to the ducting would be required to obtain the design inlet mass-flow ratio. For expediency, therefore, it was decided to reduce the inlet area $\left(A_{inlet}/A_{design} = 0.462\right)$ as shown by the inlet modification in figure 2 and, as a result, the mass-flow ratio was increased to approximately 0.75 as indicated in figure 10.

An interruption during the test program, however, permitted the internal ducting of the model to be extensively modified in order that some tests could be made to determine the aerodynamic characteristics of the model with the proper mass-flow ratio. The proper mass-flow ratio, however, could only be achieved for the configuration without a horizontal tail since the modifications consisted of increasing the internal duct areas wherever possible, removing the horizontal-tail support structure, and reducing the design-inlet area by increasing the lip radii at the duct inlets. These changes resulted in a mass-flow ratio of about 0.72 $\left(A_{inlet}/A_{design} = 1.00\right)$ for the configuration with original fuselage and 0.78 $\left(A_{inlet}/A_{design} = 1.00\right)$ for the configuration with modification 1. (See fig. 10.) Except where noted, the test program was conducted with the ducting modifications and inlet modifications on the model

$\left(A_{inlet}/A_{design} = 0.546\right)$ with a mass-flow ratio of 0.91 as shown in figure 10.

The drag analysis plots of the various configurations presented have been adjusted to account for the effects on drag of proper mass flow through the internal ducting system as shown in figure 11. The basic longitudinal data for the various model configurations are presented in figures 12 to 25. Summary plots of the longitudinal data are presented in figures 26 to 38. The basic lateral data are then given in figures 39 to 43 with the summary plots of the lateral stability characteristics in figures 44 to 47.

The effective downwash angle at a given angle of attack for the basic model shown in figure 37 was determined by finding the model stabilizer incidence at which the pitching-moment coefficient of the complete configuration was equal to that of the complete configuration less the horizontal tail. (See fig. 12.)

The aerodynamic characteristics of the basic model with the vertical and horizontal tails off and with the vertical and horizontal tails on for constant values of sideslip angle shown in figures 39 and 40, respectively represent faired values which were determined from cross-plots of the data against the indicated angles of sideslip, since the flexibility of the sting-support system made it impossible to conduct the tests at fixed values of sideslip. The aerodynamic characteristics in sideslip of the basic model with and without the vertical and horizontal tails shown in figure 41 were obtained with the model rotated 90° on the sting-support system.

Some tests of the model were conducted at supersonic speeds in the Langley 4- by 4-foot supersonic tunnel, and some of these data (labeled 4-foot data) have been included with the summary data of the present report. Curves have been faired from the transonic data through the supersonic data in order to illustrate the trends in the aerodynamic characteristics in these speed ranges.

DISCUSSION

Longitudinal Aerodynamic Characteristics

Lift characteristics.- Most of the configurations exhibited linear lift characteristics up to a lift coefficient of approximately 0.5. (See, for example, figs. 12 to 15 and 19 and 20.) Above a lift coefficient of 0.6 and at Mach numbers up to 0.95, the variation of lift coefficient with angle of attack decreased such that the lift-curve slopes were less than one-half the values measured in the lift range -0.2 to 0.5; but as

the Mach number increased, these decreases in lift-curve slope became less pronounced.

In general, the lift-curve slopes for the various configurations (fig. 26) were very nearly the same. The lift-curve slopes increased to a maximum value at Mach number of about 1.00 and then decreased gradually with increase in speed. The lift-curve slope of the basic configuration for the trimmed condition (fig. 26(a)) was approximately $2\frac{1}{2}$ percent lower than for the untrimmed condition at a Mach number of 0.60 and 19 percent lower at a Mach number of 1.13.

The addition of the speed brakes to the basic model decreased the angle for zero lift about 0.25° at a Mach number of 0.90 and 1.25° at a Mach number of 1.13 (fig. 20). In the same speed range, however, the trim lift coefficient was increased by the addition of the speed brakes.

Drag characteristics.- An examination of figure 15 shows that throughout the Mach number range at low lift coefficients the configuration with fuselage modification 1 had higher drag than did the configuration with the original fuselage. These differences were probably due to the more rapid body indentation of modification 1 and to its slightly lower effective fineness ratio (see fig. 6(a)) as compared with that of the original fuselage.

As previously mentioned, the drag results in the following discussion have been adjusted to account for the effects of mass-flow ratio on drag. This adjustment has been necessary since the basic model was chosen as the one with an inlet modification such that $A_{inlet}/A_{design} = 0.546$.

Figure 11 shows the effect on the drag coefficient of operating the model with various mass-flow ratios. It would be expected that the drag coefficient should be less for a configuration with a higher mass-flow ratio than for one with approximately one-half the mass-flow ratio, since the pressure losses in the system would be less and there would be less external spillage of the air around the model. It was therefore believed that the addition of the inlet modification to the model could have been responsible for the difference in the drag, especially in the subsonic Mach number range where it could have affected the scoop-incremental drag. As a result, some calculations were made in an attempt to determine what effect the inlet modification would have on the scoop-incremental drag. The results of these calculations indicated that only approximately one-half of the difference noted in figure 11 could be accounted for by the effect of the inlet modification on the scoop-incremental drag; as a result, the reasons for the remaining disparity in the drag are not obvious.

It can be seen in figure 27 that the minimum drag coefficient of the configuration with the cambered wing was approximately 15 percent

higher than that of the configuration with the symmetrical wing at sub-
sonic speeds and about 6 percent higher at a Mach number of 1.13. The
drag rise for both configurations occurred at approximately Mach number
of 0.95. It is interesting to note the low values of minimum drag coef-
ficients of the configurations with both wing sections measured at Mach
number of 1.00 as compared with the drag coefficients of present-day air-
planes as shown in reference 10, for example. These low values are pri-
marily due to the favorable cross-sectional area distribution of the
model (fig. 6(a)), which was obtained by indenting the fuselage in the
region of the wing in accordance with the transonic area-rule concept
discussed in reference 1.

Attempts were made to reduce further the drag of the original fuse-
lage with both the symmetrical wing and the cambered wing sections by
improving the cross-sectional area distribution of the model as shown in
figure 6(a). At a Mach number of 1.00, body modification 2 reduced the
drag of the configuration with the symmetrical wing about 10 percent
(fig. 28(a)). As was expected, due to an increase in base area, modifi-
cation 3 in combination with modification 2 increased the subsonic drag
level of the configuration with the symmetrical wing 13 percent; but at
a Mach number of 1.00, the drag was intermediate between that of the
configuration with and without modification 2. Modification 2 in combi-
nation with the cambered wing decreased the drag of the basic configu-
ration approximately 7 percent at Mach number 1.00 (fig. 28(b)).

The incremental drag coefficient based on frontal area of the air-
to-air missiles (fig. 29) was abnormally high. It should be remembered,
however, that the model incremental missile drag includes both the strut
drag and the interference drag. The drag of an isolated missile (taken
from ref. 11), which is very similar to the missile of the present tests,
is also included in figure 29 for comparison; the data indicate that the
strut-plus-interference drag is very high. As an example, at a Mach
number of 1.00 the strut-plus-interference drag is approximately 2.5
times the drag of the isolated missile. This high interference drag is
believed to be caused by the location of the missiles in relation to
the cross-sectional area distribution of the complete configuration.
As demonstrated in reference 12, external-store or nacelle configura-
tions having the highest drags were those which had the greatest total
cross-sectional areas resulting in large rates of axial development of
total cross-sectional area. As will be noted in figure 6(b), the peak
area of the air-to-air missiles in the present tests coincided with that
of the basic configuration.

The addition of the forward and aft speed brakes to the basic con-
figuration produced an incremental drag coefficient of about 0.048 at
subsonic speeds, which increased to approximately 0.060 at a Mach number
of 1.13 (fig. 30). Although the aft speed brakes alone caused somewhat

smaller increases in incremental drag coefficients, the brakes would still be very effective as speed reducers.

The drag-due-to-lift parameter $\dfrac{\partial C_D}{\partial C_L{}^2}$ of the configuration with the symmetrical wing section was approximately 30 percent higher than that of the configuration with the cambered wing section at subsonic speeds and was the same for both configurations at Mach numbers of 1.00 and above. (Compare fig. 31(a) with fig. 31(b).) The data also indicated that no leading-edge suction was developed for either wing section at Mach numbers greater than 1.00 because the values differed little from the parameter for no leading-edge suction $\left(\dfrac{1}{57.3C_{L_\alpha}}\right)$. In the trimmed condition, the drag-due-to-lift parameter for the basic configuration was increased only slightly at subsonic speeds and was increased about 26 percent at a Mach number of 1.13 (fig. 31(b)).

A study has been made to compare the drag characteristics for trimmed level flight at an altitude of 35,000 feet for the configurations with the symmetrical and cambered wing sections. The results of this study indicated that the cambered wing section had lower drag than the symmetrical wing section up to a Mach number of about 0.92. For example, at a Mach number of 0.90, the drag of the cambered wing section was approximately $9\frac{1}{2}$ percent lower than that of the symmetrical wing section. The drag characteristics of the symmetrical wing were slightly lower than those of the cambered wing at Mach numbers above 0.93.

It can be seen in figure 32 that the maximum lift-drag ratio for the trimmed condition of the basic configuration dropped abruptly above a Mach number of 0.90. It can also be noted that the lift coefficient for maximum trimmed lift-drag ratio increased from a value of 0.30 at a Mach number of 0.60 to approximately 0.40 at a Mach number of 1.13. The trimmed $(L/D)_{max}$ decreased from a value of 13.7 at $M = 0.60$ to 5.2 at $M = 1.13$ (fig. 33). The values of trimmed lift-drag ratio for level flight at sea level and an altitude of 35,000 feet for a wing loading of 64 pounds per square foot are also shown in figure 33. The advantages to be gained by proper selection of flight altitude are clearly indicated.

The various body modifications on the configuration with symmetrical wing section (fig. 34(a)) or the configuration with cambered wing section (fig. 34(b)) caused small increases in the untrimmed $(L/D)_{max}$ at Mach numbers near 1.00. The higher values of the untrimmed $(L/D)_{max}$ for the cambered wing configuration at subsonic speeds are due to the lower values of the drag due to lift as previously discussed.

Pitching-moment characteristics.- The pitching-moment characteristics for the basic configuration indicated small pitch-up tendencies at lift coefficients about 0.70 in the range of Mach numbers of 0.80 to 0.90 and no instability was indicated for Mach numbers 0.95 to 1.13. (See fig. 12.) The pitch-up tendency for the basic configuration was not due to a loss in effectiveness of the horizontal tail but rather was associated with the characteristics of the wing-fuselage combination since it was shown in figure 12 that the basic model without the horizontal tail had a larger pitch-up tendency at lift coefficients above about 0.65 for Mach numbers from 0.80 to 0.95. Since the pitch-up tendency of the basic configuration occurred over a small lift-coefficient range, this type of pitch-up may not be objectionable on the basis of dynamic-stability considerations.

The chordwise wing fences and the 0.10-chord leading-edge chord-extensions were effective in delaying the pitch-up tendency to higher lift coefficients for Mach numbers up to 0.95; whereas the configuration with the symmetrical wing section lowered the lift coefficient at which the pitch-up tendency occurred for Mach numbers up to 0.95 (figs. 13 and 14).

The effect of closing the inlets on the basic configuration (fig. 18) caused the pitching moments to have greater negative values; however, the pitching-moment characteristics were similar to those for the configuration with inlets open.

An increase in Reynolds number from about 2×10^6 to 5×10^6 made the basic configuration (the horizontal tail on or off) slightly more stable at low lifts and delayed the destabilizing break to slightly higher lift coefficients (figs. 21 and 22). Adding roughness to the nose of the fuselage and to the leading edge of the wings had a negligible effect on the pitching-moment characteristics (fig. 24).

The static-longitudinal-stability parameter $C_{m_{C_L}}$ for the basic configuration with the horizontal tail on and off (fig. 35) indicated large rearward movements of the aerodynamic center at Mach numbers above 0.90. These rearward movements would represent a shift in the aerodynamic-center location of about 26 percent of the mean aerodynamic chord. The values of the static-longitudinal-stability parameter as determined from the tests in the Langley low-turbulence pressure tunnel are also included in figure 35, and the results from the two facilities are in good agreement and indicate a forward movement of the aerodynamic-center location.

Stabilizer effectiveness.- The stabilizer effectiveness of the basic model (fig. 36) increased gradually to a value of -0.024 at a Mach number of 0.95 and then decreased approximately 28 percent through the transonic

speed range. For the maximum stabilizer deflection tested (-10°), the maximum trim lift coefficient was 0.87 at a Mach number of 0.80 and decreased to 0.44 at a Mach number of 1.13 (fig. 12).

Effective downwash characteristics.- There were large differences in the variations in the effective downwash angle with angle of attack for the basic configuration (fig. 37) throughout the Mach number range. The reductions in the variation of effective downwash angle with angle of attack at the high angles noted in figure 37 were the principal cause of the reductions in the pitch-up tendency for the basic model with the horizontal tail compared with the basic model without the horizontal tail (fig. 12).

The downwash derivative $\partial\epsilon/\partial\alpha$ for the basic configuration (fig. 38) increased quite markedly up to a Mach number of 0.95 and then decreased rapidly through the transonic speed range. These changes in the downwash derivative are responsible for the changes with Mach number up to a Mach number of 0.90 in the static-stability parameter $C_{m_{C_L}}$ for the basic model configuration with horizontal tail shown in figure 35.

Lateral Aerodynamic Characteristics

Effective dihedral.- The basic configuration without the horizontal and vertical tails indicated negative effective dihedral (that is, positive $\left(C_{l_\beta}\right)$ at low lift coefficients throughout the Mach number range (figs. 39 and 44(a)). With an increase in lift coefficient, however, the model became laterally stable. The negative effective dihedral at low angles of attack is, of course, due to the negative geometric dihedral, while the positive values at higher angles are due to the positive dihedral effect contributed by the wing sweep. The addition of the horizontal- and vertical-tail surfaces to the basic configuration (figs. 40 and 44(a)) caused the model to have positive effective dihedral with the exception of a region of instability at low lifts and Mach numbers near 1.00 and 1.07 (fig. 45).

Lateral-control characteristics.- The results of deflecting the spoiler for the basic configuration with the horizontal and vertical tails off shown in figure 42 indicated constant effectiveness up to lift coefficients of 0.4 and Mach numbers up to 0.95. The loss in rolling power above lift coefficient of 0.4 was particularly noticeable for the spoiler deflection of 28°. The spoiler effectiveness $C_{l_{\delta_f}}$ increased gradually to a value of -0.00094 at Mach number 0.95 and then decreased about 29 percent at a Mach number of 1.13 (fig. 46). Physical damage to the wing in the vicinity of the spoiler prevented the measurement of the spoiler effectiveness for the basic configuration with the horizontal and vertical tails.

Directional-stability characteristics.- The basic model without the tail surfaces was directionally unstable (figs. 39 and 44(b)) but became stable with the addition of the tail surfaces (figs. 40 and 44(b)). Some nonlinearities existed in the yawing-moment characteristics of the basic configuration which tended to reduce the directional stabililty near zero sideslip especially at an angle of attack of about 6° and at Mach numbers from 1.00 to 1.13 (see fig. 41(b)). In general, at Mach numbers of 0.60 to 0.95, the directional-stability derivative C_{n_β} for the basic model was invariant with angle of attack at least for the angle range shown (fig. 44(b)). A reduction in C_{n_β} with increase in angle of attack is indicated at Mach numbers 0.98 to 1.13; however, more important is the fact that the model retained directional stability throughout the angle-of-attack and speed ranges.

The lateral-force derivative C_{Y_β} for the basic model with and without the tail surfaces was only slightly affected by changes in angle of attack (fig. 44(c)) or by changes in Mach number (fig. 45). The incremental lateral-force derivative of the tail was approximately 0.012 throughout the Mach number range.

Directional-control characteristics.- Deflecting the rudder up to 11.27° indicated positive directional-control characteristics which remained nearly constant throughout the lift coefficient range (fig. 43). The rolling-moment coefficients due to rudder deflection were small and decreased with an increase in lift coefficient (fig. 47).

The rudder effectiveness was high at subsonic Mach numbers. The derivative β_{δ_r} had a value slightly greater than 1.0 for Mach numbers up to 0.90 and then decreased approximately 65 percent through the transonic-speed range. (See fig. 47.) This large decrease in β_{δ_r} was primarily due to the decrease in the derivative $C_{n_{\delta_r}}$ and to a lesser extent to the increase in the derivative C_{n_β}.

SUMMARY OF RESULTS

An aerodynamic investigation of a model which embodied partial body indentation based on a transonic-area-rule concept indicated the following:

1. The minimum drag coefficient of the configuration with cambered-leading-edge wing section was approximately 15 percent higher than that of the configuration with symmetrical wing section at subsonic Mach numbers and about 6 percent higher at a Mach number of 1.13. The drag-due-to-lift parameter at subsonic Mach numbers, however, was 30 percent lower for the configuration with the cambered leading-edge wing section and was the same for both sections at Mach numbers of 1.00 and above.

Investigation of the Effects of Nacelles on the Aerodynamic Characteristics of a Complete Model Configuration. NACA RM L53F22a, 1953.

TABLE I

ORDINATES FOR WINGS WITH SYMMETRICAL AND CAMBERED LEADING EDGES

[Values expressed in percent of symmetrical airfoil
chord and mean line]

	Symmetrical leading edge		Cambered leading edge			
	Root	Tip	Root		Tip	
Chord	Ordinate	Ordinate	Upper ordinate	Lower ordinate	Upper ordinate	Lower ordinate
-2.42	-----	-----	Vertical tangent to L.E. radius		------	-----
-2.00	-----	-----	-0.475	1.510	Vertical tangent to L.E. radius	
-1.88	-----	-----	------	-----		
-1.54	-----	-----	------	-----	-0.550	1.360
-1.25	-----	-----	-.070	1.730	-.395	1.435
-.75	-----	-----	.145	1.815	-.200	1.495
-.50	-----	-----	.245	1.850	-.120	1.510
0	0	0	.415	1.915	.010	1.535
.50	.464	.311	.565	1.975	.130	1.560
.75	.563	.378	.630	2.005	.175	1.570
1.25	.718	.481	.750	2.060	.270	1.590
2.50	.981	.656	.990	2.190	.455	1.640
5.00	1.313	.877	1.330	2.380	.710	1.735
7.50	1.591	1.062	1.595	2.495	.925	1.800
10	1.824	1.216	1.824	2.580	1.095	1.845
15	2.194	1.463	2.194	2.700	1.380	1.880
20	2.474	1.649	2.474	2.805	1.590	1.910
25	2.687	1.790	2.687	2.880	1.760	1.940
30	2.842	1.894	2.842	2.945	1.880	1.965
35	2.945	1.962	2.945	2.985	1.970	1.995
40	2.996	1.996	2.996	2.996	1.996	1.996
45	2.992	1.996	2.992	2.992	1.996	1.996
50	2.925	1.952	2.925	2.925	1.952	1.952
55	2.793	1.867	2.793	2.793	1.867	1.867
60	2.602	1.742	2.602	2.602	1.742	1.742
65	2.364	1.584	2.364	2.364	1.584	1.584
70	2.087	1.400	2.087	2.087	1.400	1.400
75	1.775	1.193	1.775	1.775	1.193	1.193
80	1.437	.966	1.437	1.437	.966	.966
85	1.083	.728	1.083	1.083	.728	.728
90	.727	.490	.727	.727	.490	.490
95	.370	.249	.370	.370	.249	.249
100	.013	.009	.013	.013	.009	.009
L.E. radius	.229	.102	0.250 at chord = -2.17, ordinate = -1.06		0.340 at chord = -1.54, ordinate = -0.99	
T.E. radius	.014	.010	.014		.010	

TABLE II

INDEX OF FIGURES PRESENTING RESULTS OF CONFIGURATIONS TESTED

Figure	Type of plot	Configuration	Remarks
9	C_{D_I} against α	Basic model	
10	$m/\rho_o V_o A_1$ against M	Model with and without horizontal tail and body modification	
11	α, C_D, and C_m against C_L	Basic model less horizontal tail	Effects of mass flow
12	α, C_D, and C_m against C_L	Basic model less horizontal tail; basic model; $i_t = 0°, -5°, -10°$	Effects of stabilizer incidence
13	α, C_D, and C_m against C_L	Model less horizontal tail	Effects of wing modification
14	α, C_D, and C_m against C_L	Complete model	Effects of wing modification
15	α, C_D, and C_m against C_L	Model less horizontal tail with body modification	Effects of body modification
16	α, C_D, and C_m against C_L	Model with and without horizontal tail and body modifications	Effects of body modification
17	α, C_D, and C_m against C_L	Complete model with symmetrical wing and body modifications	Effects of body modification
18	α, C_D, and C_m against C_L	Basic model	Effects of closing inlets
19	α, C_D, and C_m against C_L	Basic model with and without horizontal tail and with and without air-to-air missiles	Effects of air-to-air missiles
20	α, C_D, and C_m against C_L	Basic model with and without horizontal tail and with and without speed brakes	Effects of speed brakes
21	α and C_m against C_L	Basic model less horizontal tail	Effects of Reynolds number and Mach number
22	α and C_m against C_L	Basic model	Effects of Reynolds number

TABLE II - Continued

INDEX OF FIGURES PRESENTING RESULTS OF CONFIGURATIONS TESTED

Figure	Type of plot	Configuration	Remarks
23	α and C_m against C_L	Basic model with and without horizontal tail	Effects of Mach number and Reynolds number
24	α and C_m against C_L	Basic model less horizontal tail	Effects of leading-edge roughness
25	α and C_m against C_L	Basic model less horizontal tail	Effects of closing inlets
26	C_{L_α} against M	Complete model with symmetrical and cambered wings, leading-edge chord-extensions, and wing fences	Summary plots
27	$C_{D_{min}}$ against M	Complete model with symmetrical and cambered wings	Summary plots
28	$C_{D_{min}}$ against M	Complete model with symmetrical and cambered wings with body modifications	Summary plots
29	ΔC_{D_r} against M	Air-to-air missiles	Summary plots
30	ΔC_D against M	Speed brakes	Summary plots
31	$\partial C_D / \partial C_L^2$ against M	Complete model with symmetrical and cambered wings with body modifications	Summary plots
32	Trim L/D against C_L	Basic model	Summary plots
33	Trim $(L/D)_{max}$ against M	Basic model	Summary plots
34	$(L/D)_{max}$ against M for the untrimmed condition	Complete model with symmetrical and cambered wings with body modifications	Summary plots

TABLE II - Concluded

INDEX OF FIGURES PRESENTING RESULTS OF CONFIGURATIONS TESTED

Figure	Type of plot	Configuration	Remarks
35	$C_{m_{C_L}}$ against M	Basic model with and without horizontal tail	Summary plots
36	$C_{m_{i_t}}$ against M	Basic model	Summary plots
37	ϵ against α	Basic model	Summary plots
38	$\partial\epsilon/\partial\alpha$ against M	Basic model	Summary plots
39	α, C_X, C_m, C_l, C_n, and C_Y against C_L	Basic model less vertical and horizontal tails	Effects of sideslip angle
40	α, C_X, C_m, C_l, C_n, and C_Y against C_L	Basic model	Effects of sideslip angle
41	C_L, C_X, C_m, C_l, C_n, and C_Y against β	Basic model with and without vertical and horizontal tails	
42	α, C_X, C_m, C_l, C_n, and C_Y against C_L	Basic model less vertical and horizontal tails; $\delta_f = 0°$; $5.70°$; $27.93°$	Effects of spoiler deflection
43	α, C_X, C_m, C_l, C_n, and C_Y against C_L	Basic model; $\delta_r = 0°$; $5.65°$; $11.27°$	Effects of rudder deflection
44	C_{l_β}, C_{n_β}, and C_{Y_β} against α	Basic model with and without vertical and horizontal tails	Summary plots
45	C_{l_β}, C_{n_β}, and C_{Y_β} against M	Basic model with and without vertical and horizontal tails	Summary plots
46	$C_{l_{\delta_f}}$ against M	Basic model with vertical and horizontal tails off	Summary plots
47	$C_{l_{\delta_r}}$, $C_{n_{\delta_r}}$, $C_{Y_{\delta_r}}$, and β_{δ_r} against M	Basic model	Summary plots

View A-A
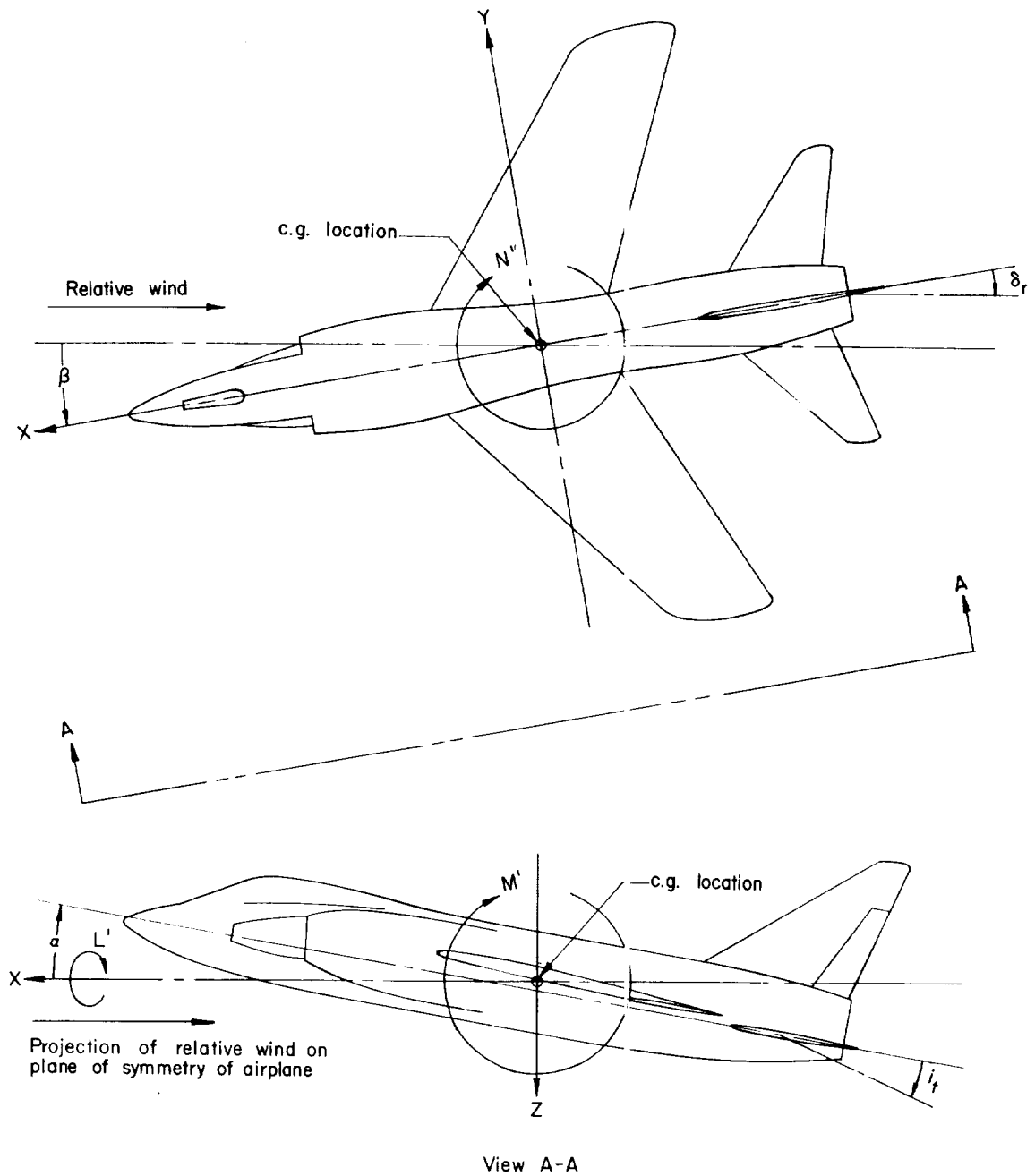
Figure 1.- System of axes and control-surface deflections. Positive
values of forces, moments, and angles are indicated by arrows.

L-476
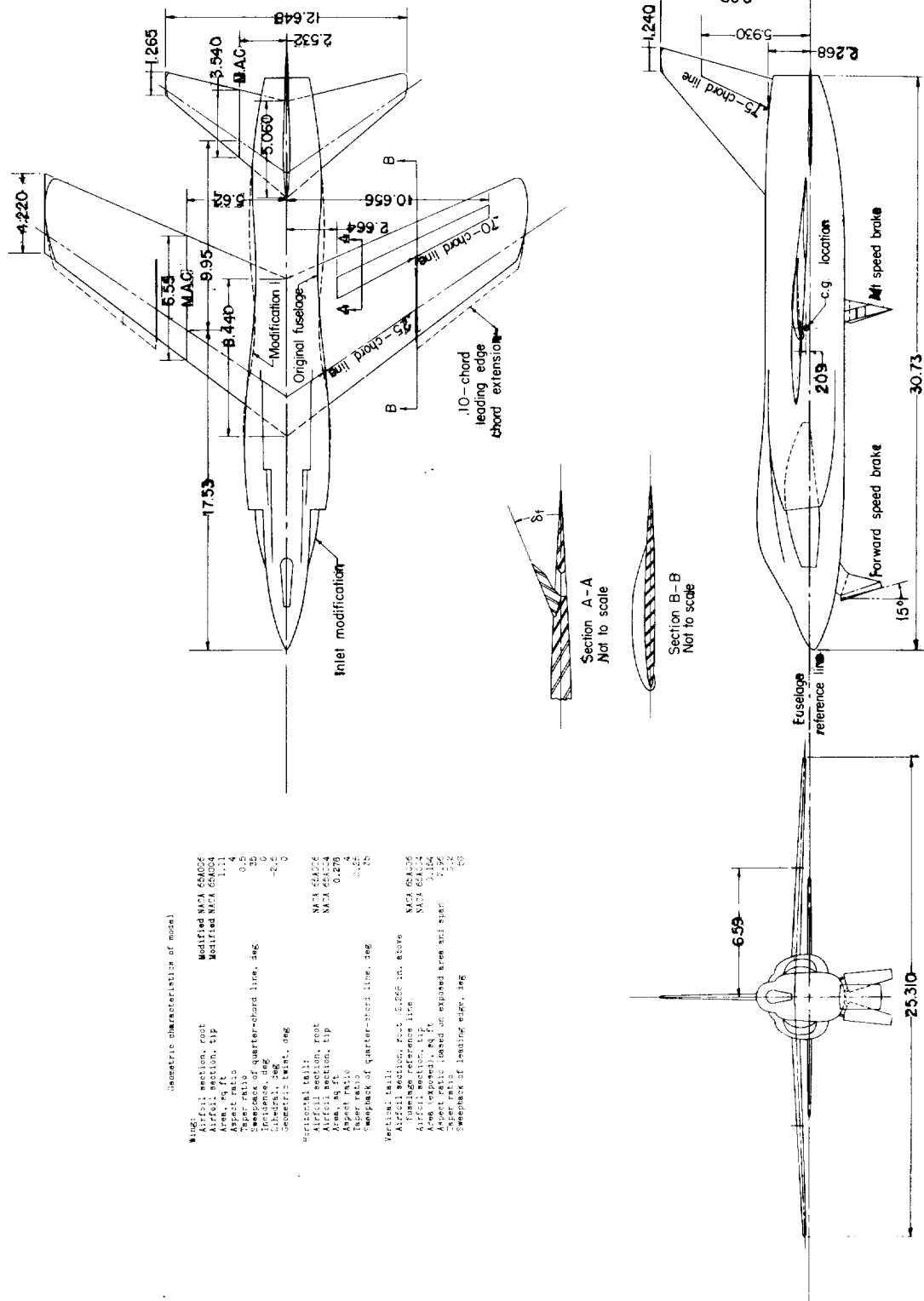
Figure 2.- A three-view drawing of the model investigated. All dimensions are in inches except as noted.

Figure 3.- View of model on sting support.

L-81850.1

L-476
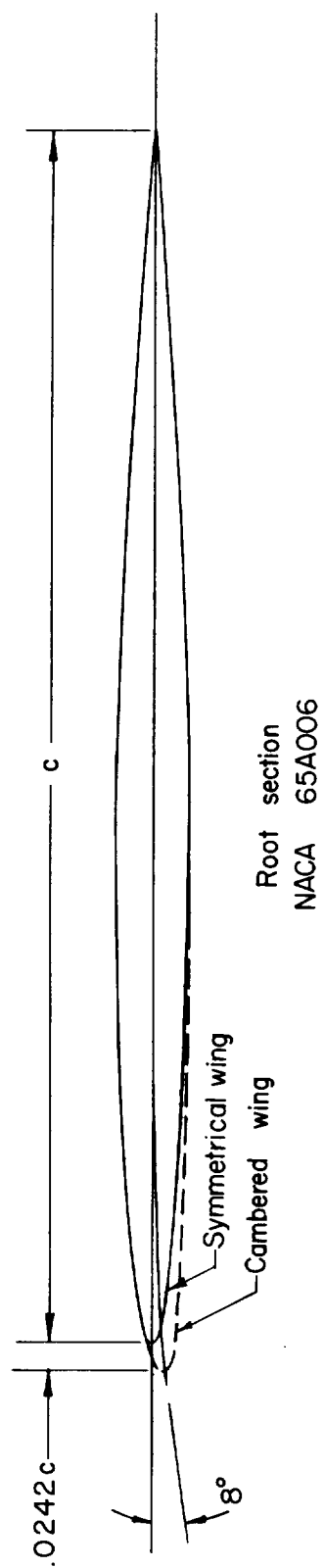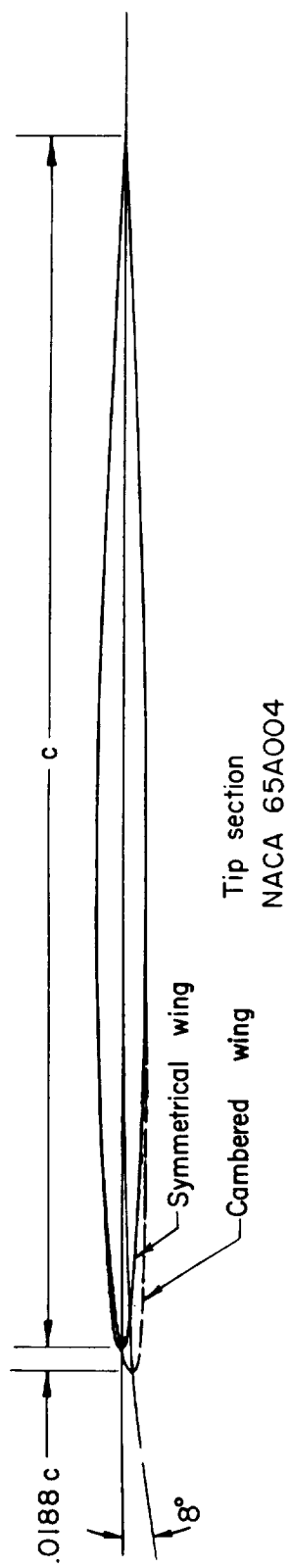
Figure 4.- Comparison of the wings with symmetrical and cambered leading edges.

Fuselage reference line

Section B-B

Modification 3

B

B

Fuselage reference line

Section A-A

A

A
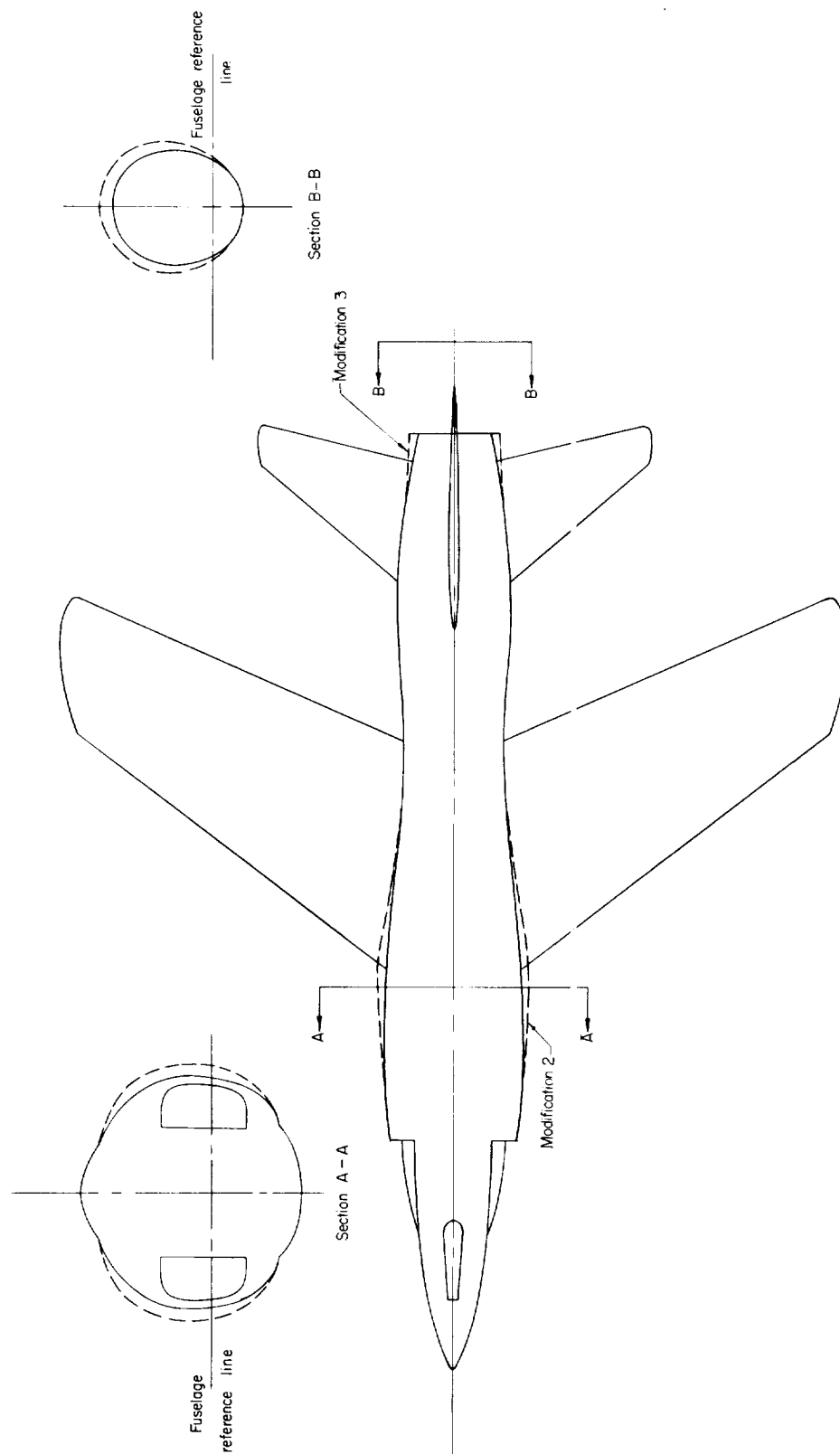
Modification 2

Figure 5.- Details of modifications made on original fuselage.
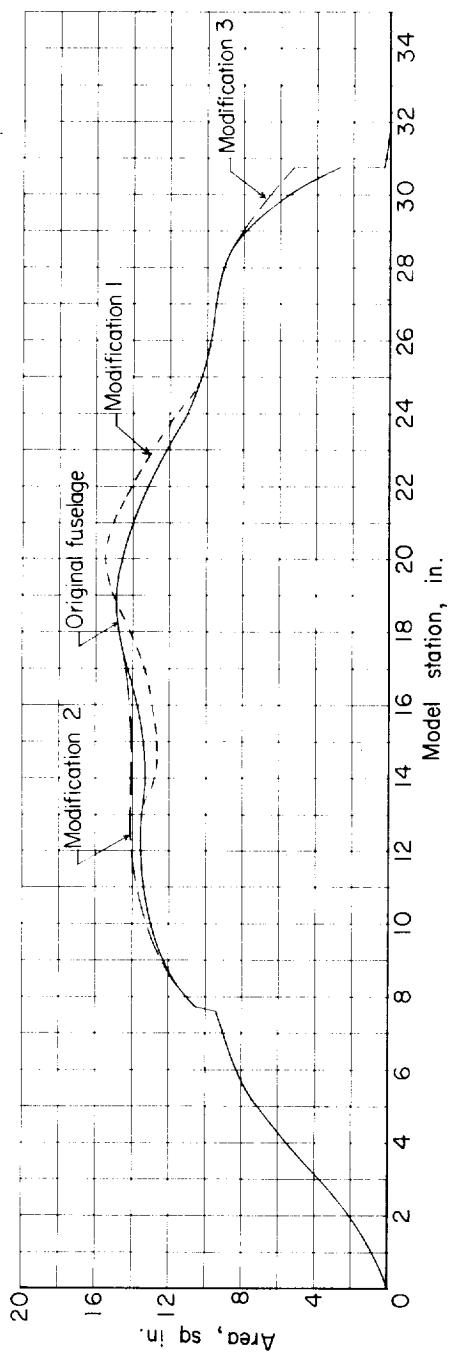
(a) Four fuselage configurations.
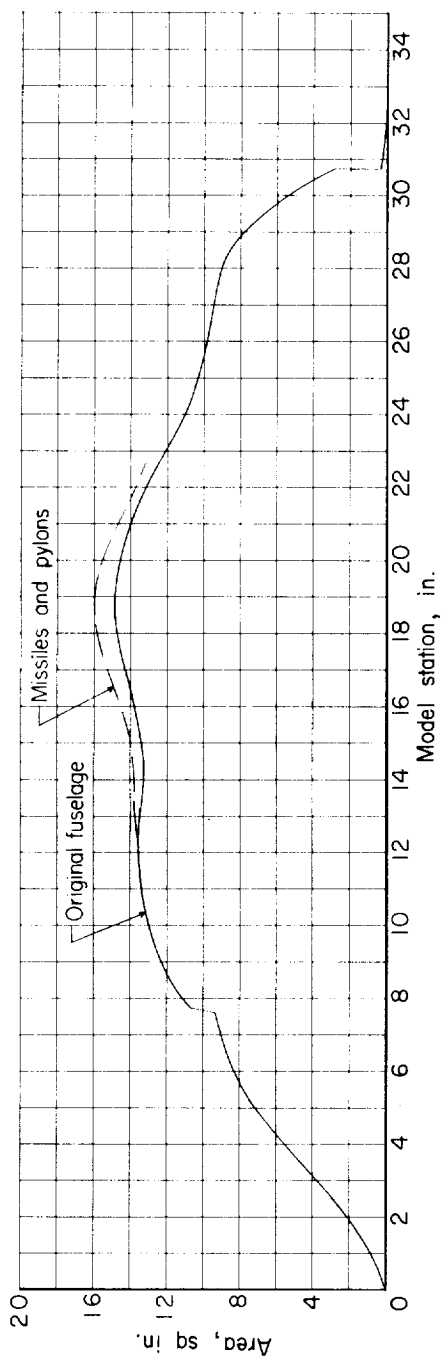
(b) Original fuselage with air-to-air missiles.

Figure 6.- Axial distribution of cross-sectional area of various configurations.

Model ₵

Pylon section

.234

7.33

1.60

2°

.07

.85

.59

4.50

8.52

1.66

11.02

.54 diam.
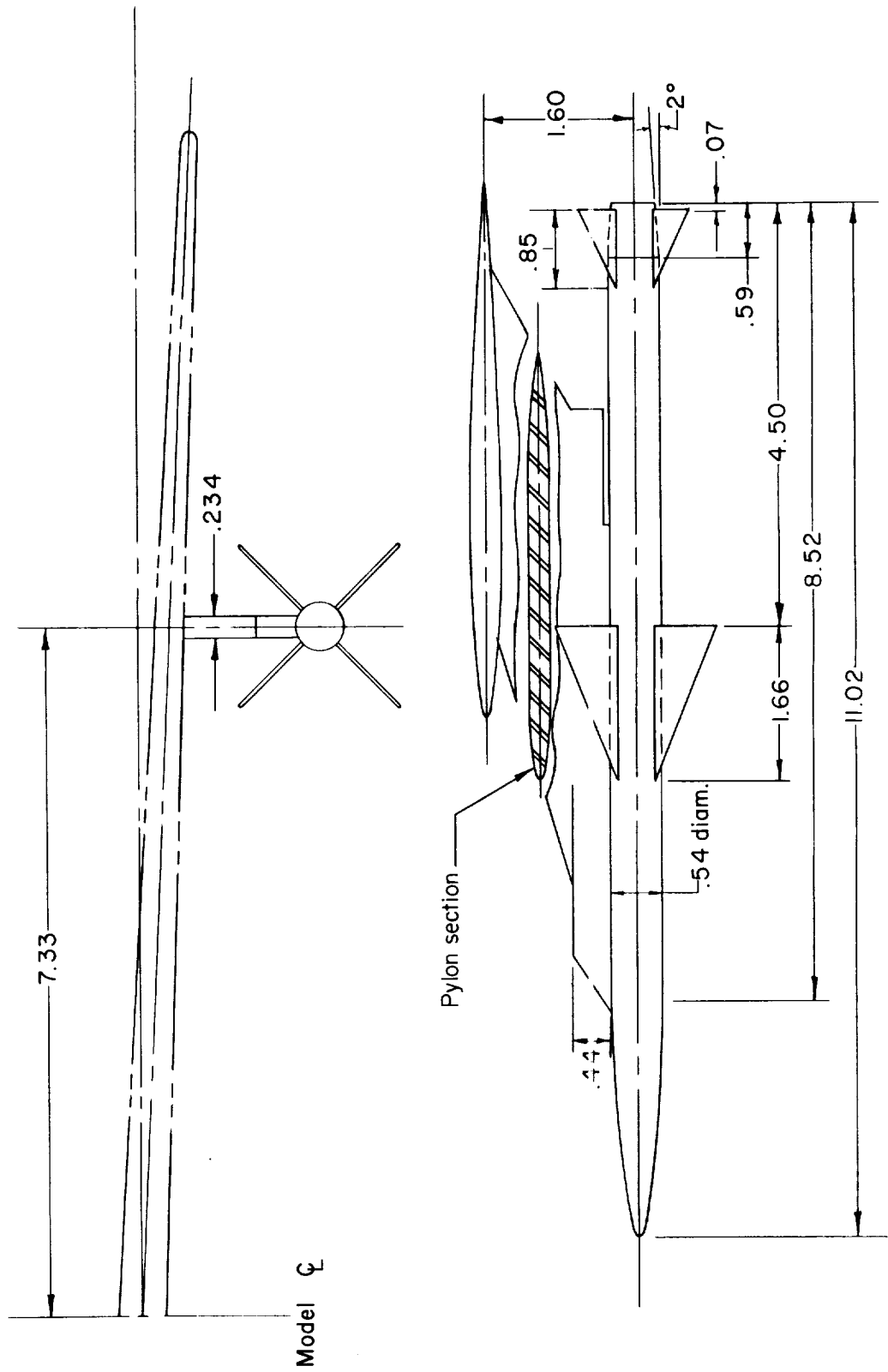
Figure 7.- Details of air-to-air missiles. All dimensions are in inches unless otherwise noted.
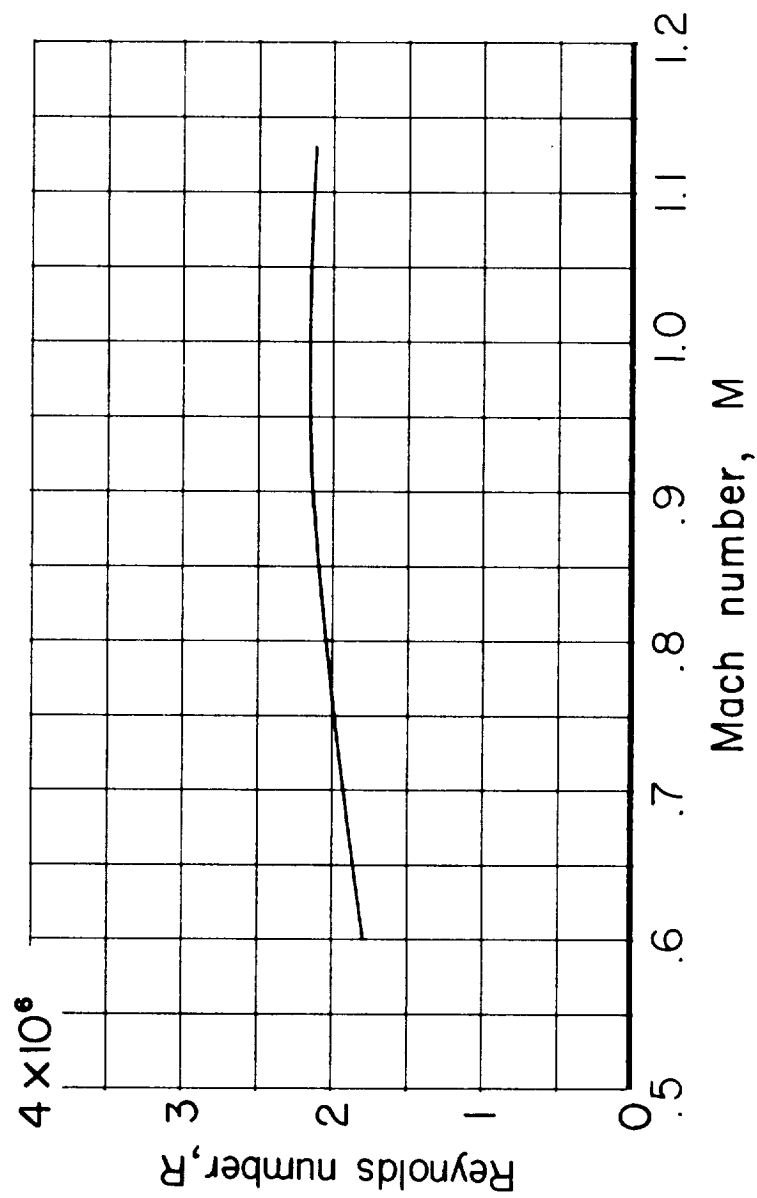
Figure 8.- Variation with Mach number of test Reynolds number based on wing mean aerodynamic chord.
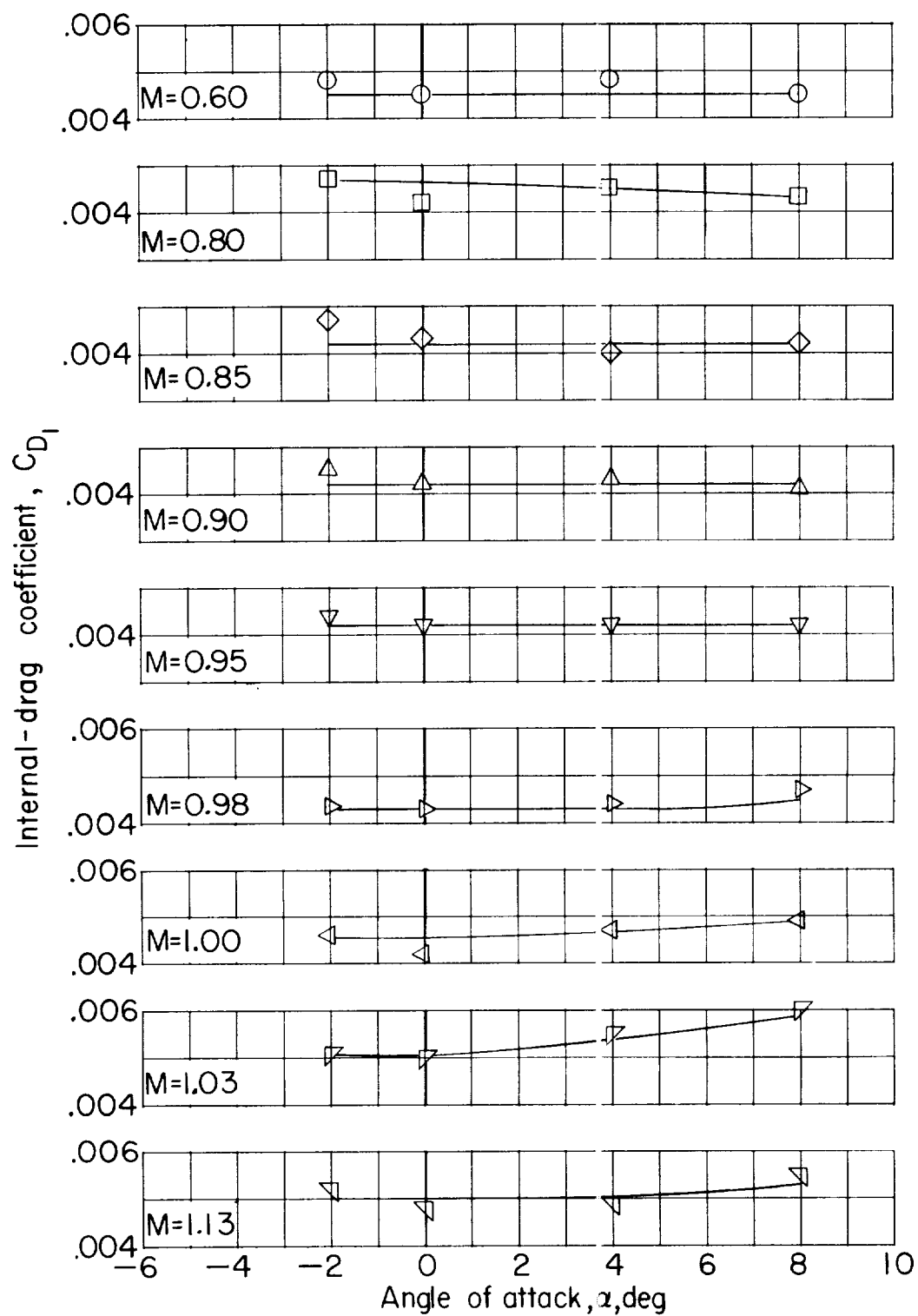
Figure 9.- Variation with angle of attack of the internal-drag coefficient for basic configuration. A_{inlet}/A_{design} = 0.546.
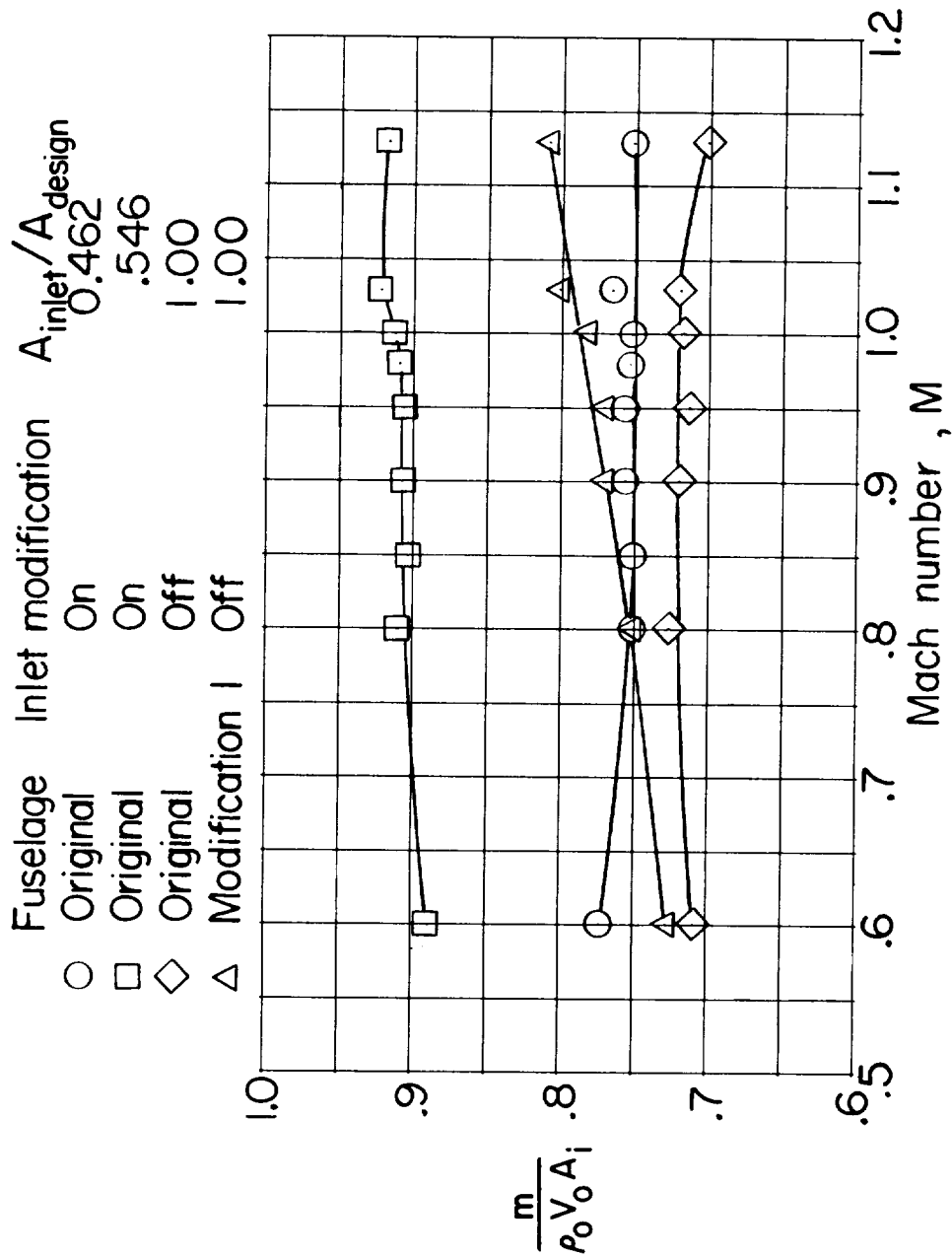
Figure 10.- Variation with Mach number of the mass-flow ratio for various configurations.
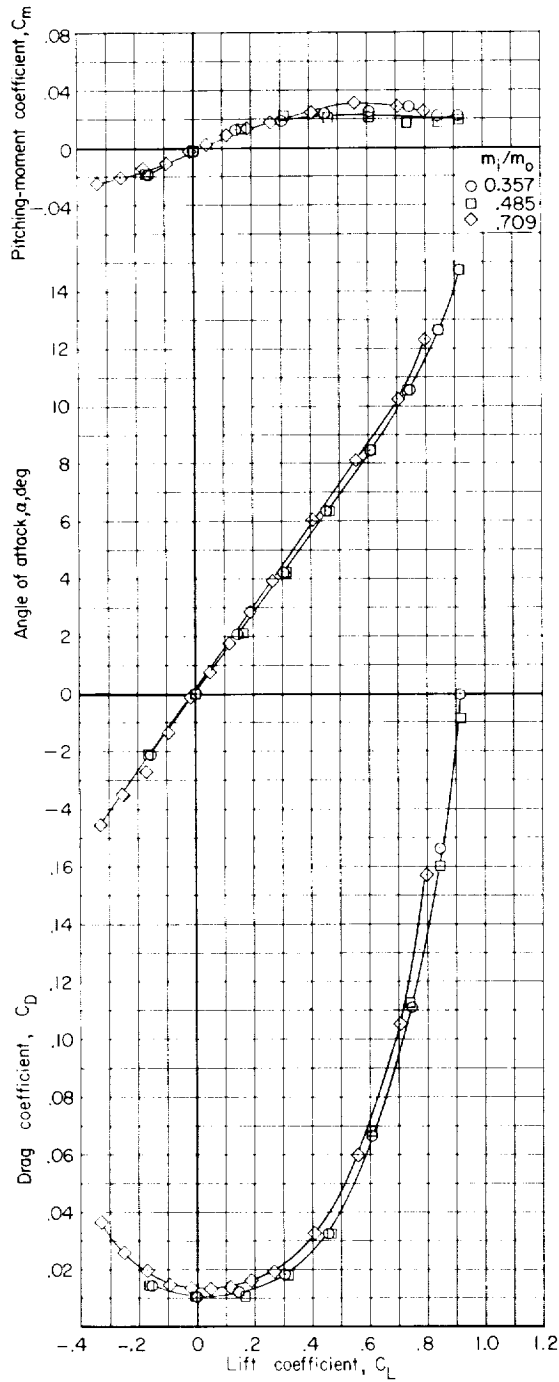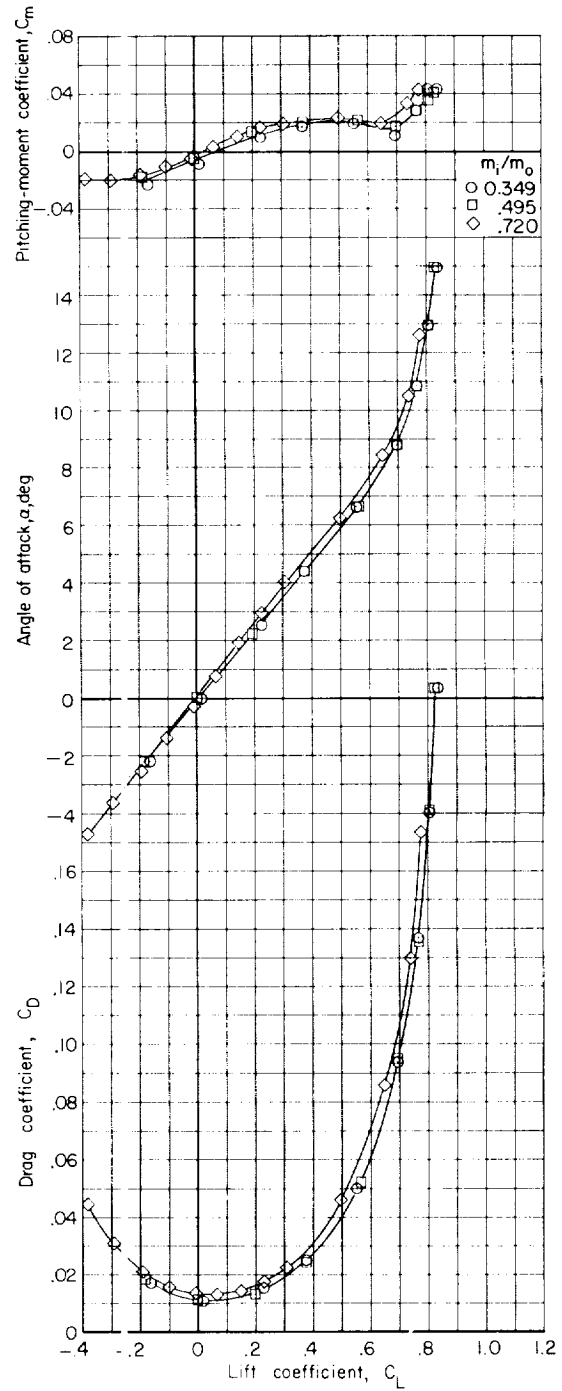
(a) M = 0.60.   (b) M = 0.80.

Figure 11.- Effects of mass-flow ratio on the aerodynamic characteristics
in pitch of the basic model. Horizontal tail off.
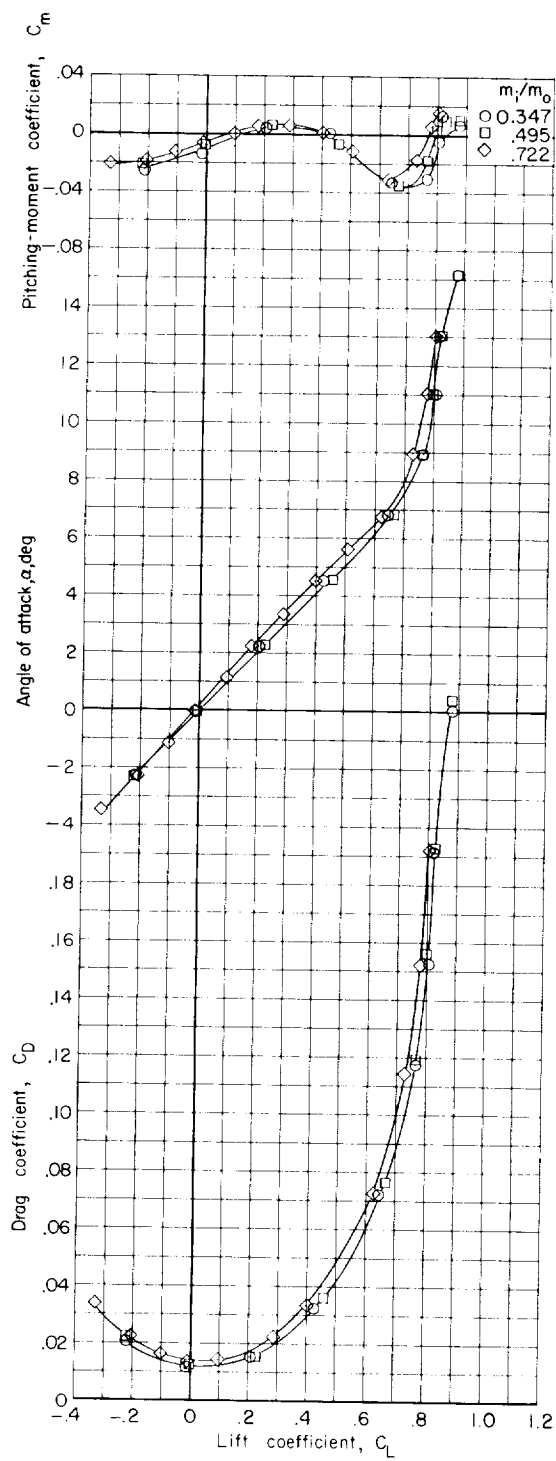
(c) M = 0.90.
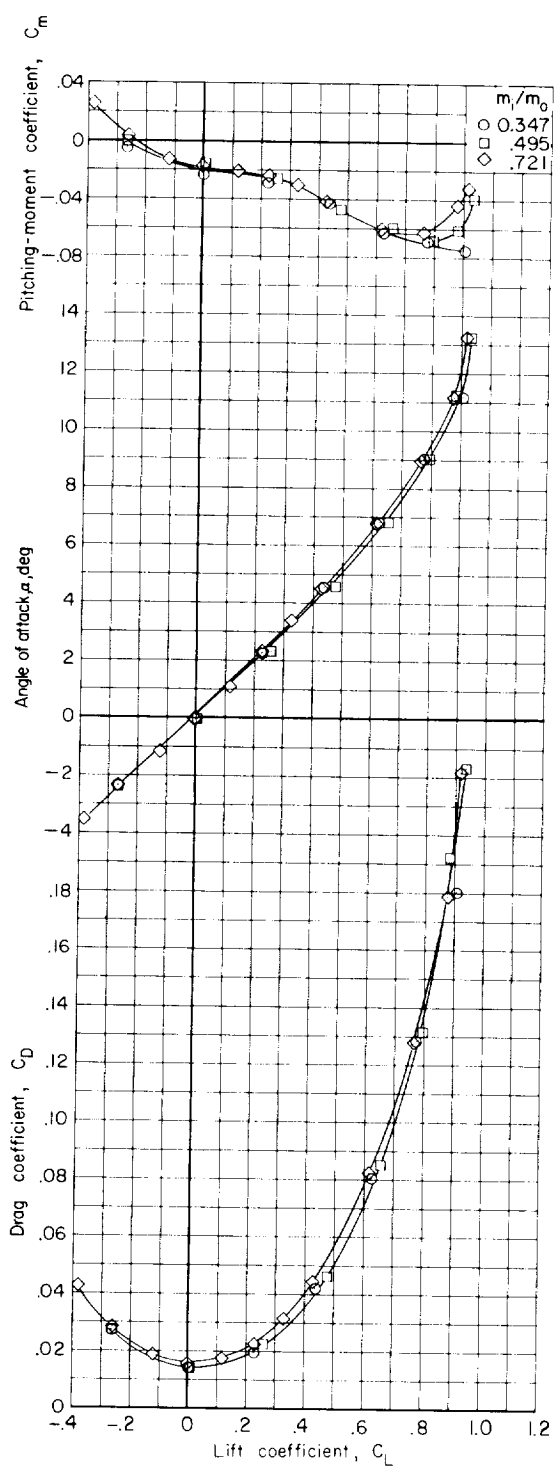
(d) M = 0.95.

Figure 11.- Continued.
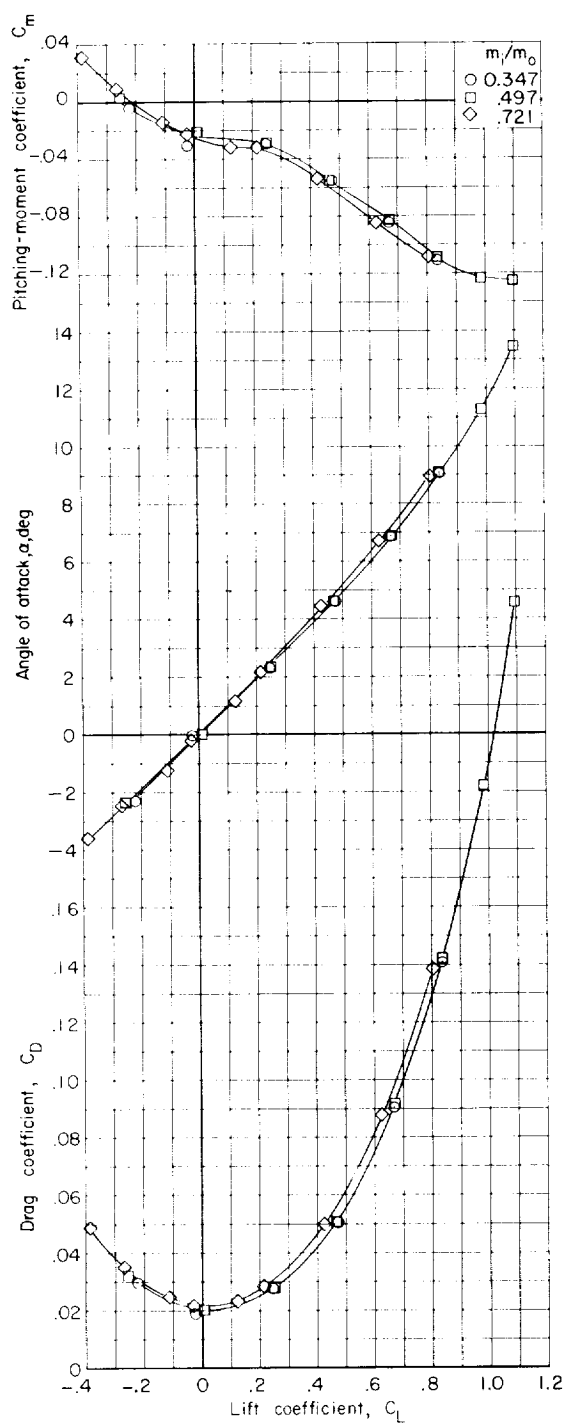
(e) M = 0.98.
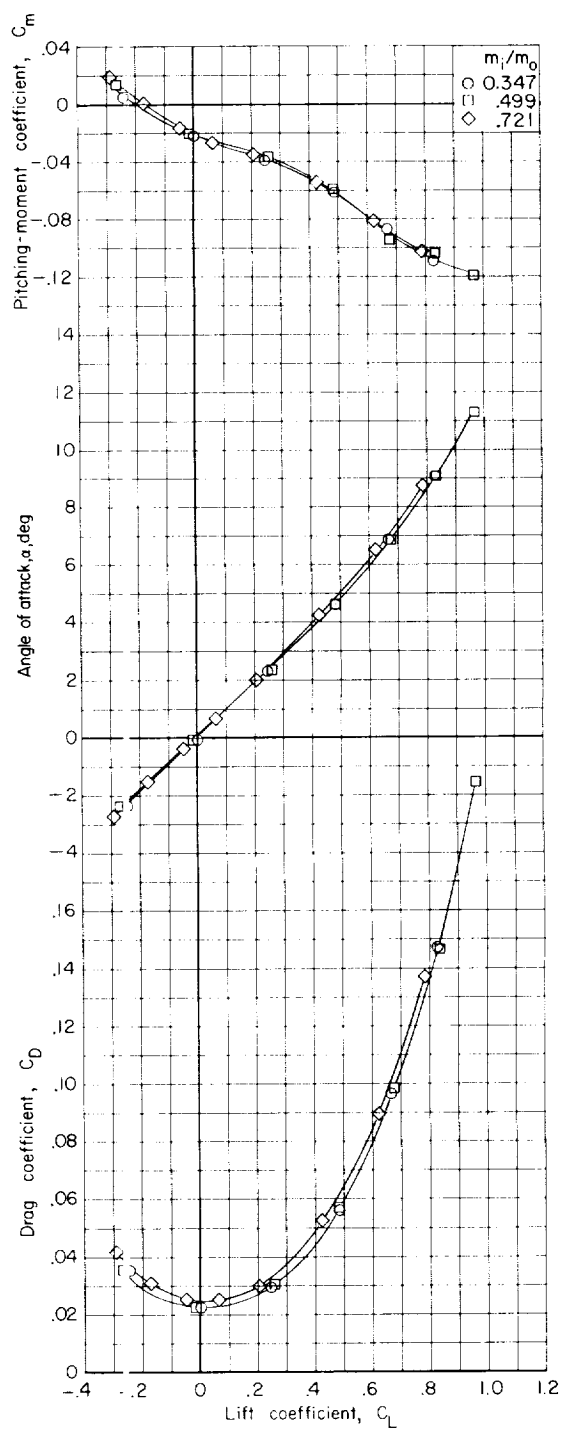
(f) M = 1.00.

Figure 11.- Continued.
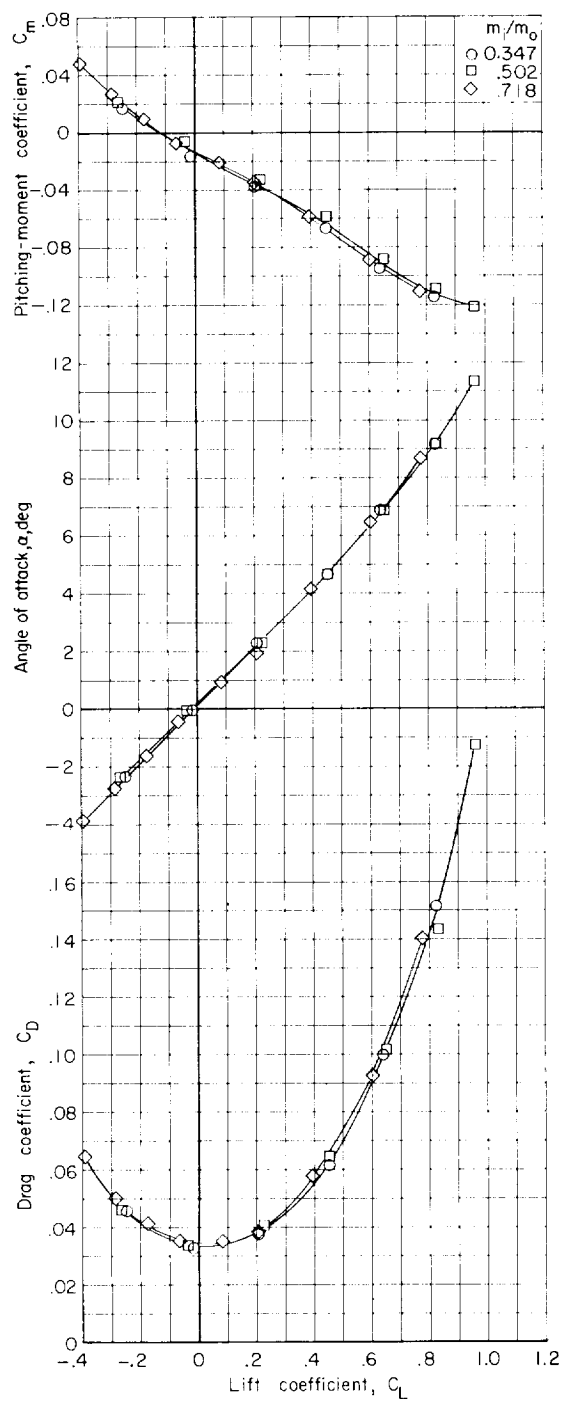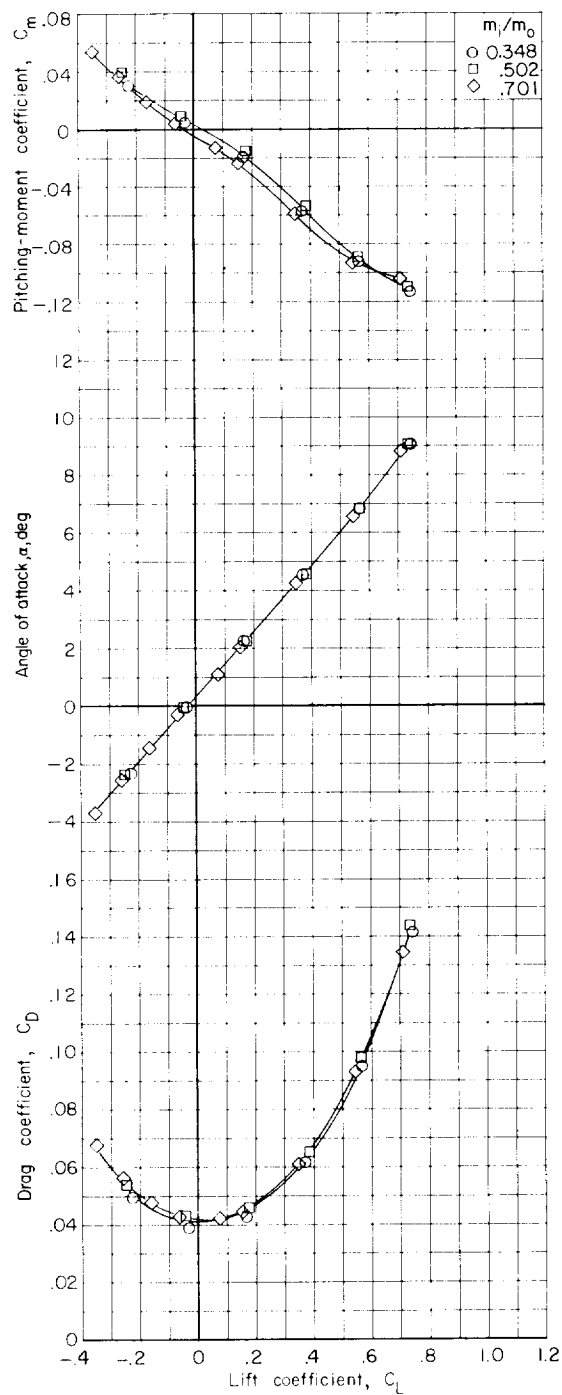
(g) M = 1.03.   (h) M = 1.13.

Figure 11.- Concluded.

38
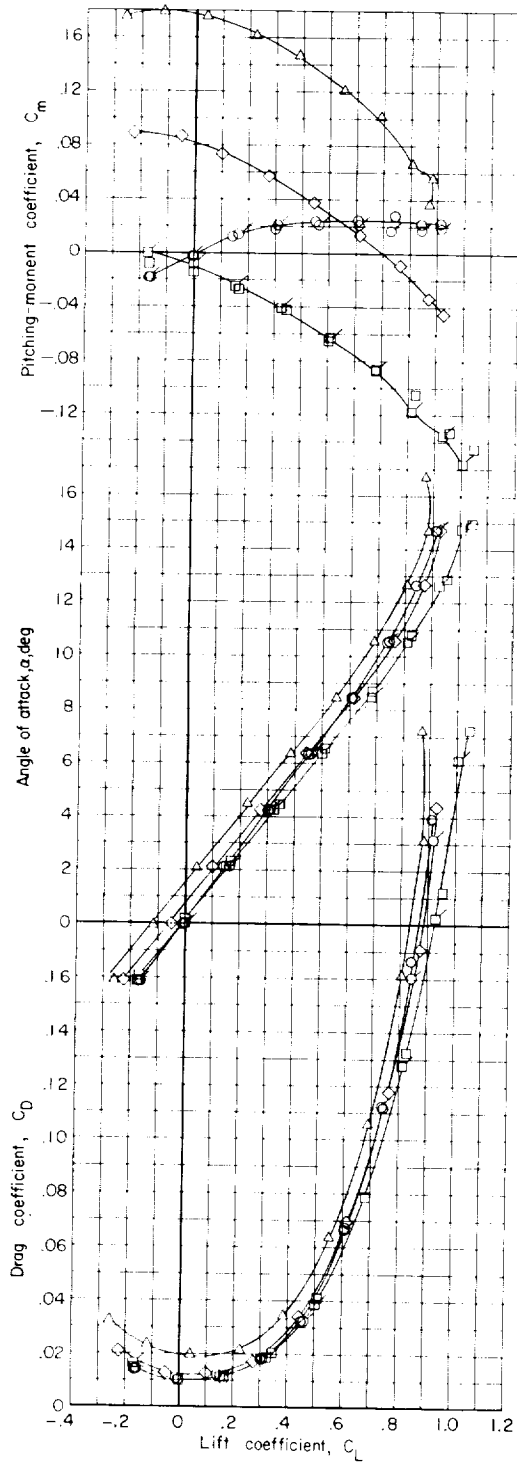
(a) M = 0.60.
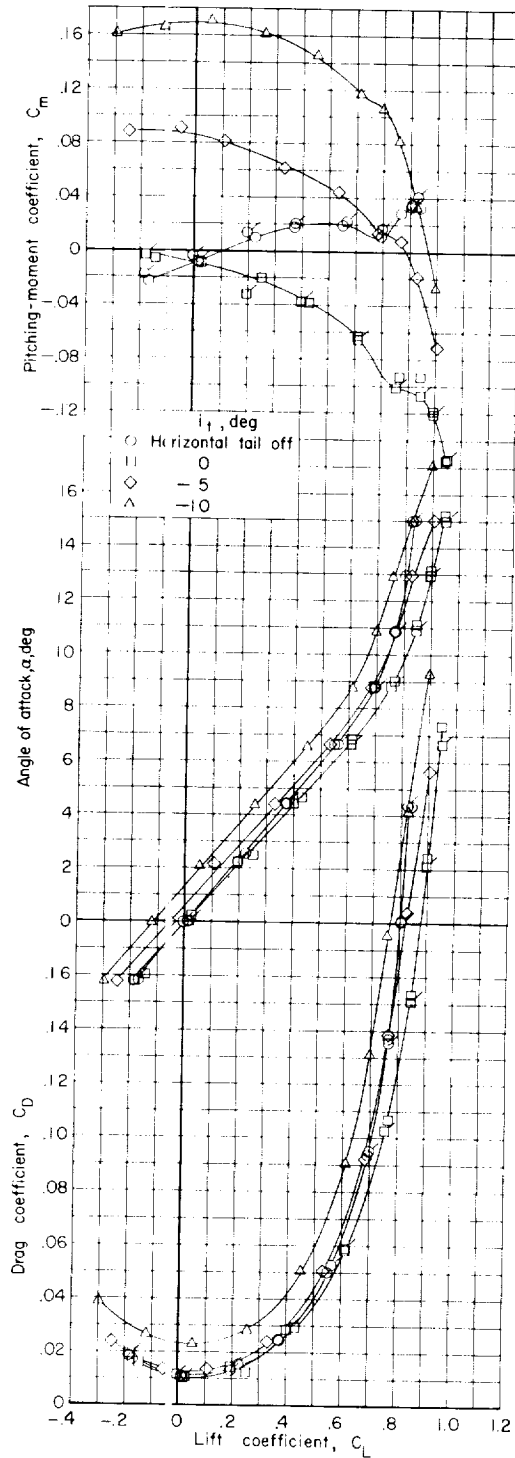
(b) M = 0.80.

Figure 12.- Effects of stabilizer incidence on the aerodynamic character-
istics in pitch of the basic model. Repeat runs shown by flagged symbols.
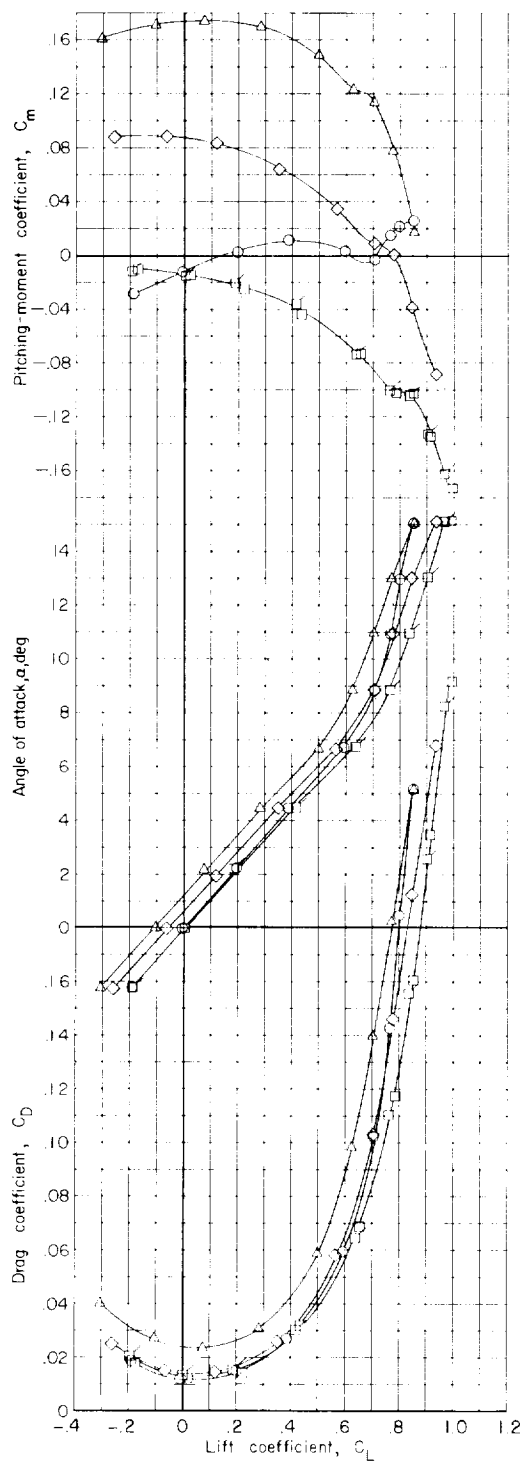
(c) M = 0.85.
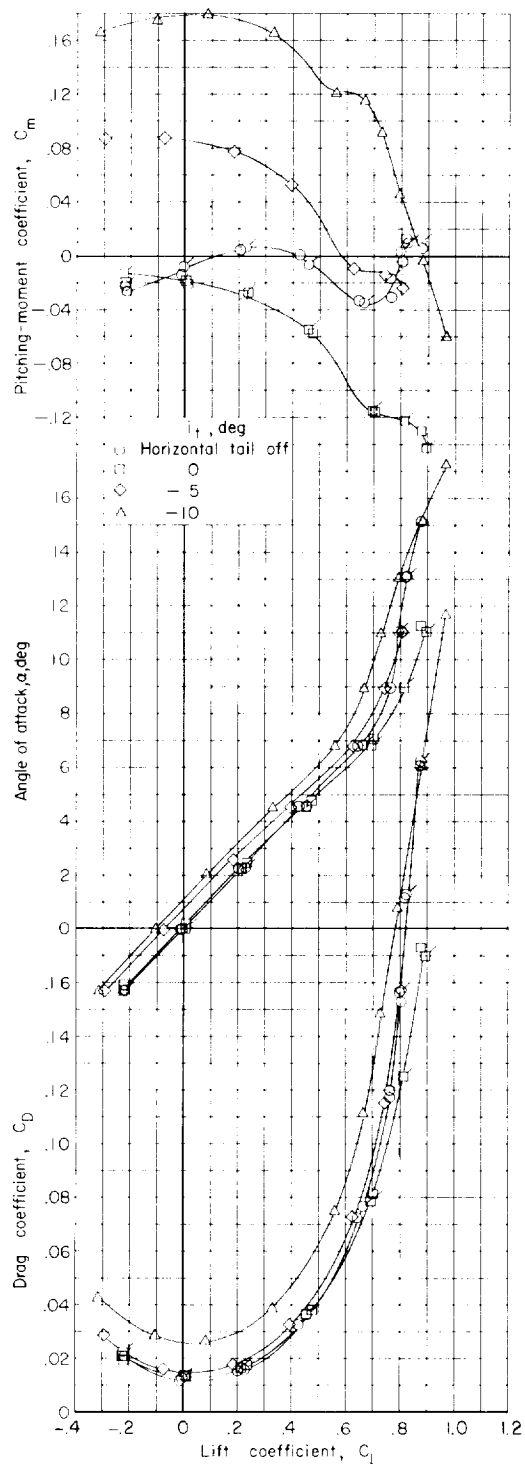
(d) M = 0.90.

Figure 12.- Continued.
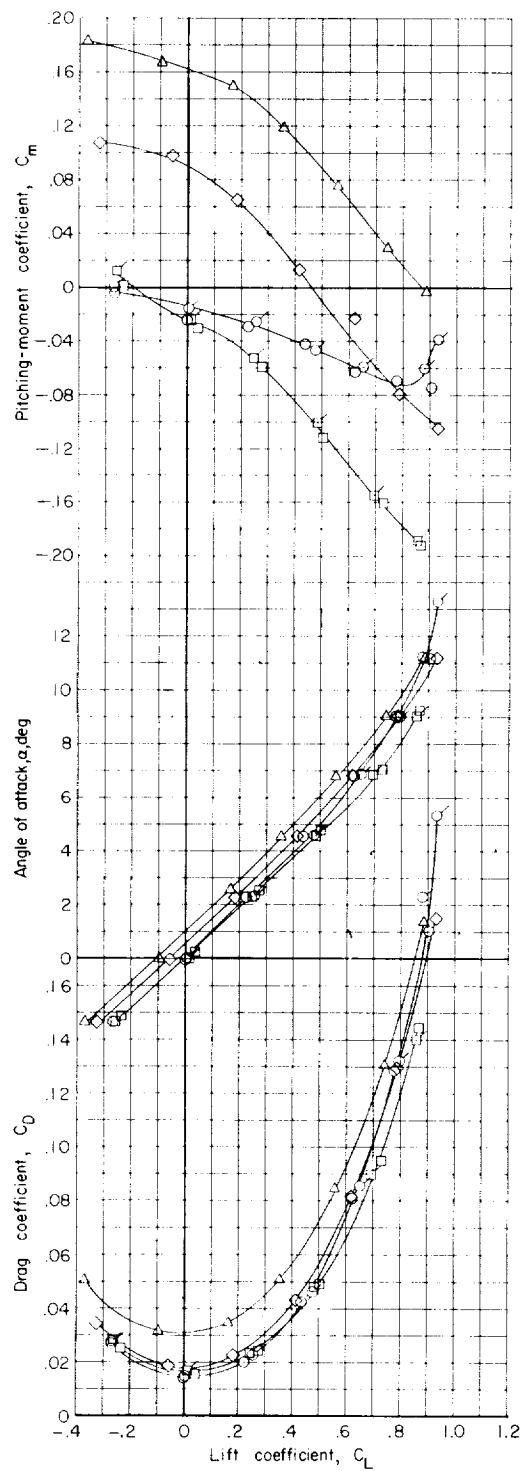
(e) M = 0.95.
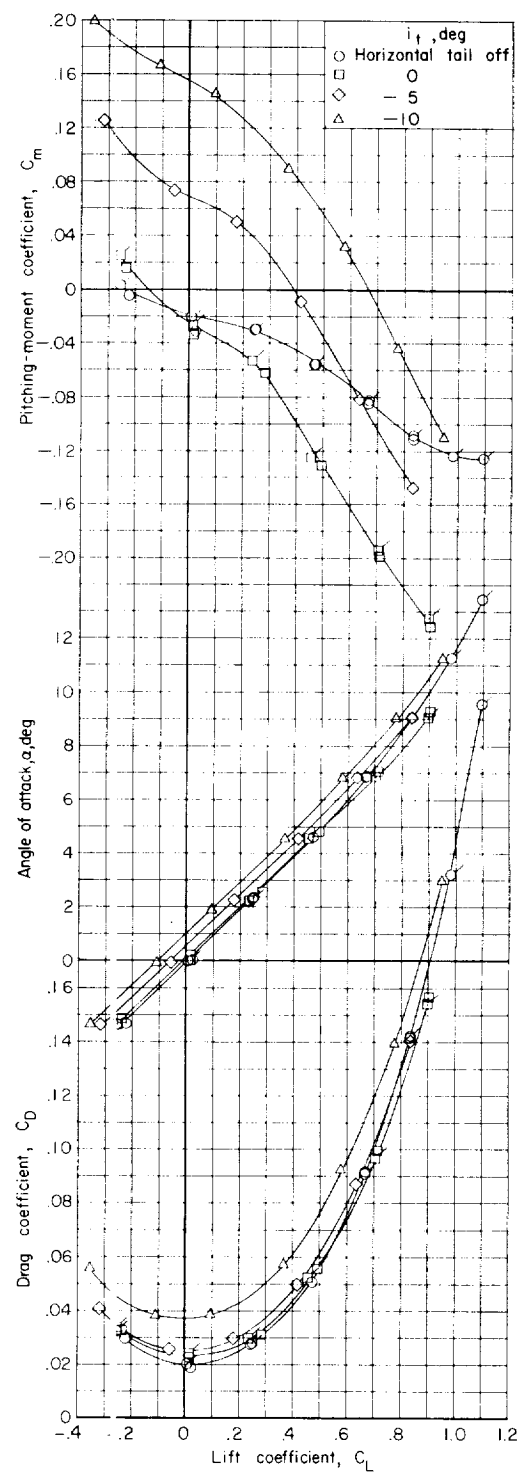
(f) M = 0.98.

Figure 12.- Continued.

L-476
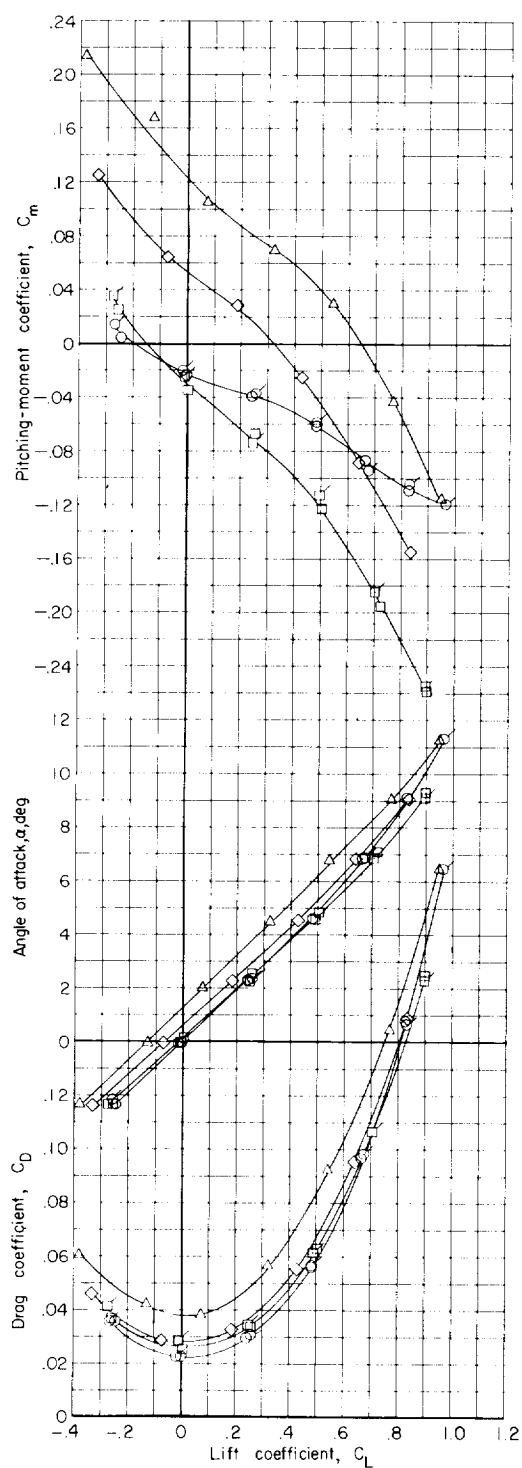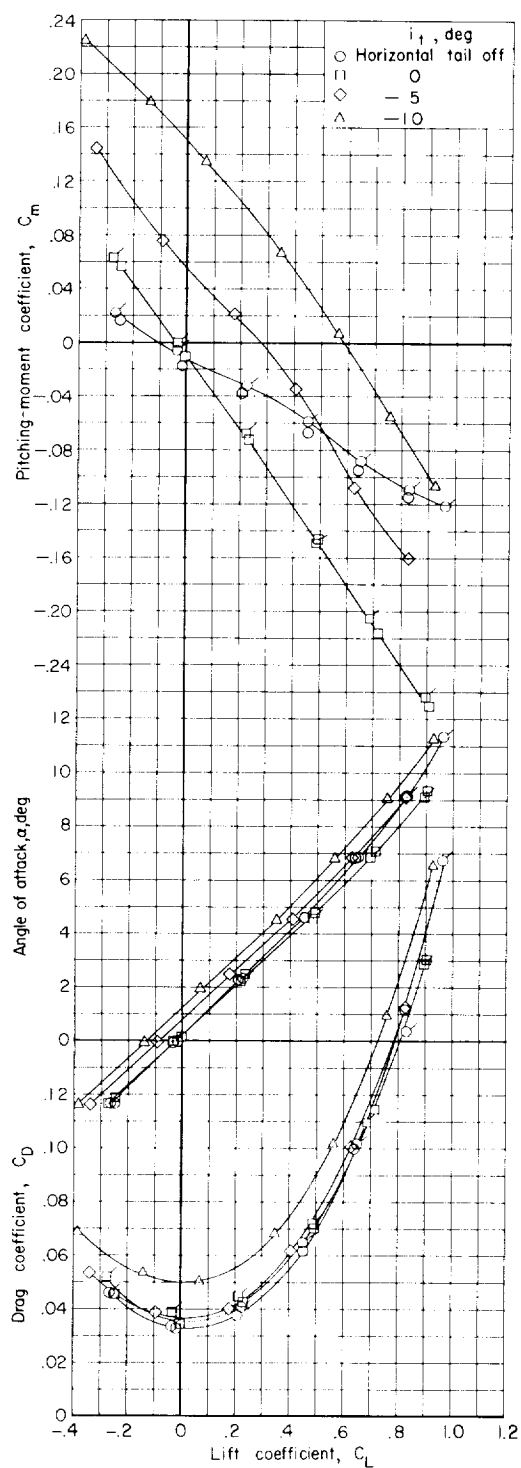
(g) M = 1.00.   (h) M = 1.03.

Figure 12.- Continued.
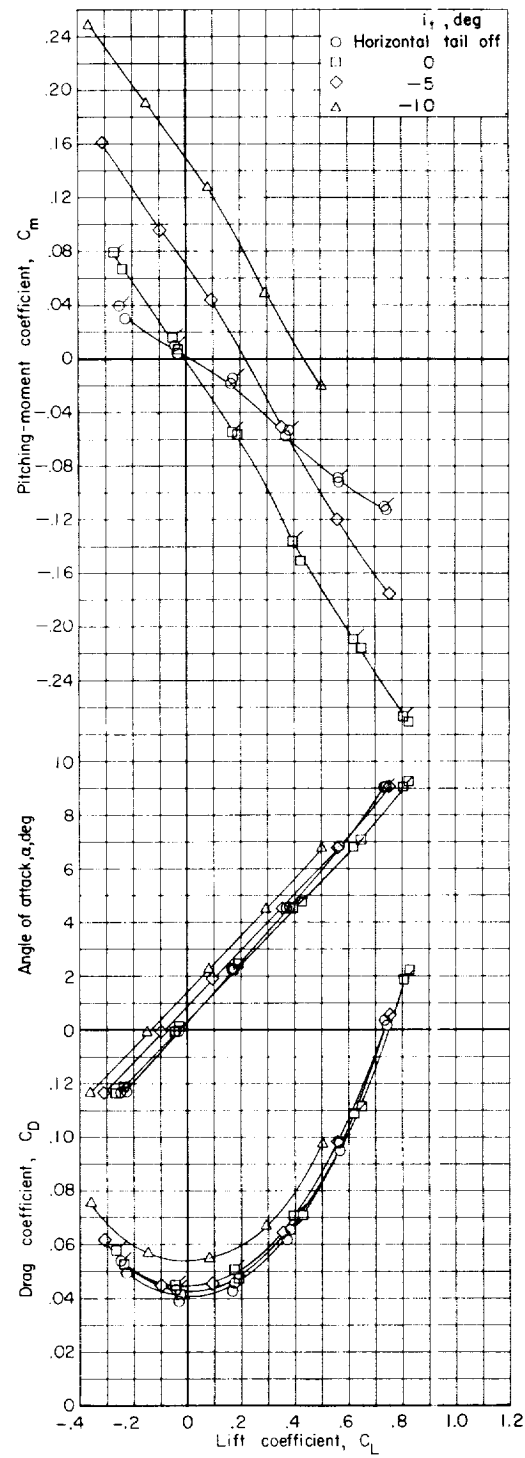
(i) M = 1.13.

Figure 12.- Concluded.
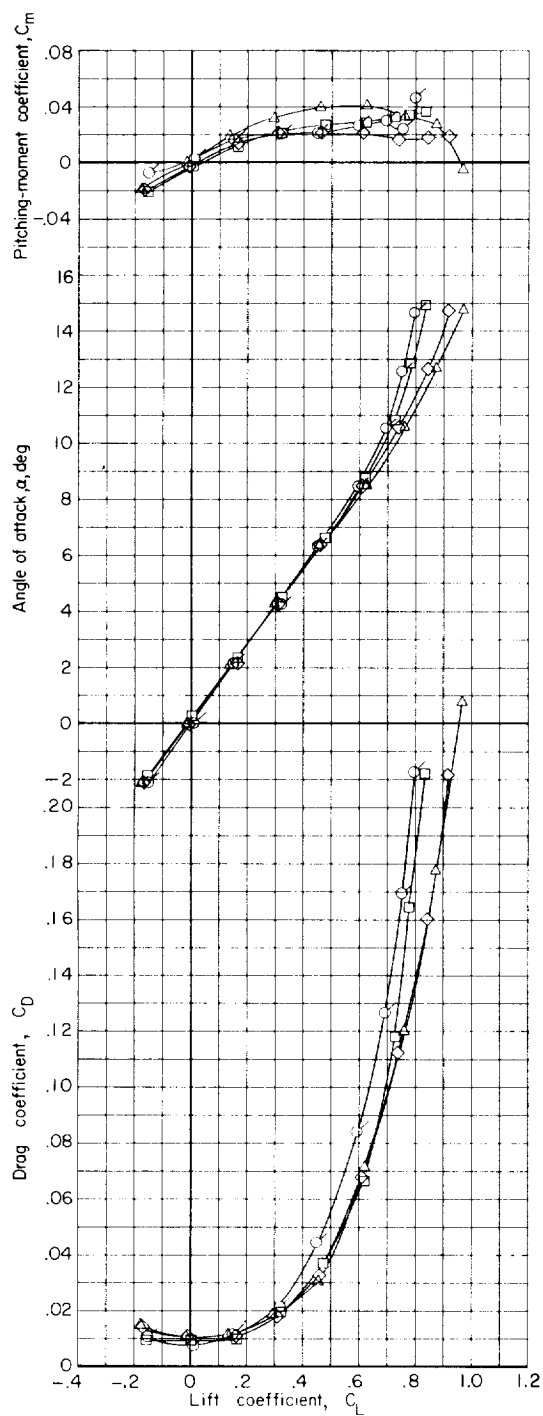
(a) M = 0.60.
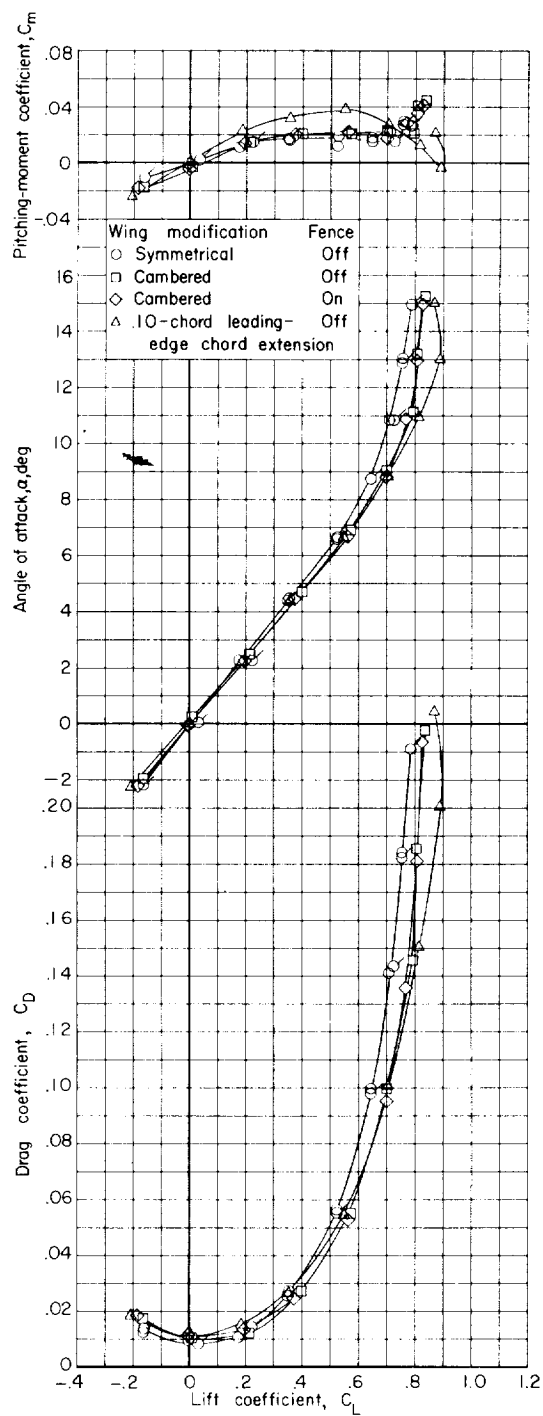
(b) M = 0.80.

Figure 13.- Effects of various wing modifications on the aerodynamic characteristics in pitch of the model. Horizontal tail off. Repeat runs shown by flagged symbols.
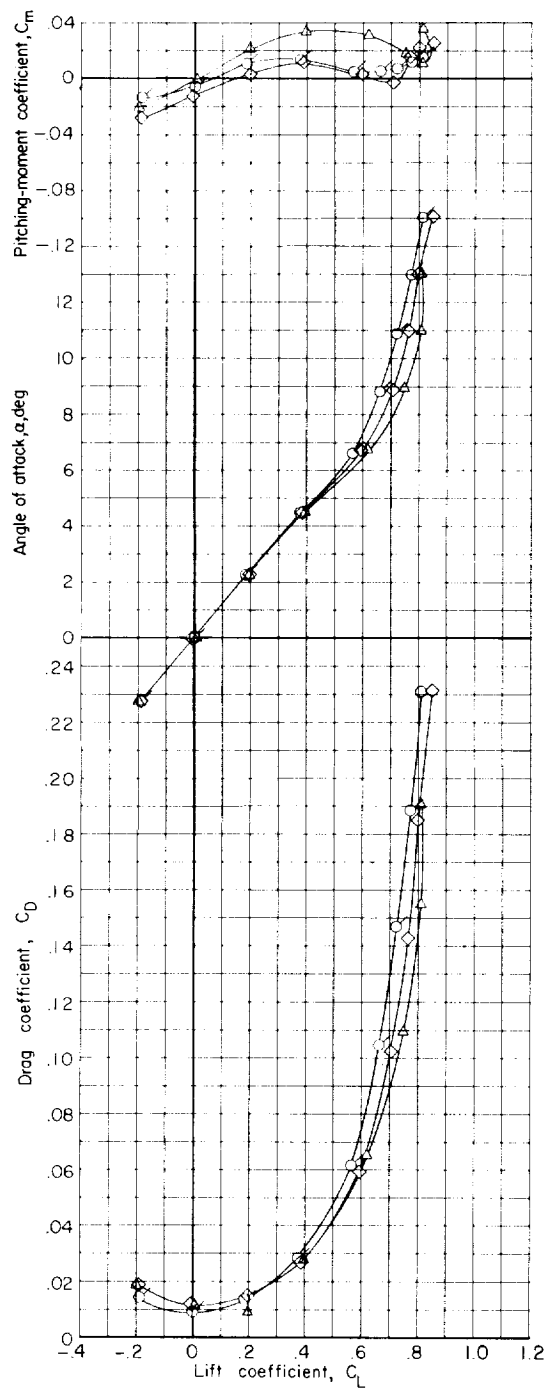
(c) M = 0.85.

(d) M = 0.90.

Figure 13.- Continued.

Wing modification | Fence
○ Symmetrical | Off
◻ Cambered | Off
◇ Cambered | On
△ .10-chord leading- | Off
    edge chord extension
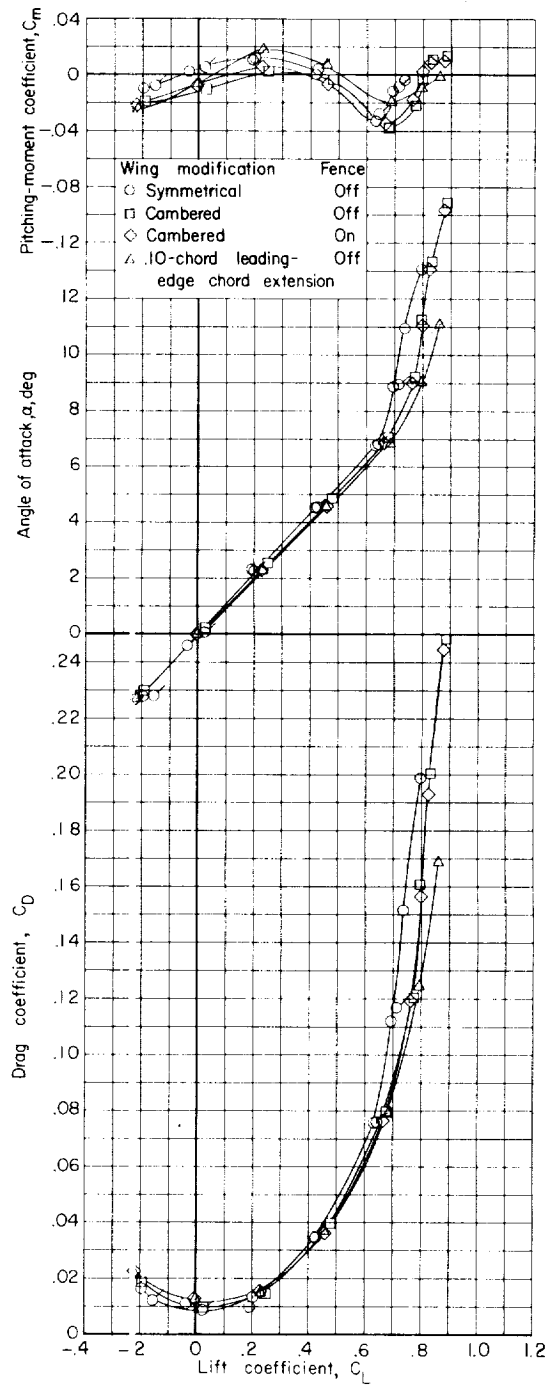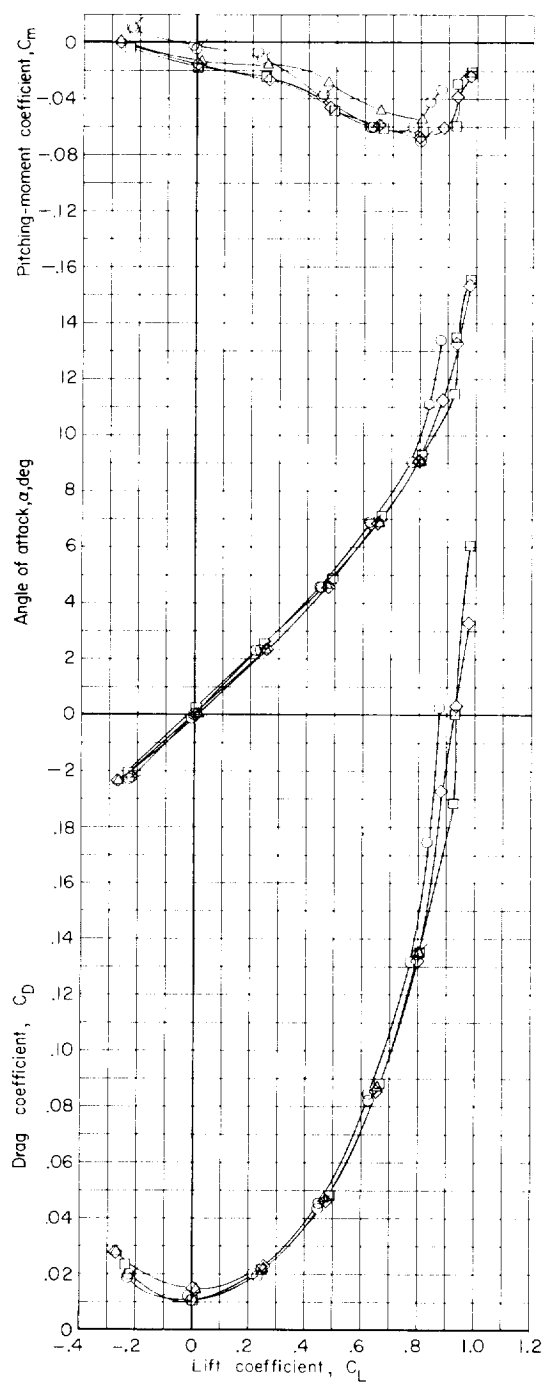
(e) M = 0.95.
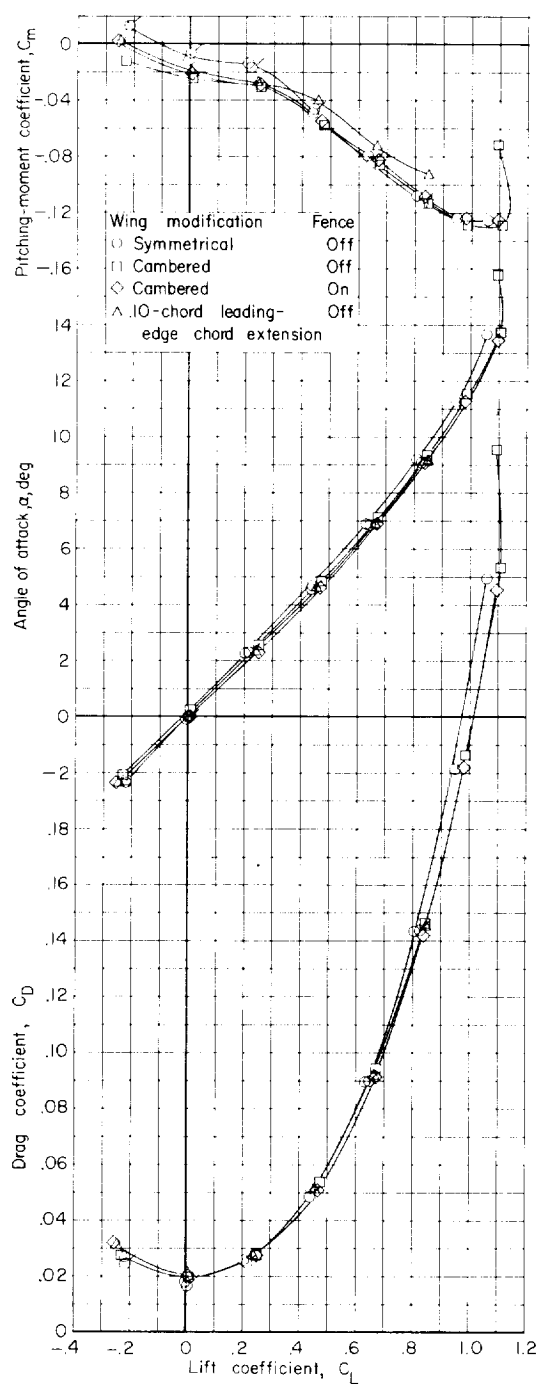
(f) M = 0.98.

Figure 13.- Continued.
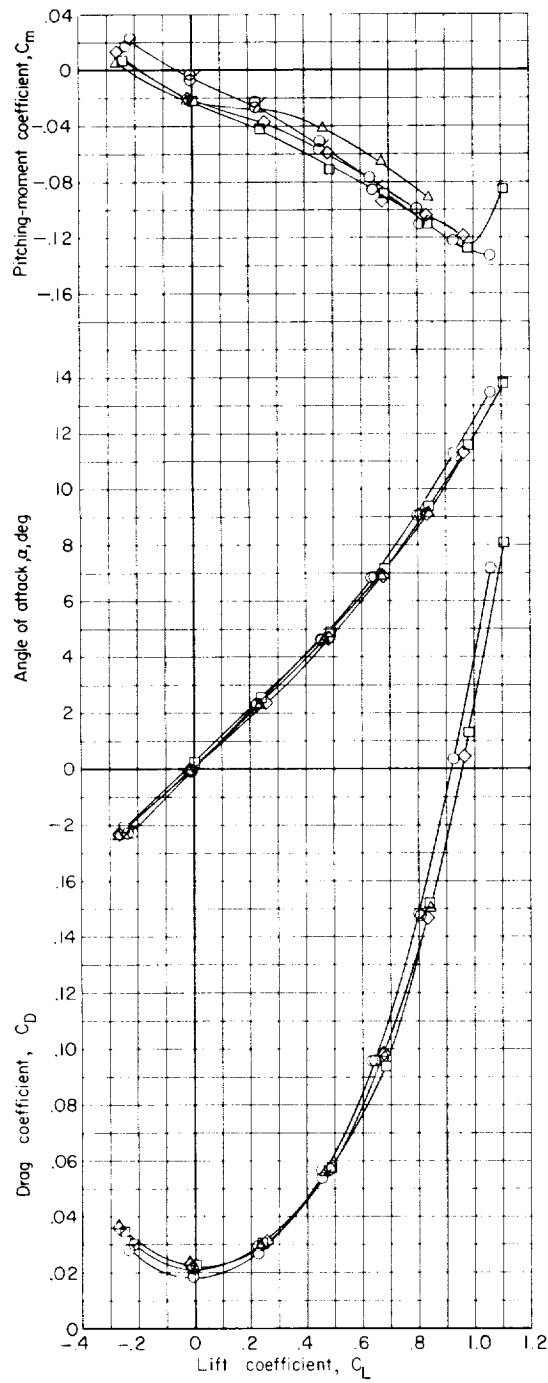
(g) M = 1.00.
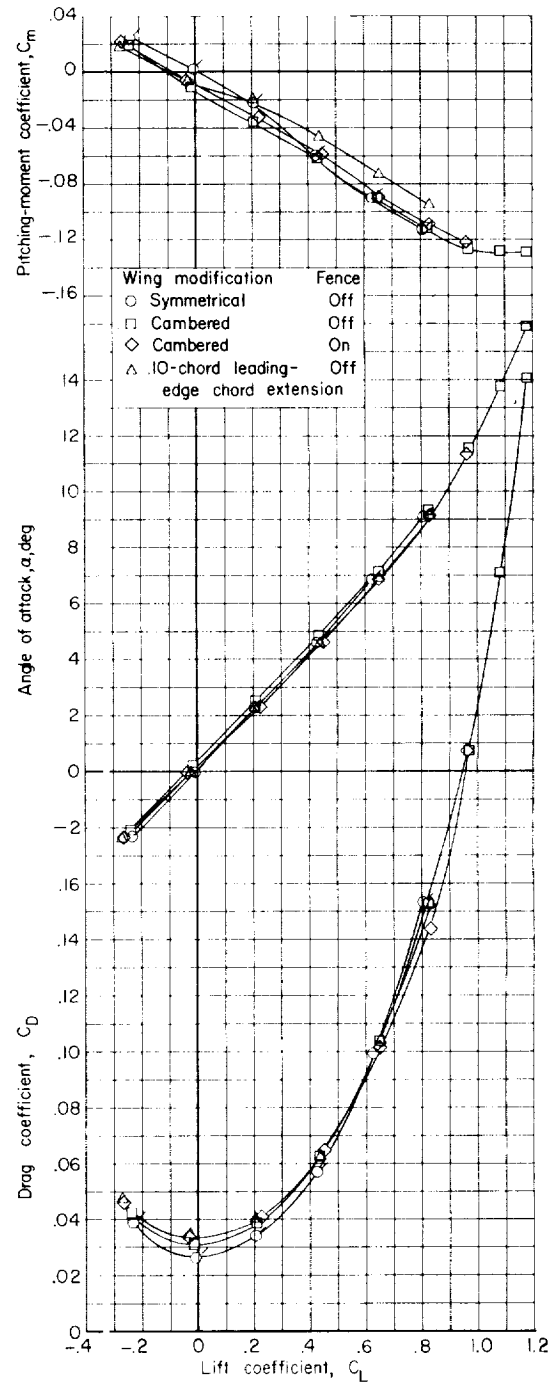
(h) M = 1.03.

Figure 13.- Continued.
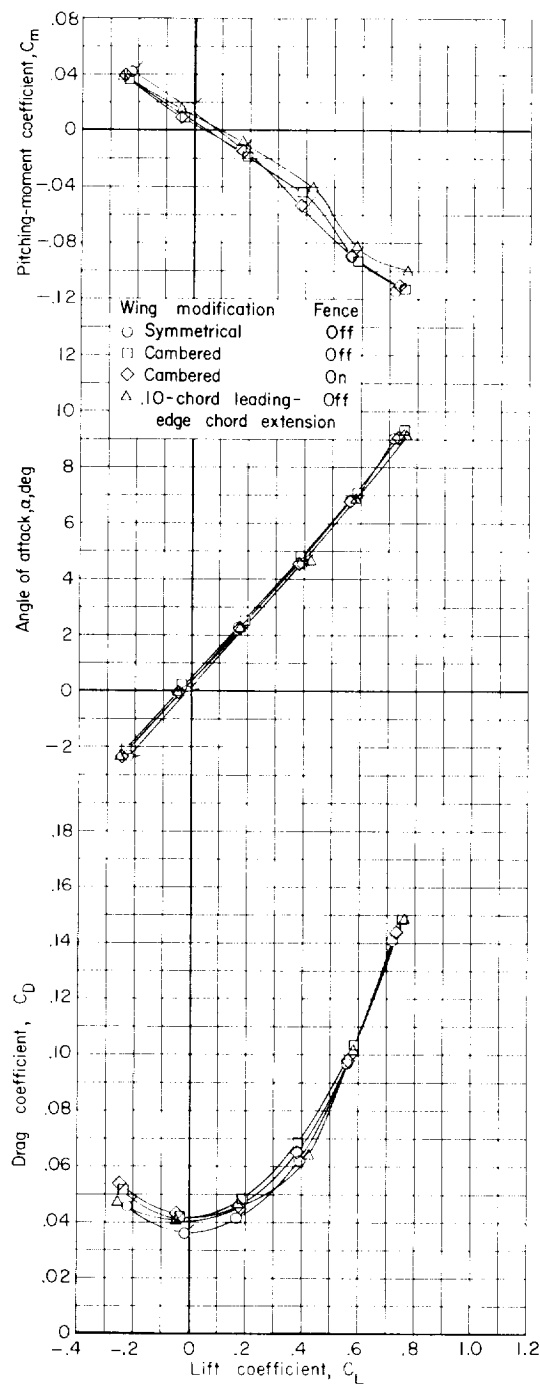
(i) M = 1.13.

Figure 13.- Concluded.
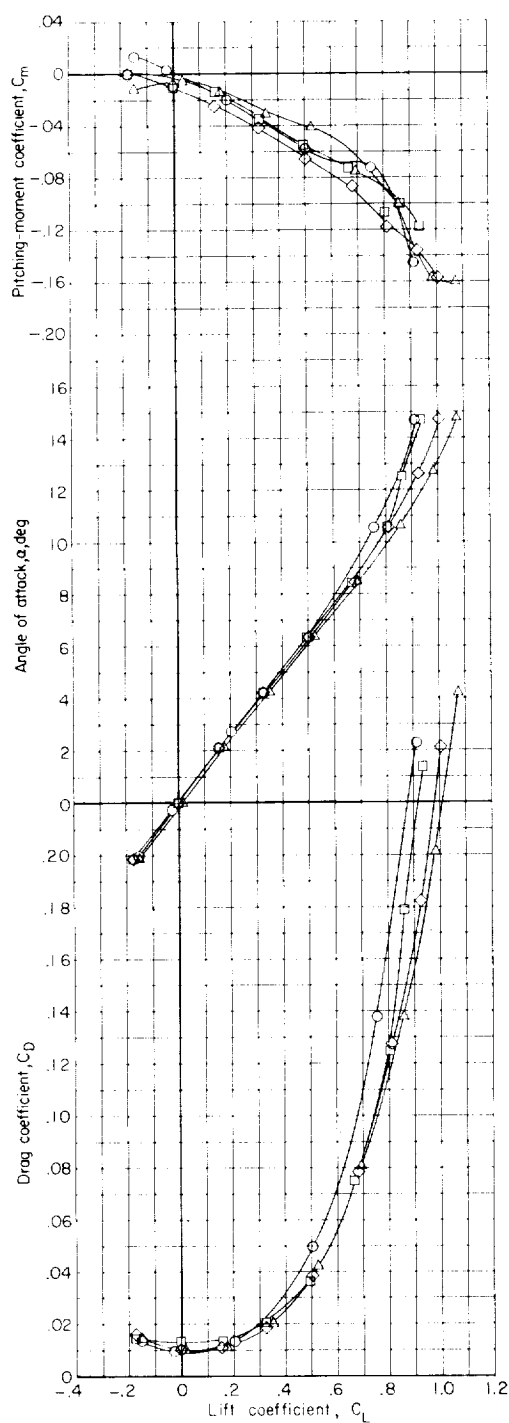
(a) M = 0.60.
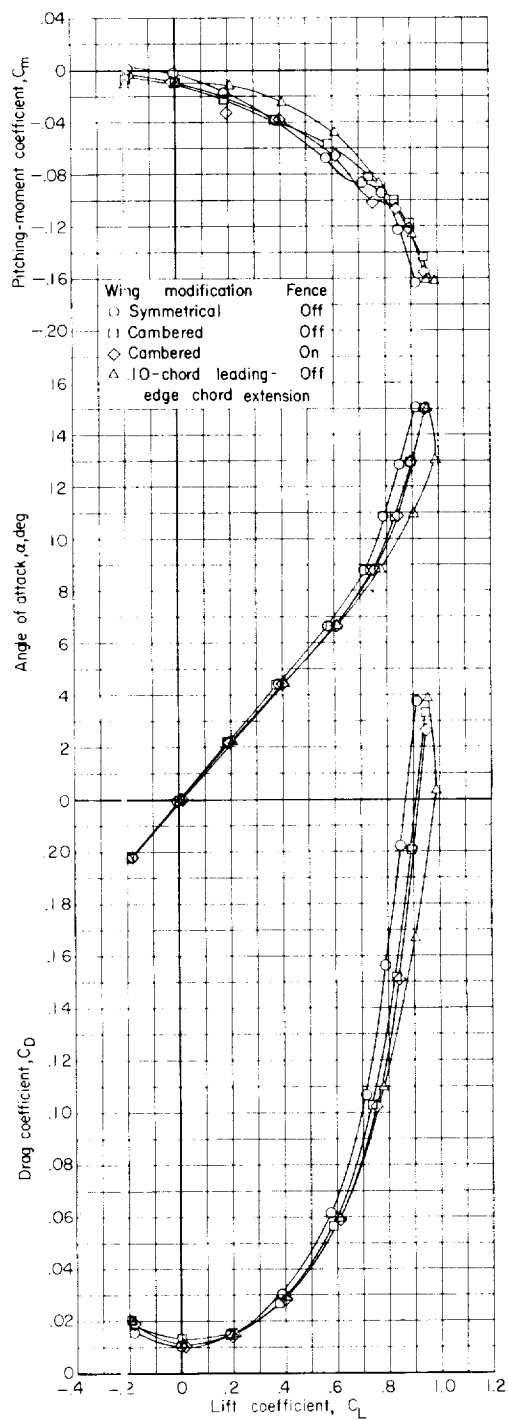
(b) M = 0.80.

Figure 14.- Effects of various wing modifications on the aerodynamic
characteristics in pitch of the model. Horizontal tail on. i_t = 0°.

L-470
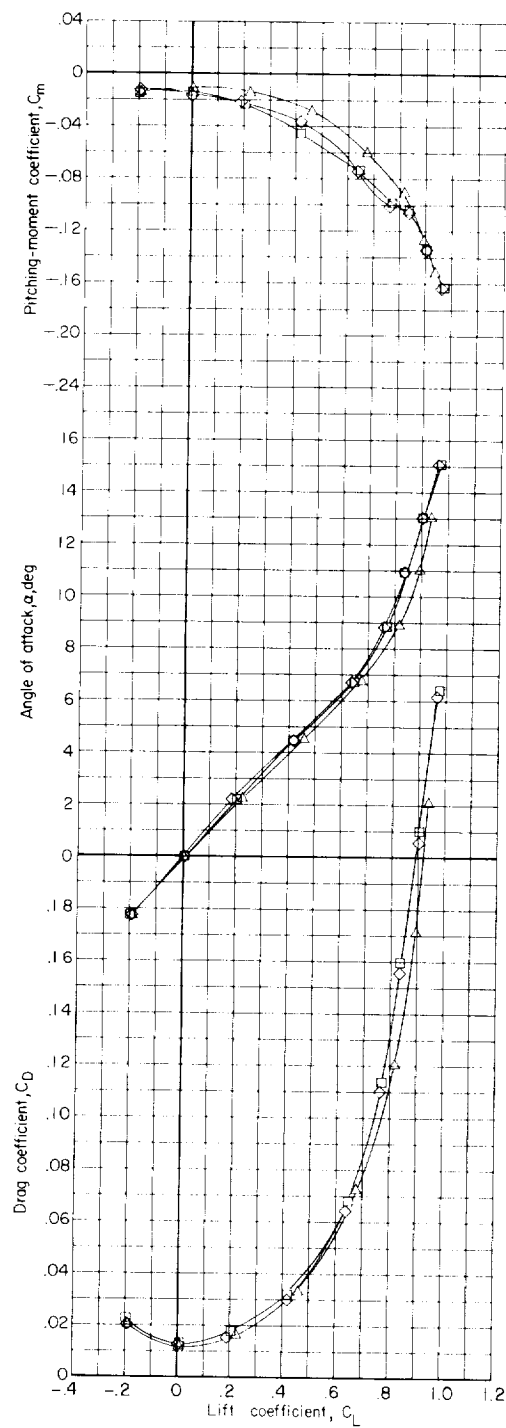
(c) M = 0.85.
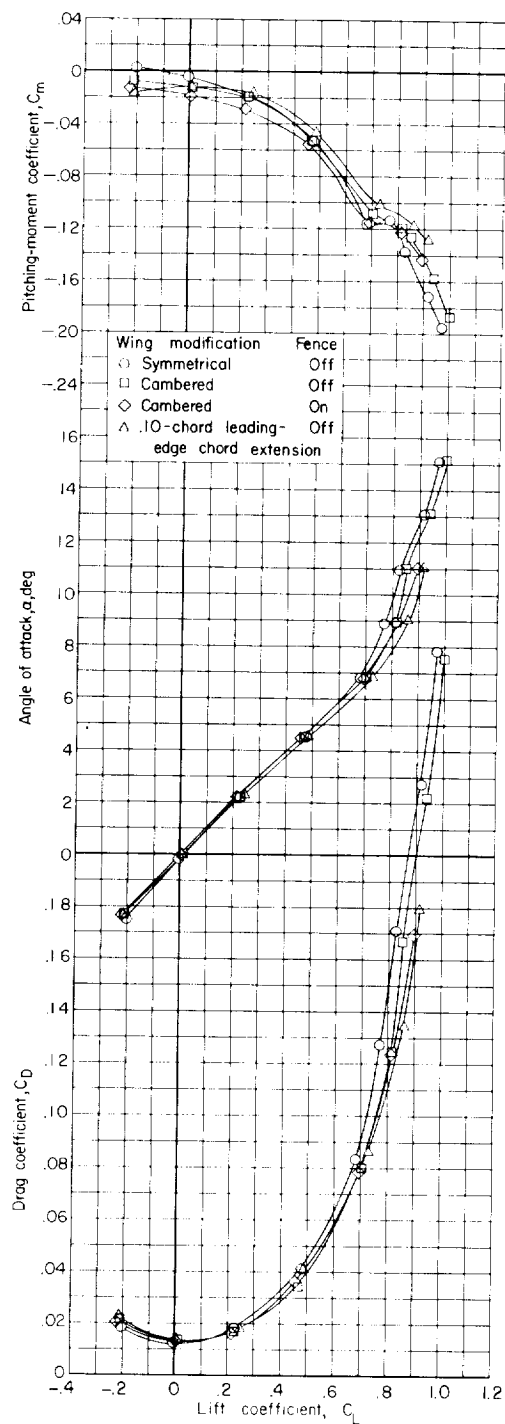
(d) M = 0.90.

Figure 14.- Continued.
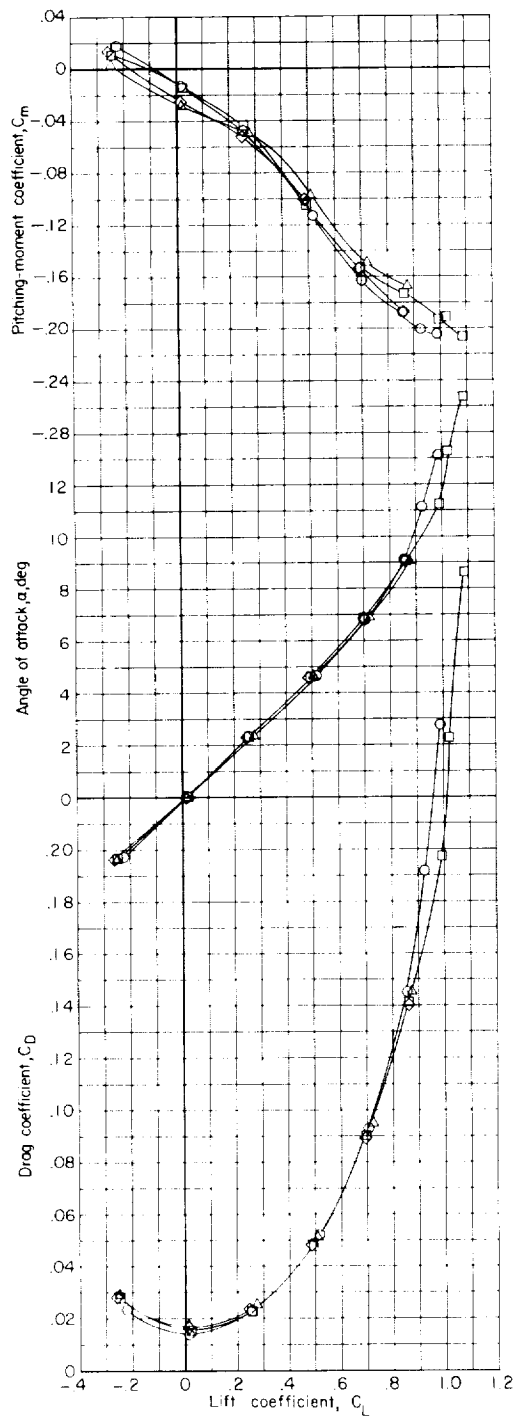
(e) M = 0.95.
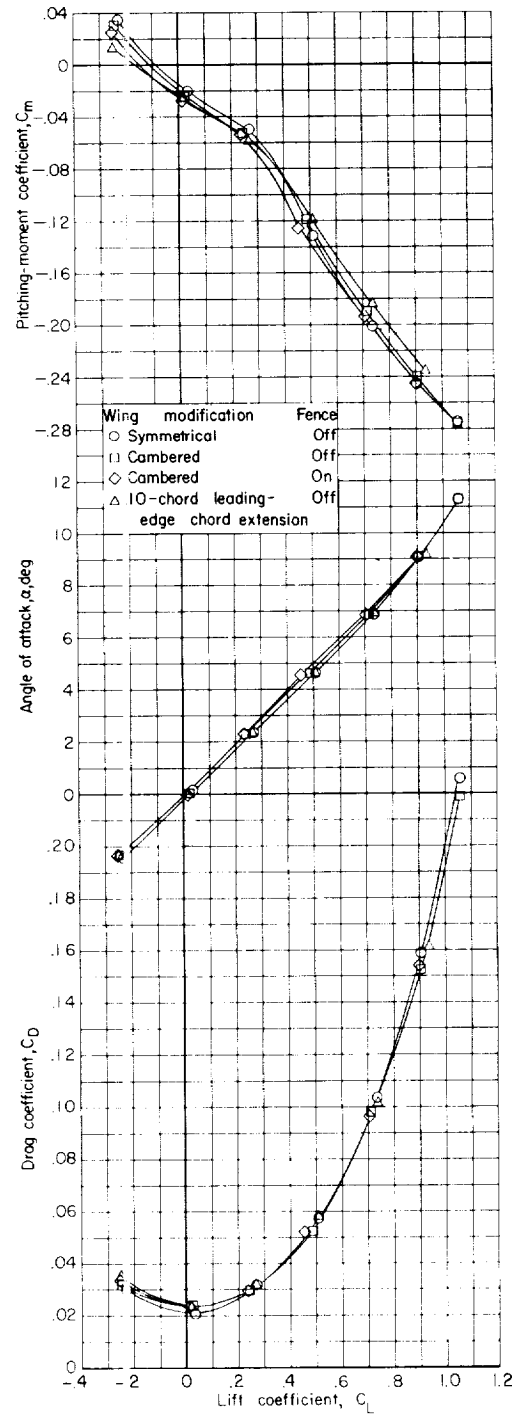
(f) M = 0.98.

Figure 14.- Continued.
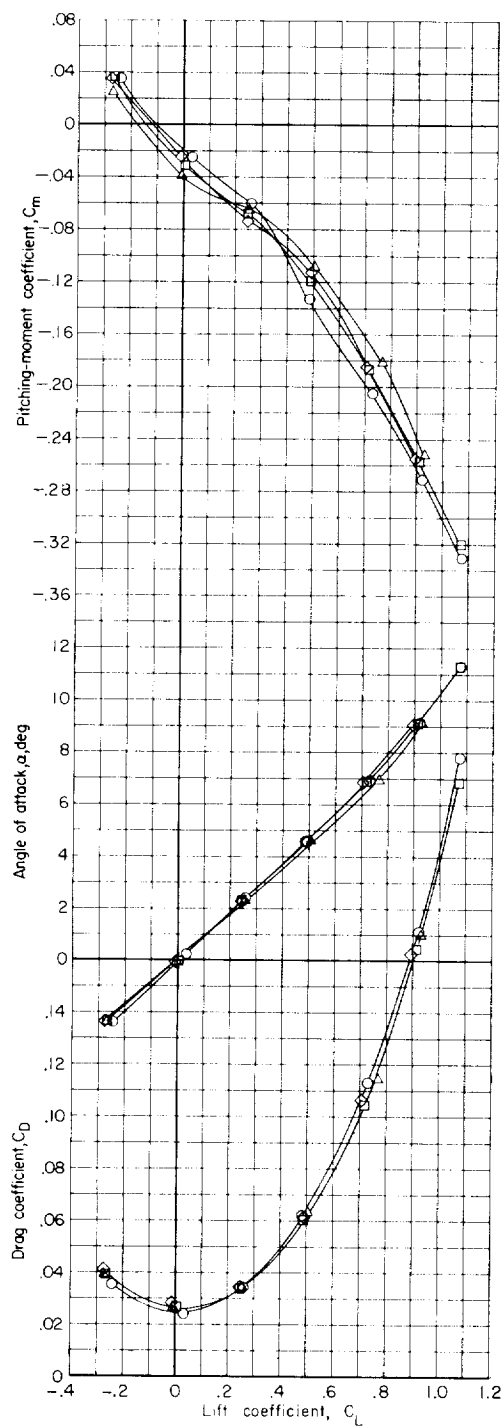
(g) M = 1.00.
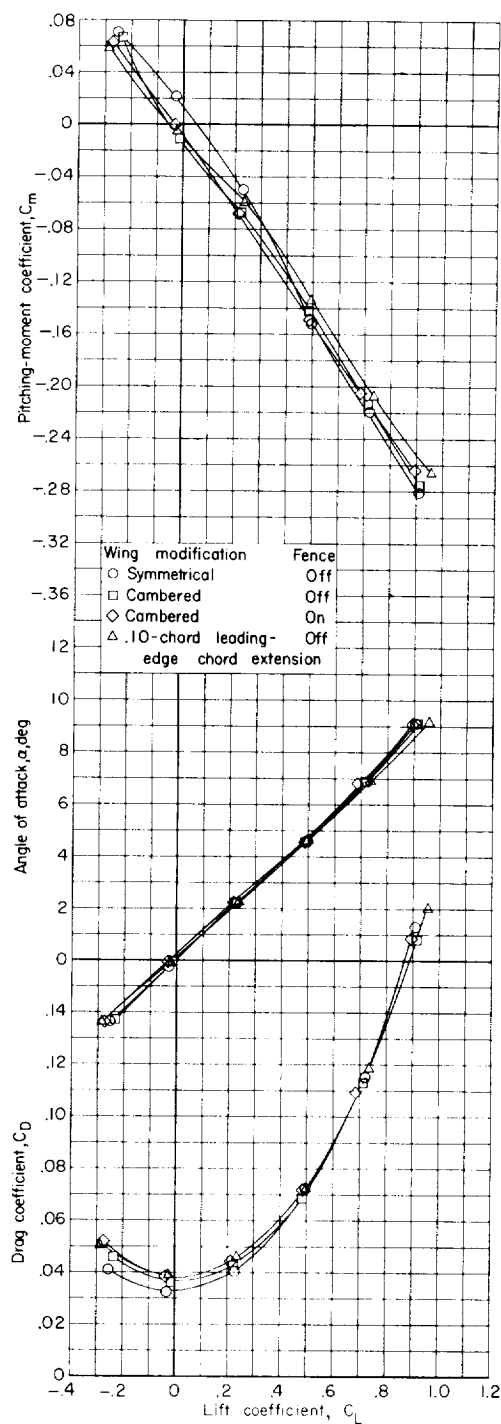
(h) M = 1.03.

Figure 14.- Continued.
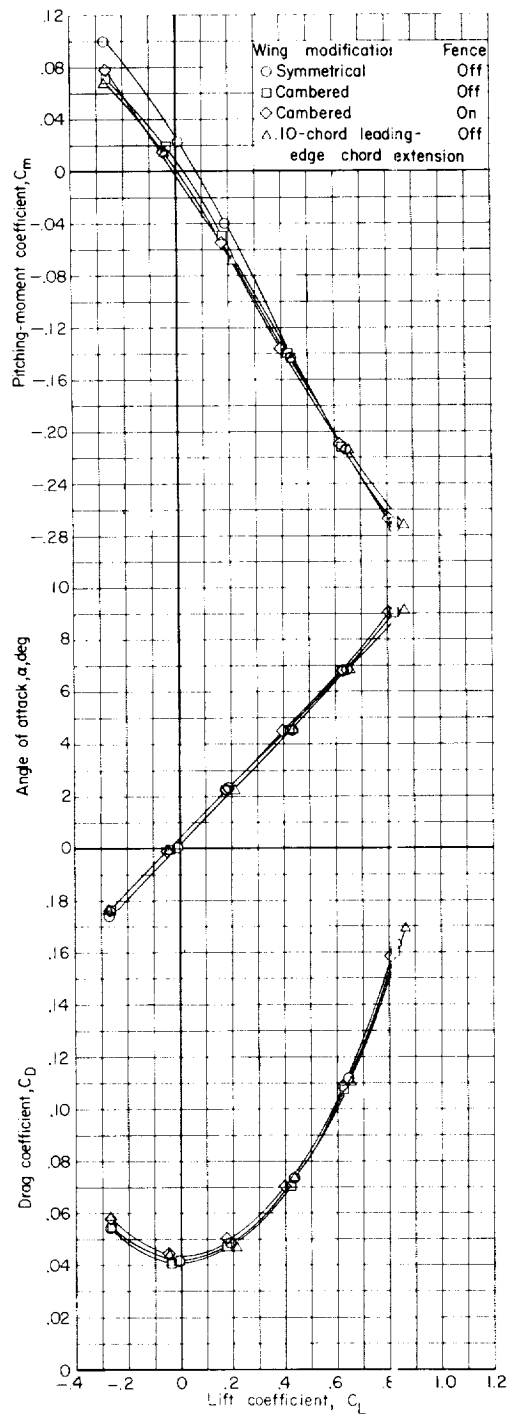
(i)   M = 1.13.

Figure 14.- Concluded.

(a) M = 0.60.
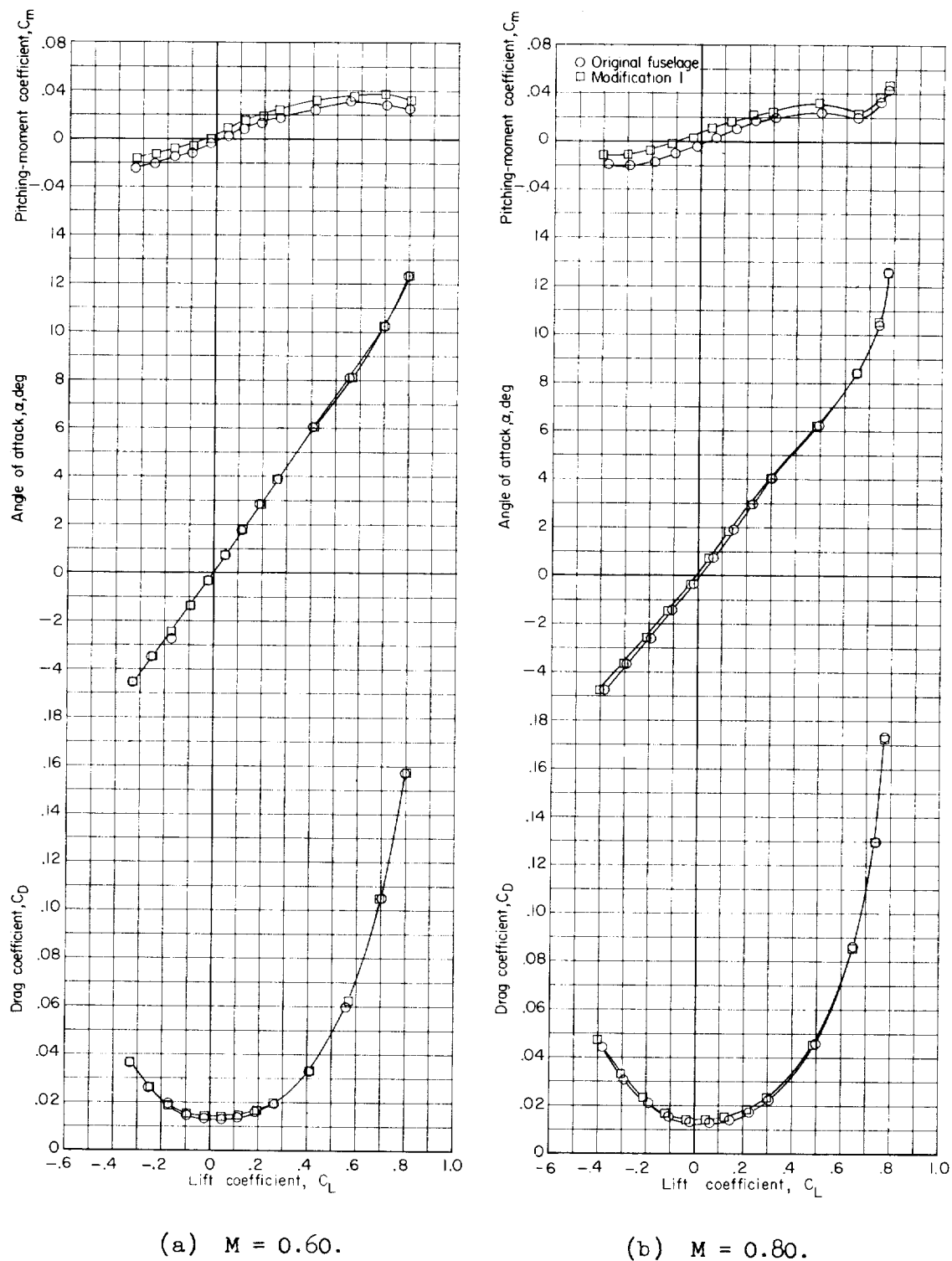
(b) M = 0.80.

Figure 15.- Effects of body shape on the aerodynamic characteristics in
pitch. Horizontal tail off.
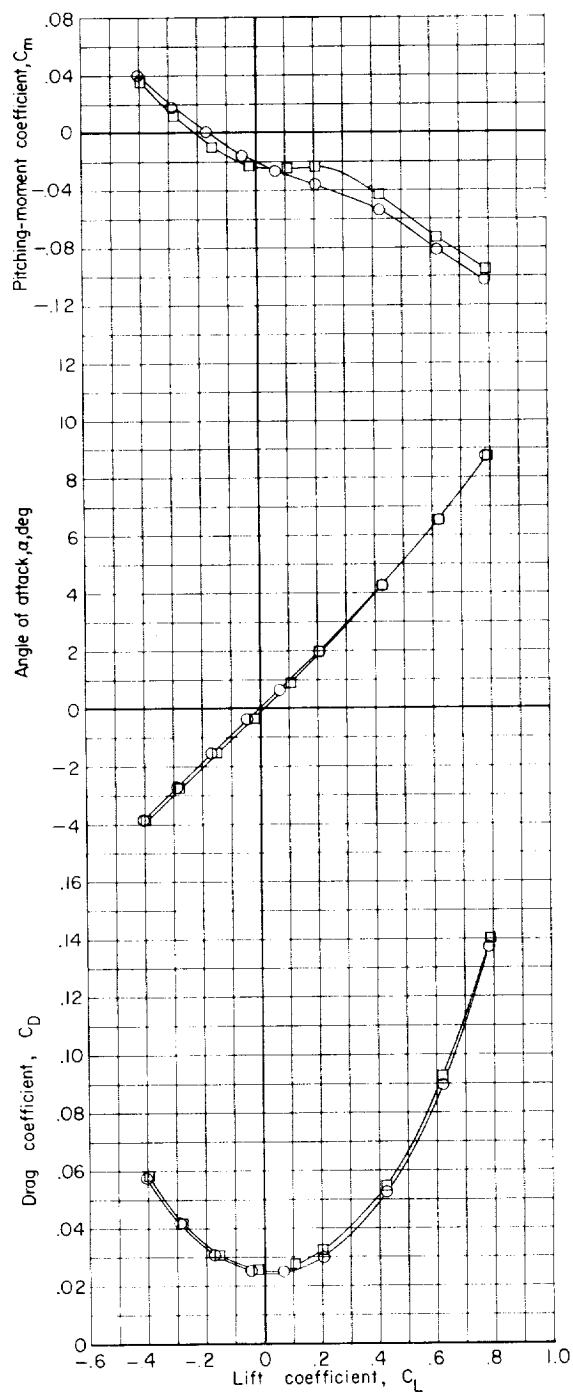
(g) M = 1.00.
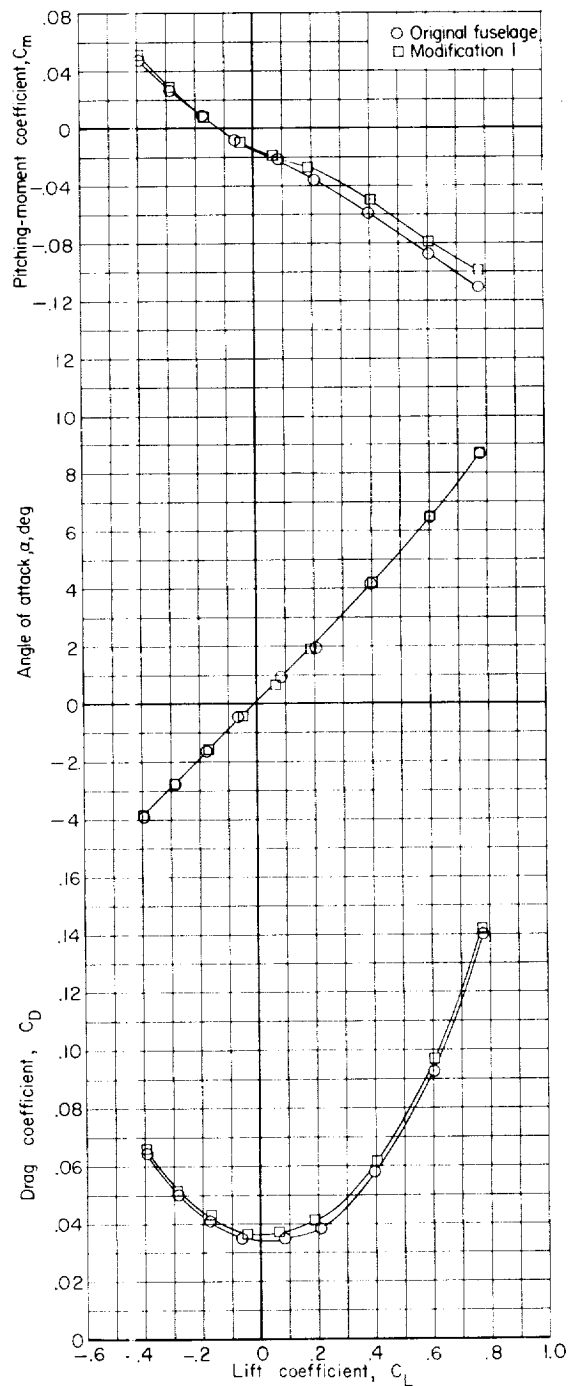
(h) M = 1.03.

Figure 15.- Continued.

L-476
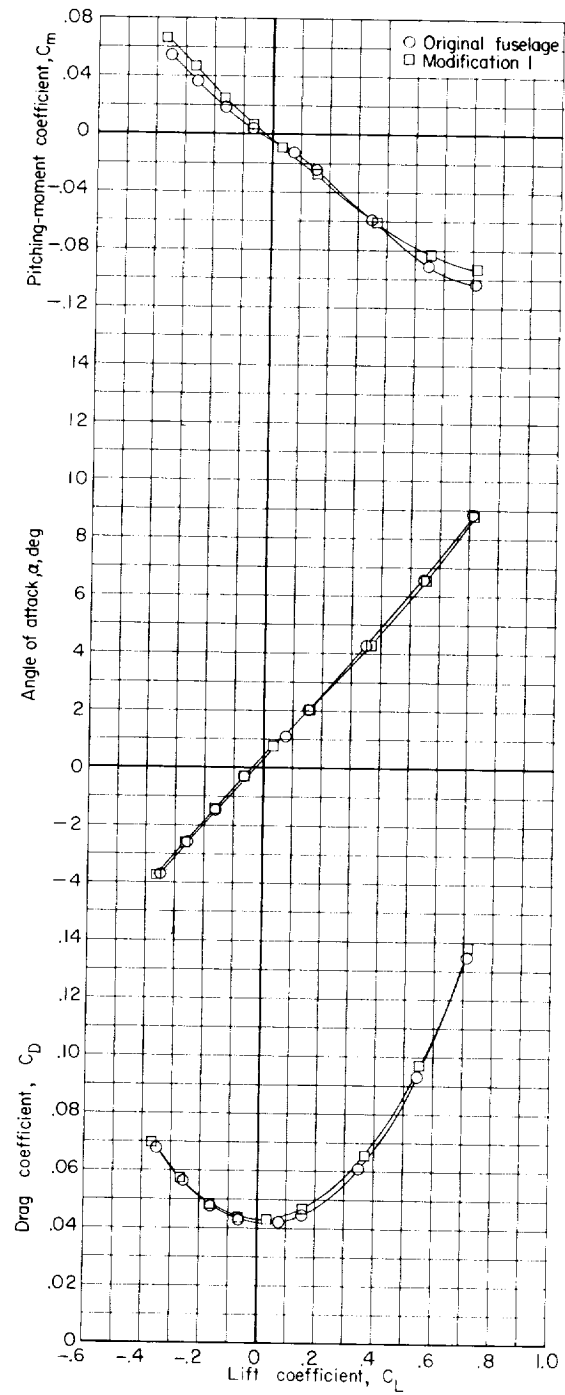
(i)   M = 1.13.

Figure 15.- Concluded.

58

Modification	Horizontal tail
◯ Off	Off
☐ 2	Off
◇ Off	On $i_1 = 0°$
△ 2	On $i_1 = 0°$
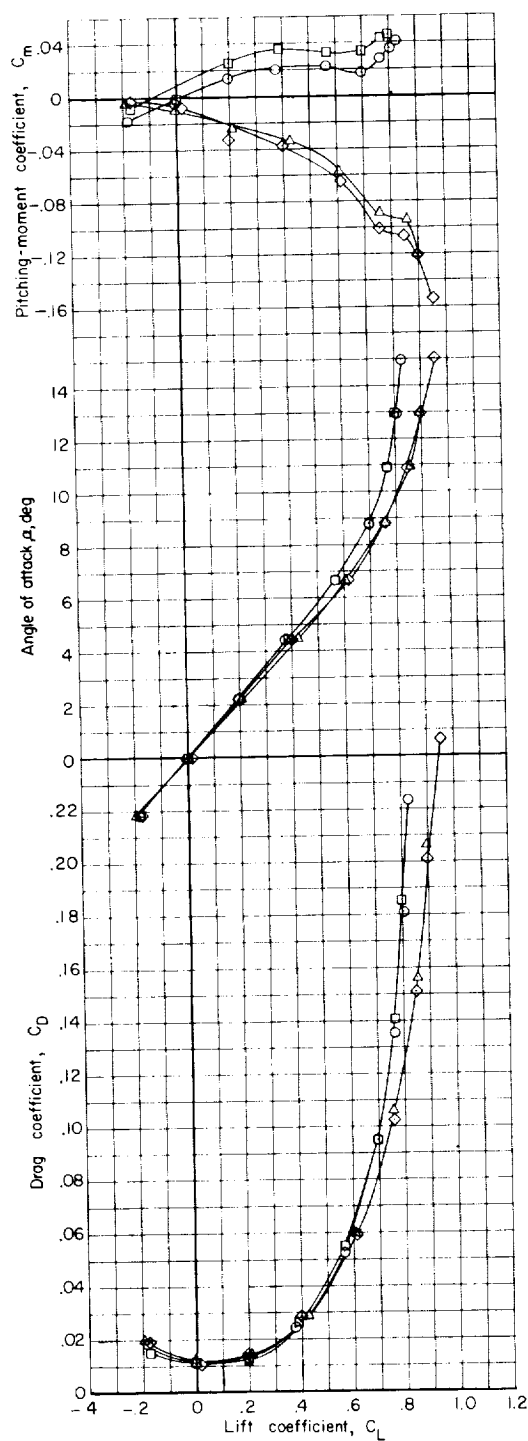
(a) M = 0.80.
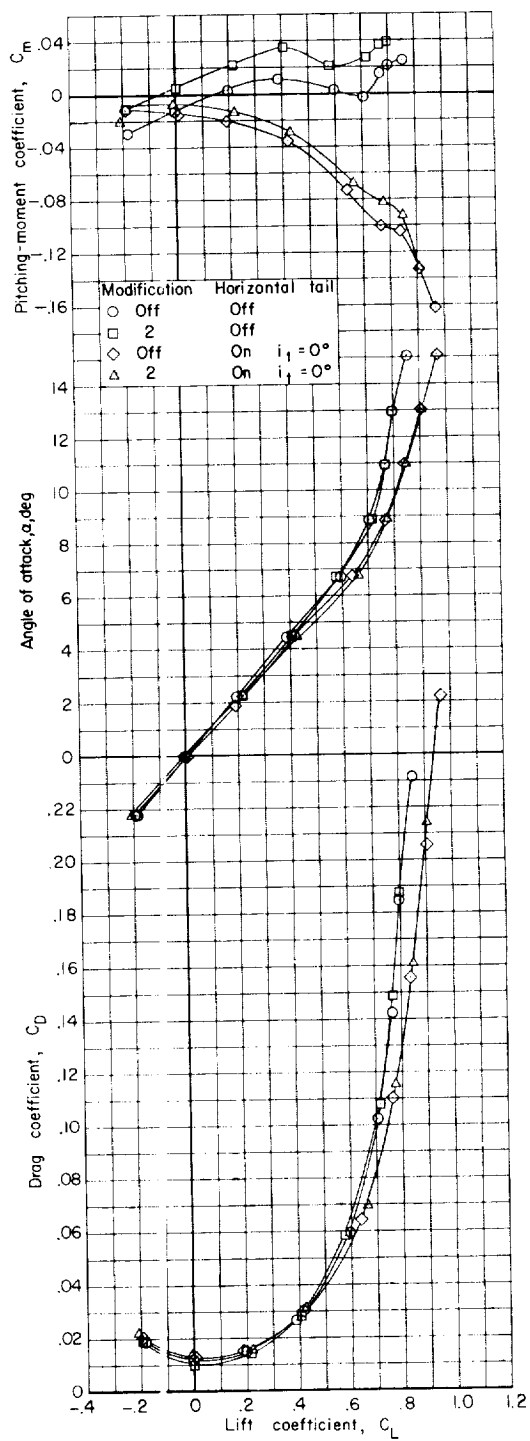
'b) M = 0.85.

Figure 16.- Effects of body modification on the aerodynamic characteristics
in pitch of the model.
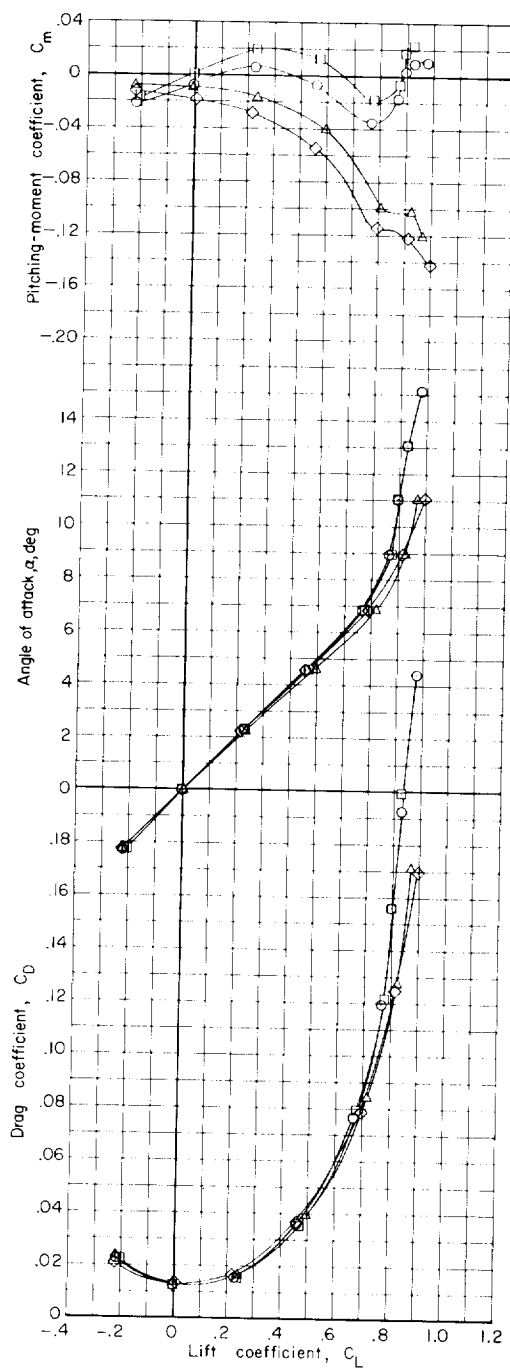
(c) M = 0.90.
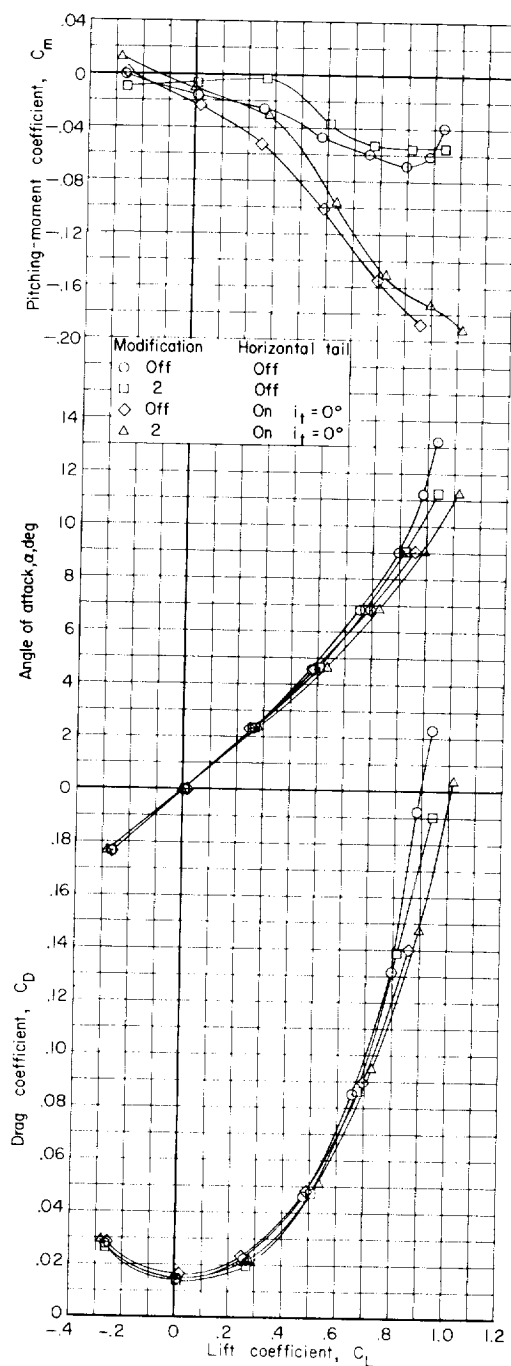
(d) M = 0.95.

Figure 16.- Continued.

60
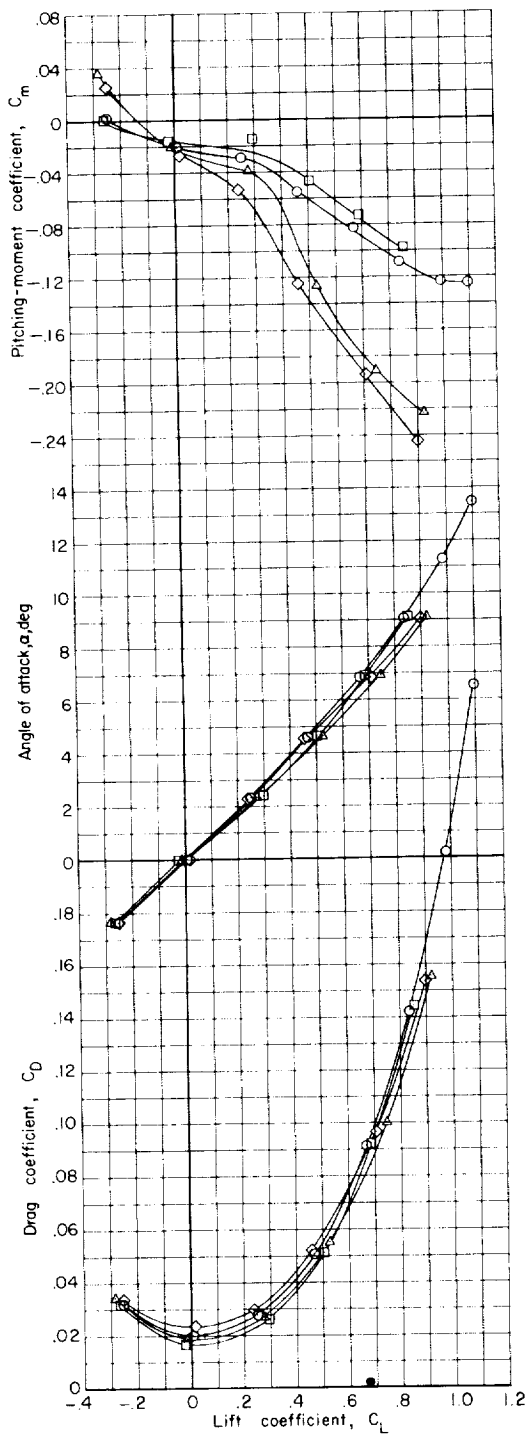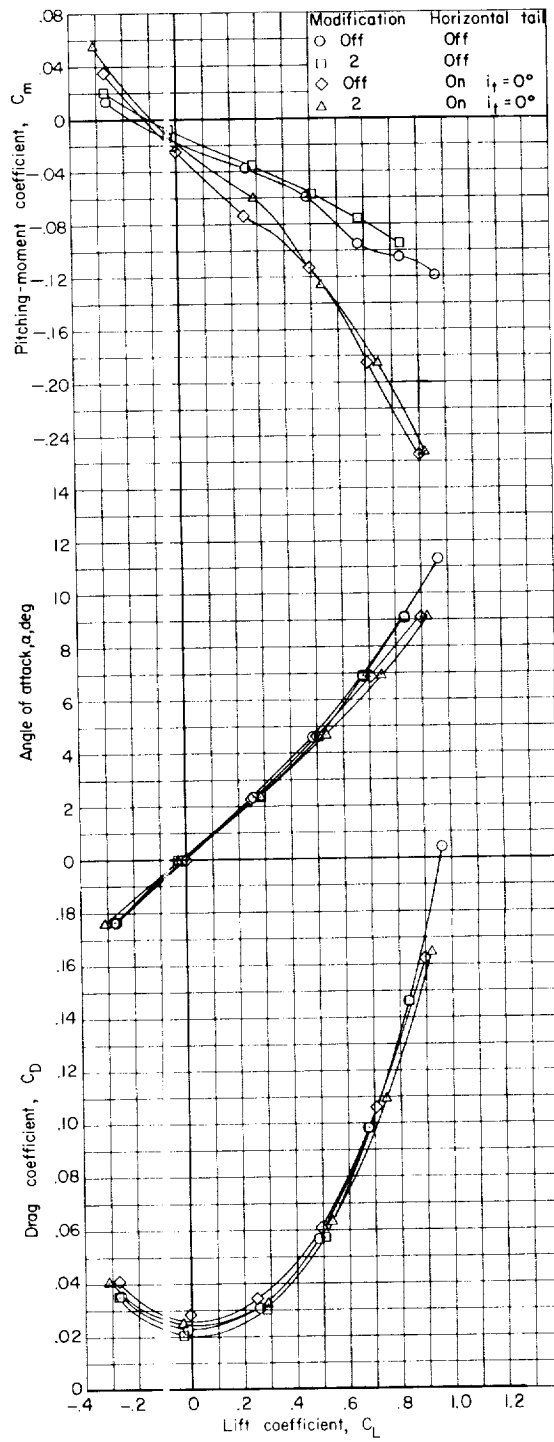
(e) M = 0.98.

(f) M = 1.00.

Figure 16.- Continued.
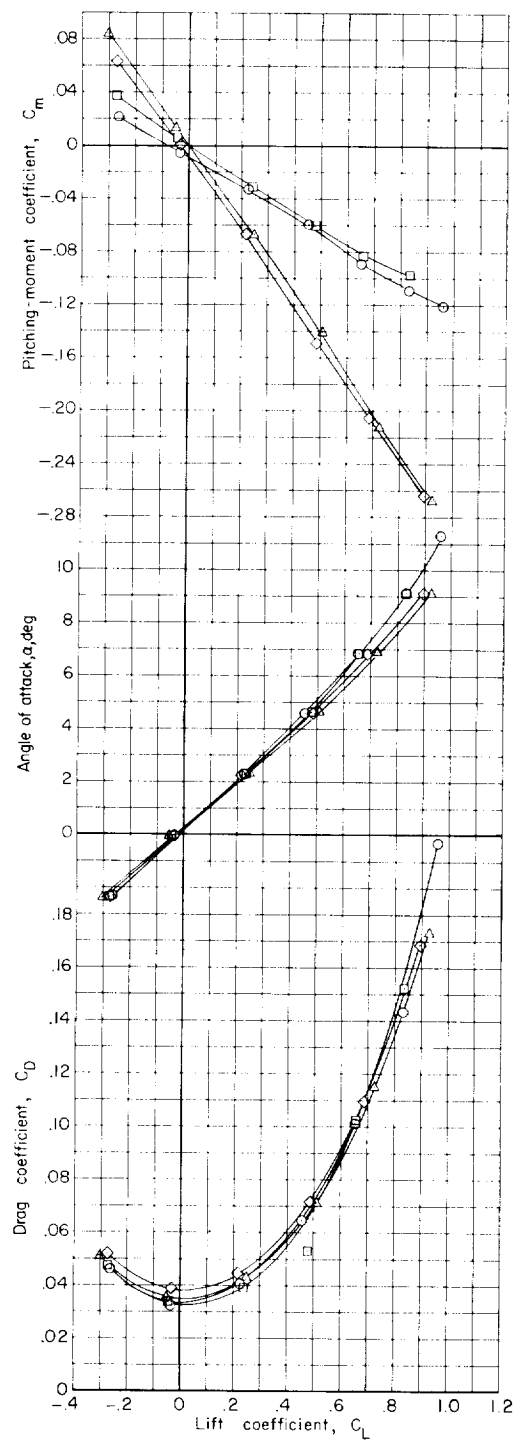
(g) M = 1.03.
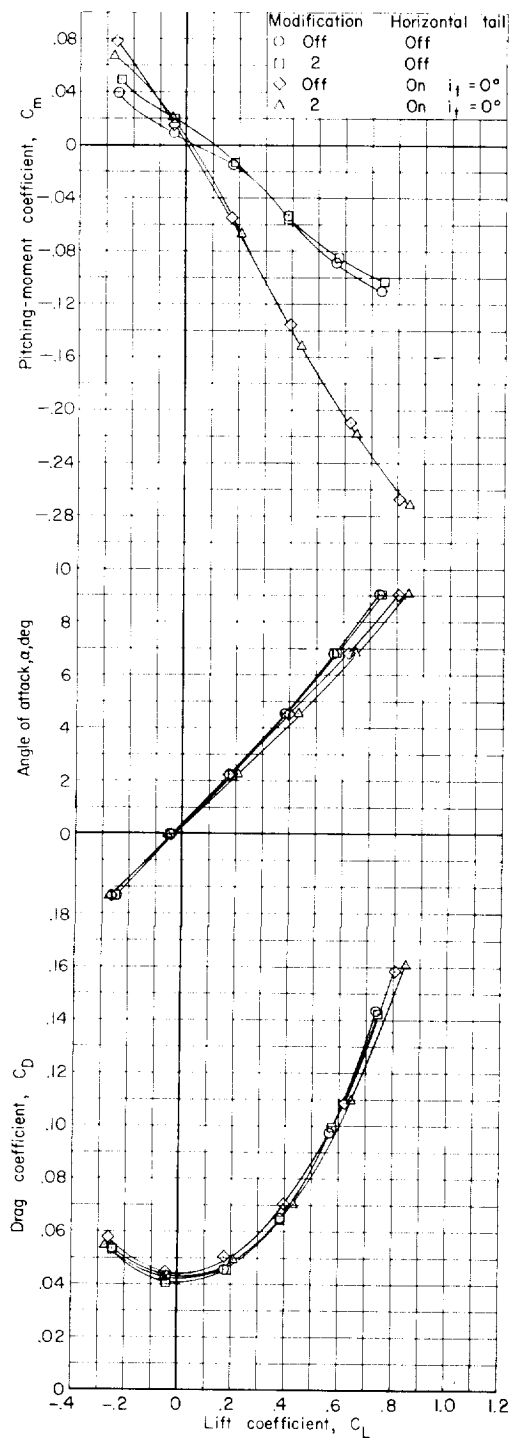
(h) M = 1.13.

Figure 16.- Concluded.

62

Modification
○ Off
□ 2
◇ 2 and 3
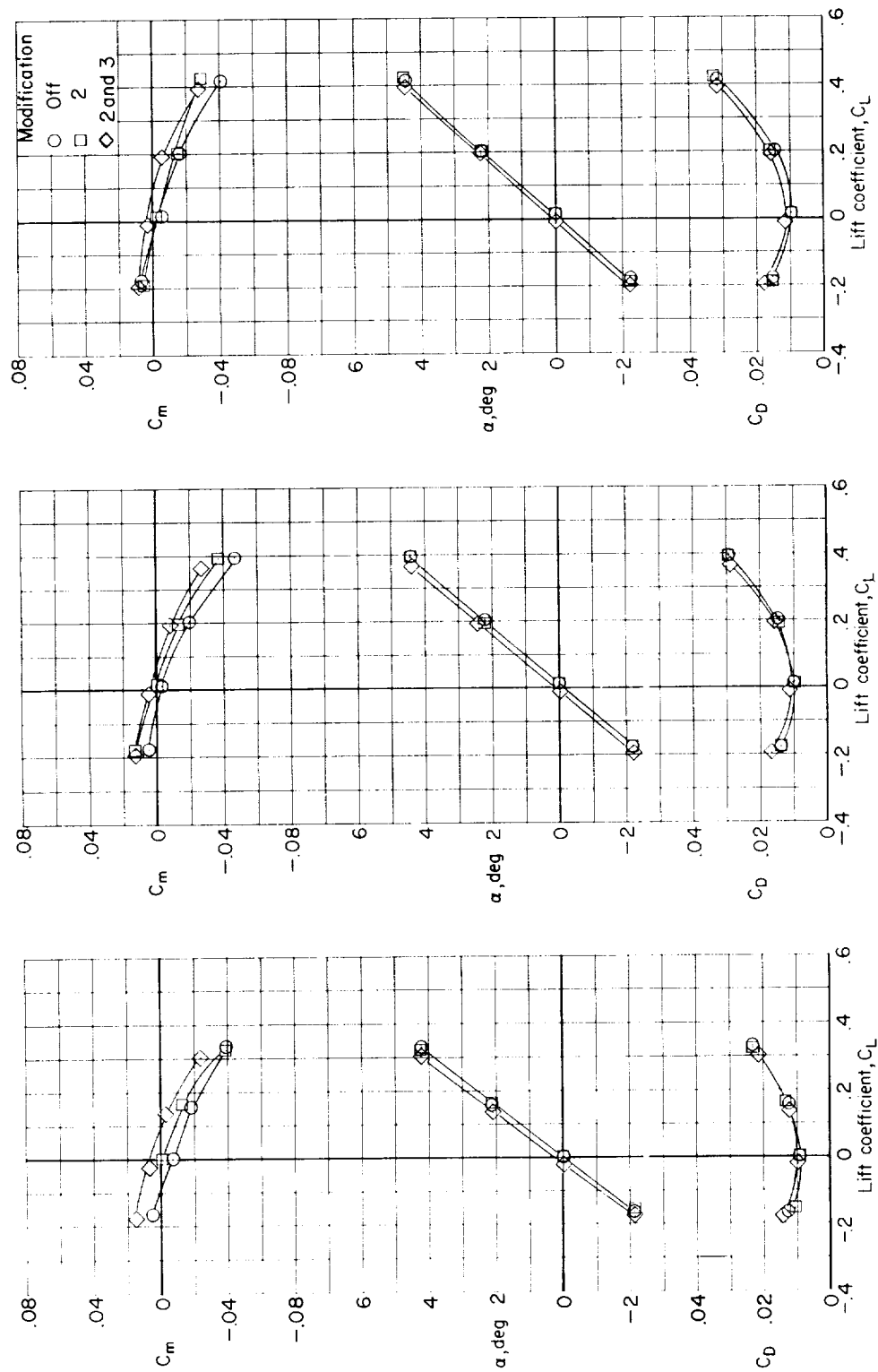
(a) M = 0.60.

(b) M = 0.80.

(c) M = 0.85.

Figure 17.- Effects of body modifications on the aerodynamic characteristics in pitch of the model with symmetrical wing. Horizontal tail on. $i_t = 0°$.
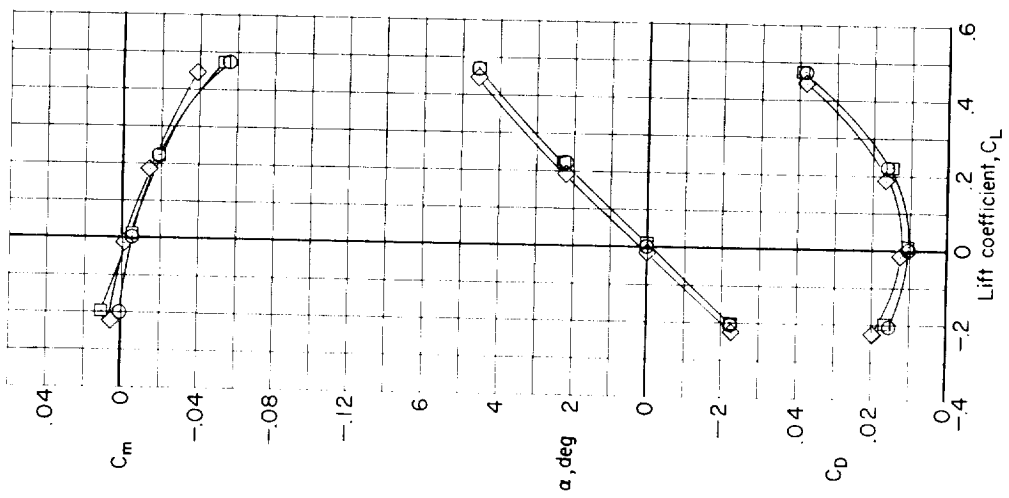
(d) M = 0.90.
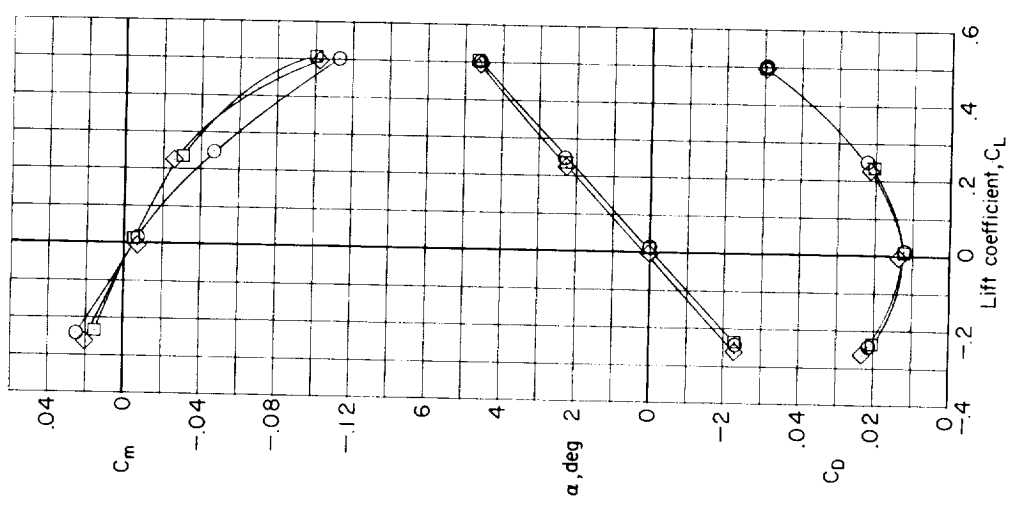
(e) M = 0.95.
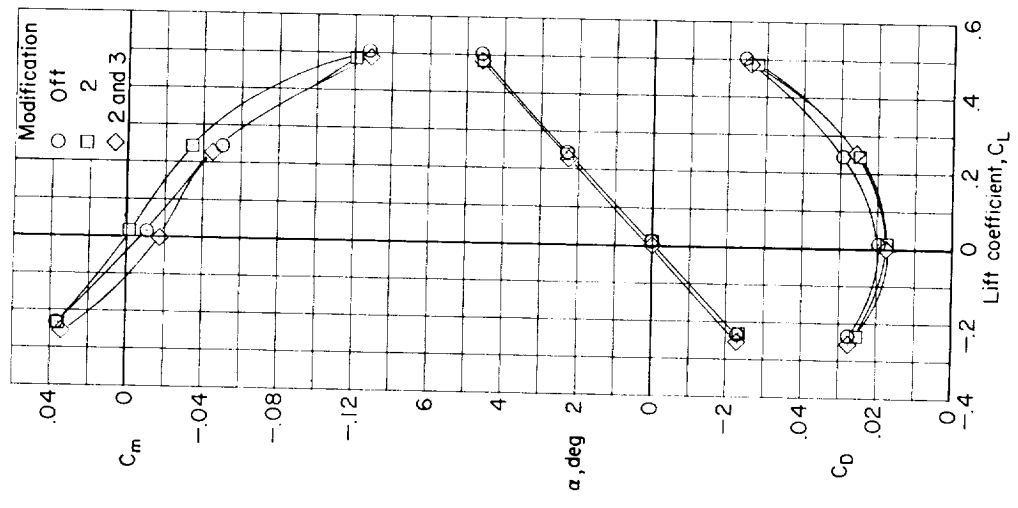
(f) M = 0.98.

Figure 17.- Continued.

63
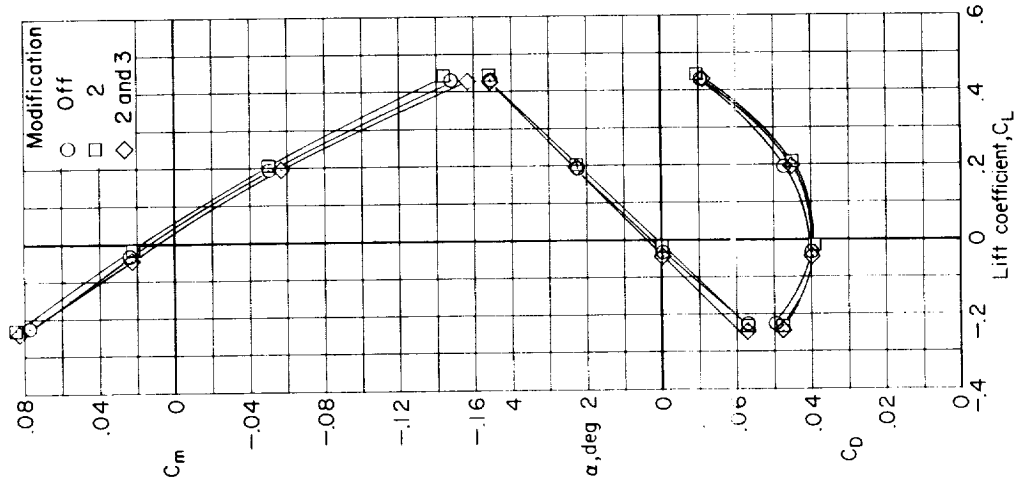
(i) M = 1.13.
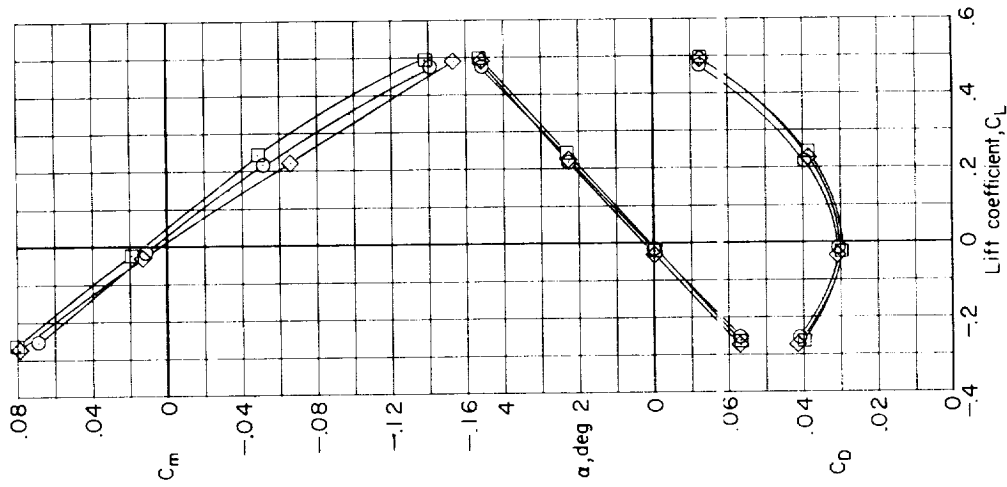
(h) M = 1.03.
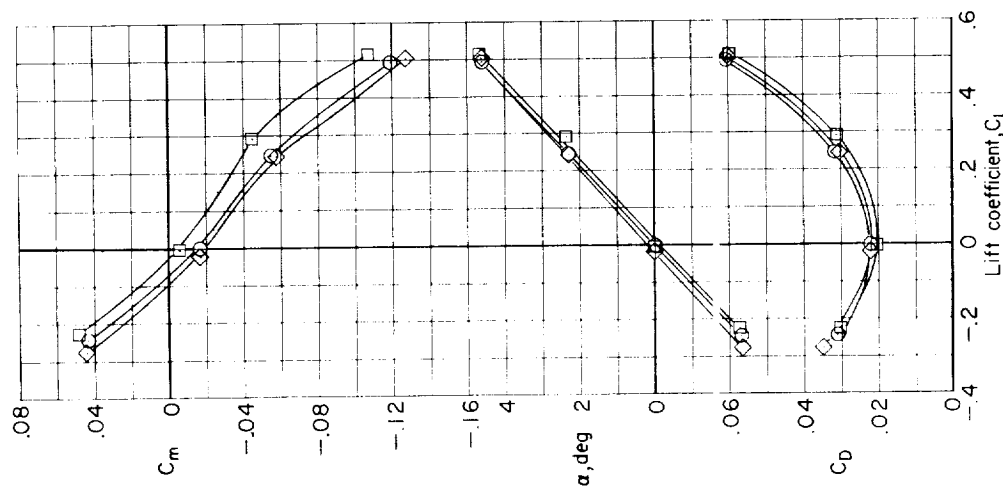
Figure 17.- Concluded.

(g) M = 1.00.

L-476
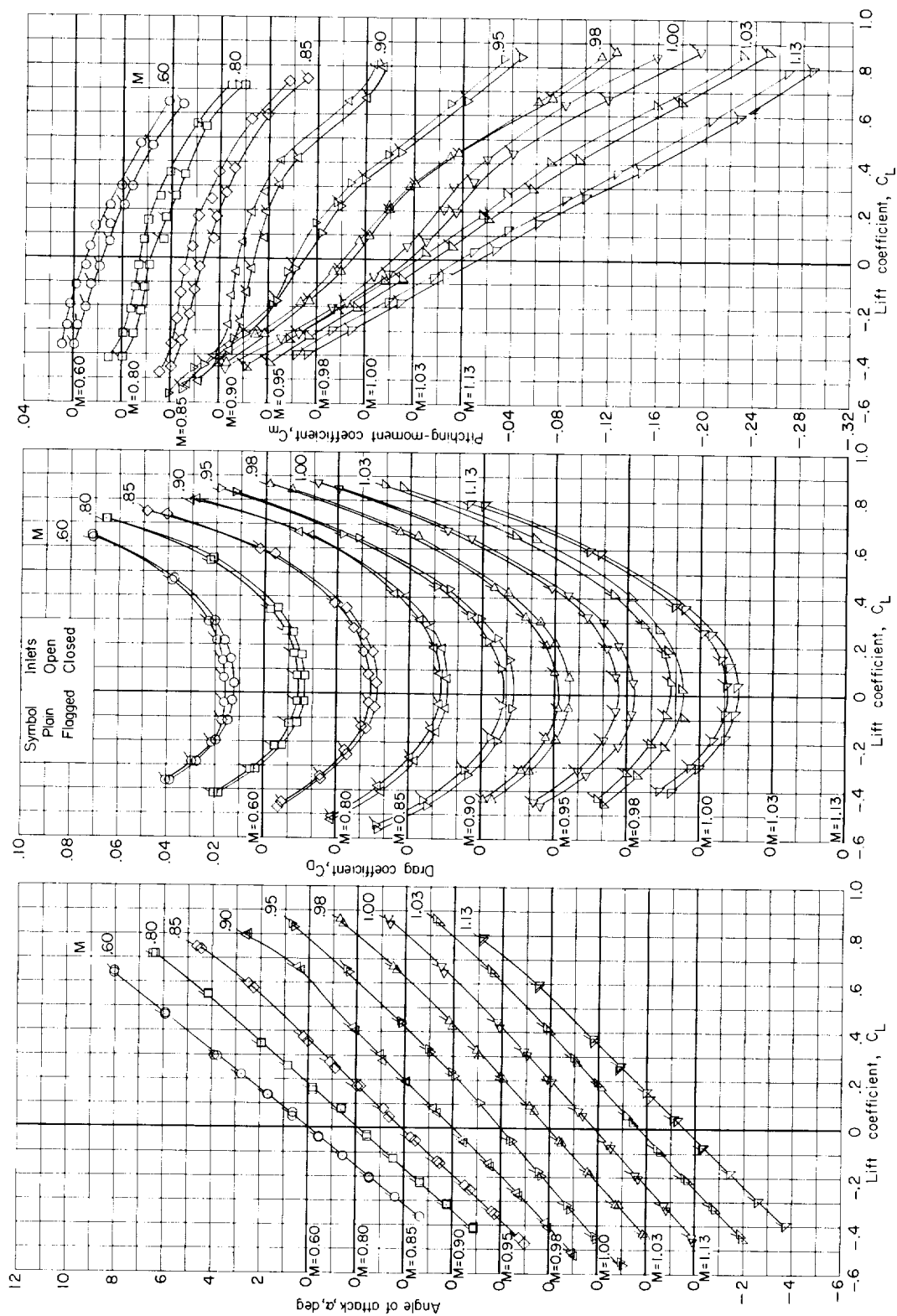
Figure 18.- Effects of closing inlets on the aerodynamic characteristics
in pitch of the basic model. Horizontal tail on. $i_t = 0^{\circ}$.
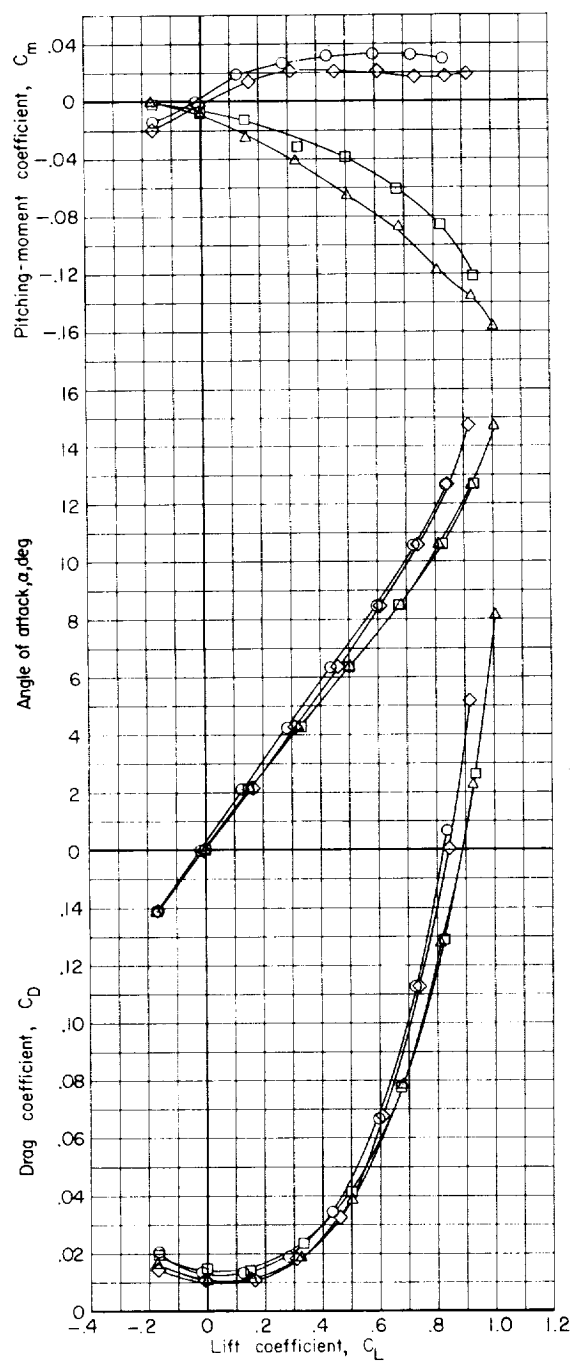
(a) M = 0.60.
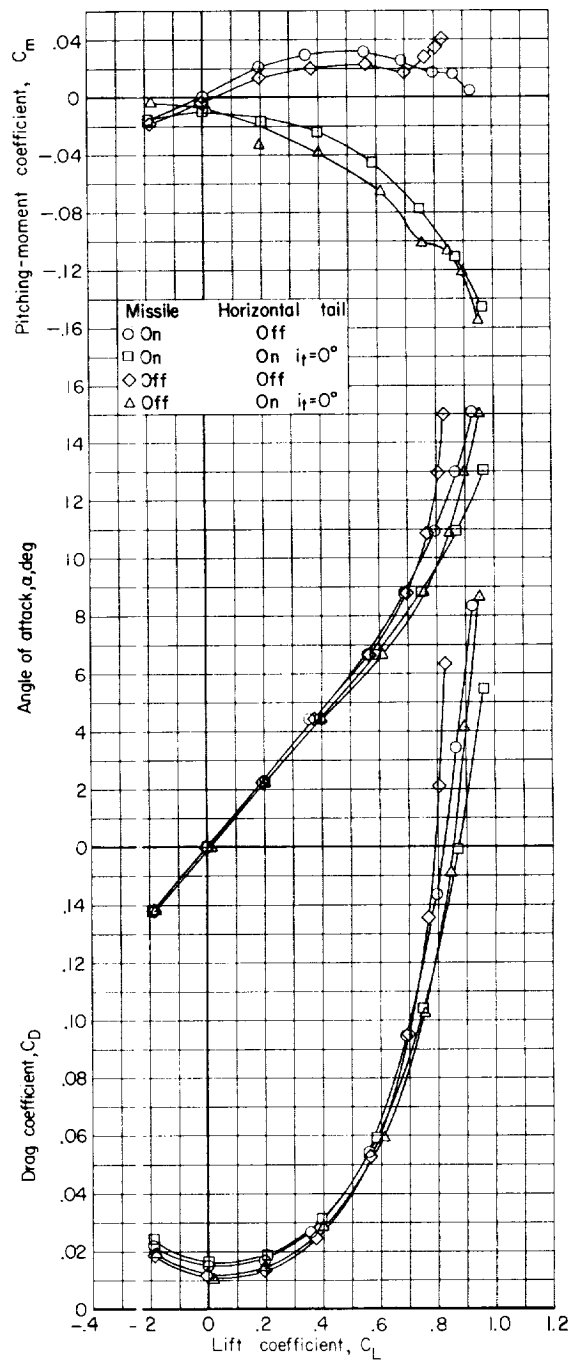
(b) M = 0.80.

Figure 19.- Effects of air-to-air missiles on the aerodynamic character-
istics in pitch of the basic model.
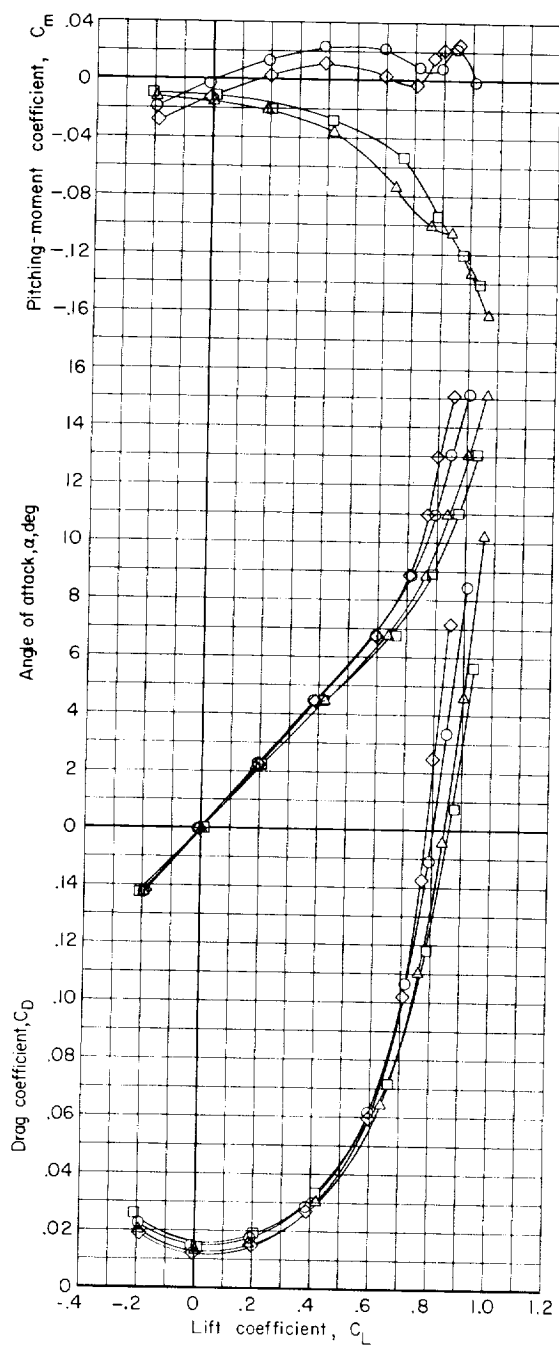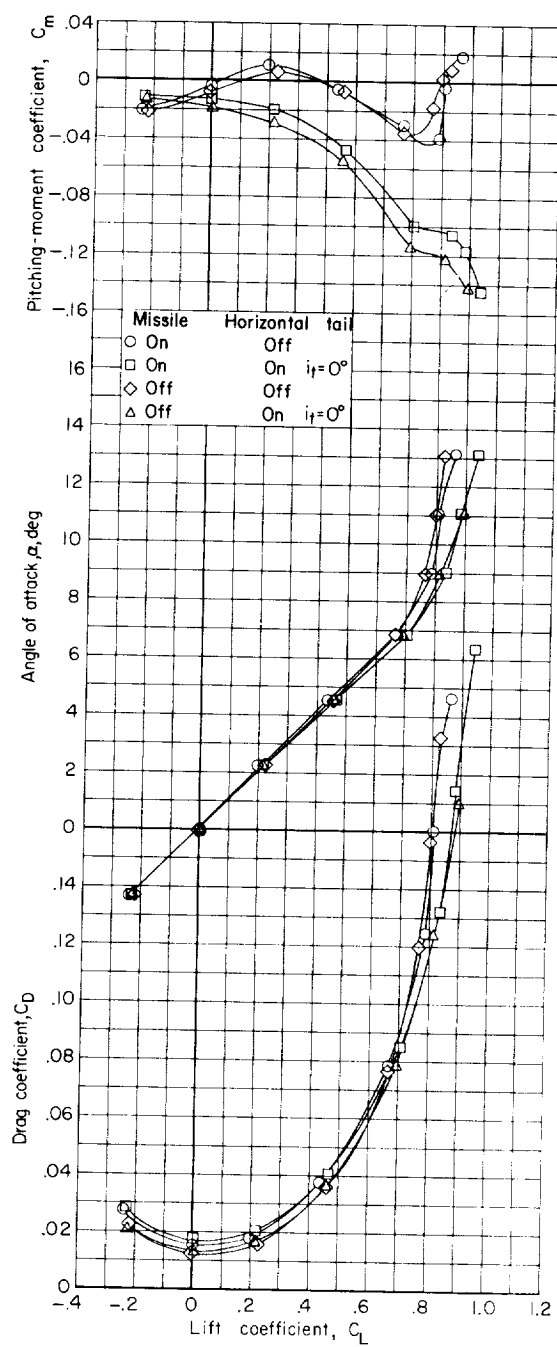
(c) M = 0.85.   (d) M = 0.90.

Figure 19.- Continued.

68
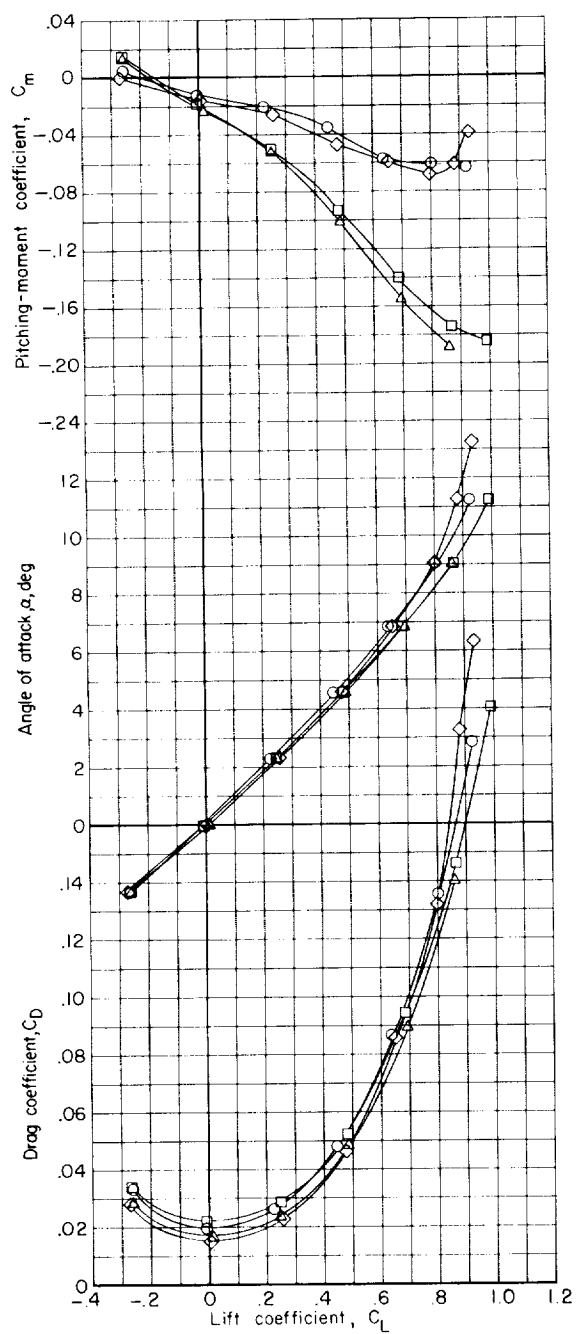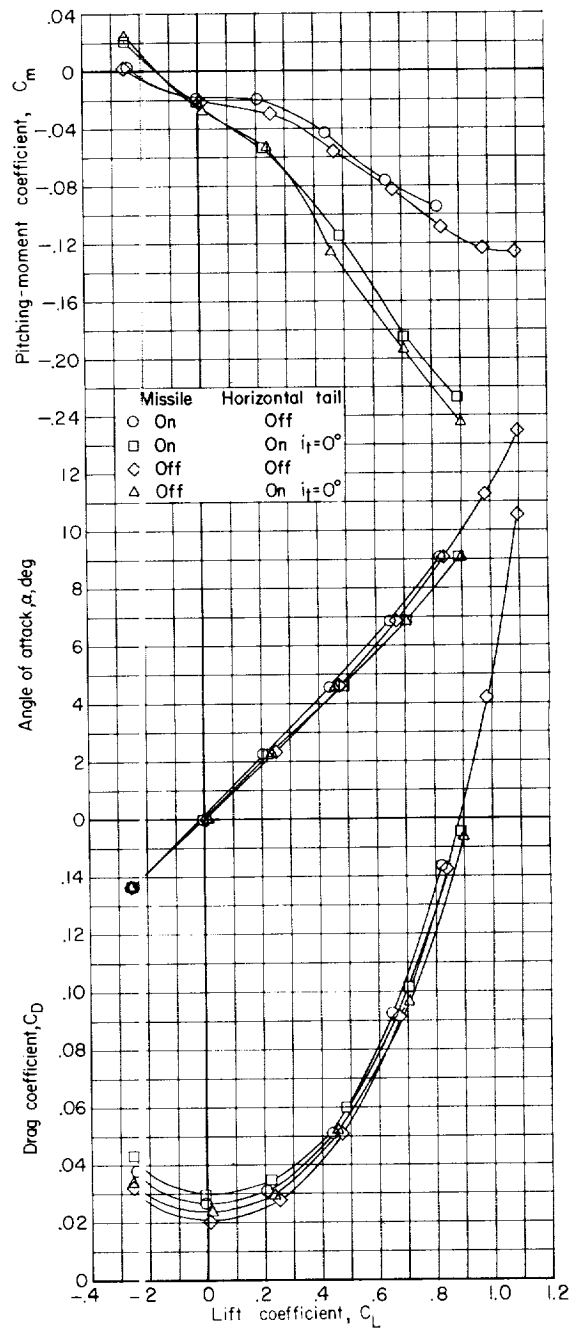
(e) M = 0.95.   (f) M = 0.98.

Figure 19.- Continued.
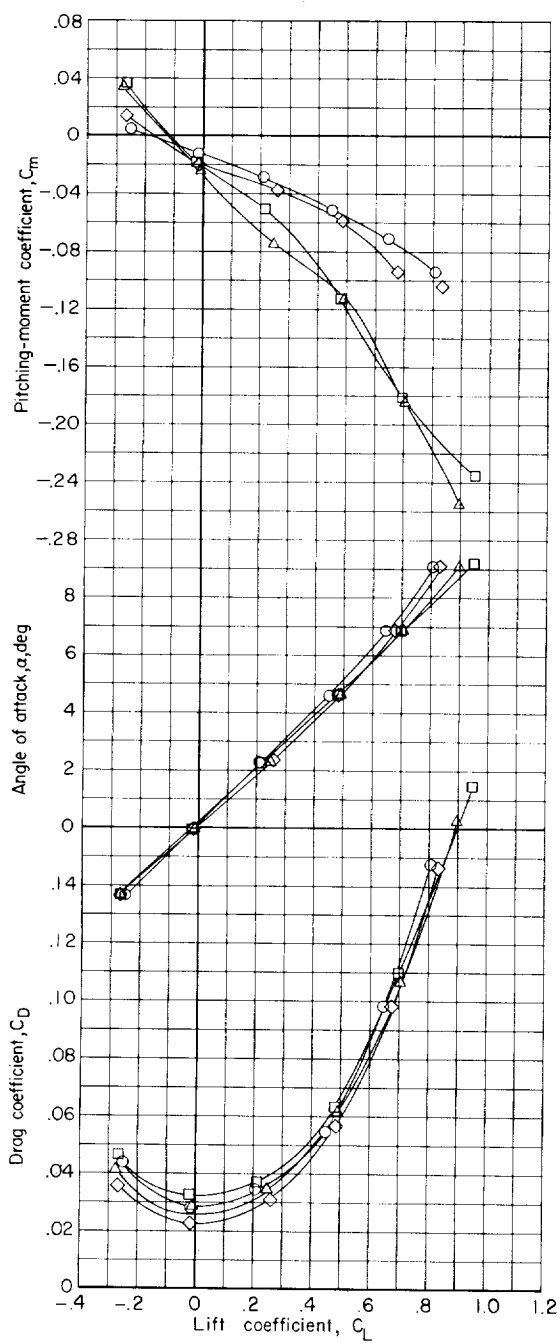
(g) M = 1.00.
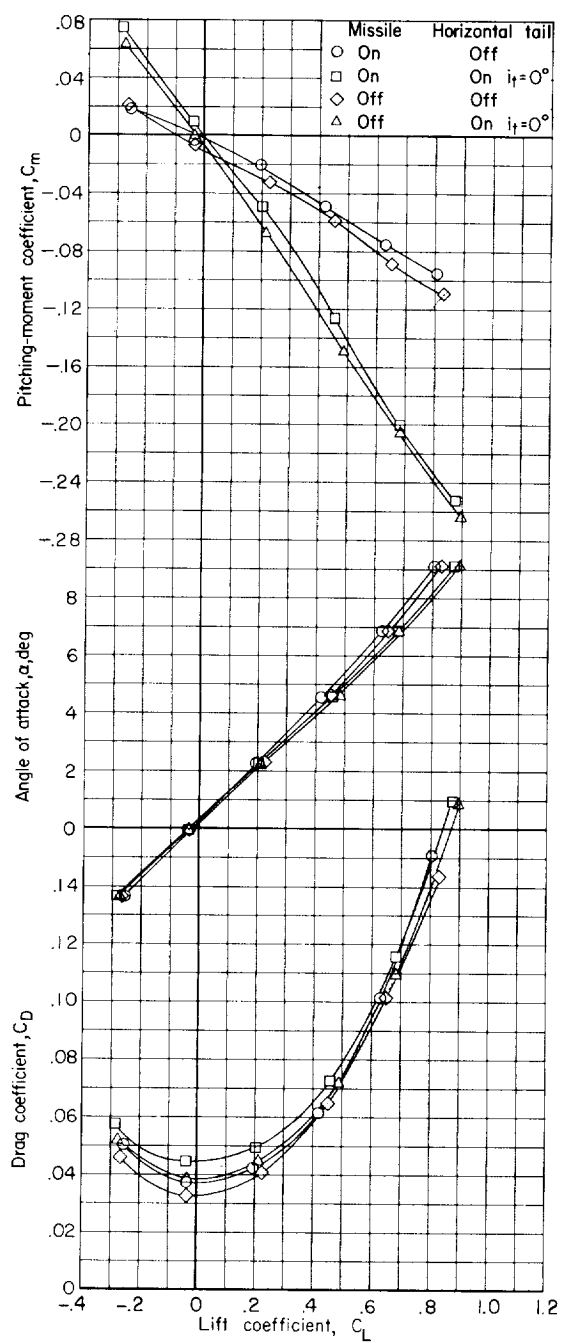
(h) M = 1.03.

Figure 19.- Continued.
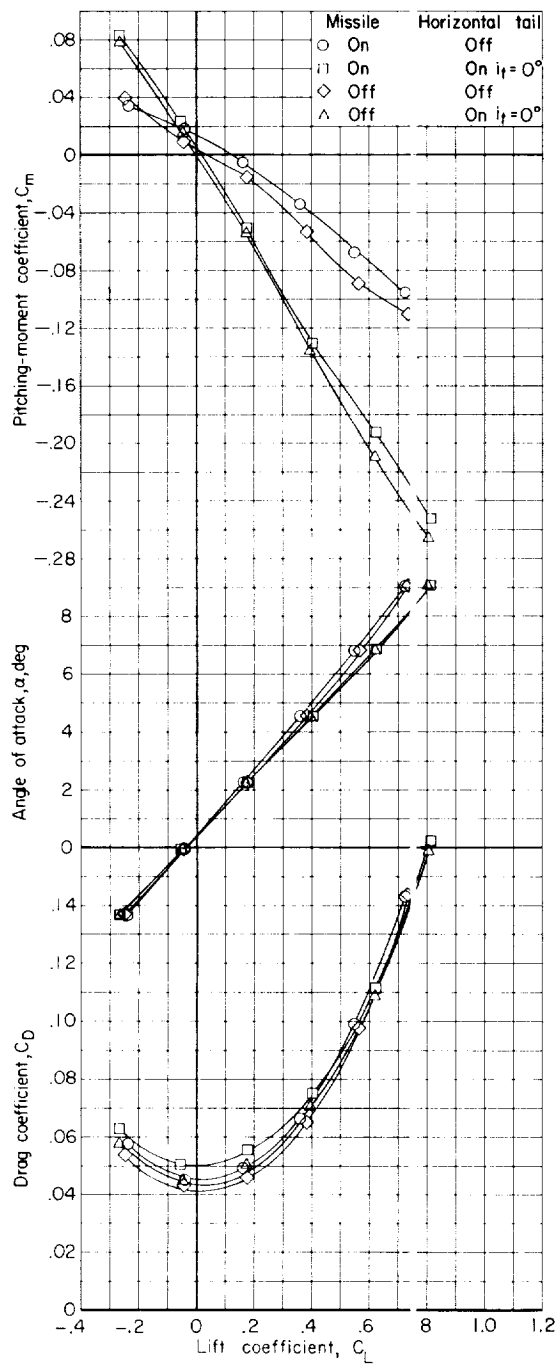
(i) M = 1.13.

Figure 19.- Concluded.
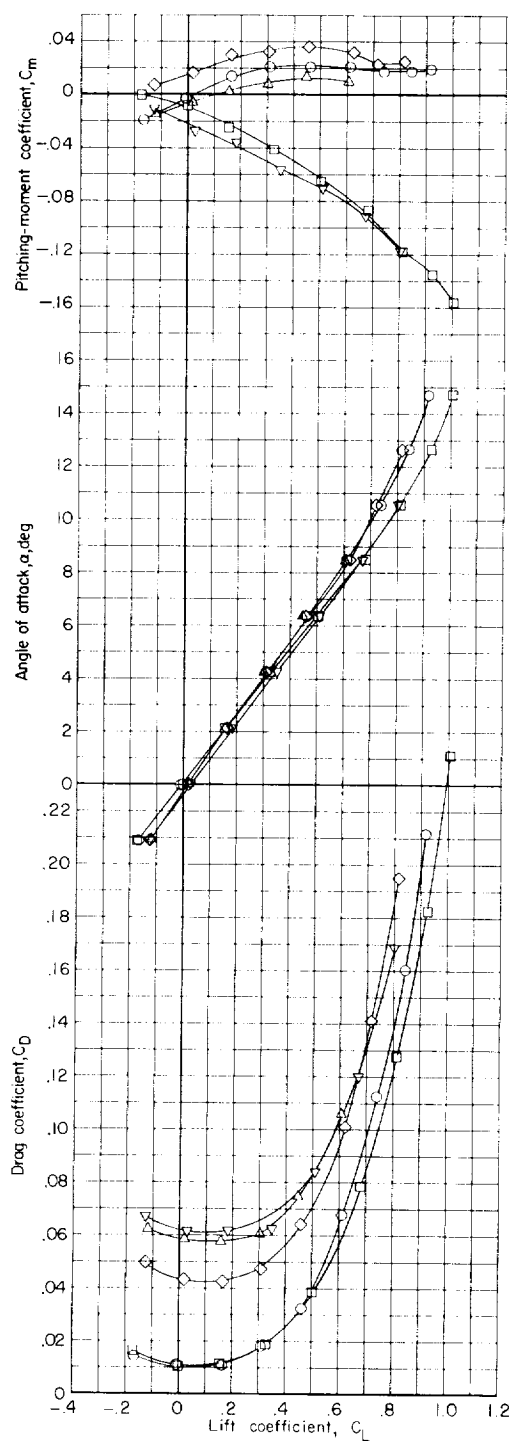
(a) M = 0.60.
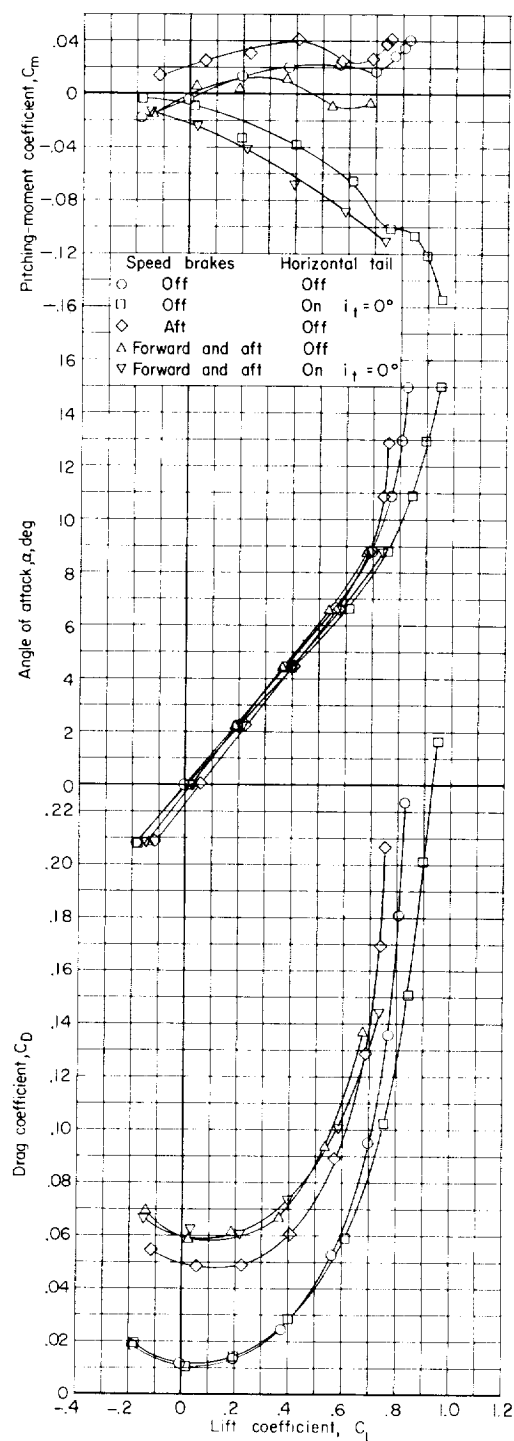
(b) M = 0.80.

Figure 20.- Effects of speed brakes on the aerodynamic characteristics
in pitch of the basic model.

72

Figure 20.- Continued.

L-476

Speed brakes | Horizontal tail
- ○ Off — Off
- □ Off — On $i_t = 0°$
- ◇ Aft — Off
- △ Forward and aft — Off
- ▽ Forward and aft — On $i_t = 0°$
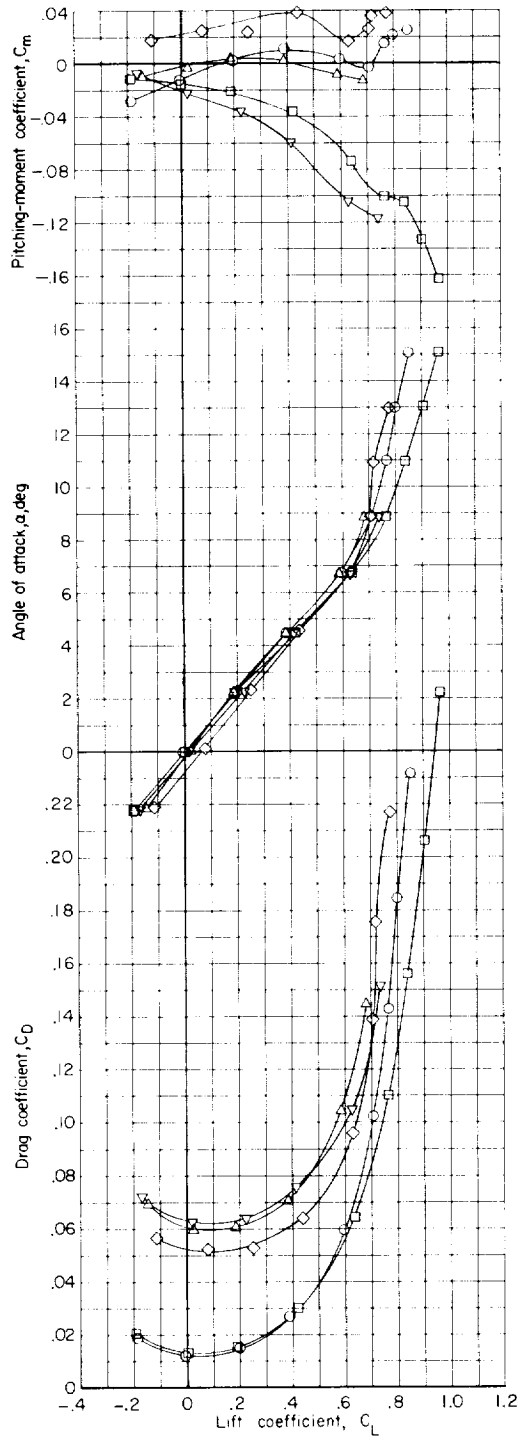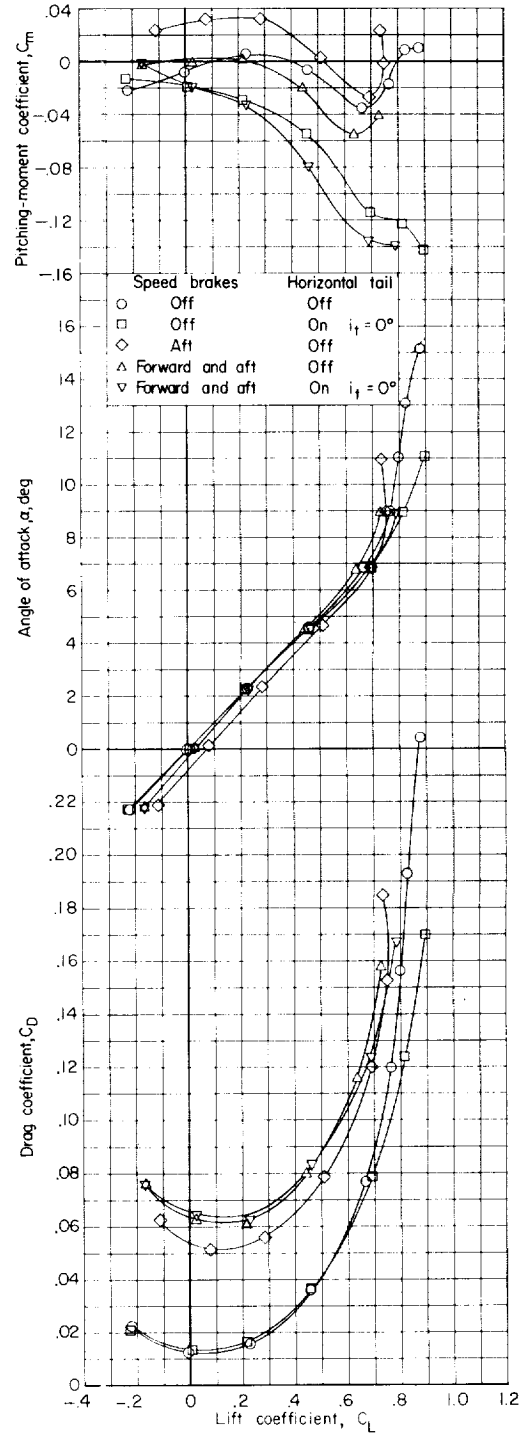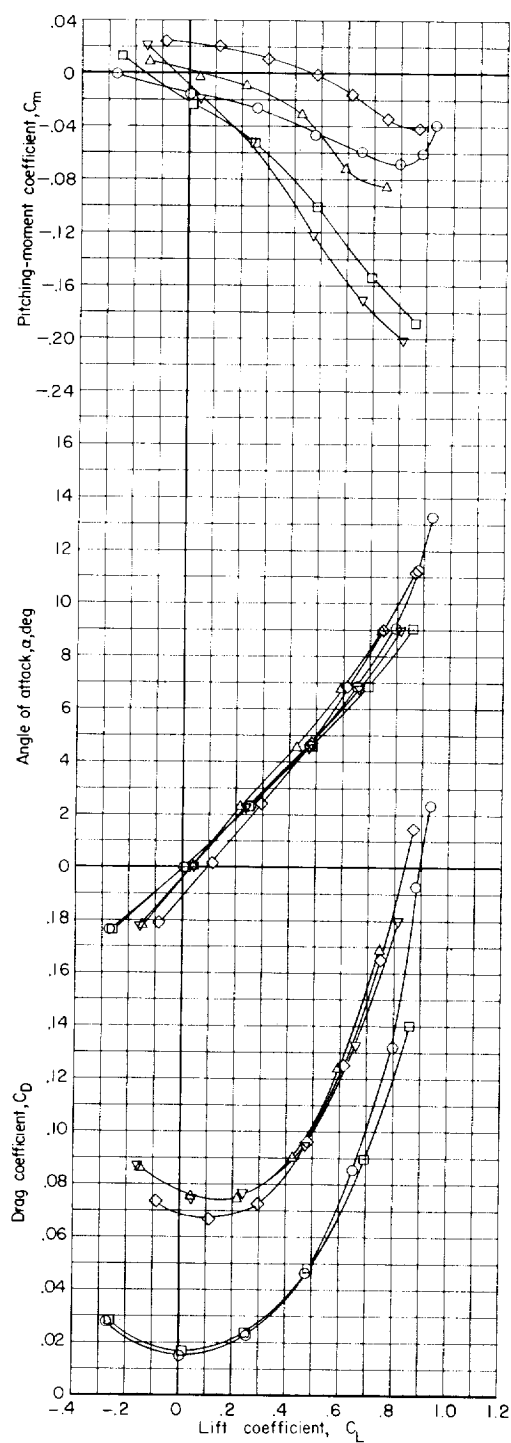
(e) M = 0.95.
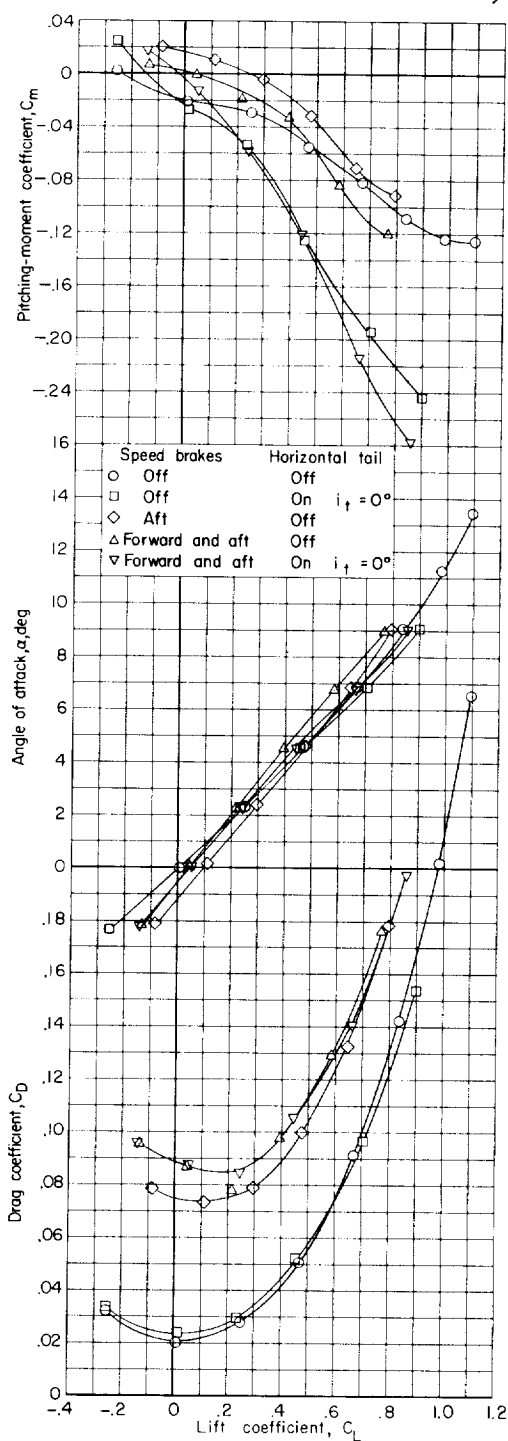
(f) M = 0.98.

Figure 20.- Continued.
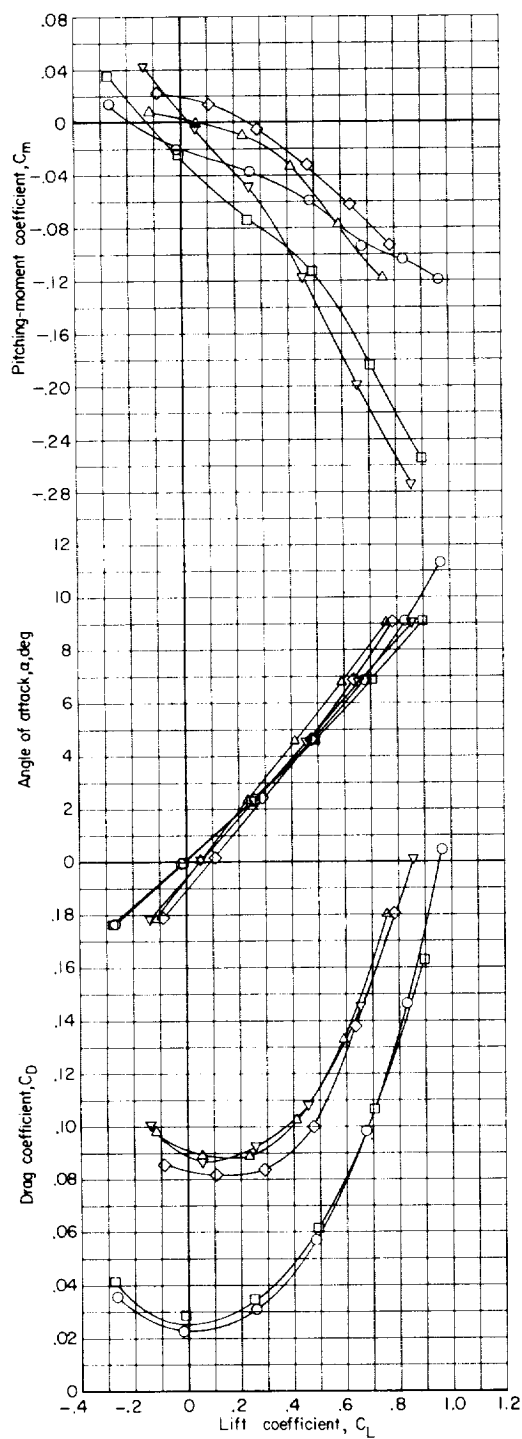
(g) M = 1.00.
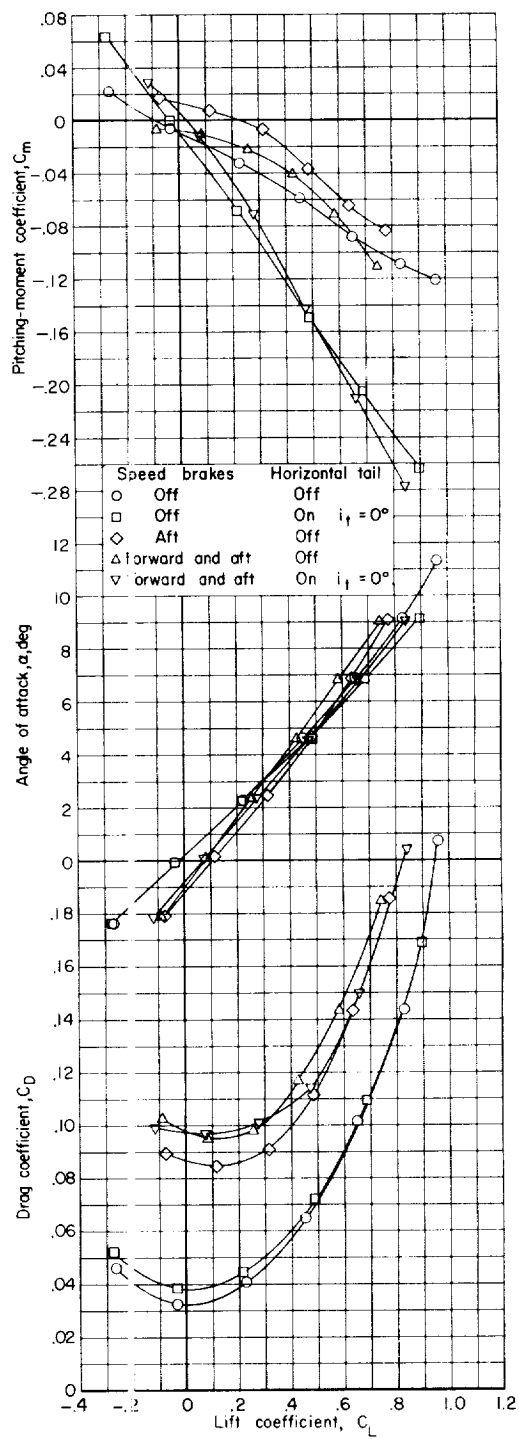
(h) M = 1.03.

Figure 20.- Continued.
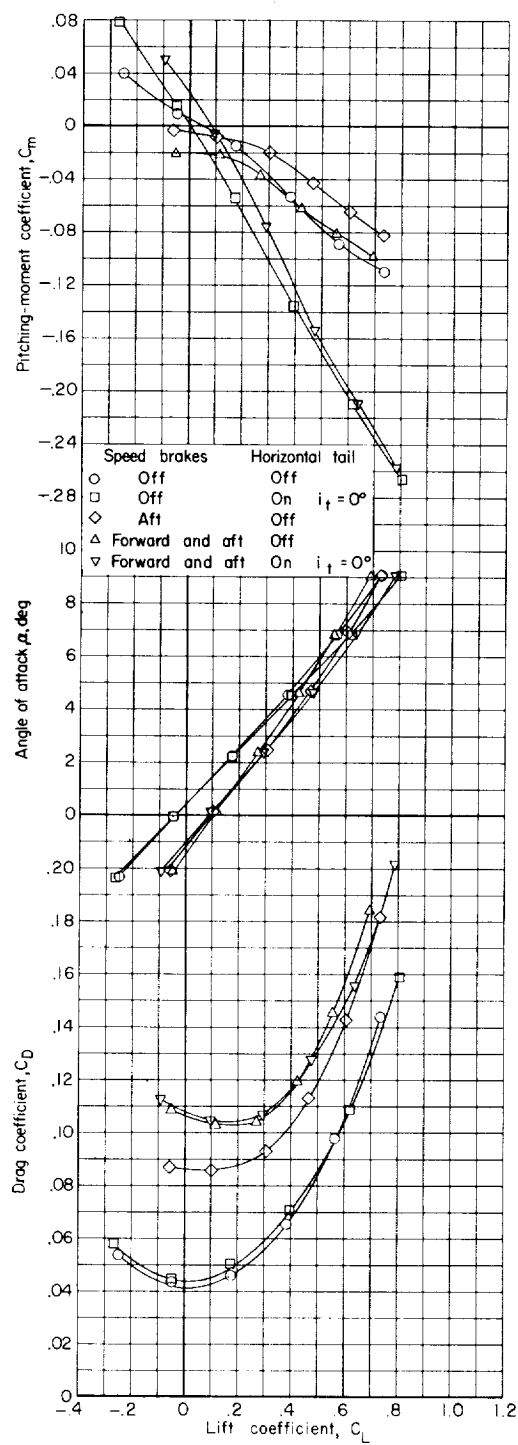
(i) M = 1.13.

Figure 20.- Concluded.
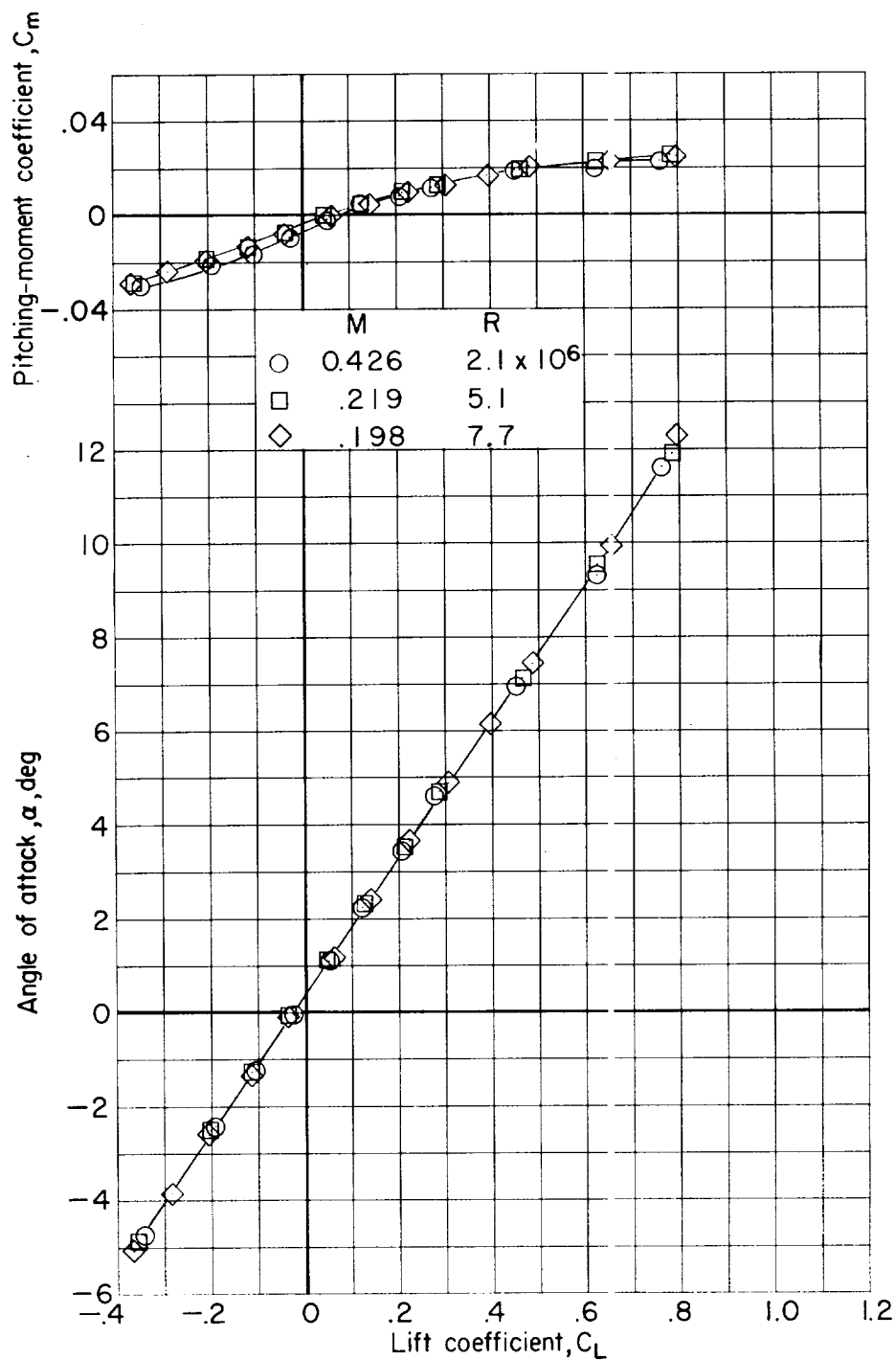
(a) M = 0.198, 0.219, and 0.426.

Figure 21.- Effects of Reynolds number and Mach number on the aerodynamic
characteristics in pitch of the basic model. Horizontal tail off.
Data from Langley low-turbulence pressure tunnel.
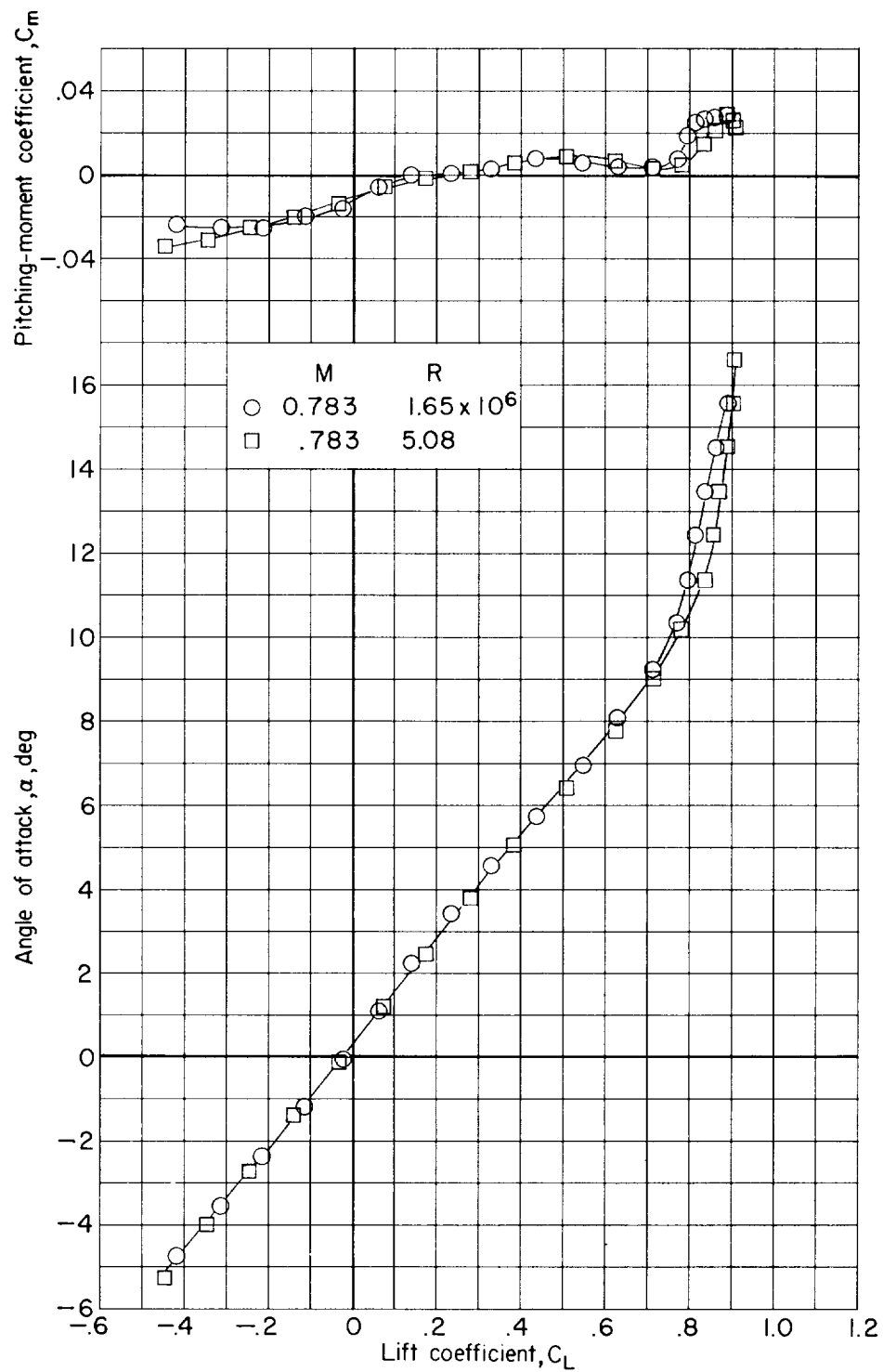
(b) M = 0.783.

Figure 21.- Concluded.
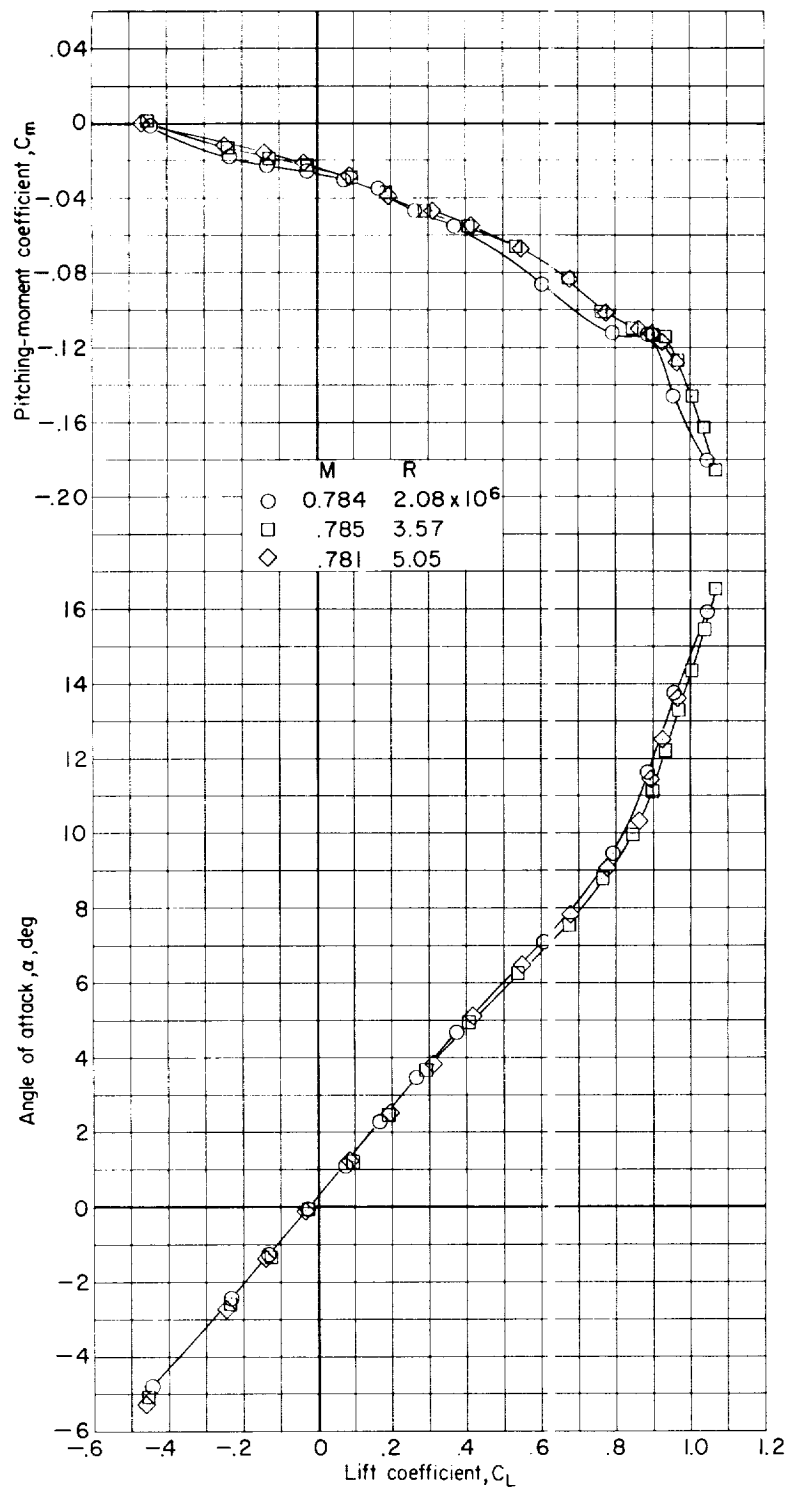
Figure 22.- Effects of Reynolds number on the aerodynamic characteristics in pitch of the basic model. Horizontal tail on. $i_t = 0°$. Data from Langley low-turbulence pressure tunnel.
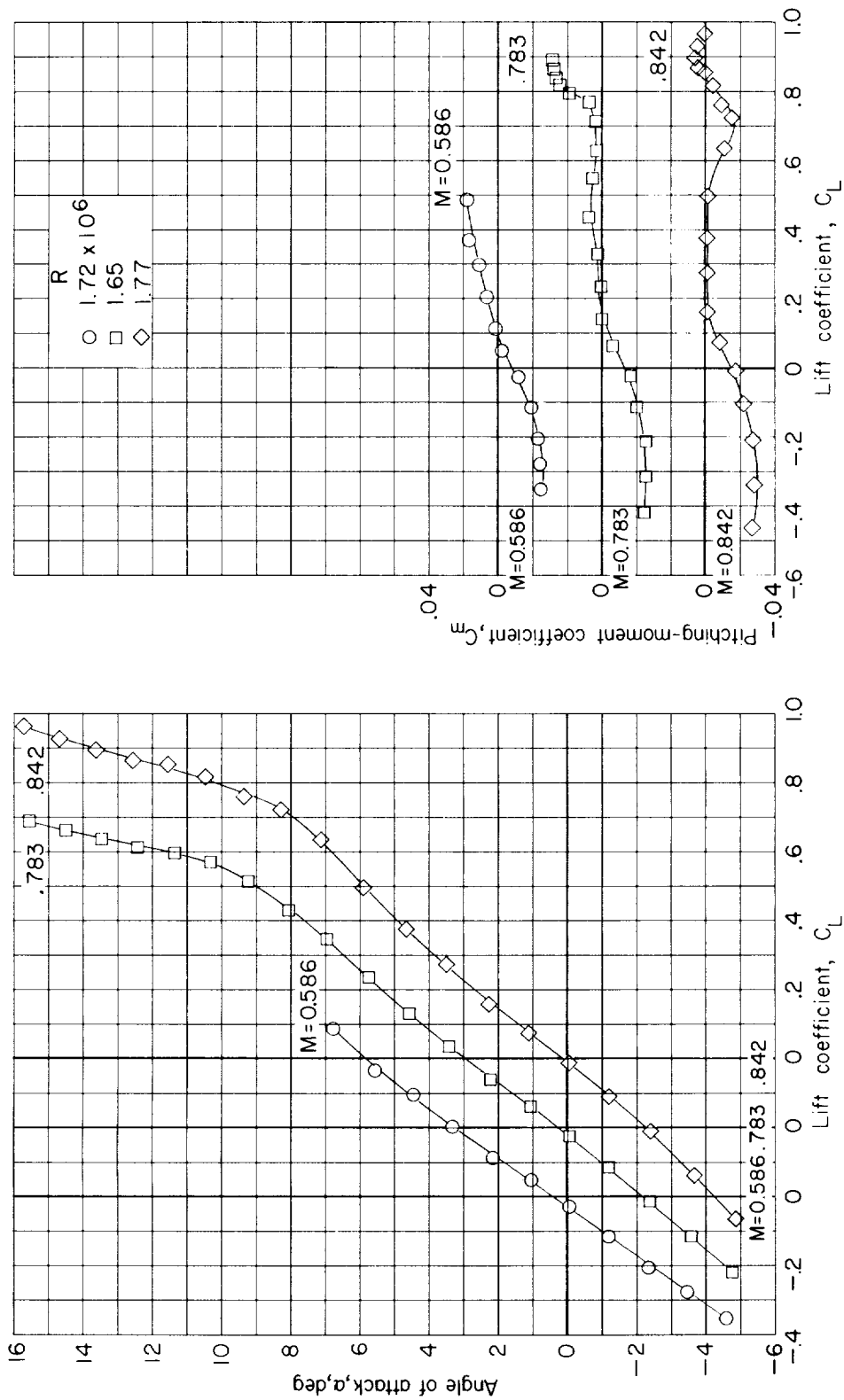
(a) Horizontal tail off.

Figure 23.- Effects of Mach number on the aerodynamic characteristics in pitch of the basic model. Data from Langley low-turbulence pressure tunnel.

80
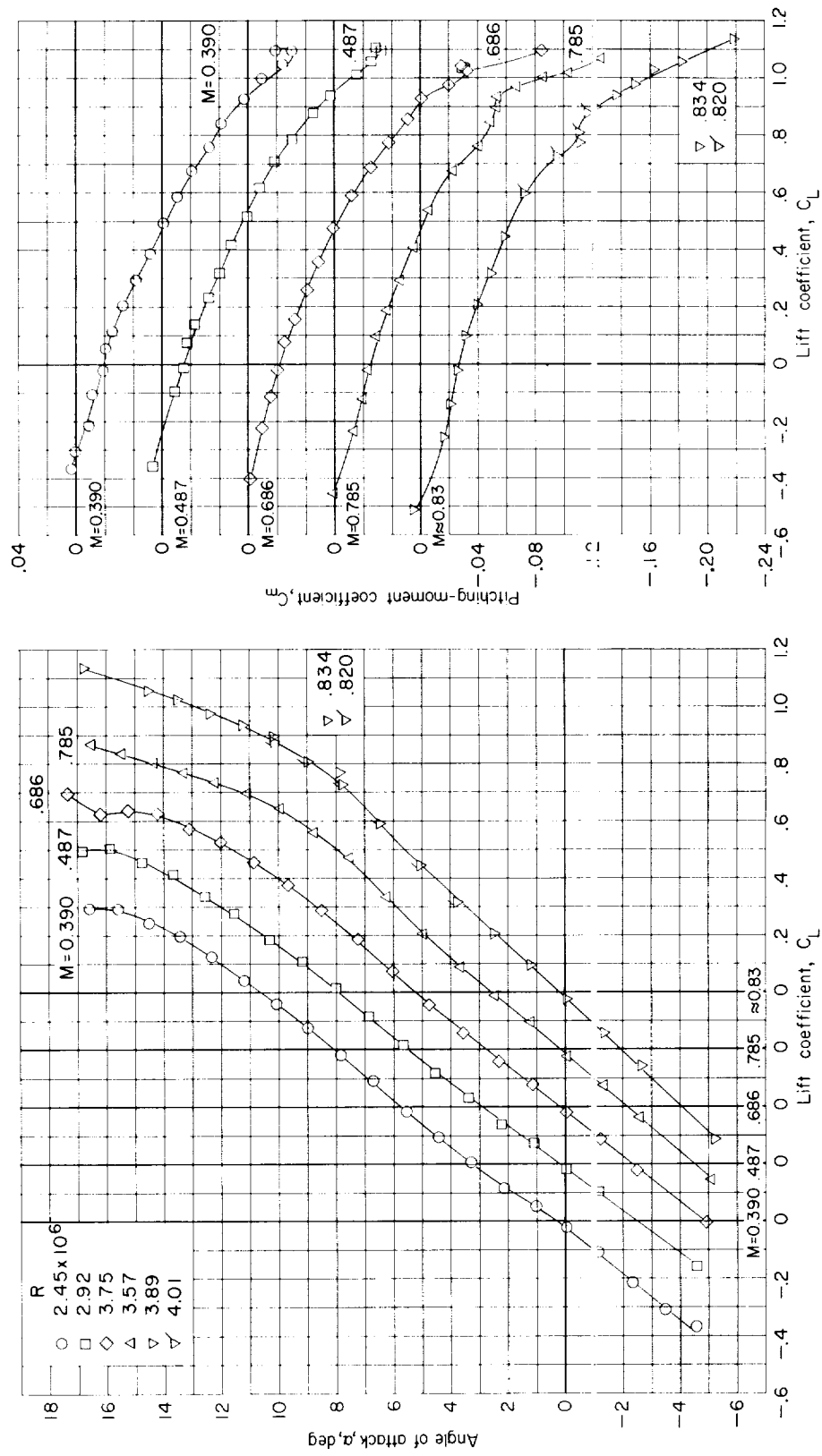
(b) Horizontal tail on. $i_t = 0°$.

Figure 23.- Concluded.
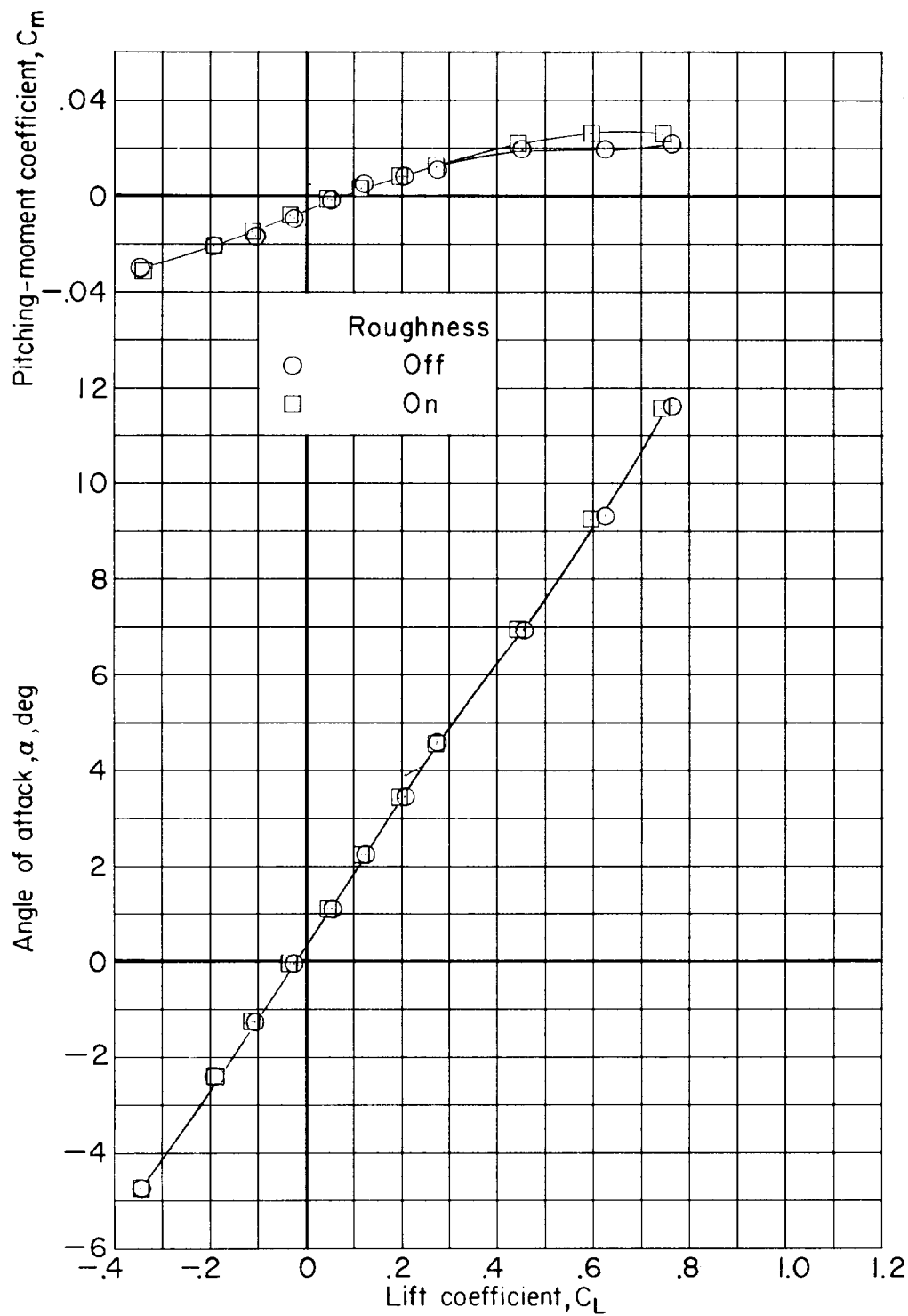
Figure 24.- Effects of leading-edge roughness on the aerodynamic charac-
teristics in pitch of the basic model. Horizontal tail off. M = 0.426;
R = 2.1 × 10^6. Data from Langley low-turbulence pressure tunnel.
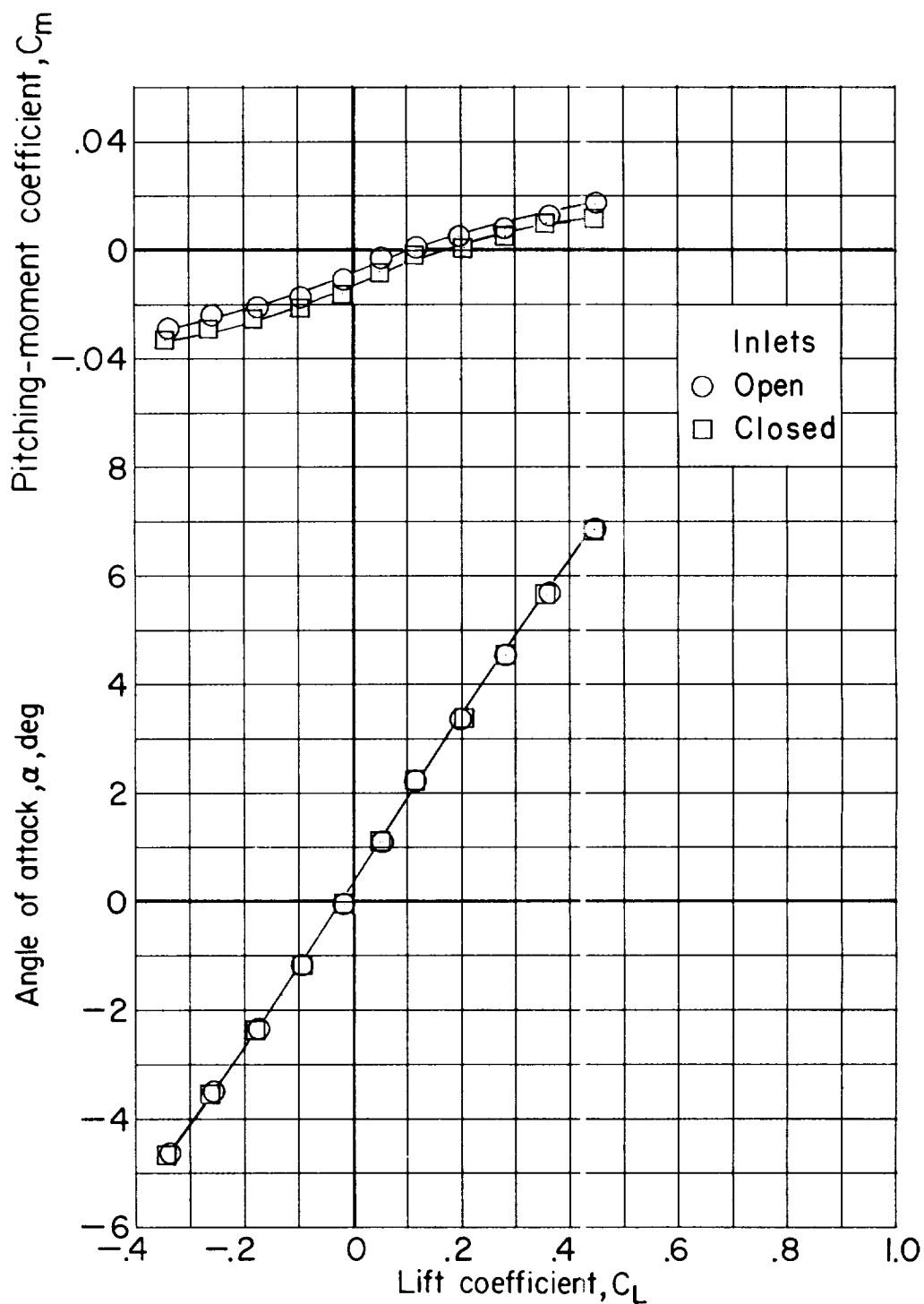
Figure 25.- Effects of closed inlets on the aerodynamic characteristics in pitch of the basic model. Horizontal tail off. M = 0.441; R = 1.6 × 10^6. Data from Langley low-turbulence pressure tunnel.

Wing modification	Fence
Cambered	Off
Cambered	On
Symmetrical	Off
.10-chord leading- edge chord extension	Off

O   4-ft data
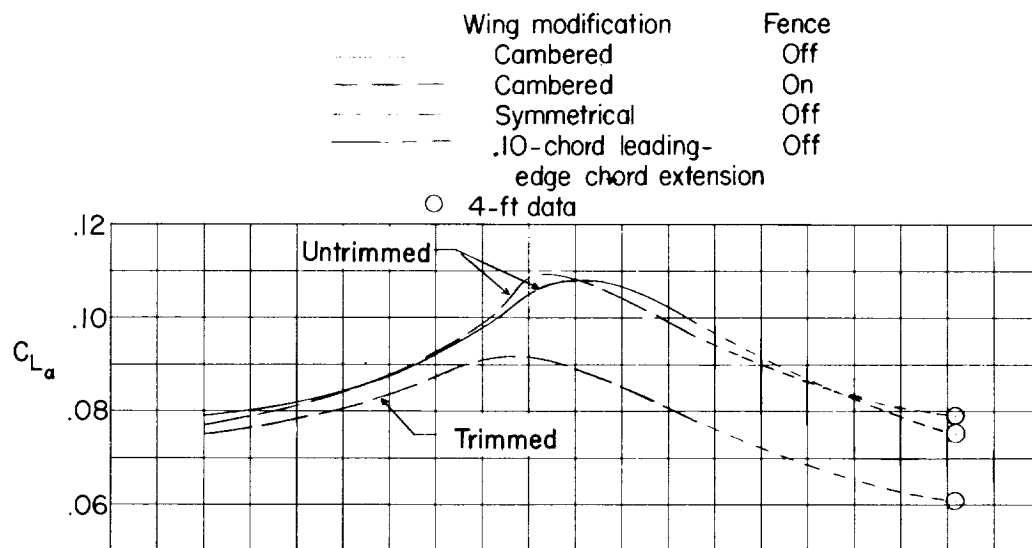
(a) Effect of wing fences.
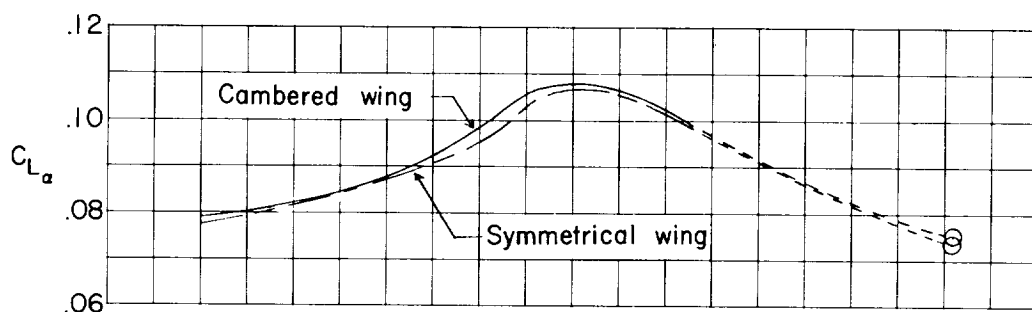
(b) Effect of wing section.
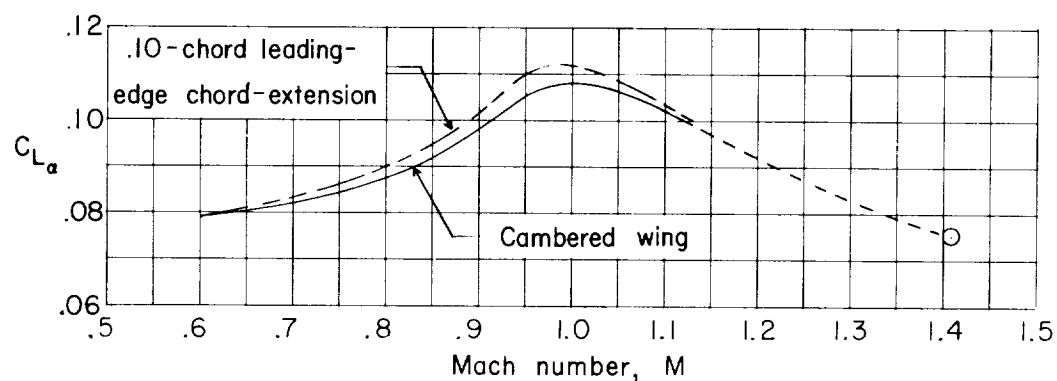
Mach number, M

(c) Effect of leading-edge chord-extension.

Figure 26.- Variation with Mach number of the lift-curve slope for various configurations.
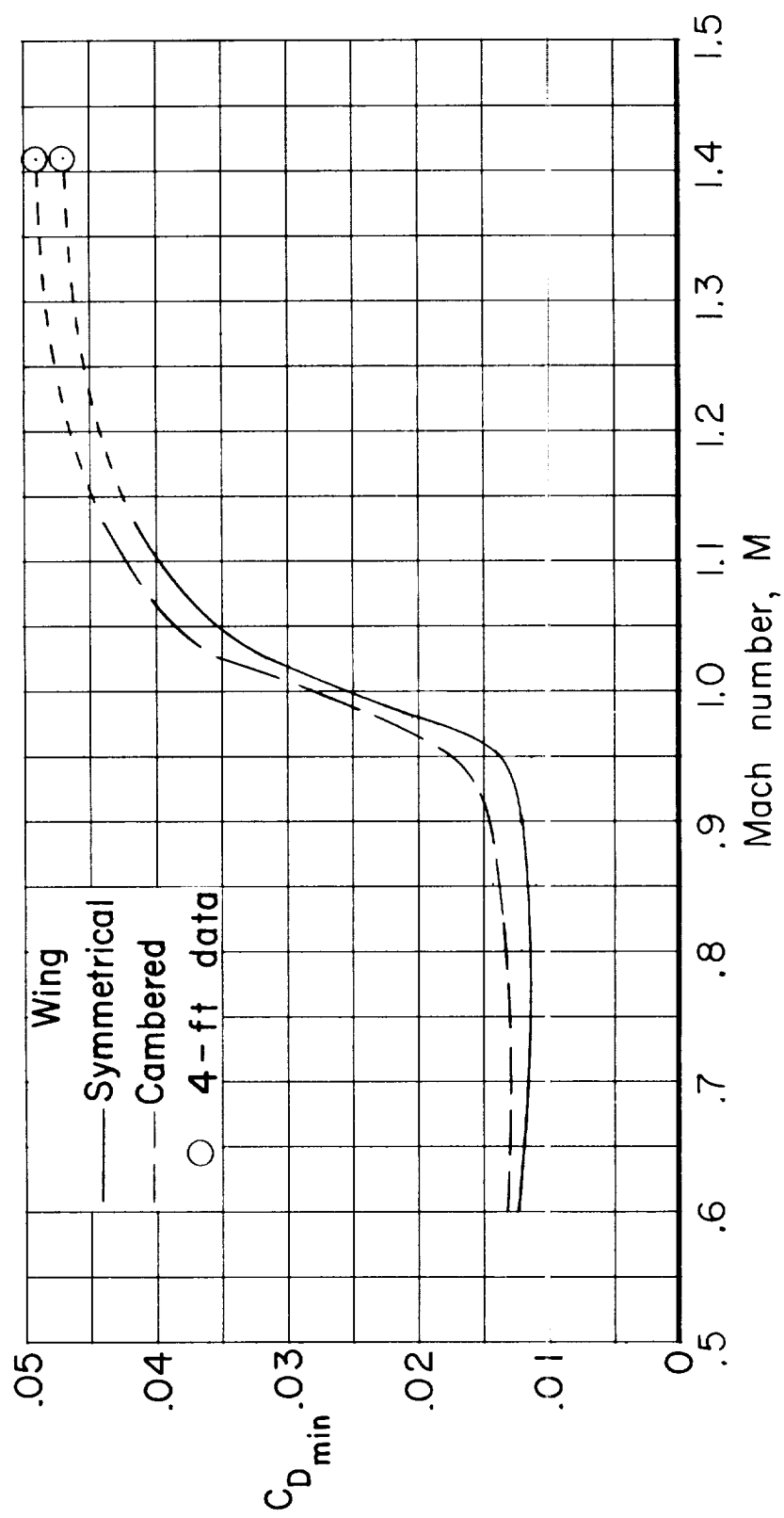
Figure 27.- Comparison of the minimum drag coefficients for the model with cambered wing and symmetrical wing sections. $i_t = 0°$.
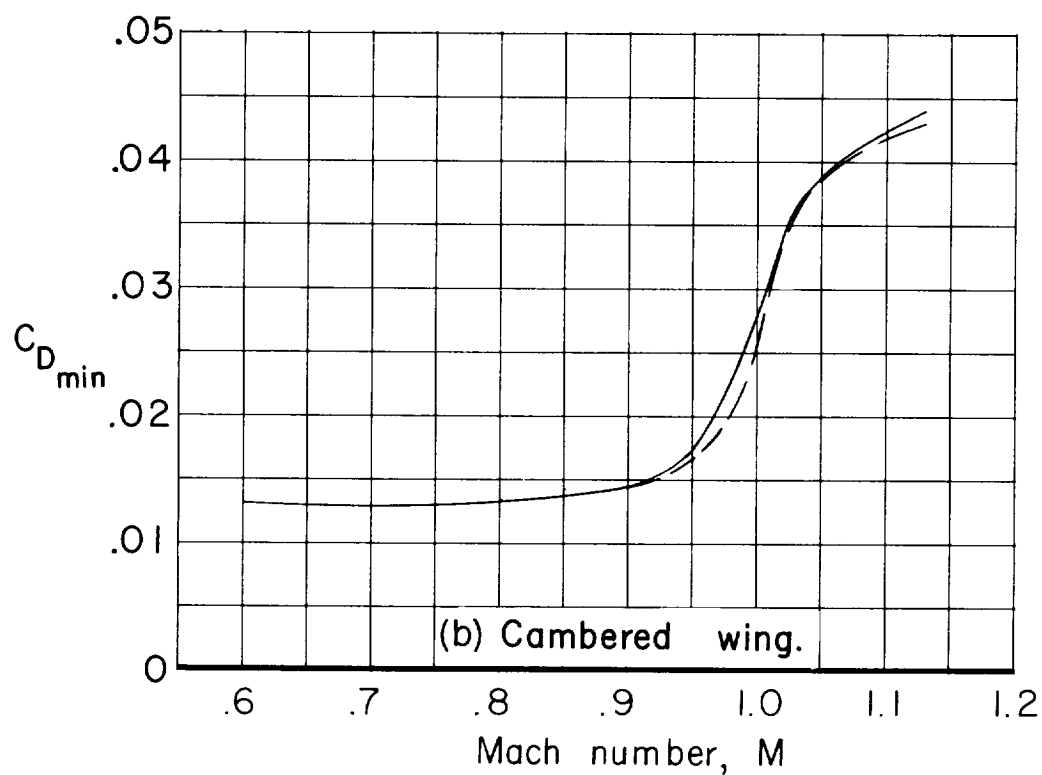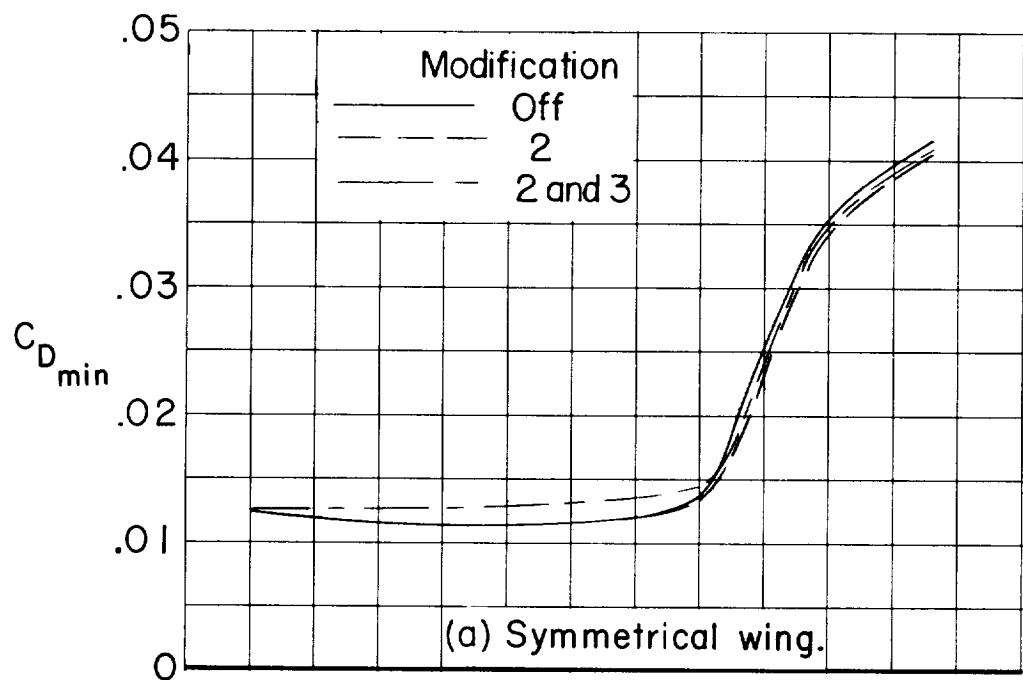
Figure 28.- Variation with Mach number of the minimum drag coefficients for various body modifications. $i_t = 0°$.
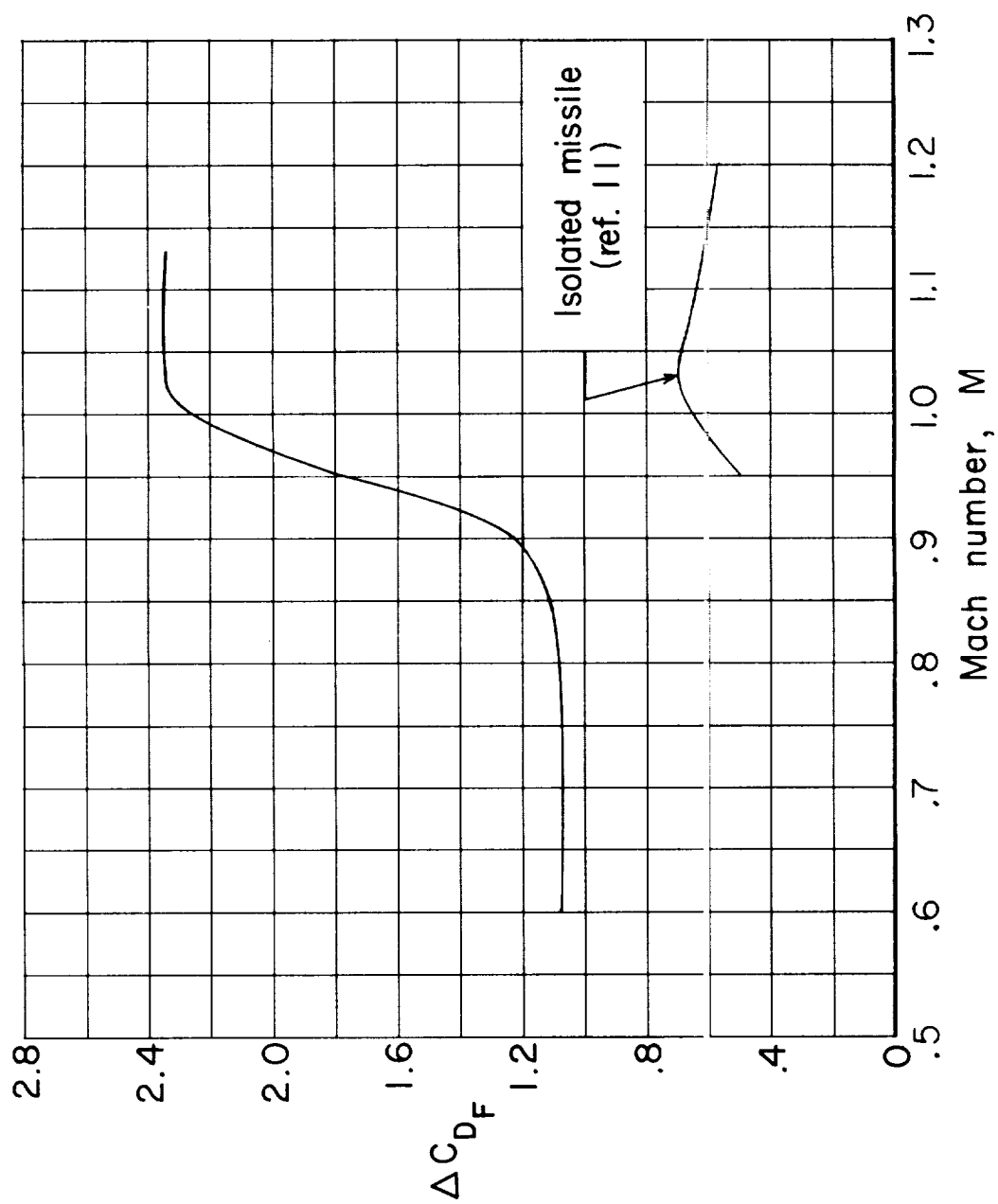
Figure 29.- Variation with Mach number of incremental drag coefficient of air-to-air missiles.
$C_L = 0$.
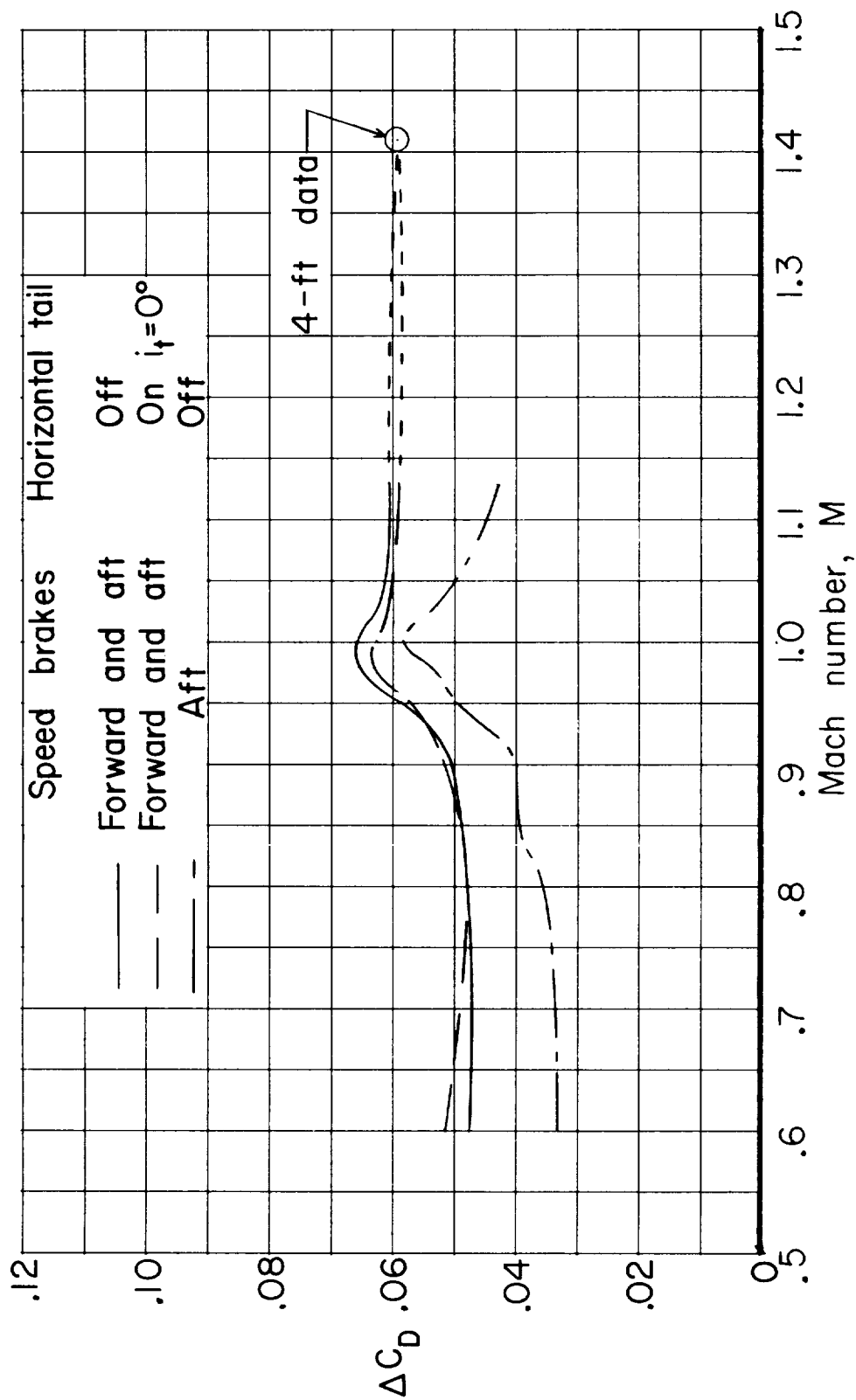
Figure 30.- Variation with Mach number of incremental drag coefficient produced by speed brakes. $\alpha = 0^{\circ}$.
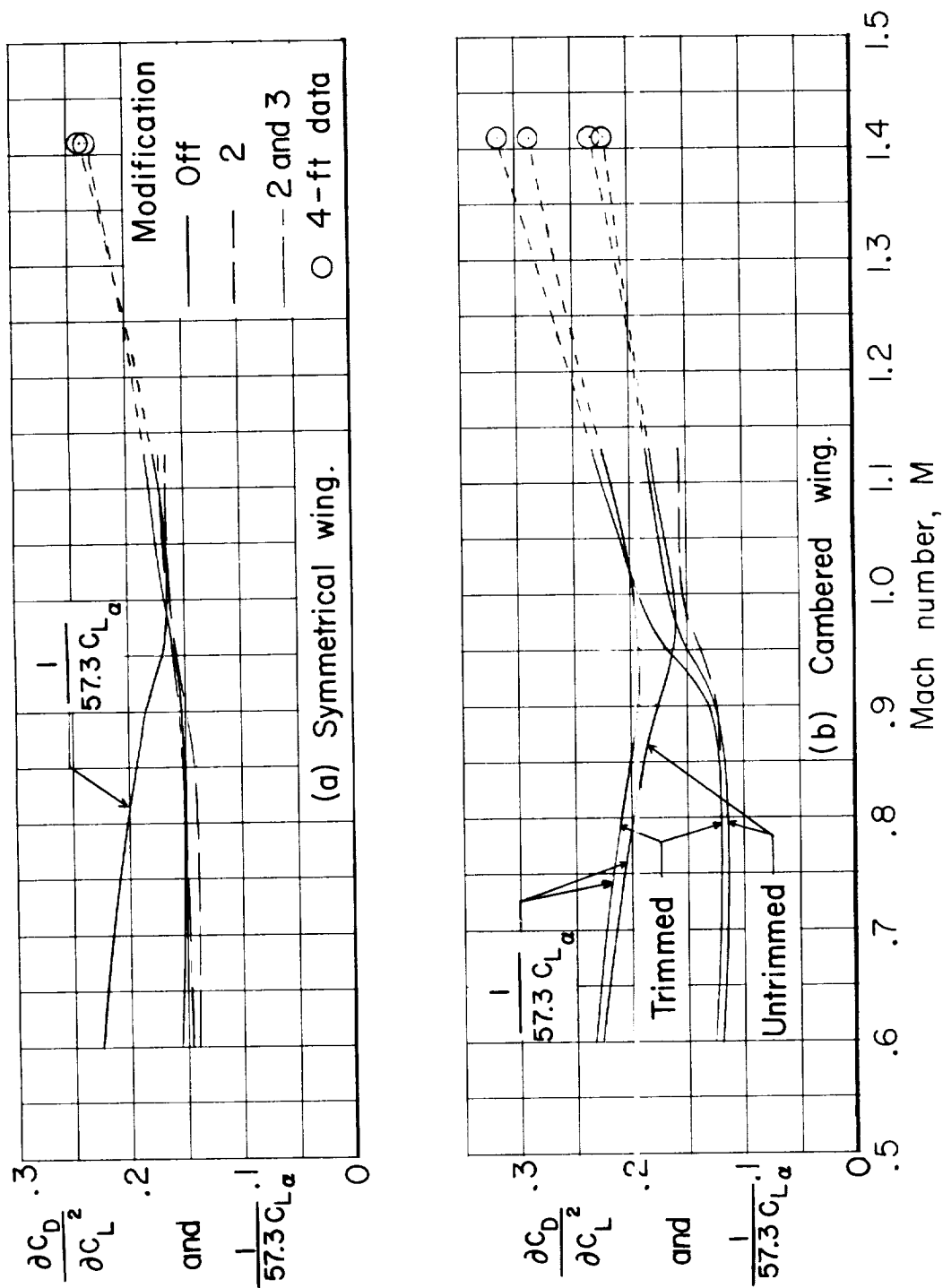
Figure 31.- Variation with Mach number of drag-due-to-lift parameter for various configurations. $C_L = 0.2$ to 0.4.

Figure 33.- Variation with Mach number of the max-
imum trim lift-drag ratio and of the trim lift-
drag ratio in level flight for sea level and
35,000 feet altitude for W/S = 64 pounds per
square foot.

Figure 32.- Variation with lift coef-
ficient of the trim lift-drag ratio
at various Mach numbers for the basic
model.
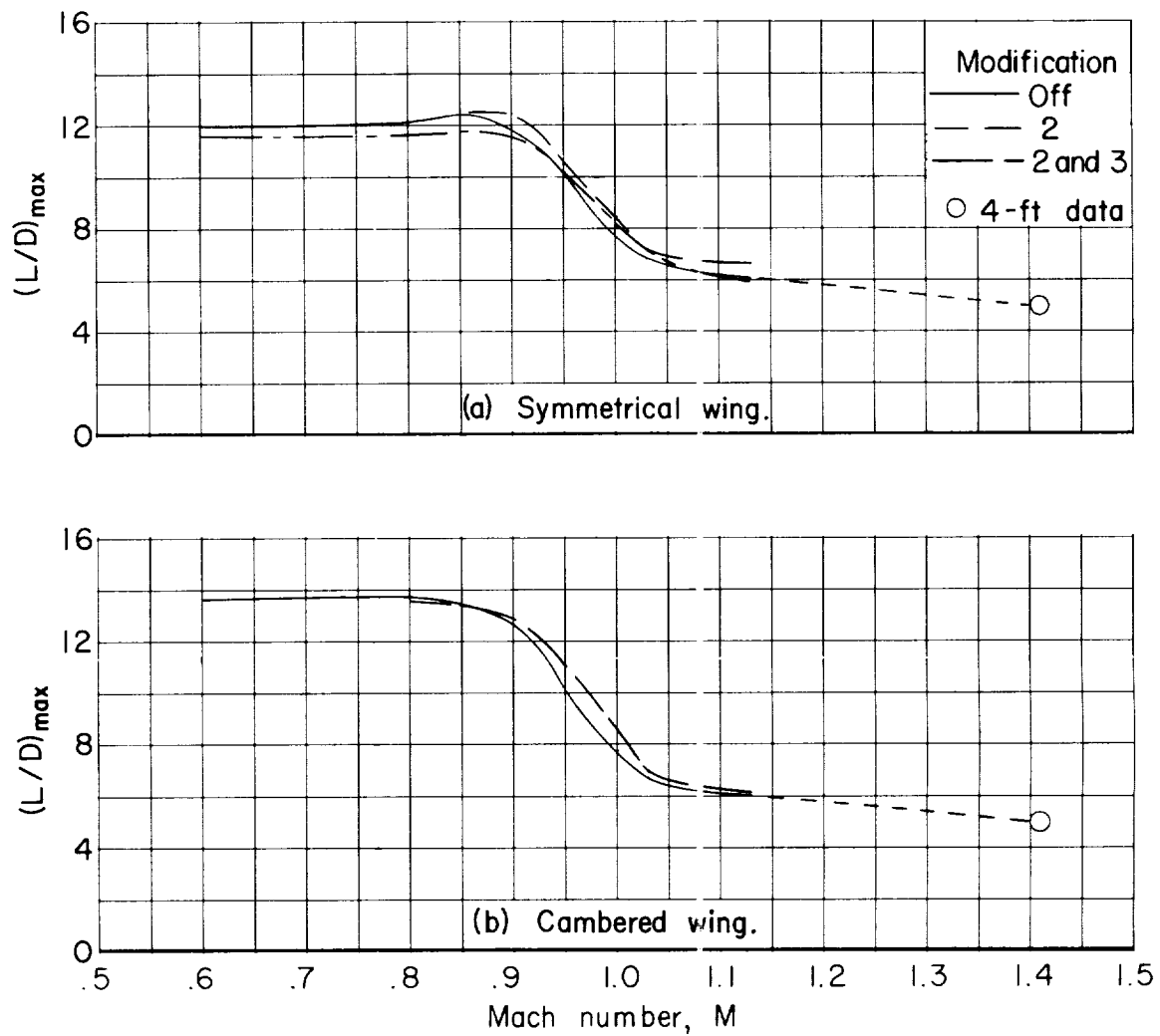
Figure 34.- Variation with Mach number of maximum lift-drag ratio for various configurations. Untrimmed model. $i_t = 0°$.
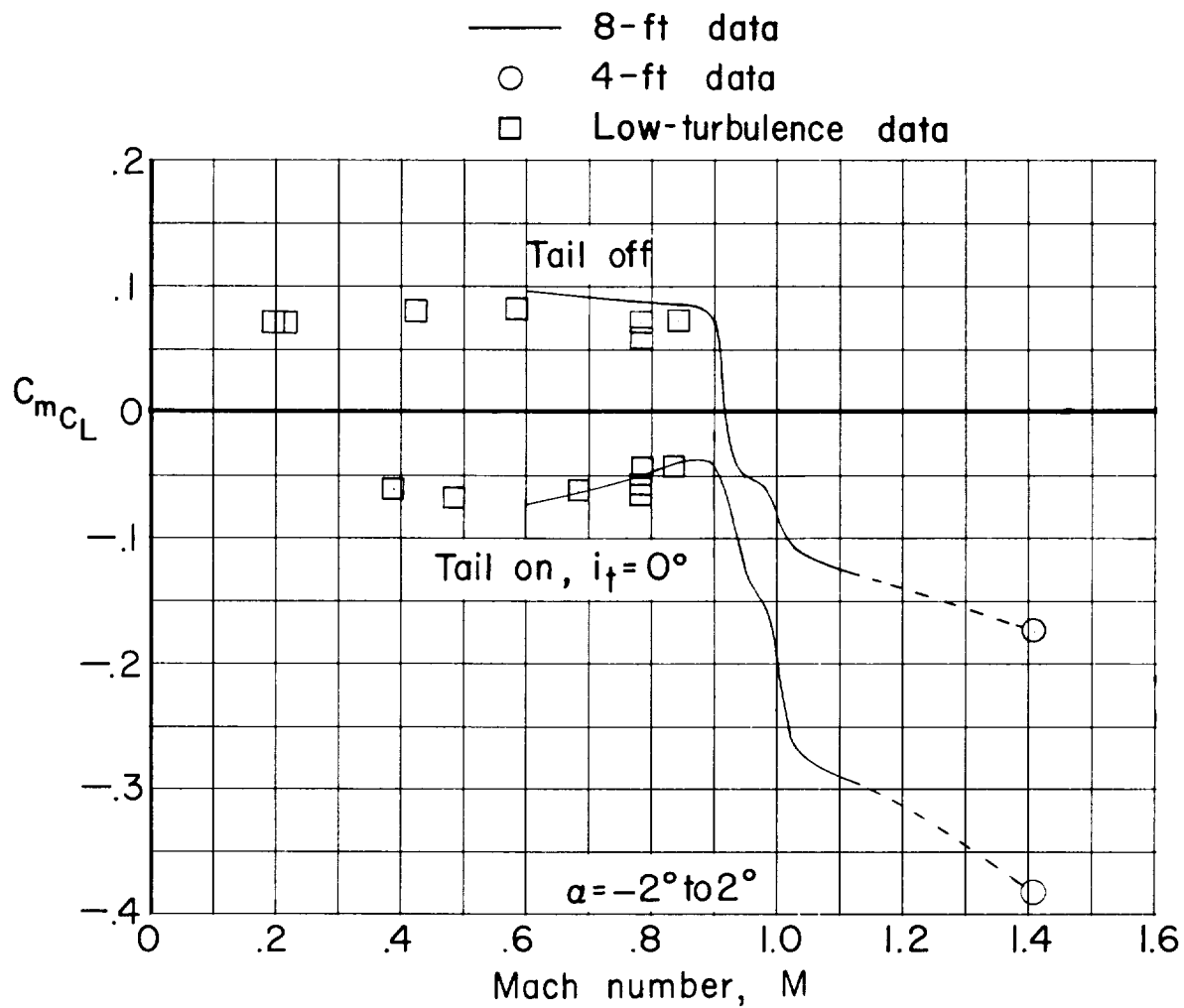
Figure 35.- Variation with Mach number of static-longitudinal-stability parameter for the basic configuration.
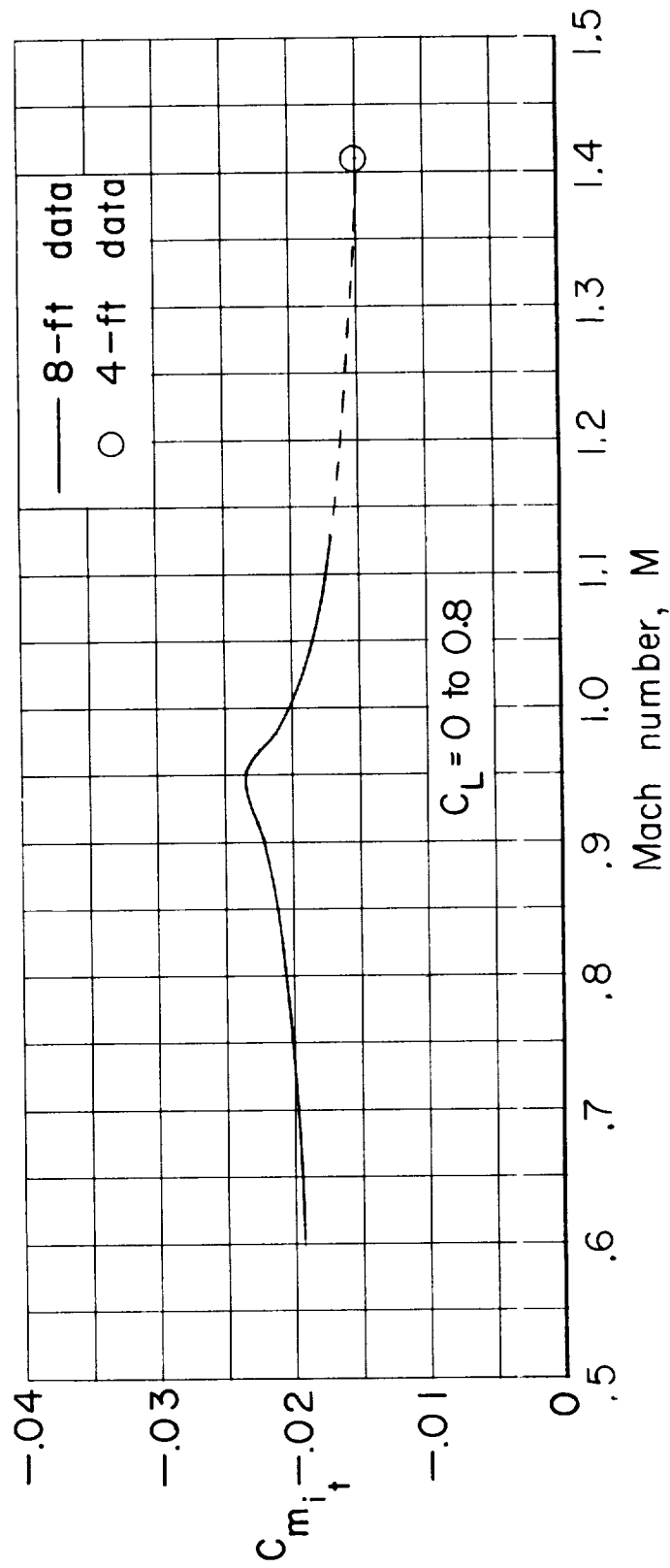
Figure 36.- Variation with Mach number of the stabilizer-effectiveness parameter for the basic model.
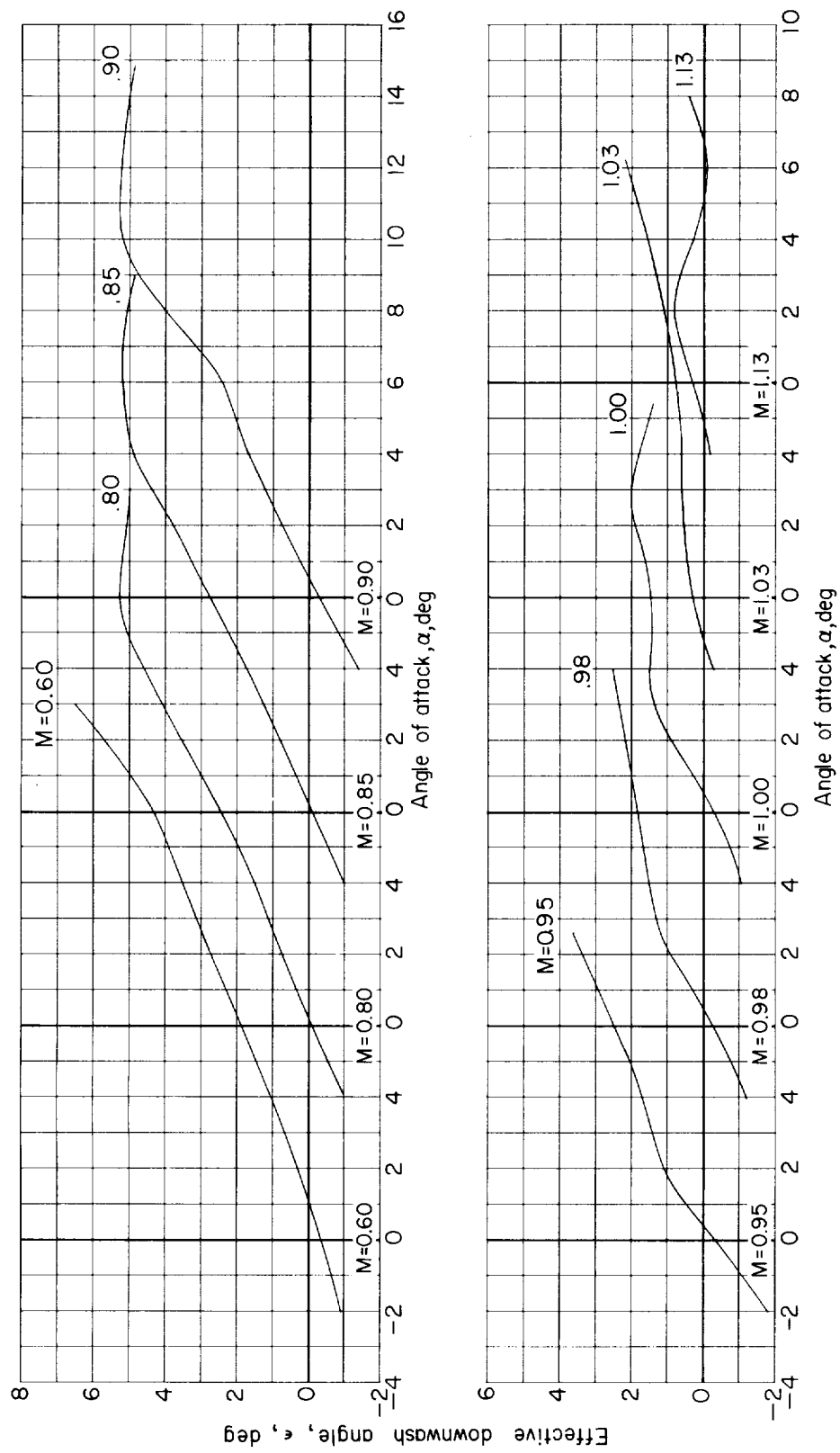
Figure 37.- Variation with angle of attack of the effective downwash angle for the basic model.
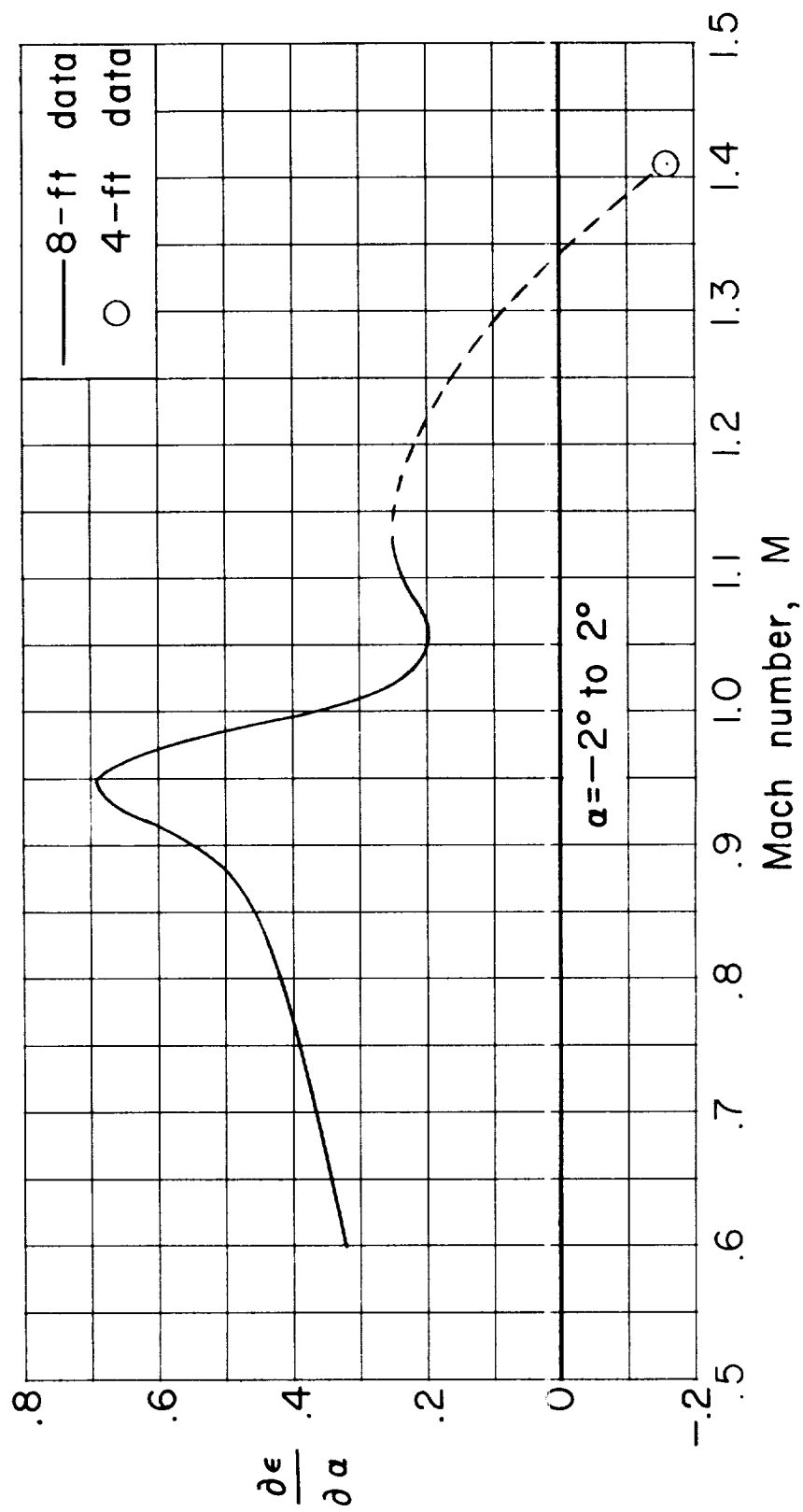
Figure 38.- Variation with Mach number of the rate of change of effective downwash angle with angle of attack for the basic model.
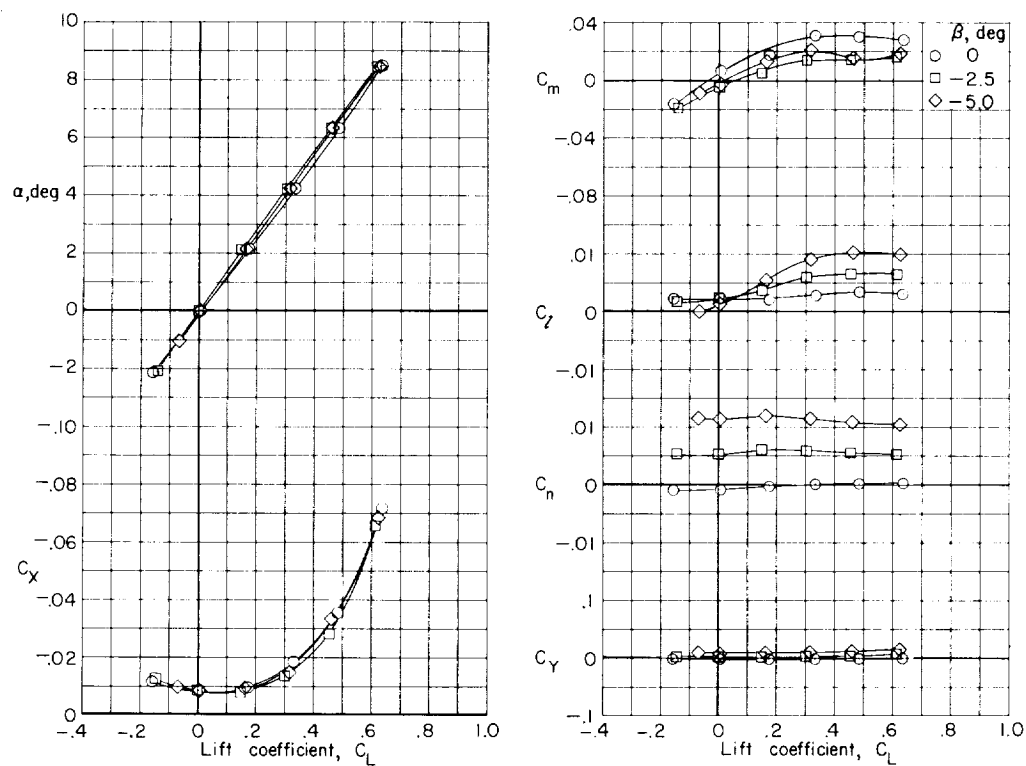
(a) M = 0.60.

Figure 39.- Variation with lift coefficient of the aerodynamic character-
istics of the basic model for various angles of sideslip. Vertical
and horizontal tails off.

96
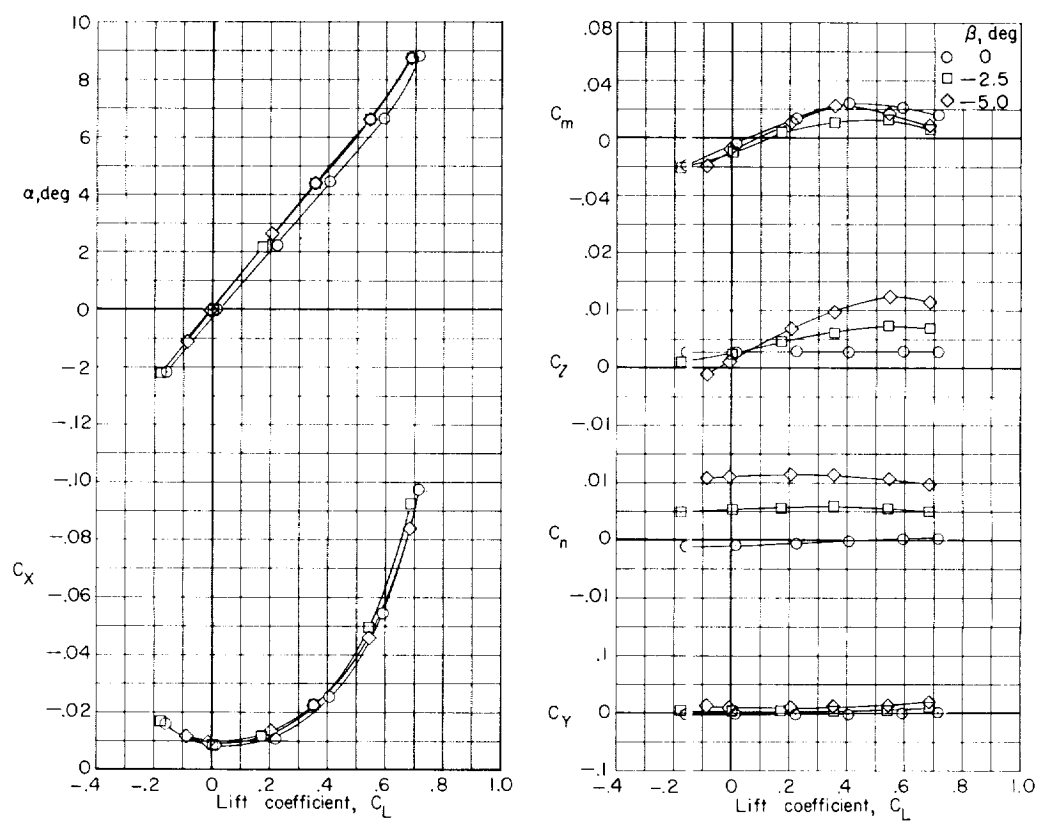
(b)   M = 0.80.

Figure 39.- Continued.
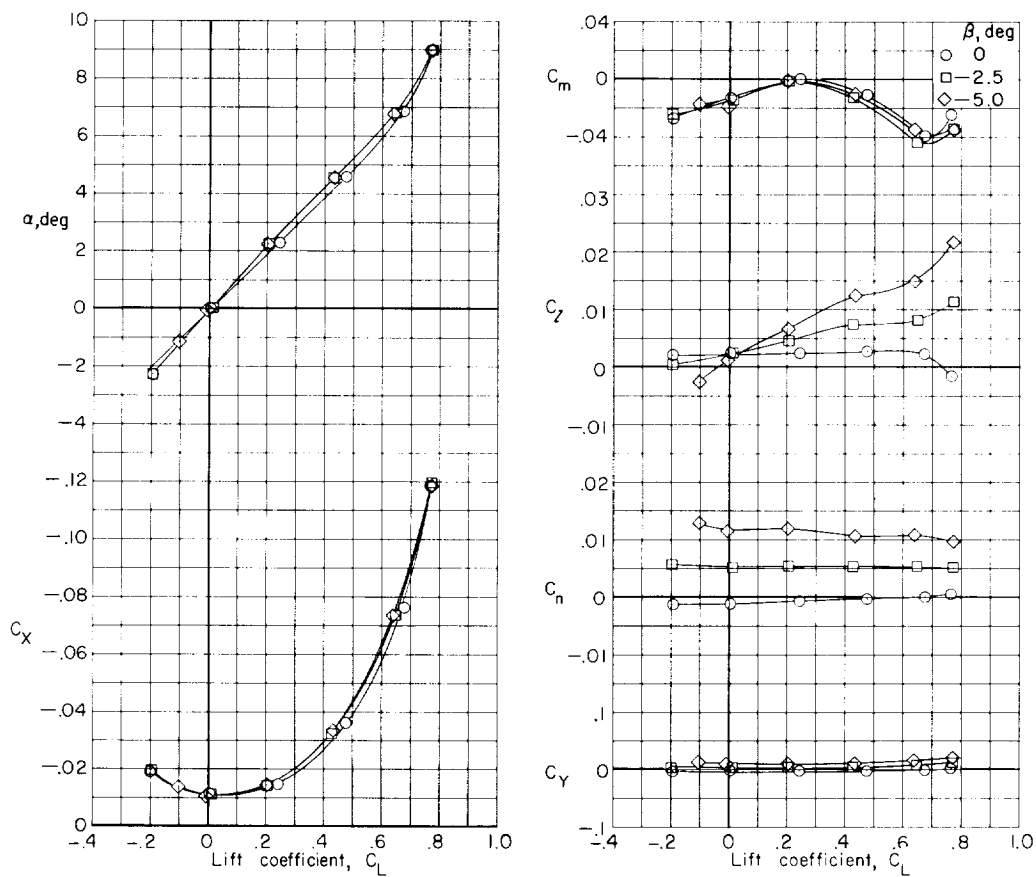
(c) M = 0.90.

Figure 39.- Continued.
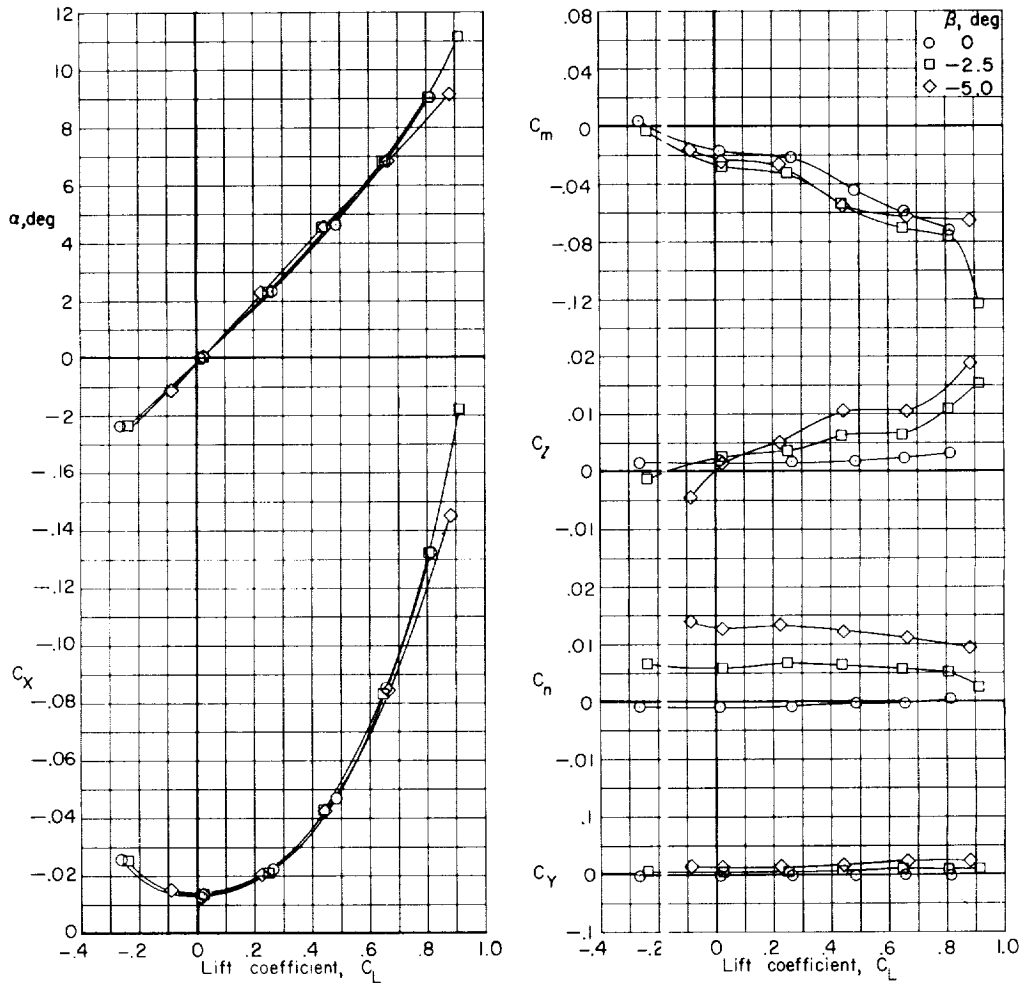
(d) M = 0.95.

Figure 39.- Continued.
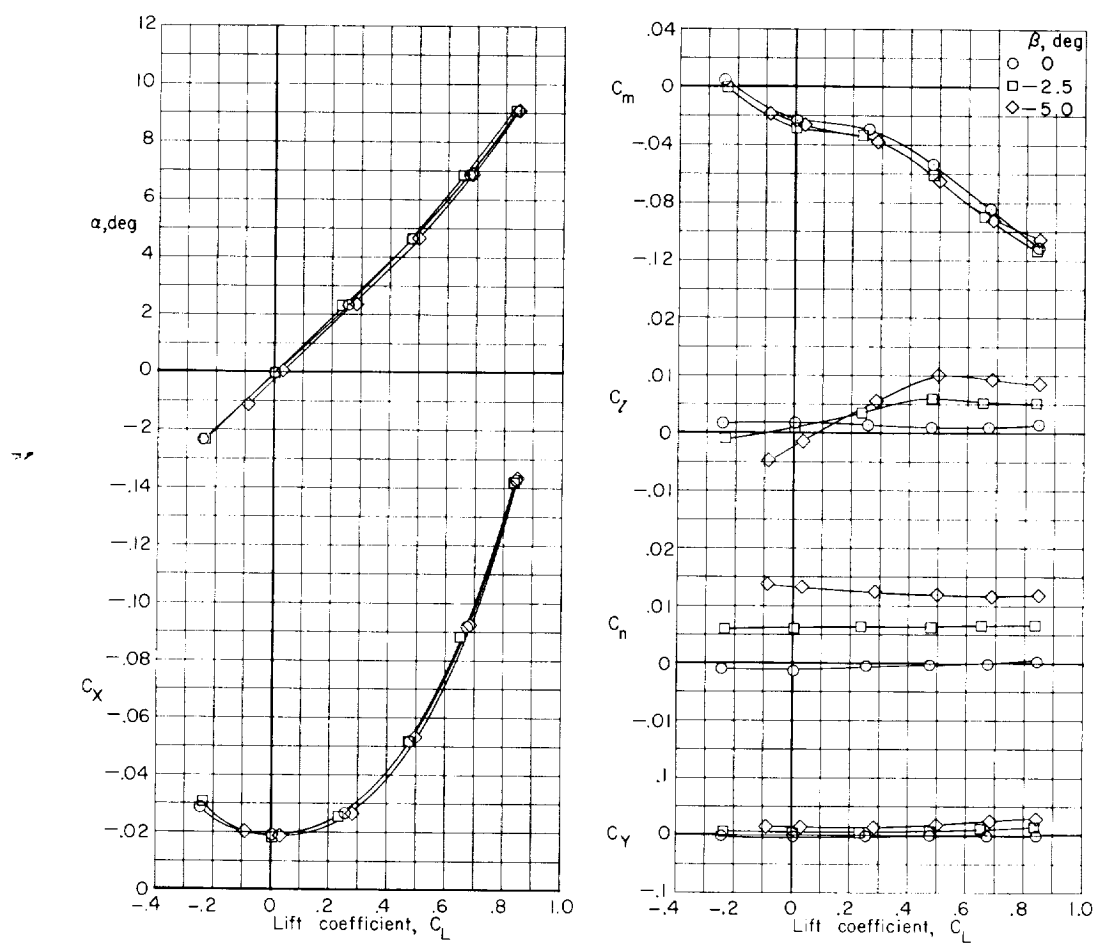
(e)   M = 0.98.

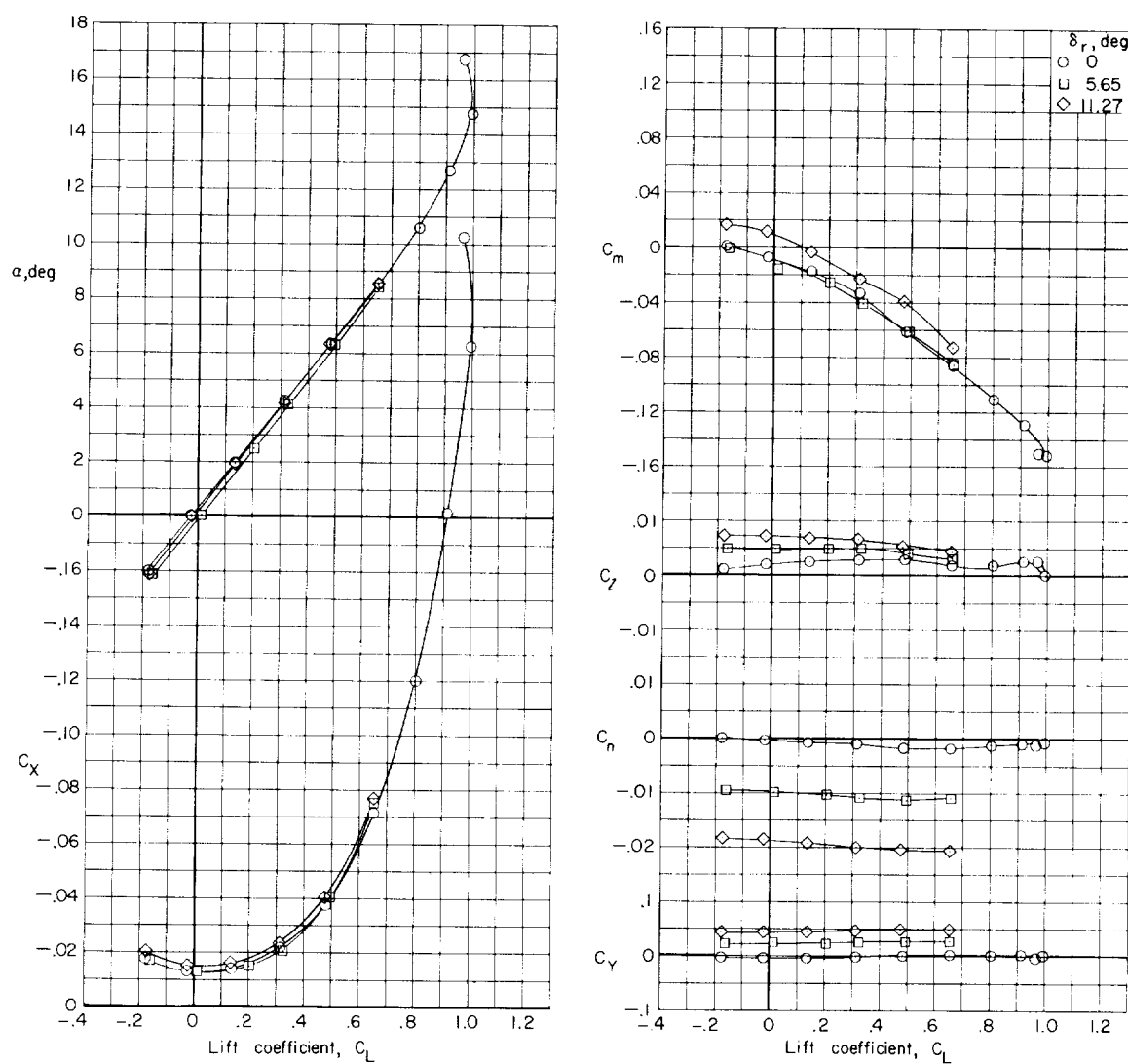Figure 39.- Continued.
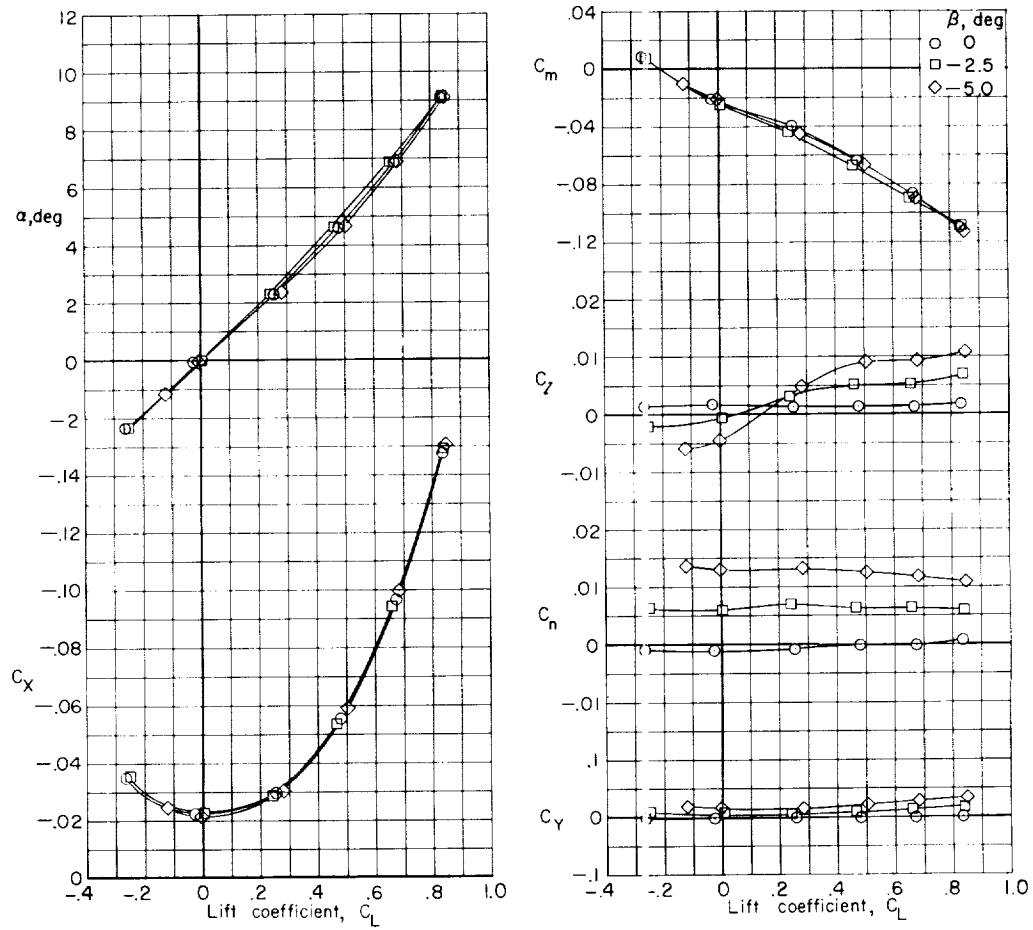
(f) M = 1.00

Figure 39.- Continued.
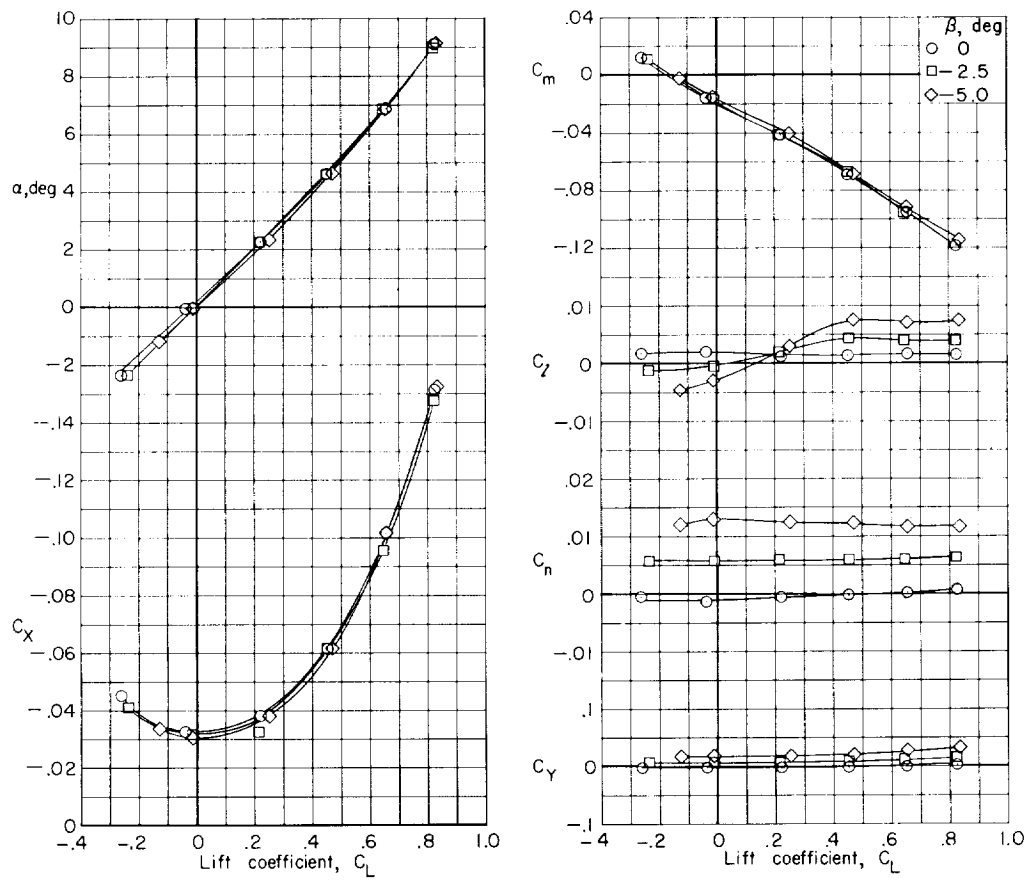
(g)   M = 1.03.

Figure 39.- Continued.
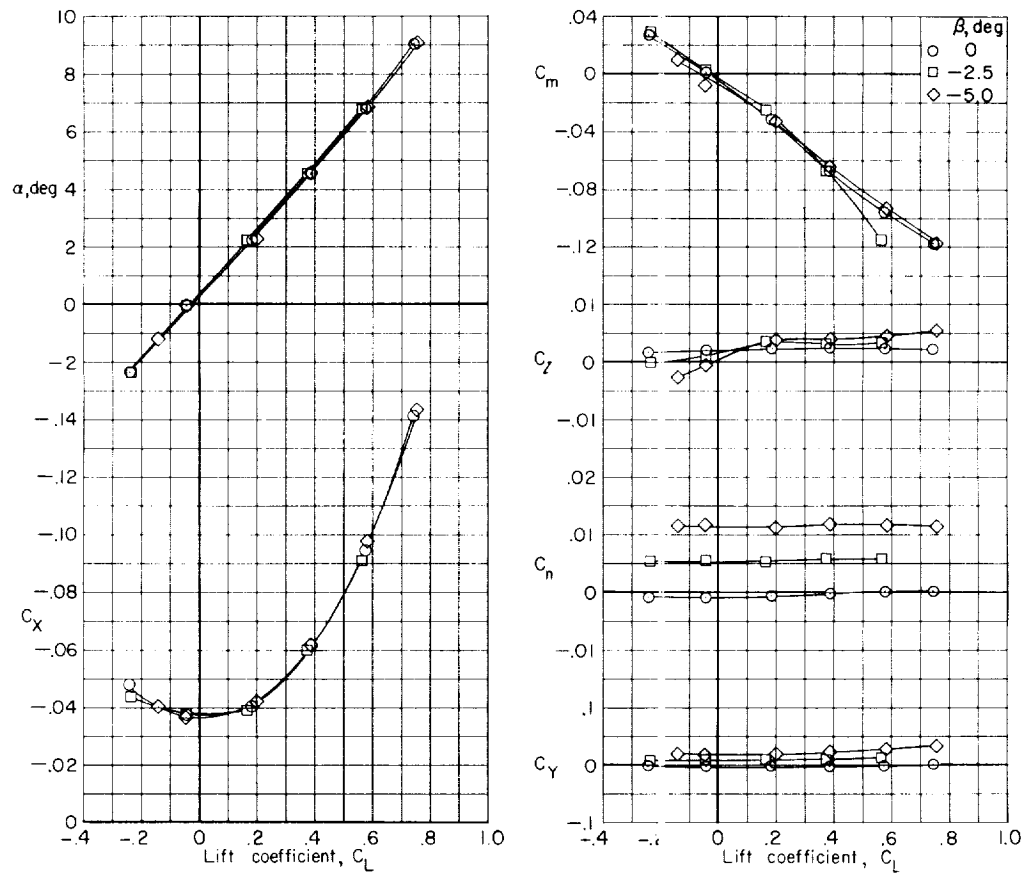
(h) M = 1.13.

Figure 39.- Concluded.
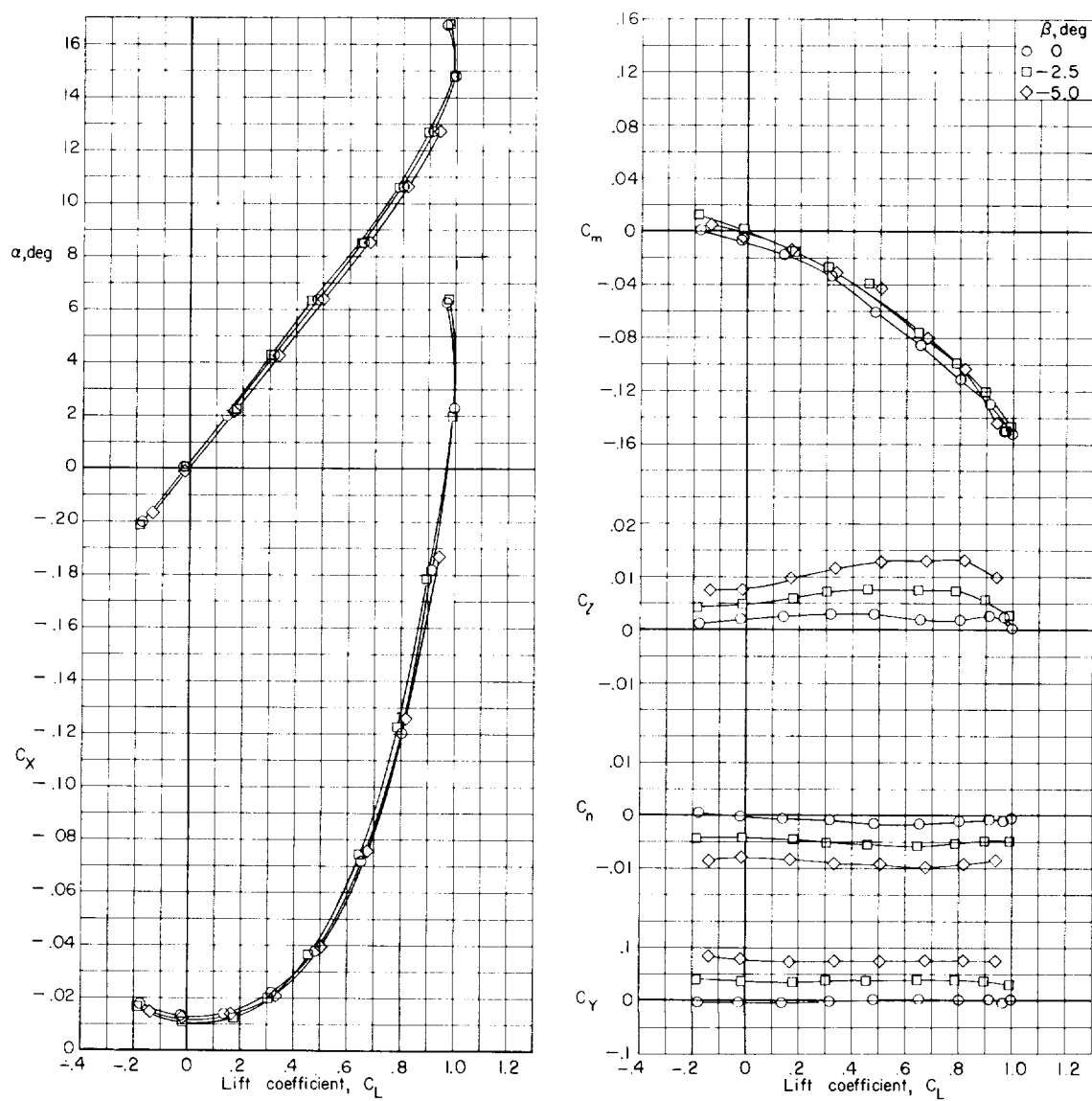
(a) M = 0.60.

Figure 40.- Variation with lift coefficient of the aerodynamic character-
istics of the basic model for various angles of sideslip. Vertical
and horizontal tails on. i_t = 0°.
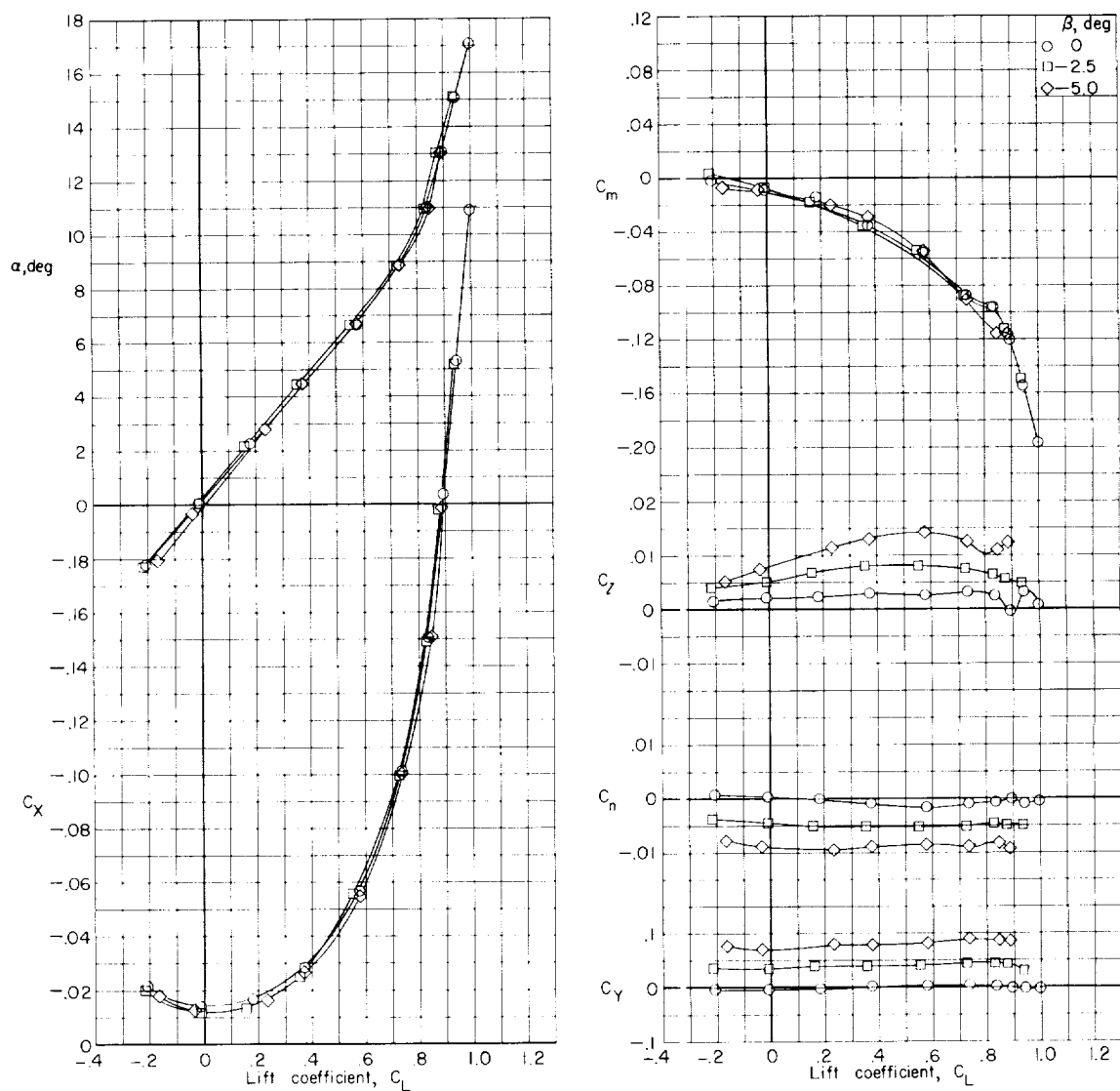
(b) M = 0.80.

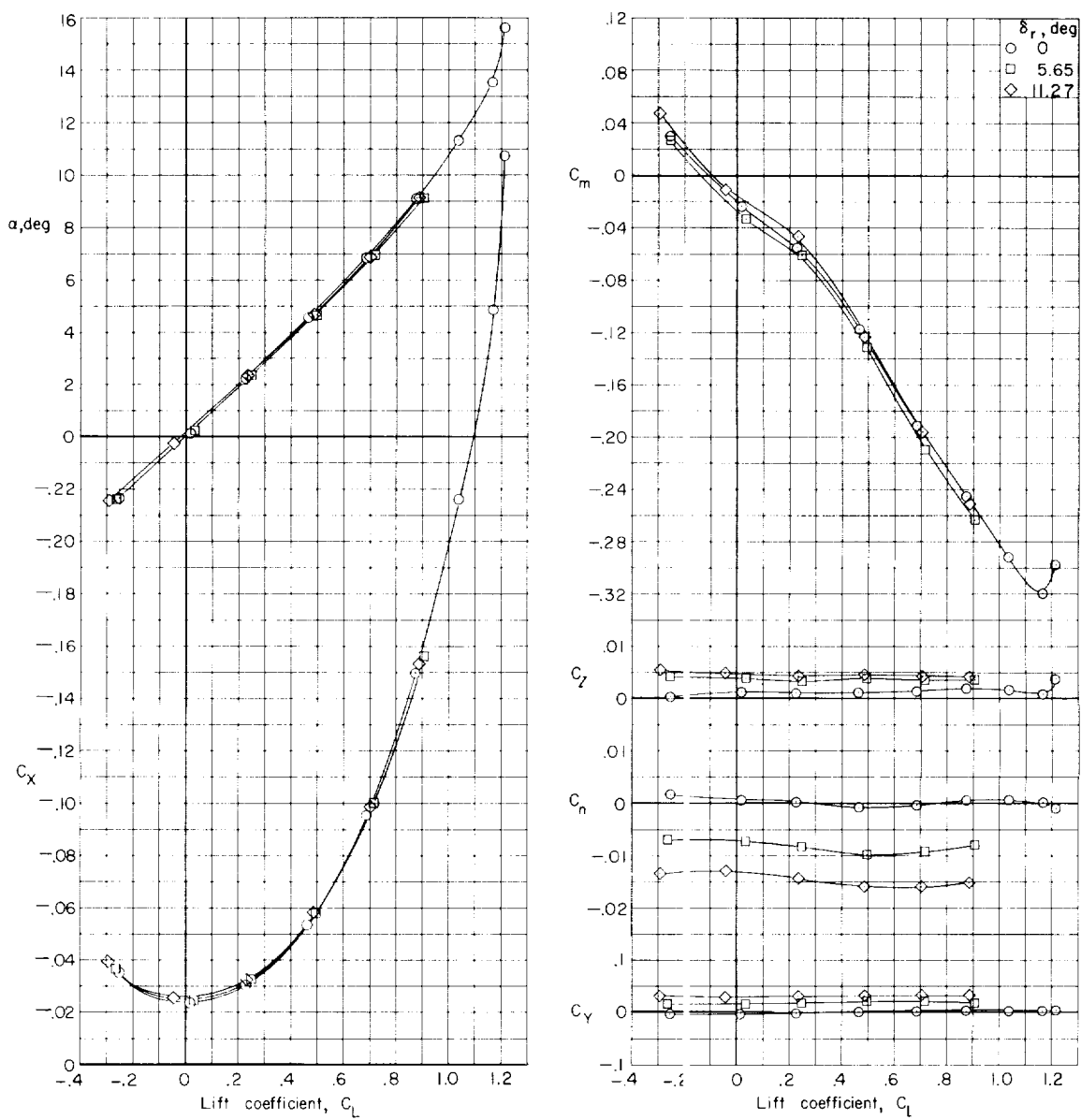Figure 40.- Continued.
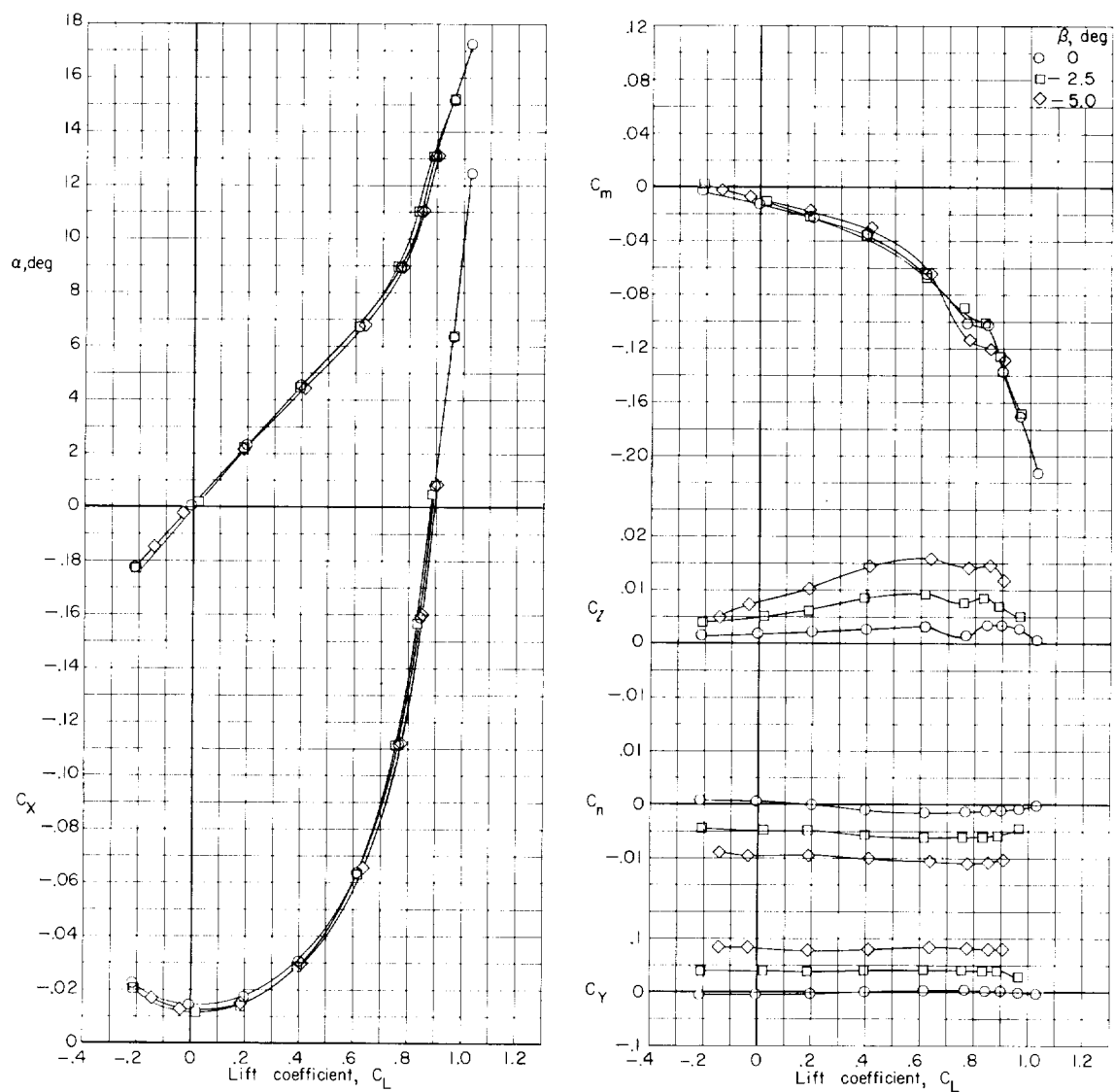
(c) M = 0.85.

Figure 40.- Continued.
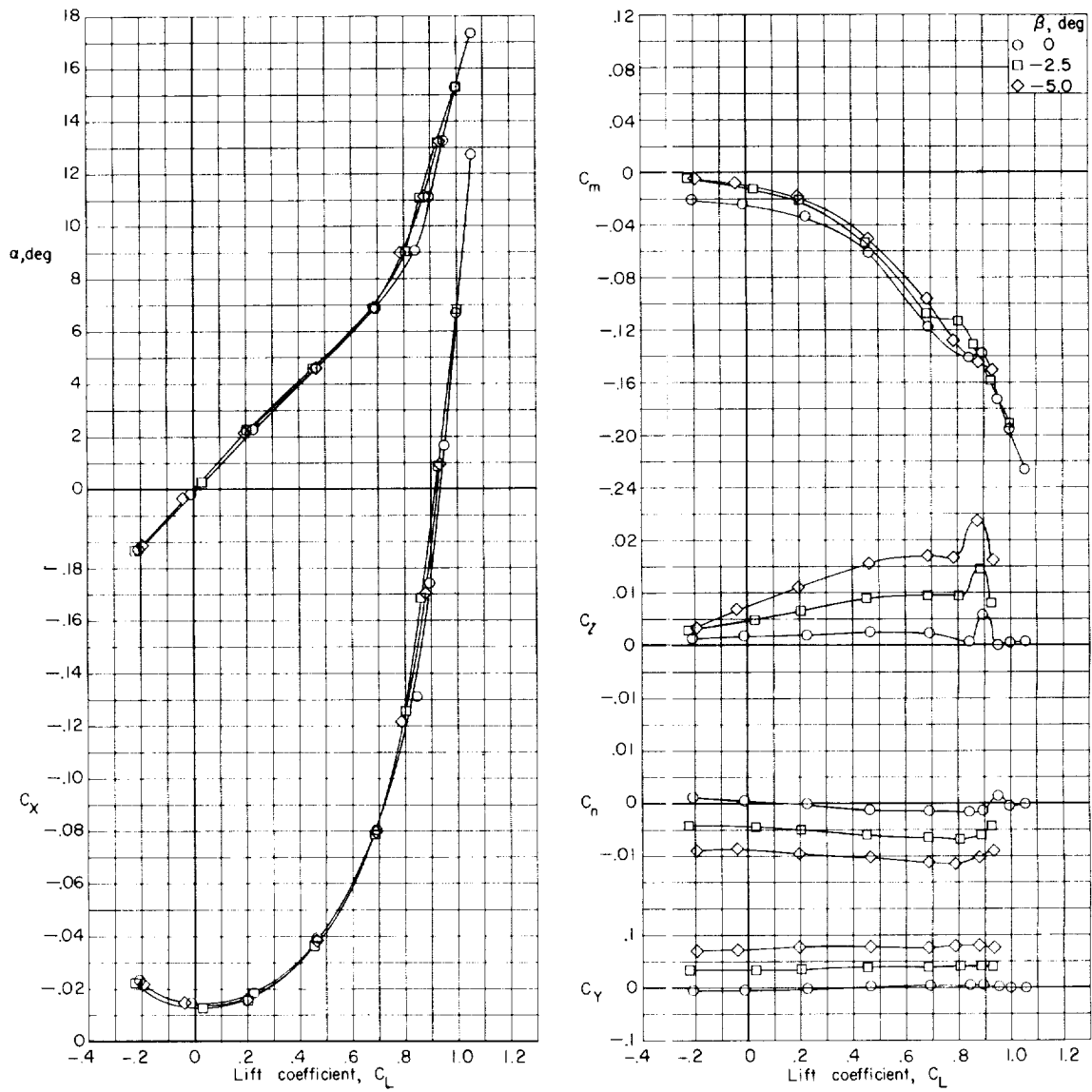
(d) M = 0.90.

Figure 40.- Continued.
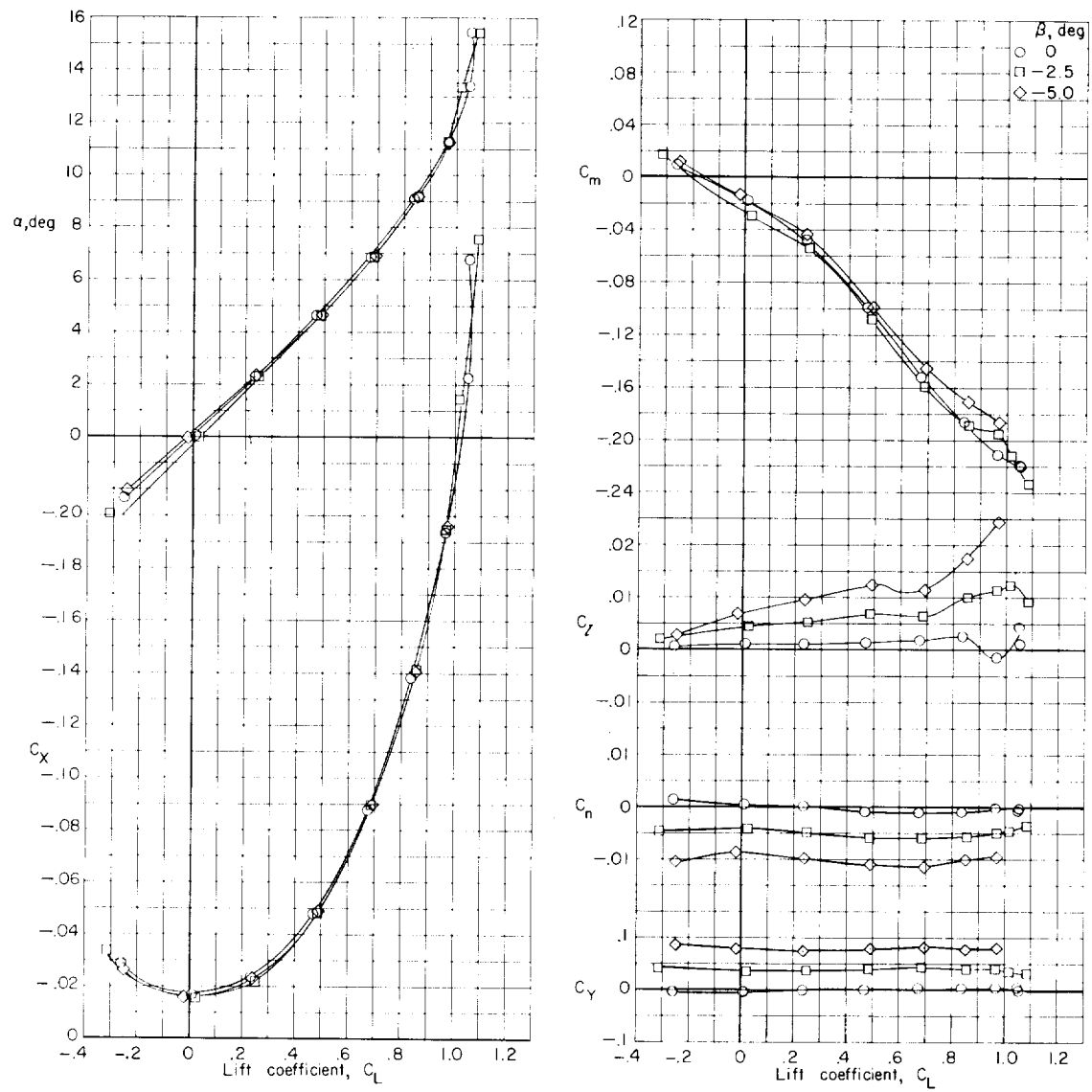
(e) M = 0.95.

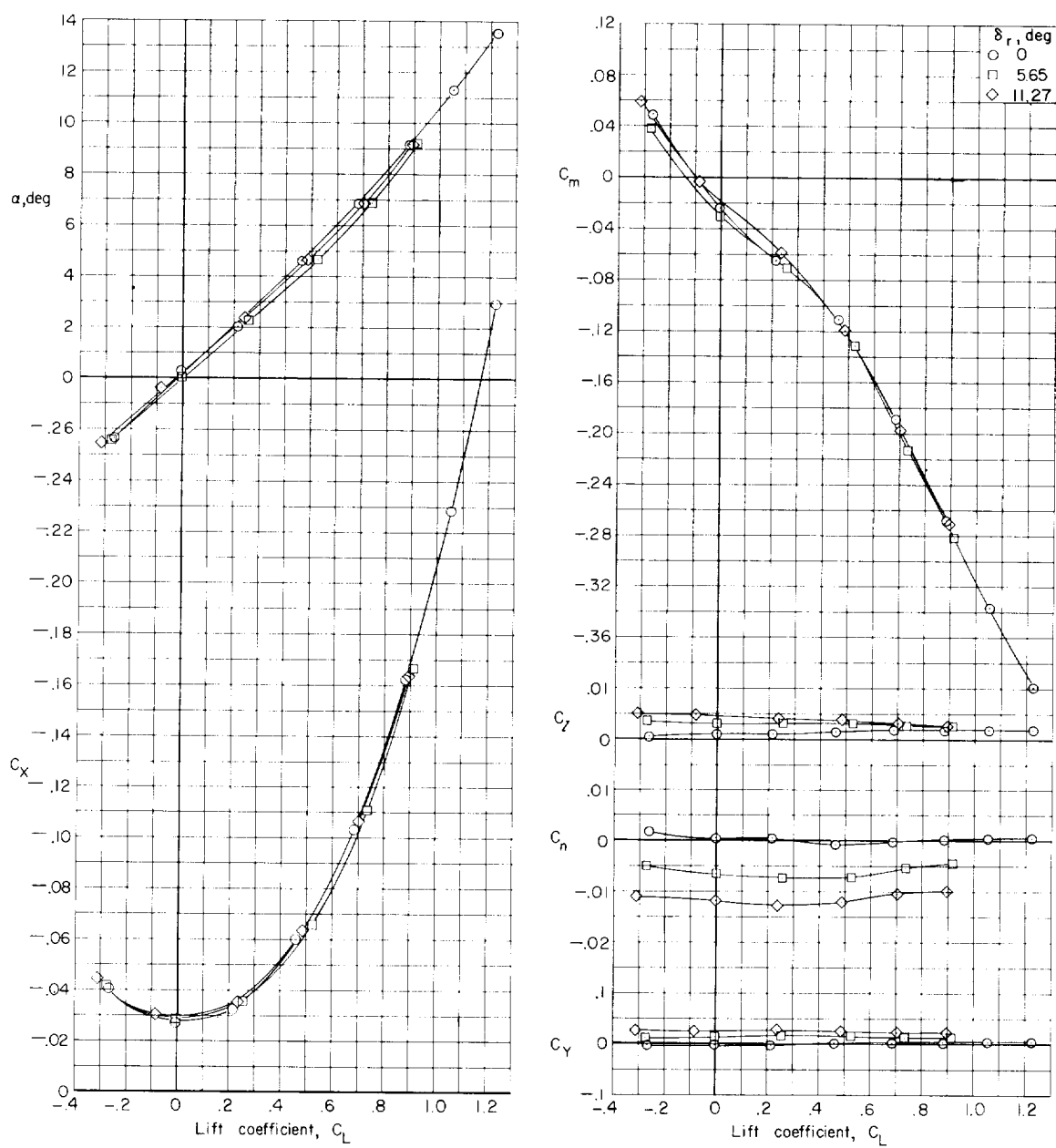Figure 40.- Continued.
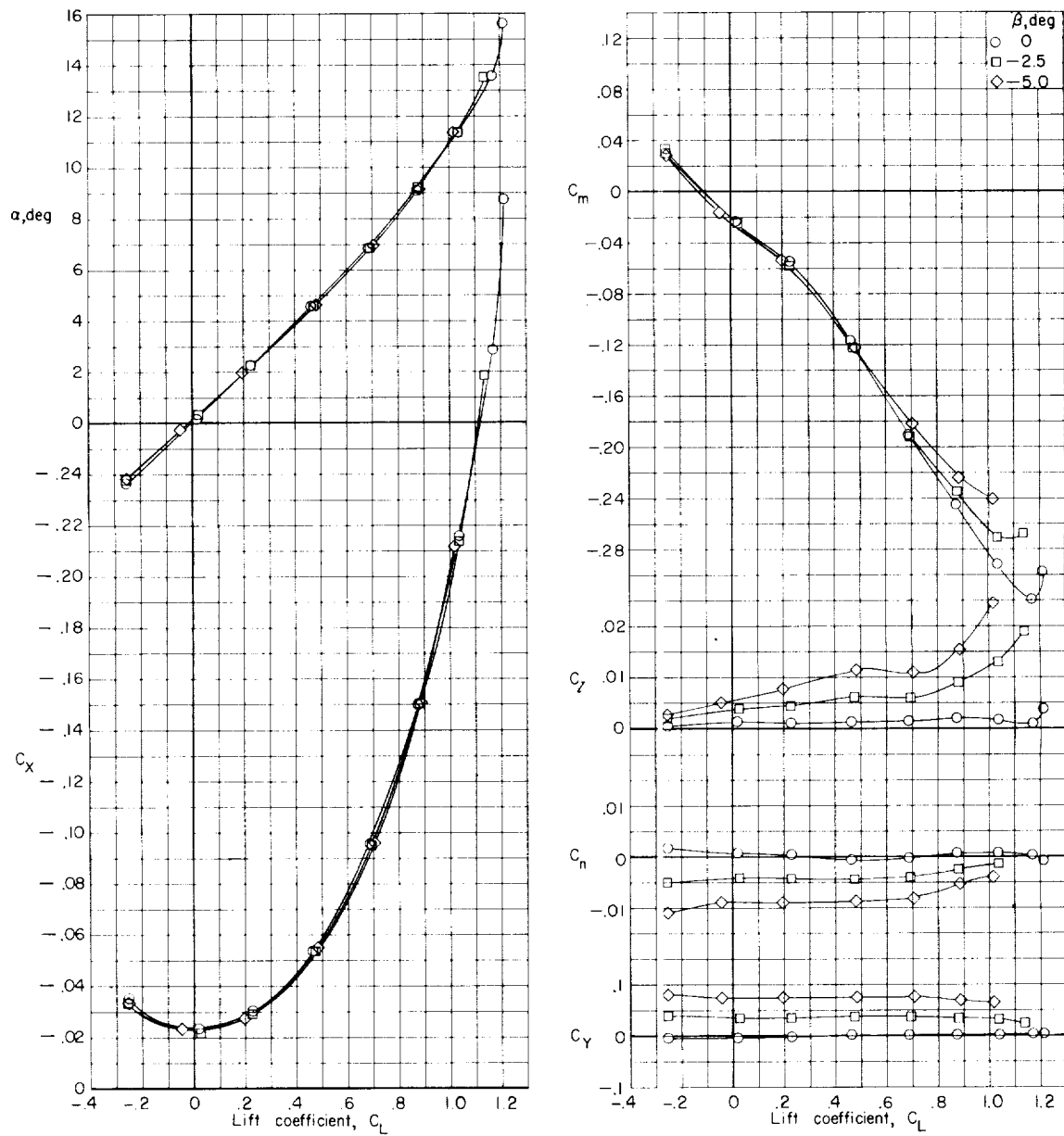
(f) M = 0.98.

Figure 40.- Continued.
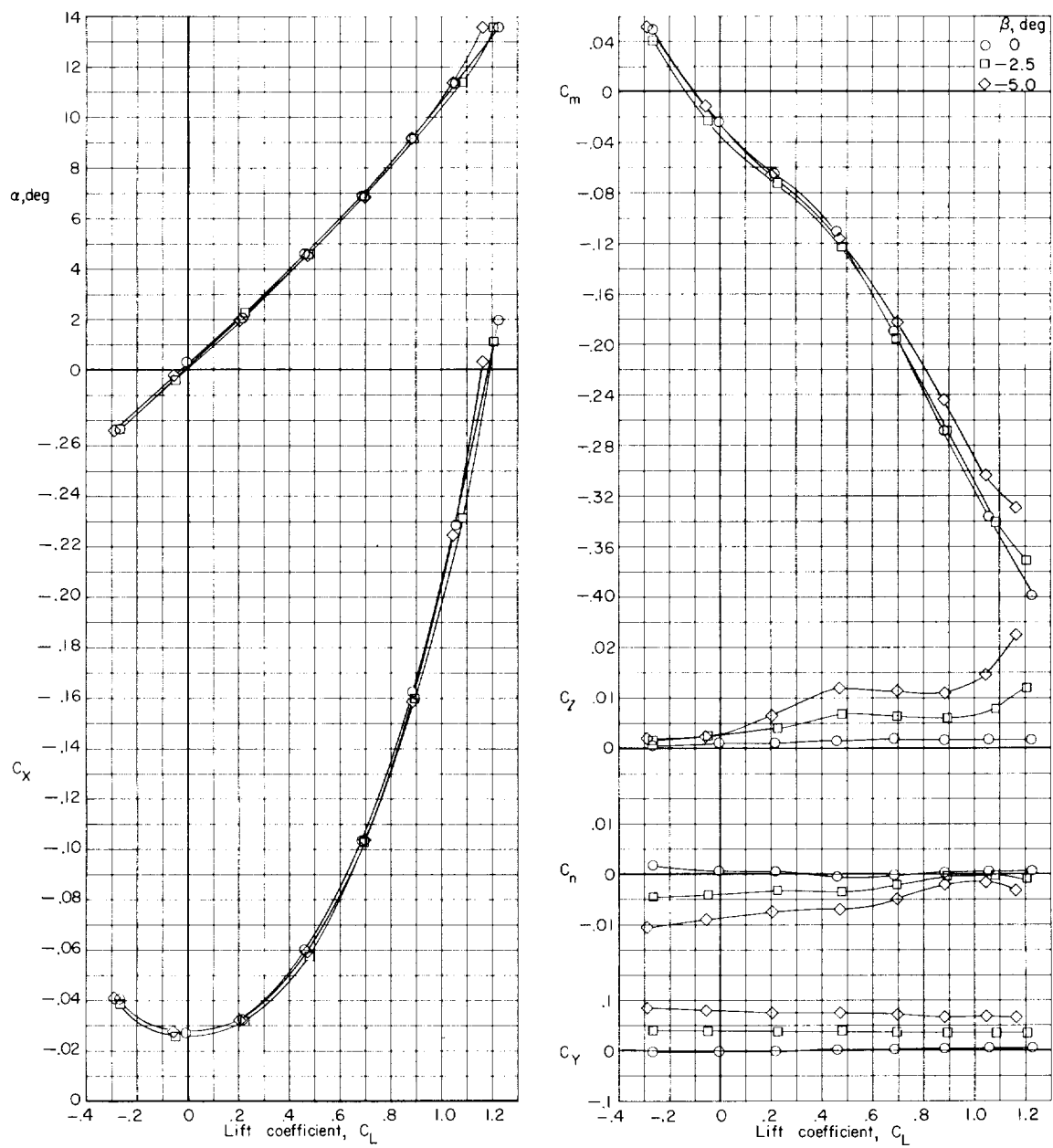
(g) M = 1.00.

Figure 40.- Continued.
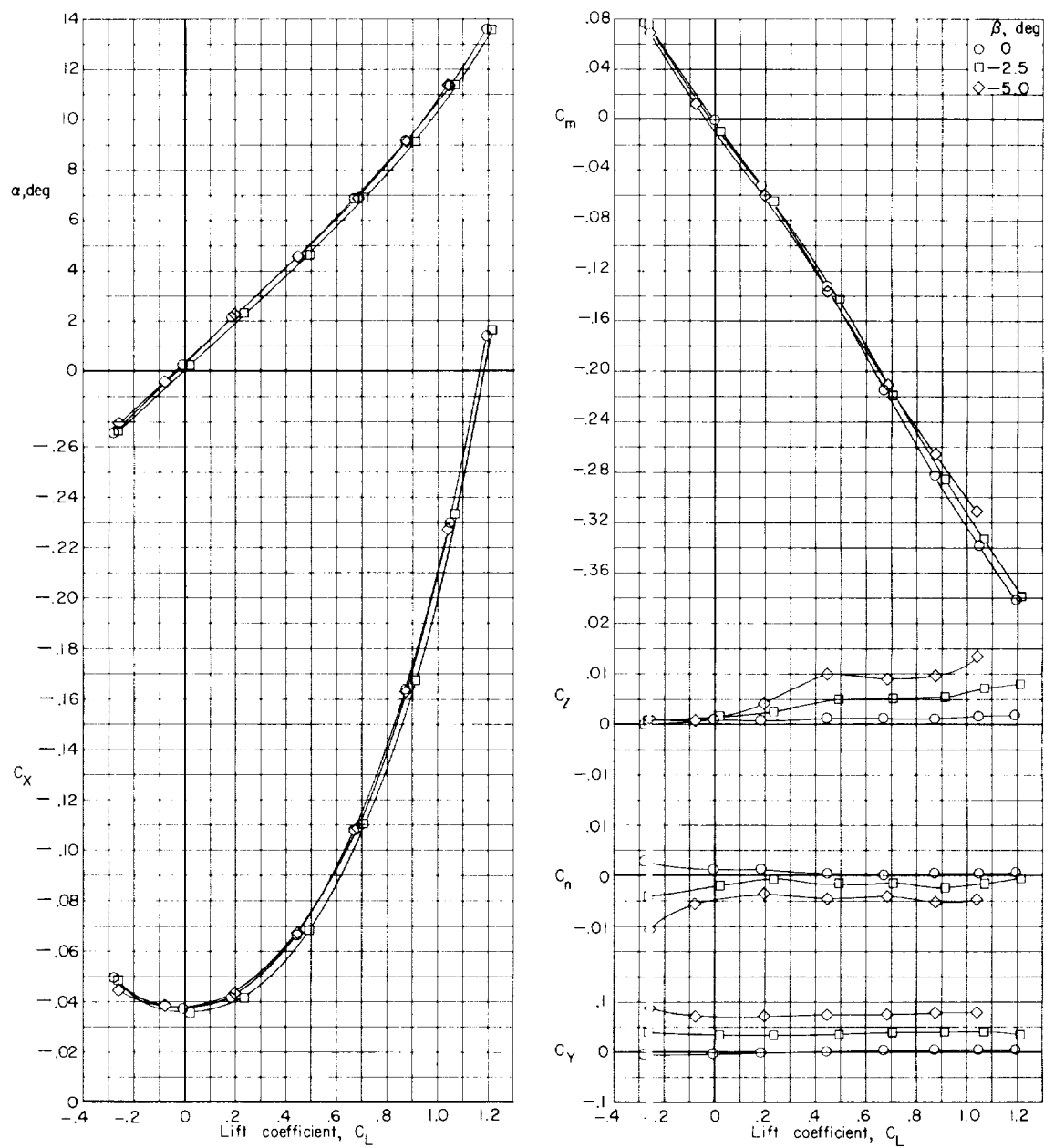
(h) M = 1.03.

Figure 40.- Continued.
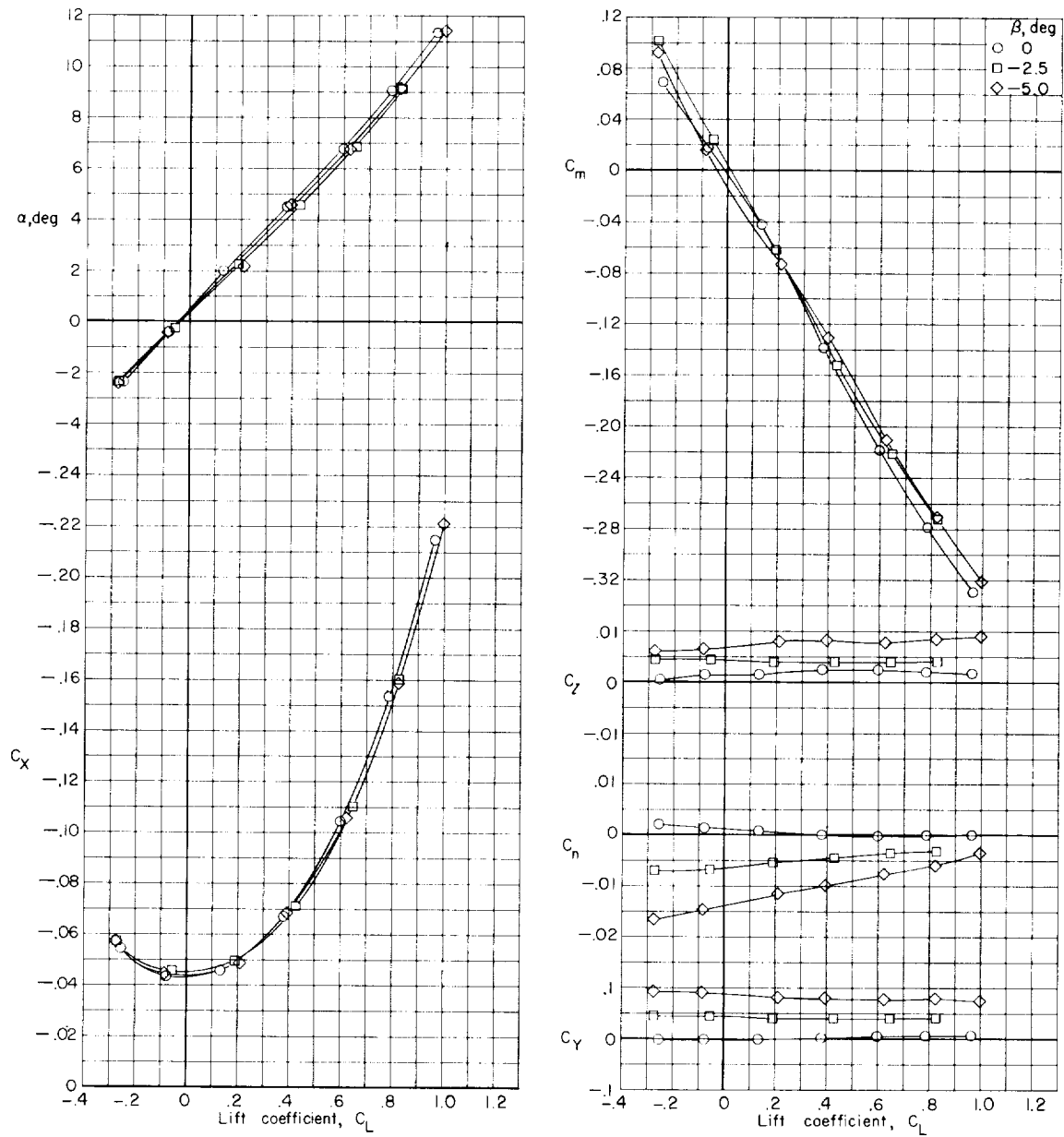
(i) M = 1.13.

Figure 40.- Concluded.

112
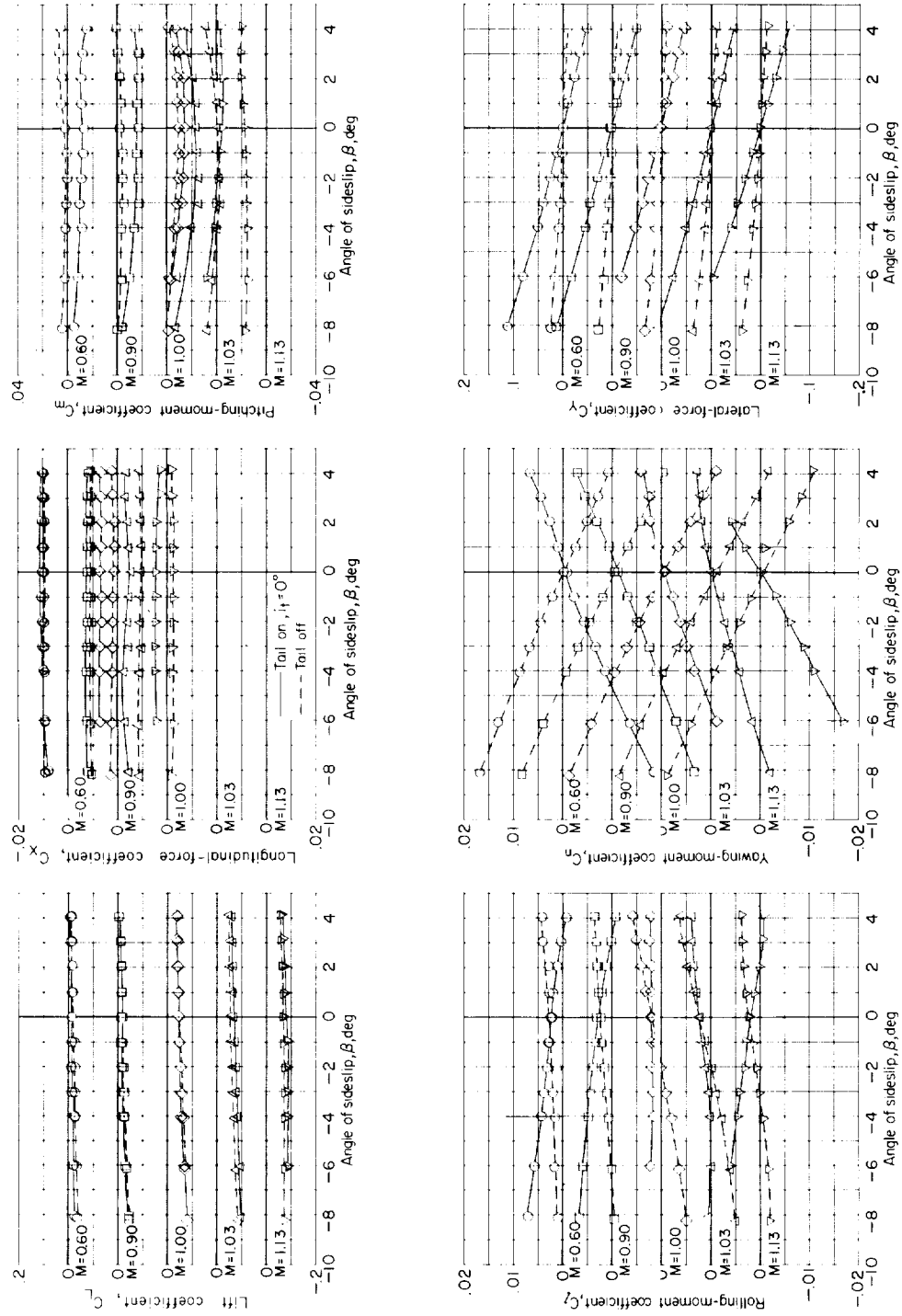
(a) α ≈ -0.3°.

Figure 41.- Aerodynamic characteristics in sideslip of the basic model with and without the horizontal and vertical tails.
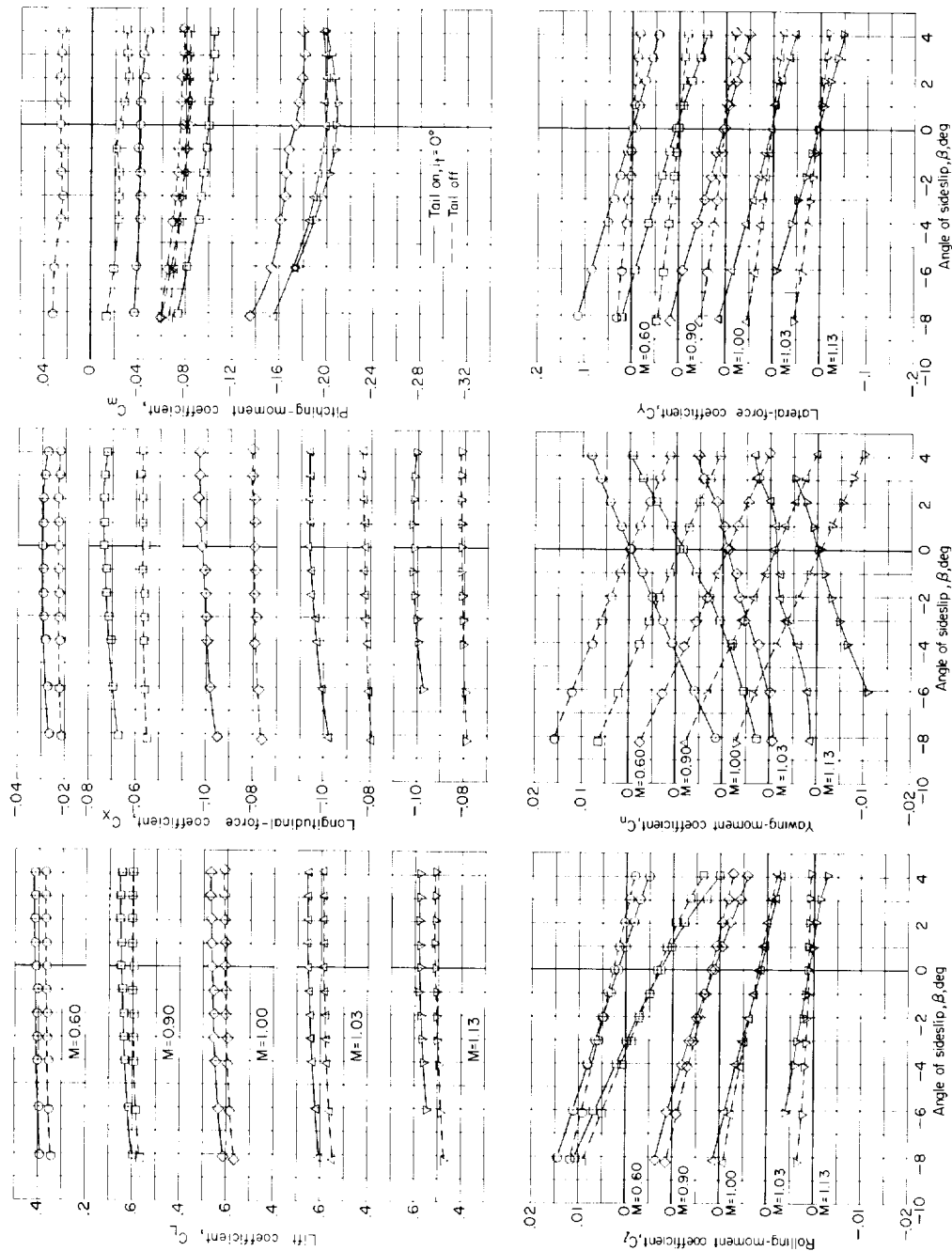
(b) $\alpha \approx 6.0^\circ$.

Figure 41.- Concluded.
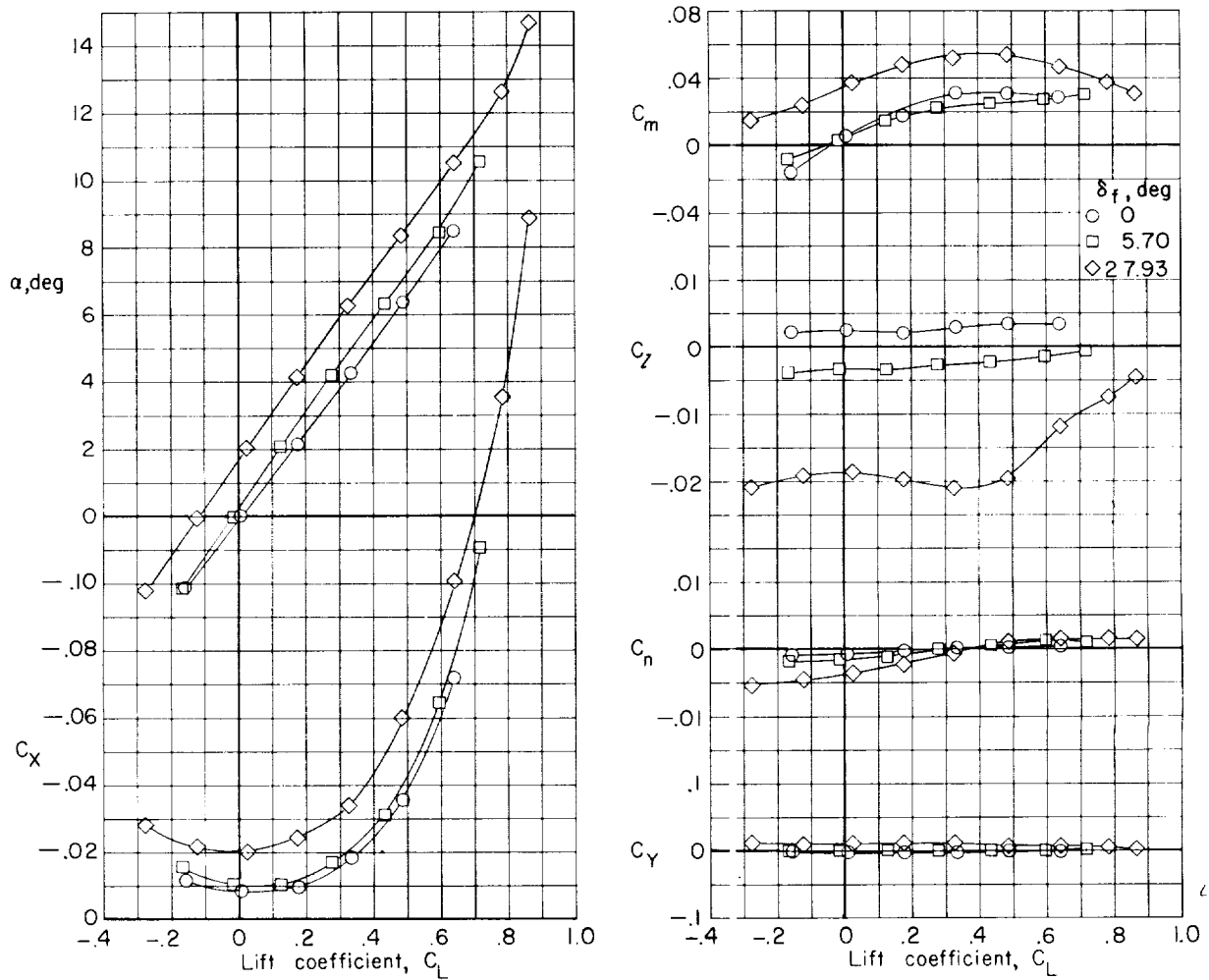
(a) M = 0.60.

Figure 42.- Effects of lift coefficient on the lateral-control character-
istics for the basic model. Horizontal and vertical tails off.
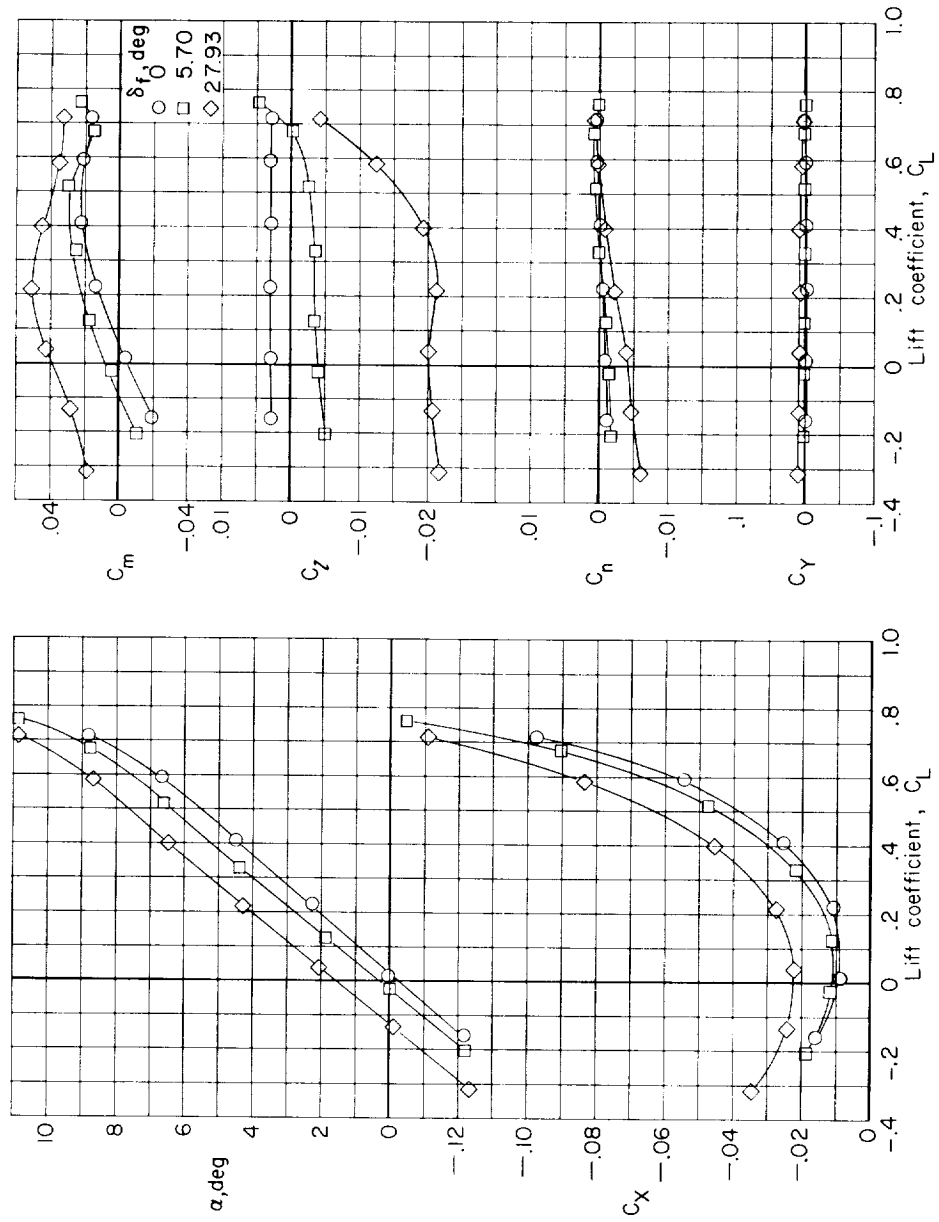
(b) M = 0.80.

Figure 42.- Continued.

115
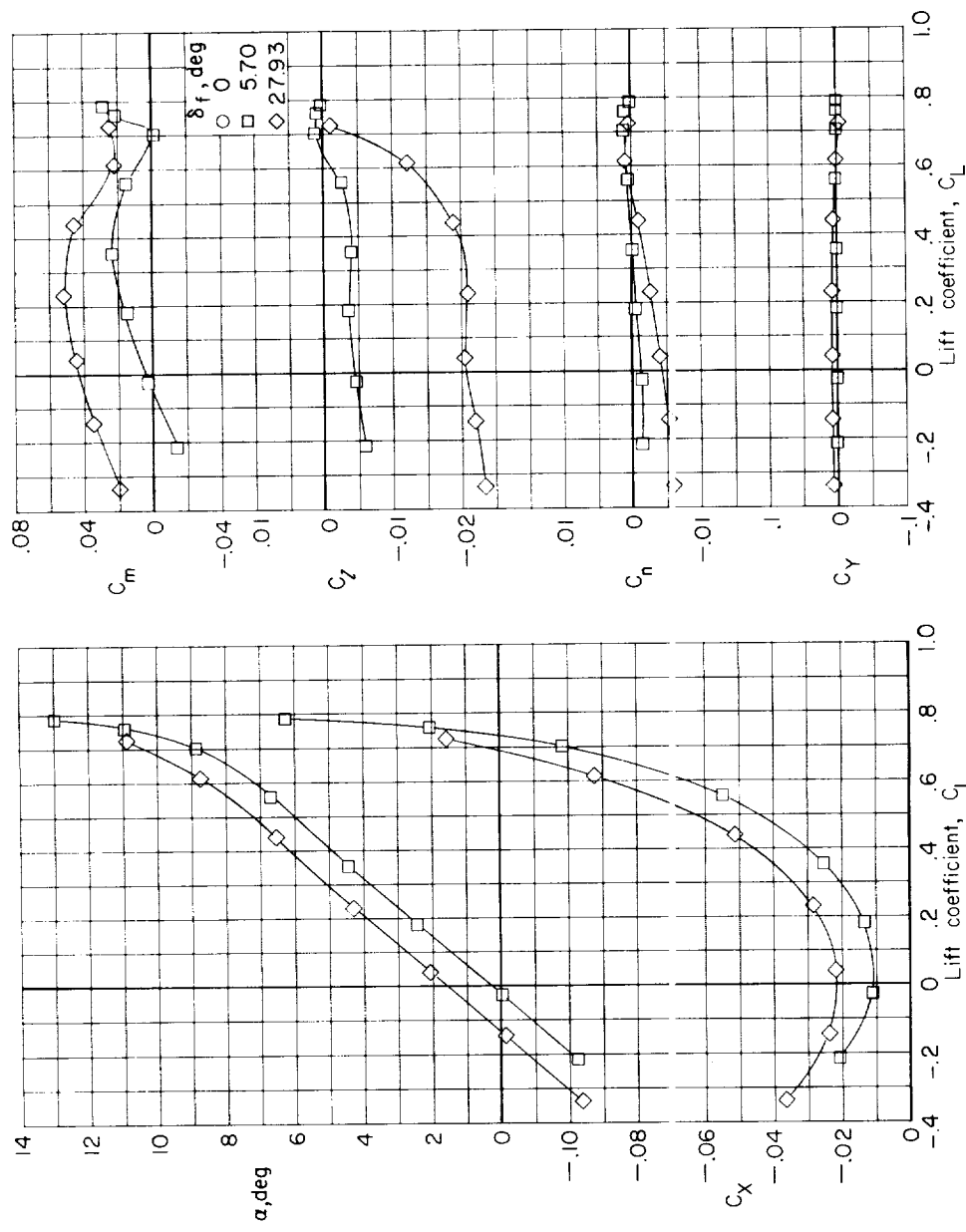
(c) M = 0.85.

Figure 42.- Continued.
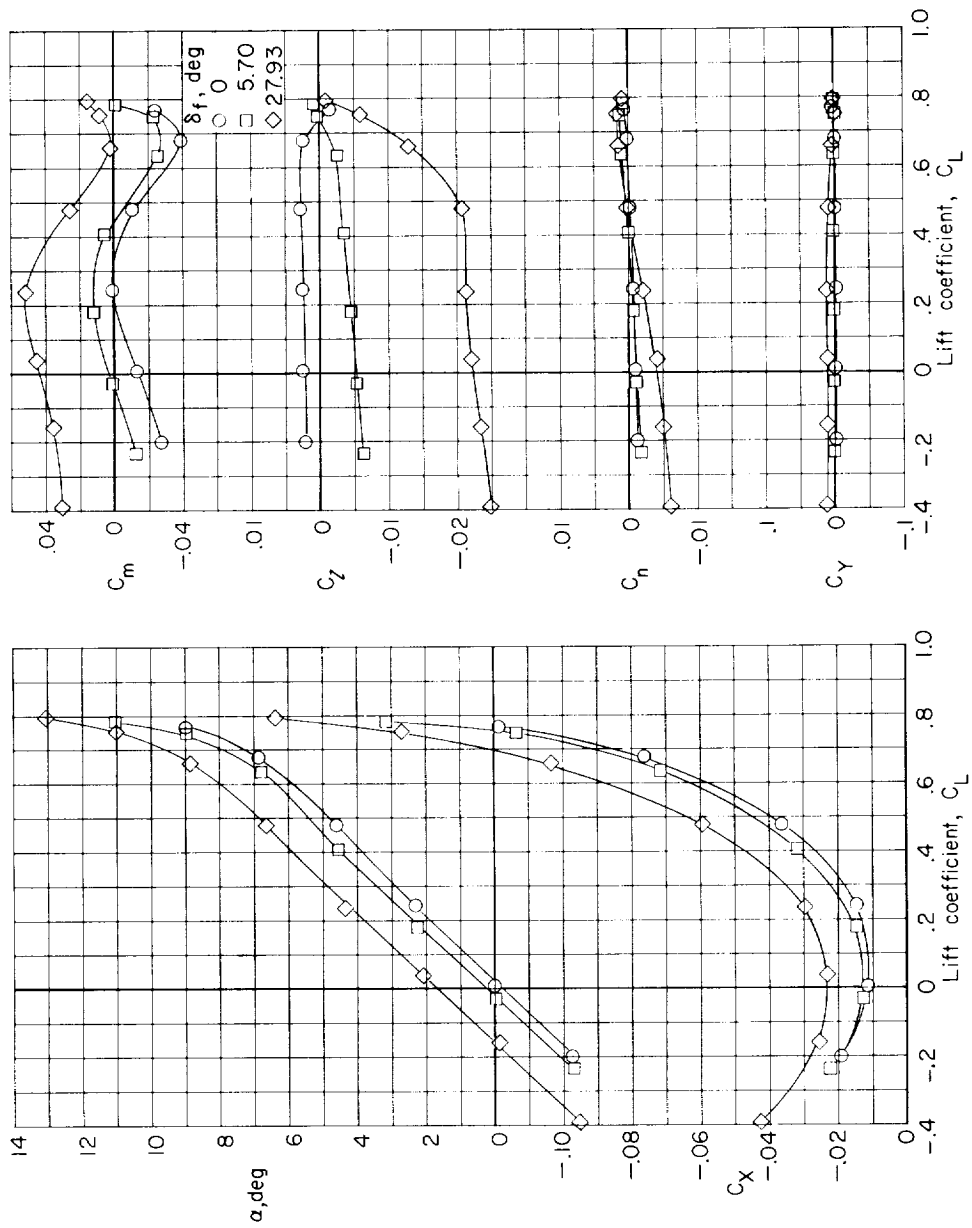
(d) M = 0.90.

Figure 42.- Continued.

118
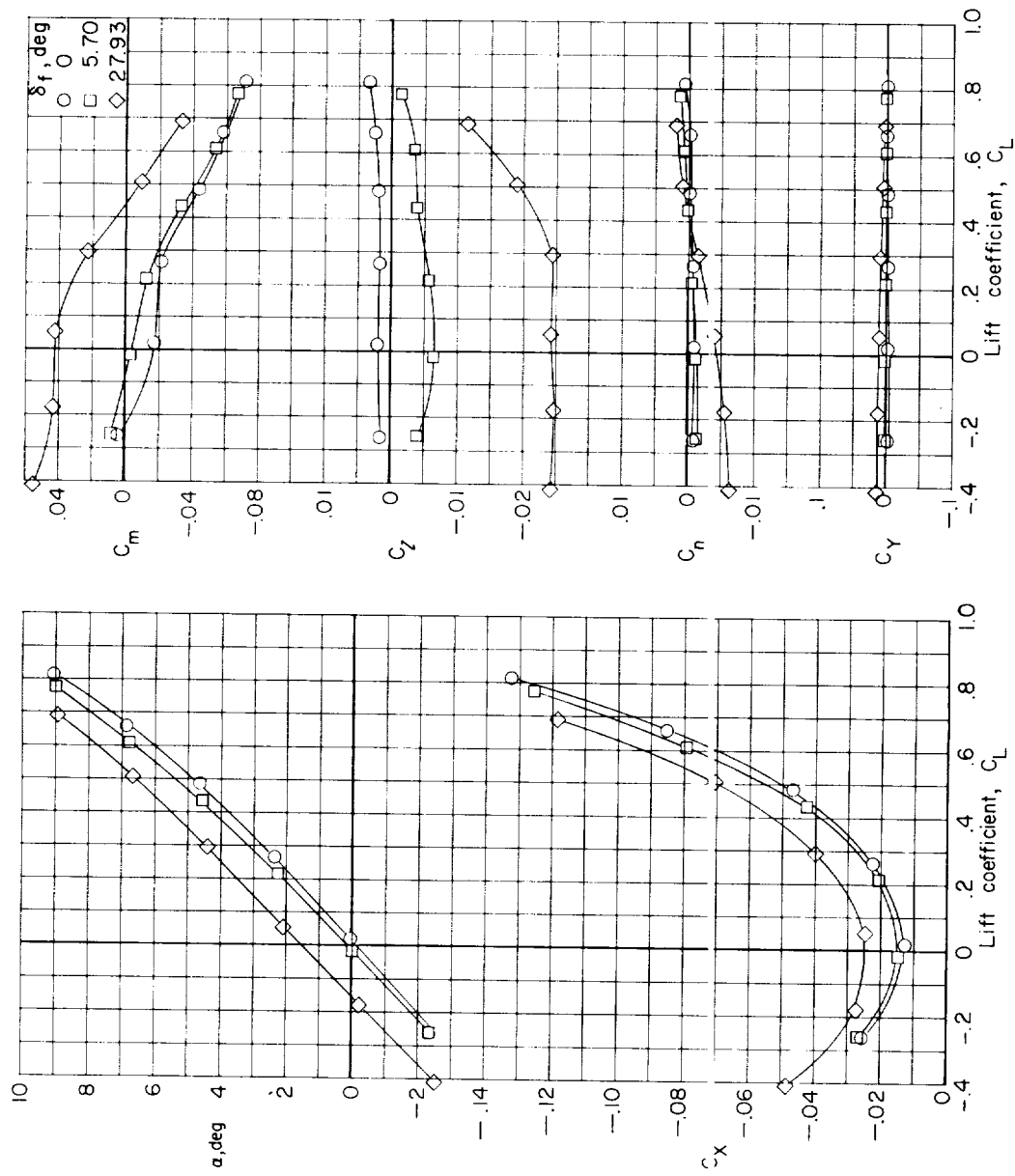
(e) M = 0.95.

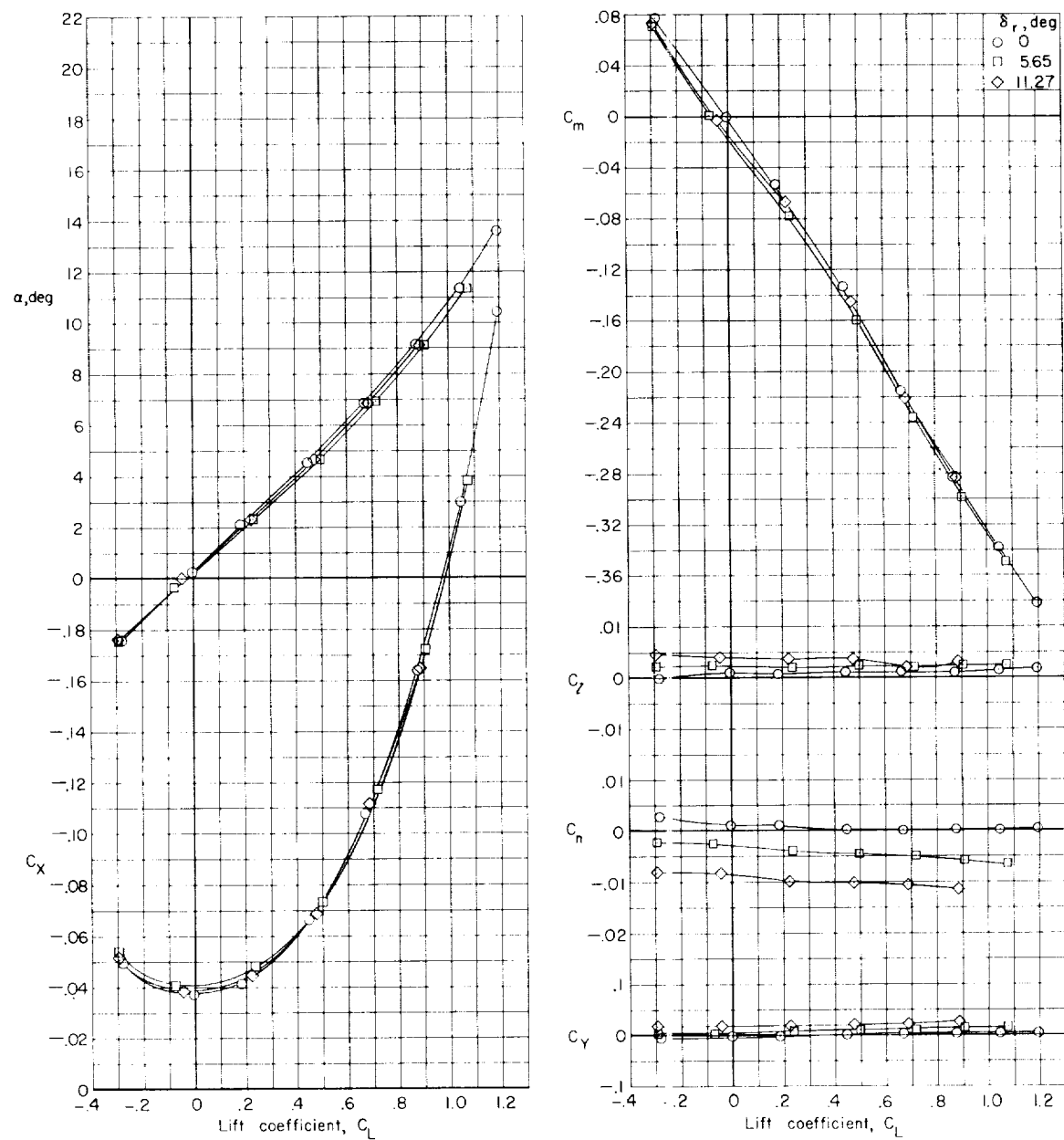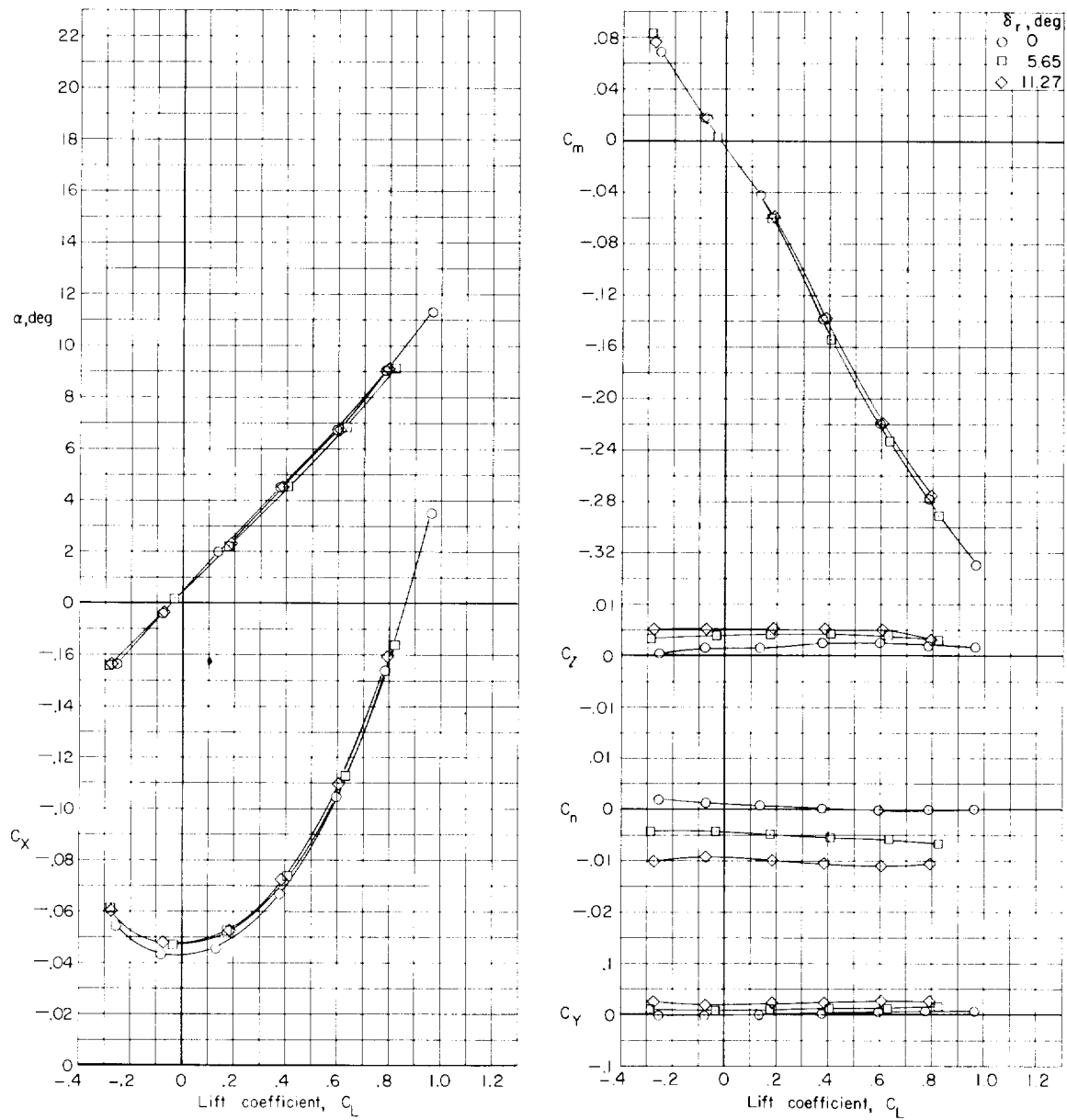Figure 42.- Continued.
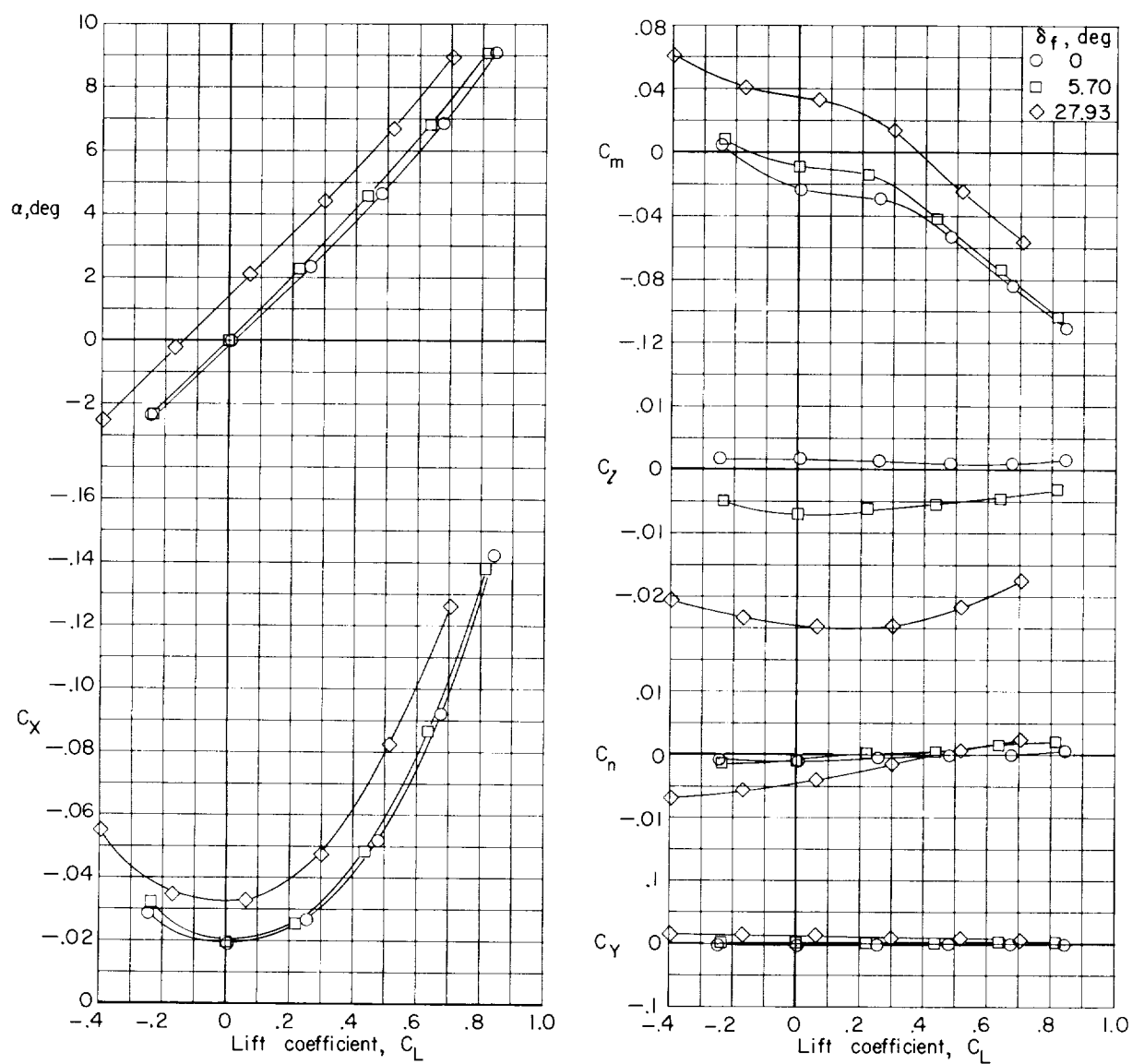
(f) M = 0.98.

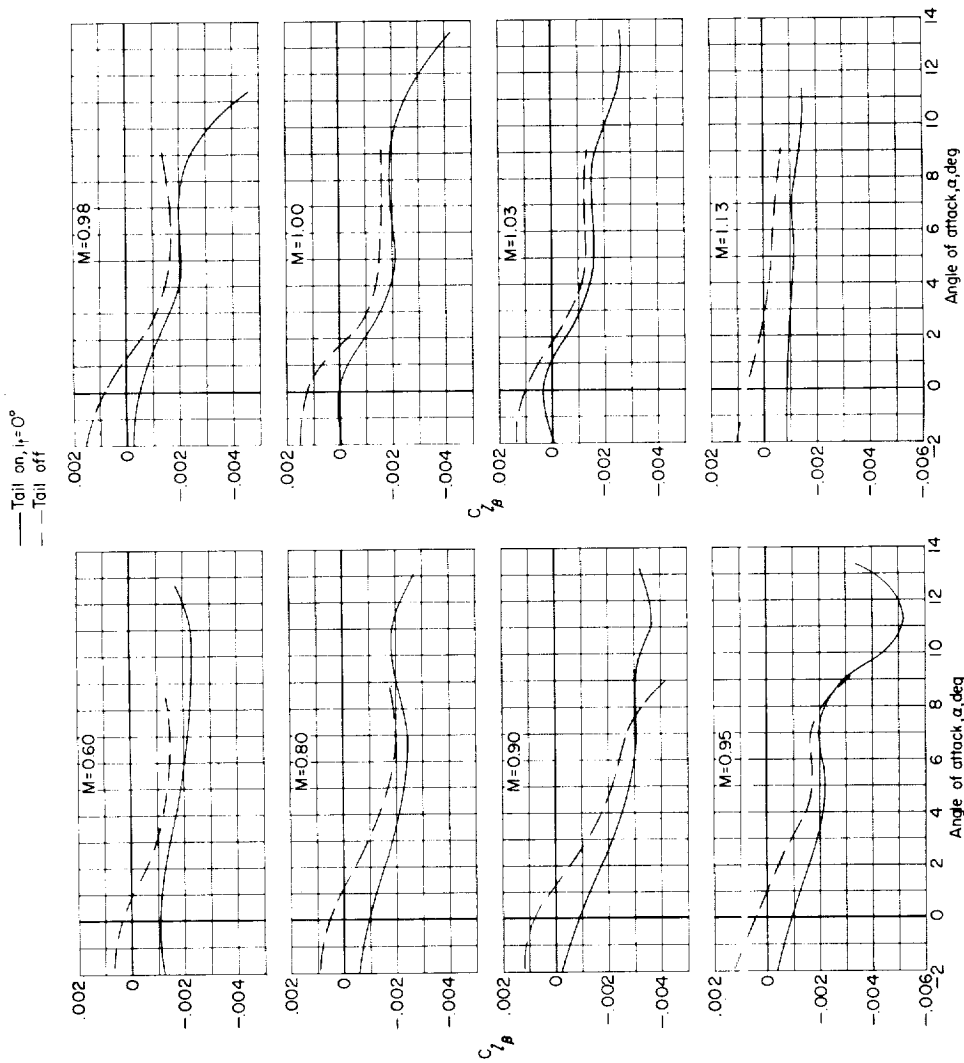Figure 42.- Continued.
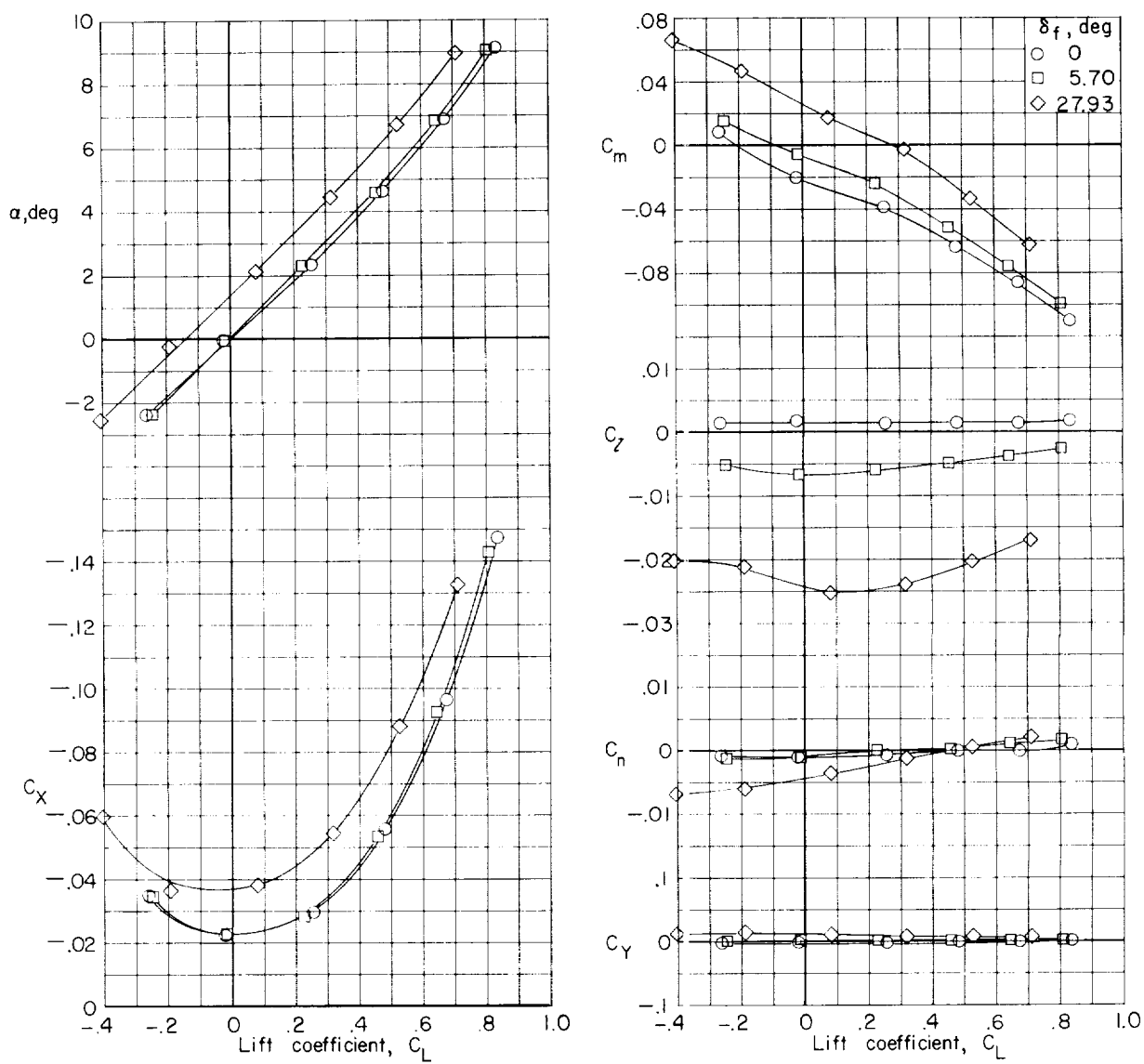
(g) M = 1.00.

Figure 42.- Continued.
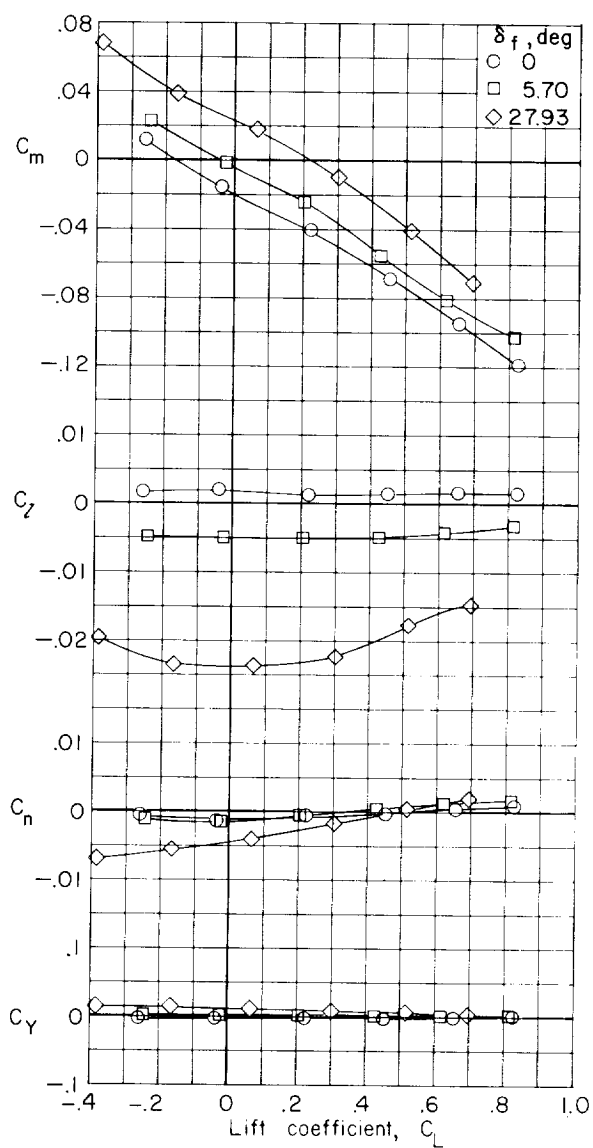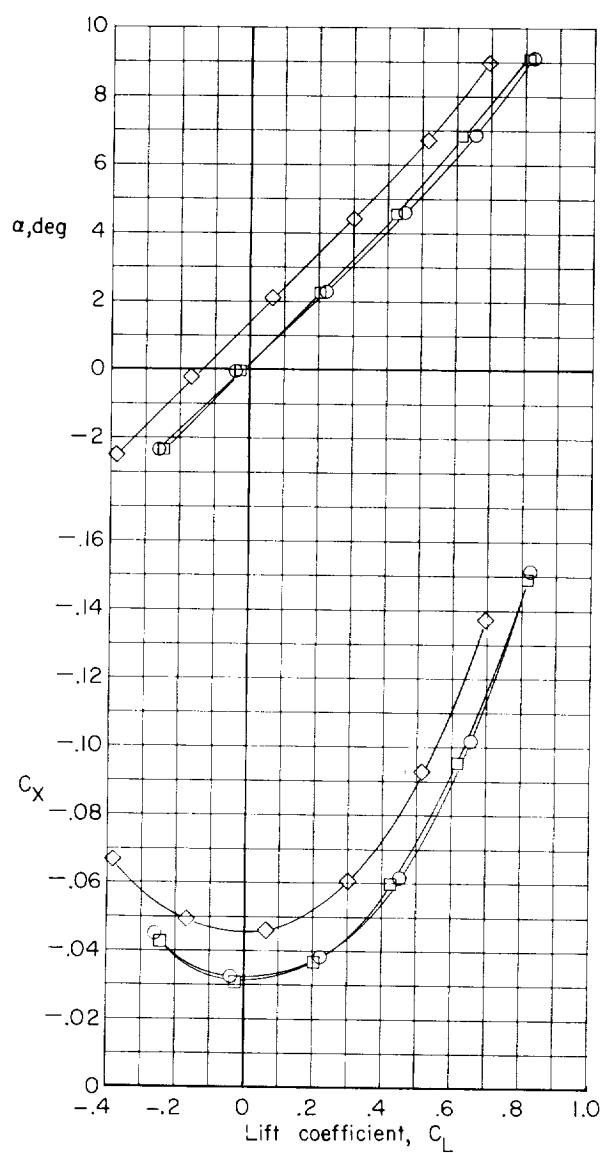
(h)   M = 1.03.

Figure 42.- Continued.
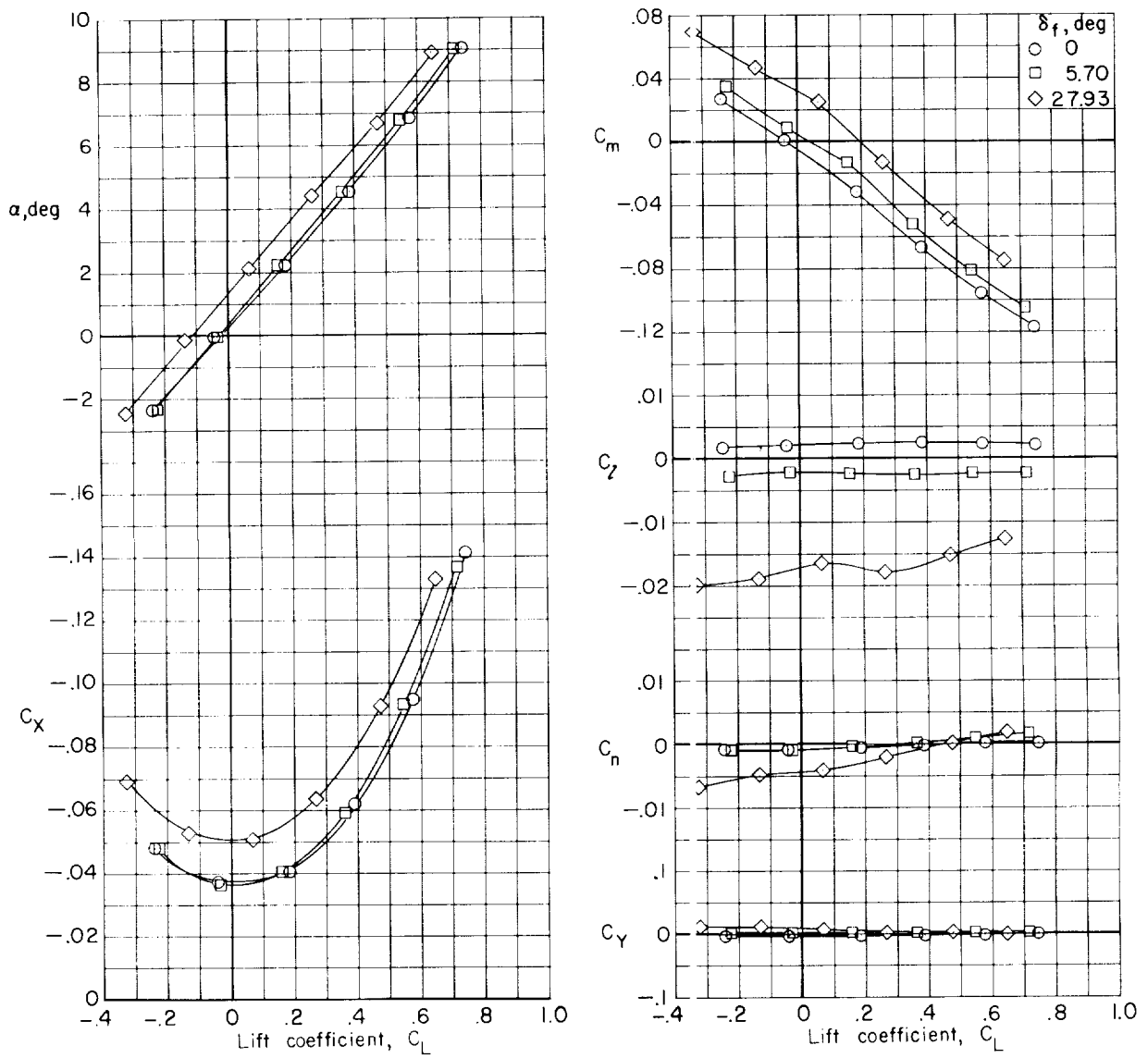
(i) M = 1.13.

Figure 42.- Concluded.

(a) M = 0.60.

Figure 43.- Effects of lift coefficient on the directional control
characteristics for the basic model at zero sideslip. Horizontal
tail on. i_t = 0°.

124
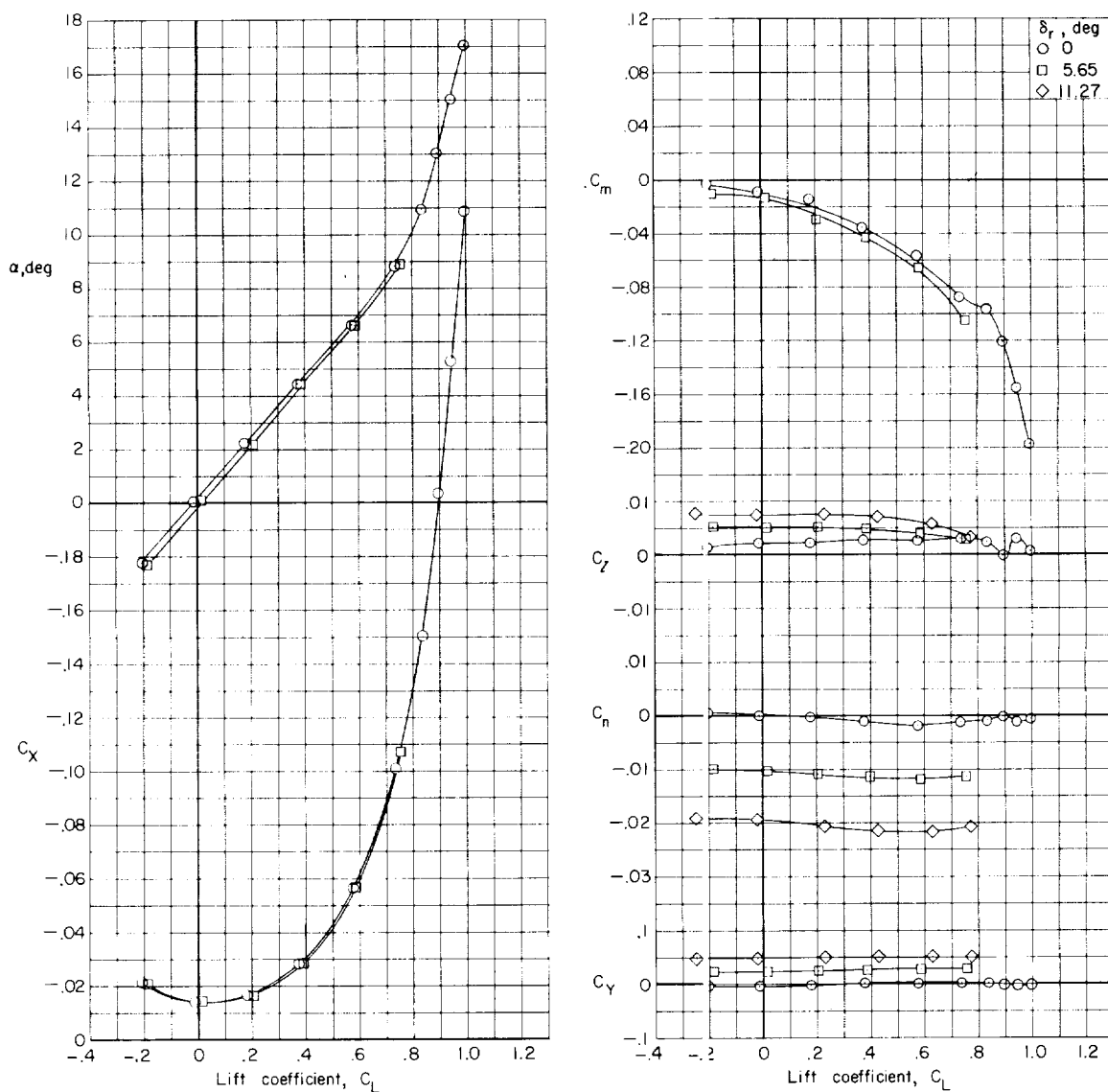
(b) M = 0.80.

Figure 43.- Continued.
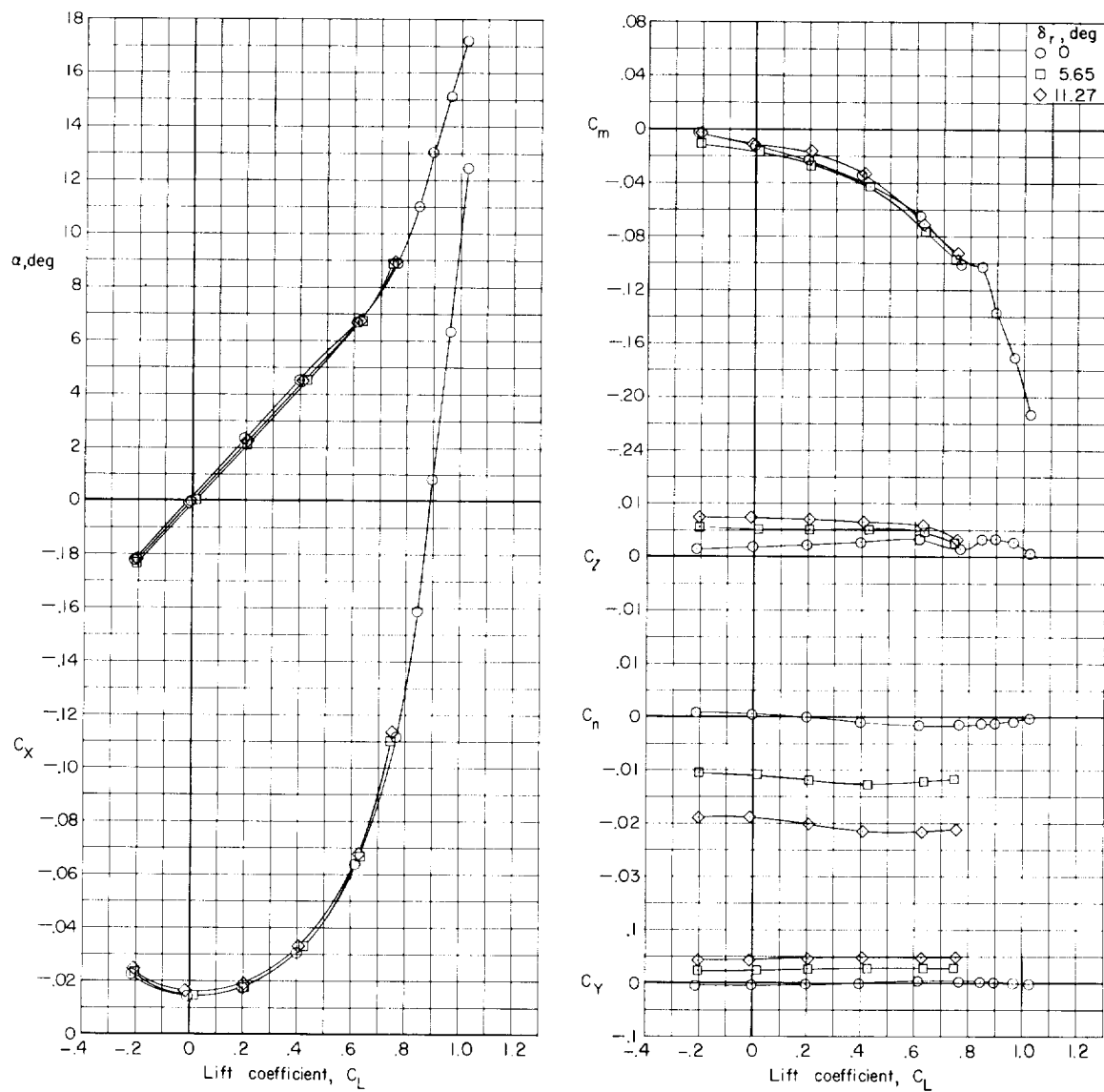
(c) M = 0.85.

Figure 43.- Continued.

126
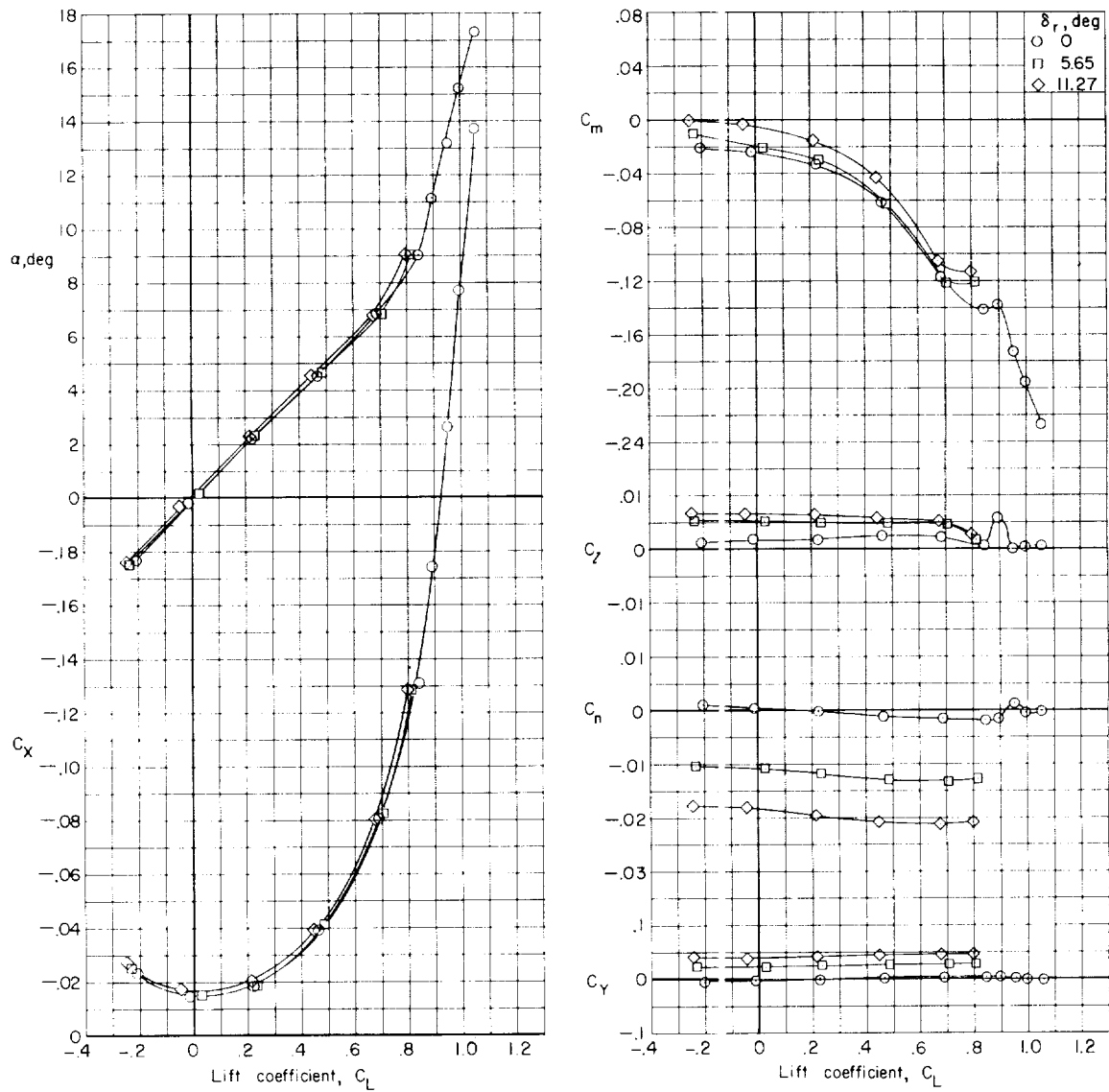
(d) M = 0.90.

Figure 43.- Continued.
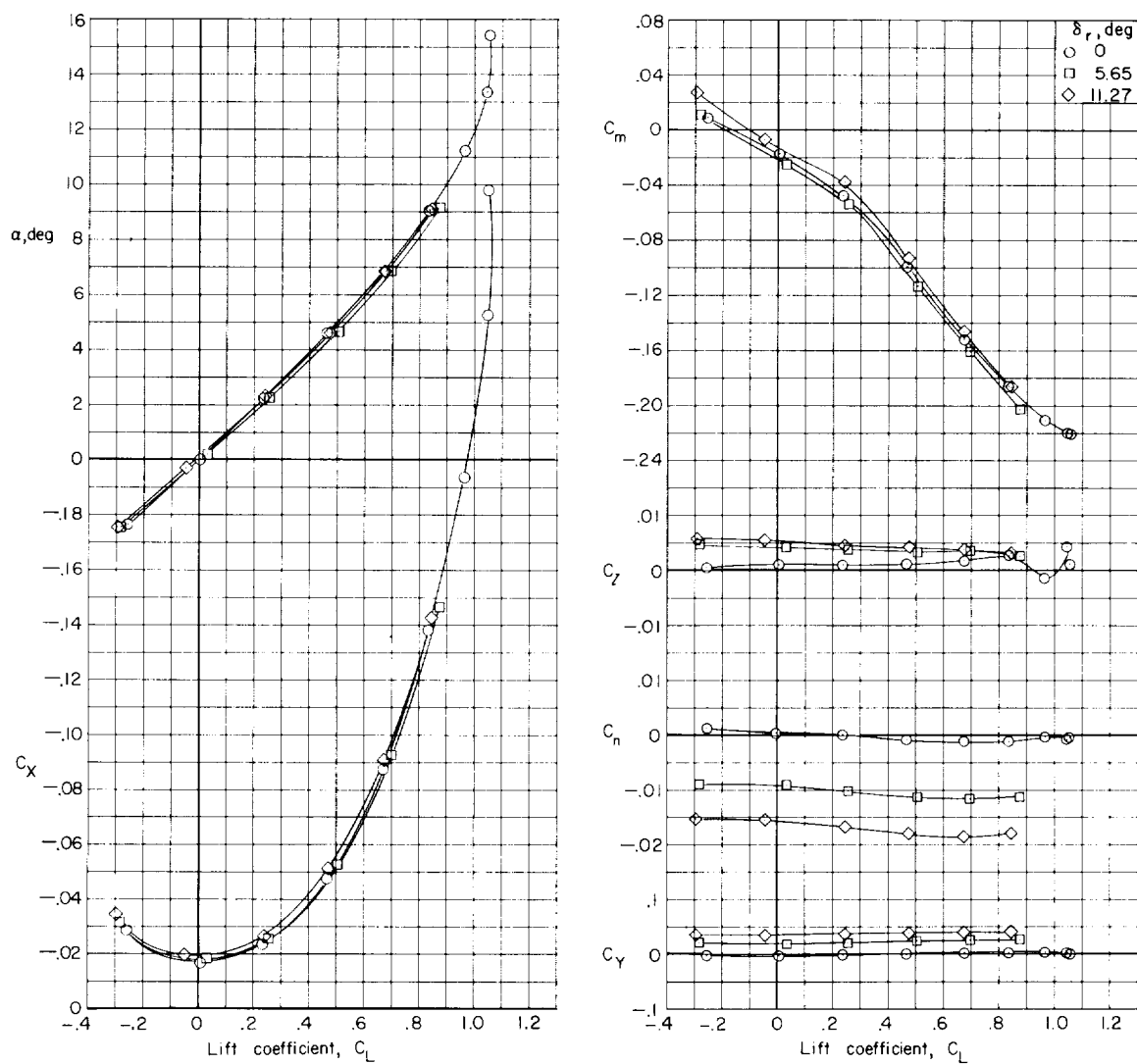
(e) M = 0.95.

Figure 43.- Continued.

128

(f) M = 0.98.

Figure 43.- Continued.

(g) M = 1.00.

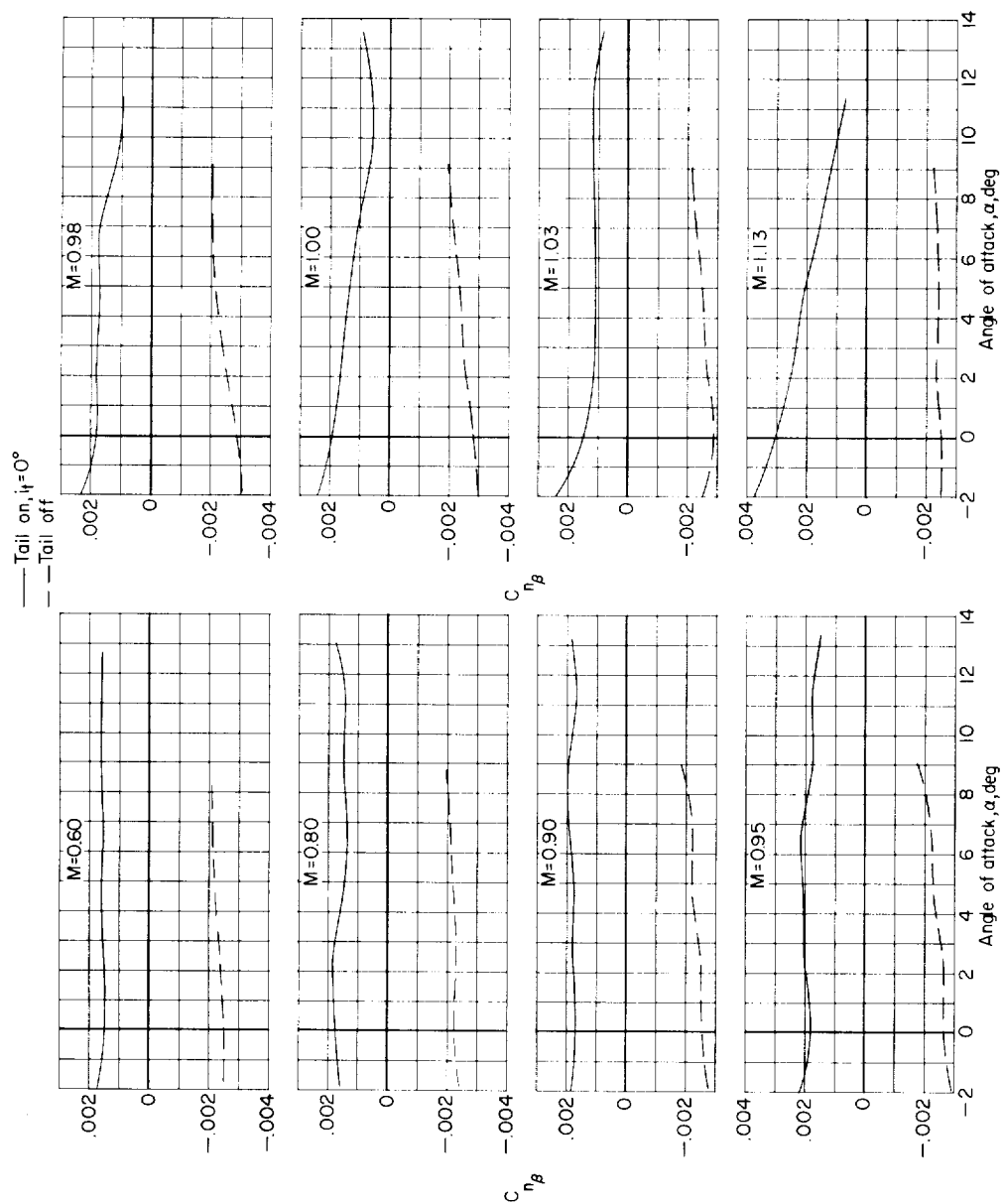Figure 43.- Continued.

(h) M = 1.03.

Figure 43.- Continued.
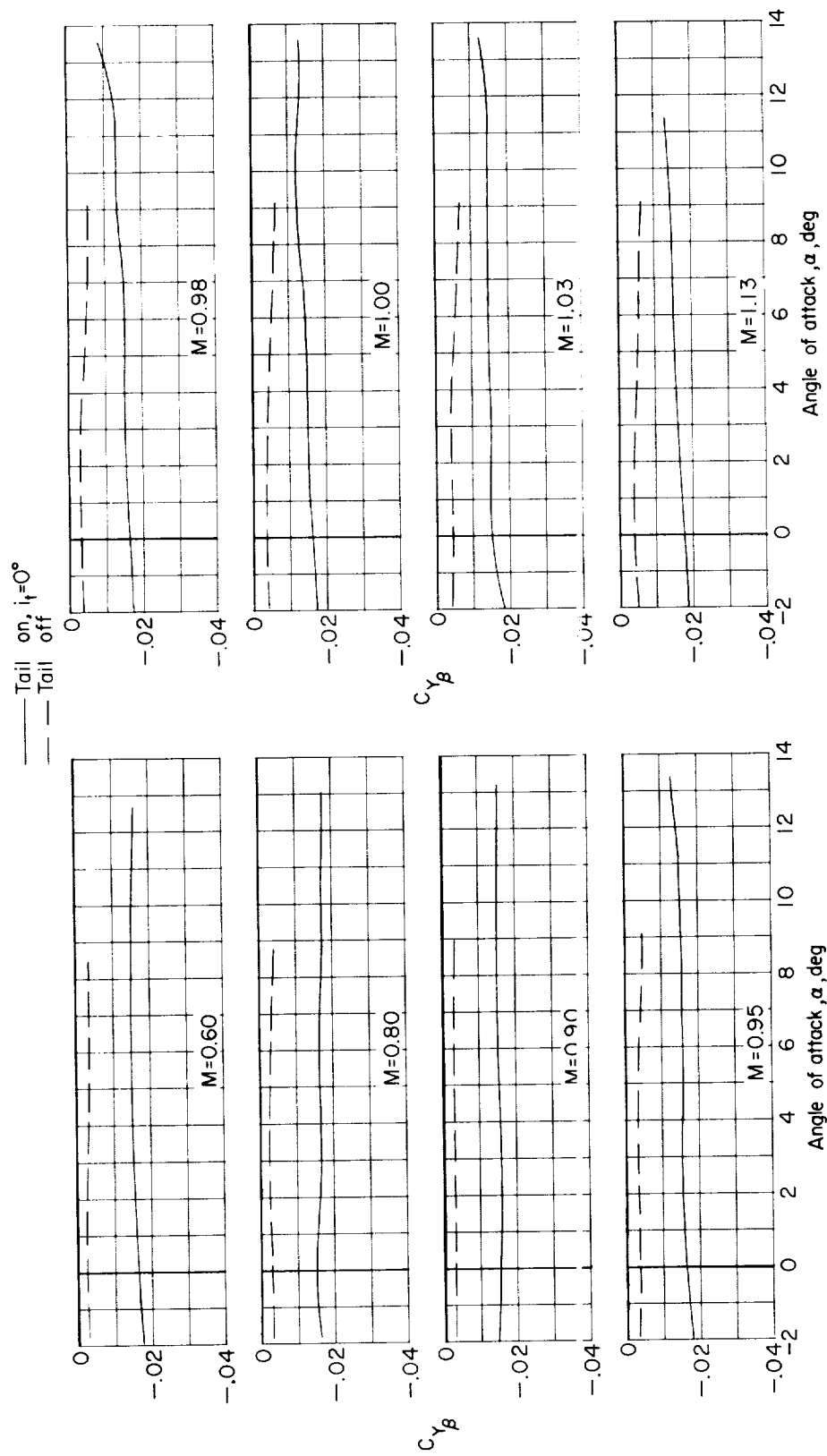
(i) M = 1.13.

Figure 43.- Concluded.

(a) Effective-dihedral derivative.

Figure 44.- Variation with angle of attack of the lateral-stability derivatives for the basic model.

(b) Directional-stability derivative.

Figure 44.- Continued.

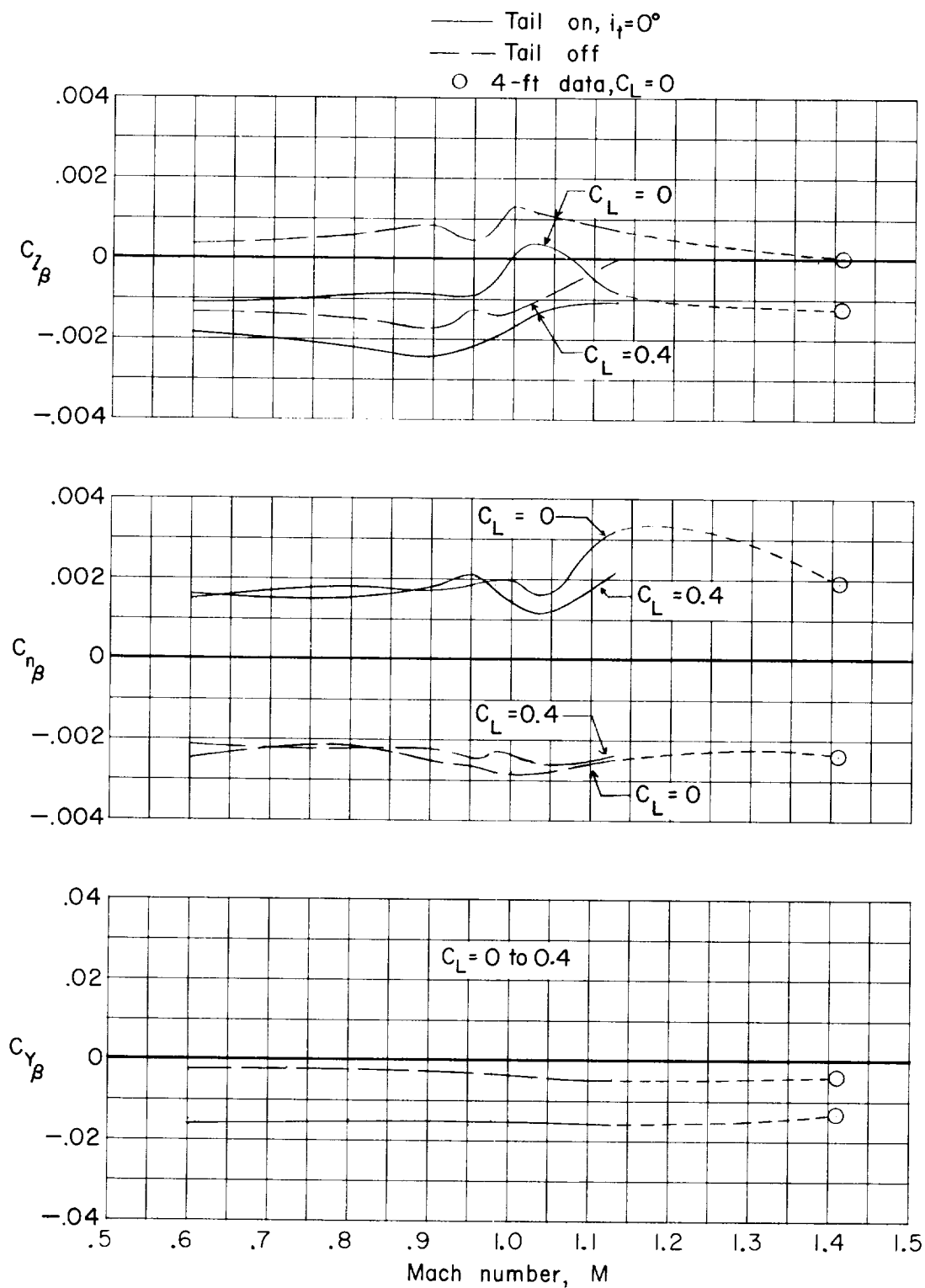(c) Lateral-force derivative.

Figure 44.- Concluded.

Figure 45.- Variation with Mach number of the lateral-stability derivatives for the basic model.
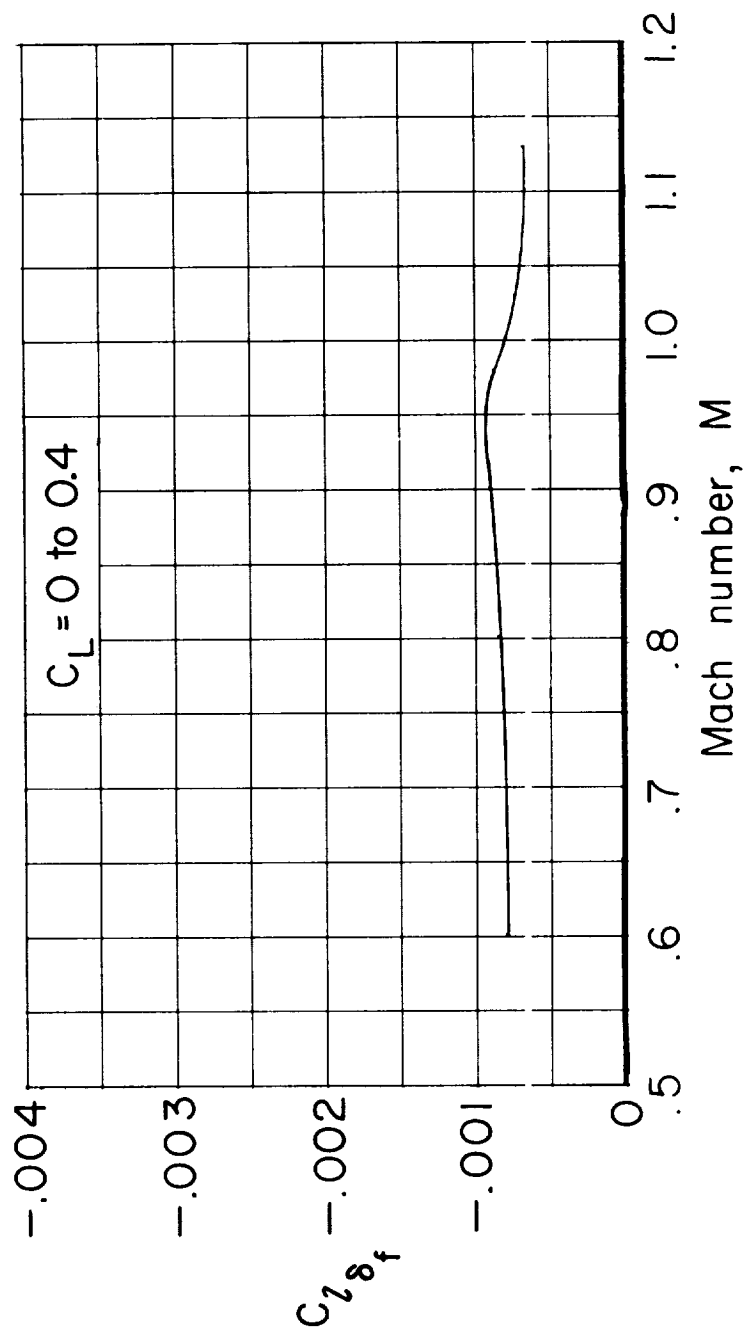
$C_L = 0 \text{ to } 0.4$

Figure 46.- Variation with Mach number of the spoiler effectiveness for the basic model with vertical and horizontal tails off.
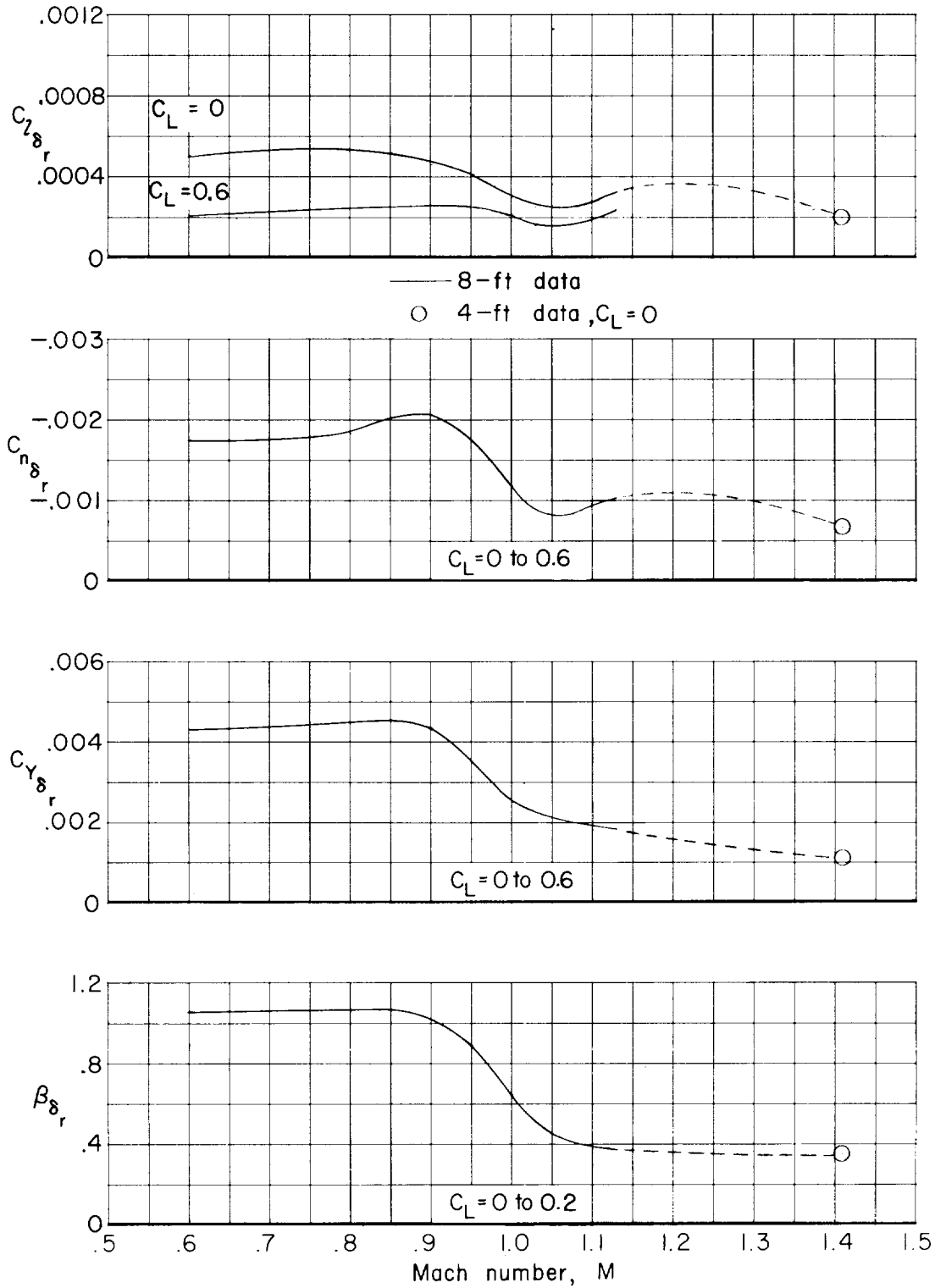
Figure 47.- Variation with Mach number of the directional control characteristics for the basic model. $i_t = 0°$.